Infra-Red Observations of Globular Clusters

Richard Igor John Dmitri Asoka Thomas Dixon

Ph.D. Thesis

University of Edinburgh

1991

to Science

To which end, I hereby relinquish all copyright on material solely owned by myself. This does not include the present data, for which an appropriate acknowledgement is required.

'October the first is too late' - Fred & Geoffrey Hoyle

This thesis has been composed of my own work, except where specifically noted in the text. In particular, chapter 1 is the largely-unaltered text of a paper by three authors.

Richard Dixon

December 1991

Abstract

Near-infra-red imaging observations of the two highly reddened globular clusters M4 and M71 are presented. These data represent the deepest K observations yet published for any cluster.

The photometric accuracy and repeatability of the infra-red camera IRCAM is investigated. Observations made at wavelengths of 1.25 μm (J) and 2.2 μm (K) show clearly that the camera-array combination is capable of a photometric accuracy of better than 1% on bright stars, with no evidence of residual non-linearity of $> 2\%$ over 6 magnitudes.

The reduction procedure is discussed in detail. The profile fitting package DAOPHOT produces accurate and repeatable results from these small frames with large pixels. Zero-point calibrations are examined, and the data are combined with optical data.

M71: Fitting new (V-K)-V and (V-K)-K isochrones finds for the four free parameters: E(B-V)=0.26 $\pm$ 0.03; $(m\text{-}M)_o$=12.85 $\pm$ 0.15; age=13 $\pm$ 1 Gyr and [Fe/H]=-0.78 $\pm$ 0.3, which agree very well with the adopted values from the literature. Combining these with the unified literature results gives the best yet estimates of the cluster parameters: E(B-V)=0.266 $\pm$ 0.015; $(m\text{-}M)_o$=12.87 $\pm$ 0.07; age=14.5 $\pm$ 2 Gyr and [Fe/H]=-0.7 $\pm$ 0.4. No significant binary fraction is detected on the main sequence.

M4: An extensive re-assessment of the literature concludes that a value of R of 4.0 $\pm$ 0.2 is appropriate and that the 'best' literature parameters are: E(B-V)=0.37 $\pm$ 0.01; $(m\text{-}M)_o$=11.22 $\pm$ 0.11 ; age=16 $\pm$ 2 Gyr and [Fe/H]=-1.1 $\pm$ 0.25. The Alcaino and Liller (1984) V magnitudes are found to contain a zero-point error. Allowing for this, isochrone fitting finds an age of 16 $\pm$ 3 Gyr and [Fe/H]=-1.0 $\pm$ 0.4.

Two-colour (V-K)-(B-V) models are constructed and agree well with the M4 and M71 data for metallicities of -1 and -0.5 respectively. The relative offsets between the two clusters in the two-colour diagram are in excellent agreement with the predictions of the models, based on the adopted metallicities.

The K-magnitude luminosity function is constructed for M4, although no allowance can be made for field star contamination. Once converted into a synthetic V-magnitude LF, it compares well with previous work and supports the proposition that the more metal-rich clusters have flatter mass functions, with x=0 for M4.

Acknowledgements

Scientific

I would like to thank the following for generously providing essential data: Roger Bell, Greg Fahlman and Harvey Richer.

I am grateful for useful scientific discussions with the following: Colin Aspin, Roger Bell, Dr V Buckley, Russell Cannon, Bruce Carney, Mark Casali, Bob Dickens, John Fernley, Richard Jameson, Ian McLean, Alan Penny, Harvey Richer, Ian Skillen, Peter Stetson and Bob Stobie.

I am very greatful to both of my supervisors for their care, particularly to Andy for his concern, good sense and friendship.

It is a pleasure to thank Dolores, Joel, Thor and Tom for their skillful telescope operation and their ability to stay awake.

The observations present in this thesis were taken using the infra-red camera IRCAM mounted on the 3.8m infra-red telescope UKIRT on the summit of Mauna Kea on the island of Hawaii, and were reduced using the STARLINK facilities at the Royal Observatory in Edinburgh, and in Hawaii.

Without whom ...

There have been many people who have made my time in Edinburgh and Hawaii more pleasant; I apologise in advance for those I leave out - nothing personal.

Thanks to Ajax, Bobbsy, Chris & Caroline, Colin, Colin, Hugh, Jane, Jane, Jo, Jocelyn, Justin, Kaffy, Karl, Lucy, Lucy, Mandy & Richie, Mick & Kathryn, Nick, Nick, Quentin, Robert, Roof, Rory, Shaun & Jackie, Suzie, Tim.

In particular, thanks for keeping me (in)sane go to Philbo, Rachel, Elin, Diana, John, Alison, Anna, Anna, Anna (Kirsti), Brian, Dave, Helen, Penny, Pippa & Paul.

And finally thanks for the company ('the NiTe cRew'): Brain, Dave, Karly, Penny and, of course, Philbo for always knowing he was right even when he was wrong.

Abbreviations and conventions

The physical sciences converted to using SI (mks) units in 1960. Since no-one would understand log g_{mks} of 0 as being the same as log $g_{cgs} = 3$ I have used these eldritch units where tradition dictates, otherwise SI units are used.

Some abbreviations are so general that they are used in most chapters and so are defined here to avoid repetition. For clarity these abbreviations always appear in upper case.

HB - horizontal branch	CMD - colour-magnitude diagram
RGB - red giant branch	2CD - two-colour diagram
SGB - sub-giant branch	HR - Hertzsprung-Russell
MSTO, TO - main sequence turn-off	GB - giant branch
IR - infra-red	CCD - charge-coupled device
BC - bolometric correction	LF - luminosity function

Symbols

X,Y,Z - respectively mass densities of hydrogen, helium and everything else (X+Y+Z=1).

$\mathcal{M}$ - stellar mass	L - luminosity.
T, T_{eff} - temperature, effective temperature	g - stellar effective gravity
[Fe/H] - metallicity. Used synonymously with [M/H]	t - stellar and cluster age

Conventions

Optical astronomy is taken to refer to astronomy in the visible region of the spectrum, although of course IR astronomy uses very similar optical technology.

Important diagrams are sometimes printed sideways. This is so that they can be shown large enough to do them justice, and I apologize to the reader for the inconvenience.

For instrumental magnitudes lower-case letters are used, e.g. k, v, (b-v), whereas true apparent magnitudes use upper case letters, such as K, V, (B-V), and absolute magnitudes use the capital M notation, M_K, M_V. Reddening corrected magnitudes are denoted by a nought subscript, e.g. V_o, $M_{K,o}$.

Contents

Introduction

This thesis concerns infra-red observations of globular clusters. Specifically, I will present near-IR K-band imaging observations in the two clusters M71 Sge and M4 Sco. This is pioneering work; imaging detectors have been available to IR astronomers for only the last five years and the data presented here were taken with one of the first camera systems available. Reduction and analysis techniques have had to be developed along the way, and these are discussed in some detail.

In this Introduction I will attempt to provide a brief introduction to IR astronomy, the huge and complex topic of globular clusters, and how the two are linked. For the reader who is less familiar with these areas of astronomy and its arcane terminology I have included short definitions for some important terms in the boxes to be found scattered throughout the following pages.

1 Infra-red astronomy

The infra-red (IR) portion of the electromagnetic spectrum lies between the visible and mm-wave regions, that is between wavelengths of $\sim 0.7\,\mu$m and $\sim$1mm. Traditionally, the IR may be further sub-divided into the photographic infra-red from 0.7 to $\sim 1.1\,\mu$m, the

globular clusters - gravitationally bound systems of $10^5 - 10^6$ stars found in our Galaxy and others. There are nearly 200 known in the Galaxy, where they form part of the population II halo.

population II - old, metal-poor stars making up the Galactic halo.

infra-red - the region of the electromagnetic spectrum between visible light and microwaves - that is, 0.7 - 1000 μm.

near-IR - approximately the region from $\sim$1 - 5 μm, depending upon your prejudice.

K-band - Johnson's broad-band filter centred around 2.2 μm.

near IR from 1.1 to $\sim$5 μm with the mid- and far-IR beyond 5 μm. These divisions are a matter of taste and vary between authors, but this thesis is concerned with observations near 2.2 μm - in Johnson's K-band (Johnson, 1964) of the near-infra-red.

1.1 History

Infra-red astronomy is a young science, even though the first infra-red astronomer was actually Sir William Herschel, who discovered the infra-red radiation beyond the red part of the Sun's spectrum at the end of the eighteenth century. Like astronomy in the radio and microwave regions, the development of IR astronomy has been dependent on technological advances, often military cast-offs. It is only in the last 30 years that IR astronomy has started to produce really significant results.

Harold Johnson introduced the UBV photometric system to optical astronomers in the 1950s and this was extended, first to the R and I bands in the photographic IR, and then to the J, H, K, L, M and N bands ranging from 1.25 - 10 μm. At optical wavelengths the centres and widths of the bands can be chosen to measure critical features in stellar spectra, for instance, the Strömgren u and v filters bracket the Balmer discontinuity. In the IR the bands are where they have to be (!) - in those regions of the spectrum not completely blocked due to absorption by atmospheric carbon dioxide and water molecules. Johnson et al (1966) published near-IR photometry of a large sample of field stars, providing calibration for this filter system.

In 1969 NASA's 2 μm catalogue (Neugebauer and Leighton, hereafter the IRC) was published, containing all objects brighter than third magnitude at 2 μm and north of declination -33°.

In the 1980s the Infra-red Astronomical Satellite, IRAS, conducted a survey of the whole sky at four wavelengths between 12 and 100 μm. It is only in the last five years that near-IR astronomers have been able to use imaging detectors, rather than having to

CCD - charge-coupled device - 2D semi-conductor array detector used between the near-UV and the photographic-IR. Highly efficient and linear.

laboriously scan a telescope, equipped with a single-channel detector, to produce a map or to measure the brightness of a number of individual objects. The day when, as in optical CCD photometry, a simple image can be taken reaching faint magnitudes and covering a large enough area of the sky to allow many objects and calibration sources to be included at one time is still some way off, but even so many tasks are two orders of magnitude faster (in the observing phase, although definitely not in the reduction phase !) than they were 10 years ago. It is only this sort advance in observing efficiency that has made a project such as the present one feasible.

1.2 Observing in the infra-red

Observing in the IR has been compared to using an optical telescope made of fluorescent tubes during daylight. The reality is even worse. At near-IR wavelengths the telescope, the dome, the astronomer and the air between the detector and the astronomical source are all glowing brightly, simply because of their temperature. Typically the brightness of the sky at K is comparable to a star of around 13^{th} magnitude. For single-channel photometry the technique of chopping is used, with phase-sensitive detector electronics, to continuously subtract the sky flux from the source observations. With an imaging detector observations quickly become background limited as the dynamic range of the device is filled up with sky flux. Indeed, the practical limitation on broad-band exposure times at all wavelengths is how fast the device saturates on the sky.

There is a rule-of-thumb approximation to Wien's law that the peak wavelength, in microns, of a black-body distribution is given by $\lambda = 3000/T$, where T is the temperature of the black-body. Thus, the J-N bands cover the peak wavelengths of objects with temper-

magnitudes - logarithmic brightness scale with smallest numbers brightest.
absolute magnitudes - the magnitude measured at a standard distance of 10pc.
RR Lyraes - population II pulsating variable stars. Most globular clusters contain a some, M3 has ~200.
chopping - switching (usually at ~10Hz) between sky and object.
background limited - when the Poisson noise from the sky is the dominant noise source.

atures ranging from ~3000-300K. For this reason IR observations have traditionally been thought most useful for cool sources like the dust shells around protostars, dust and gas in HII regions and solar-system bodies, for heavily obscured regions, such as the Galactic Centre and the Orion star-forming region, and for energetic objects such as active galaxies.

2 Globular clusters

Were we to live on a planet circling a star like the Sun, but located near the centre of a globular cluster, astronomy would be a very different subject. The sky would never be dark - with stars separated by only ~1000 AU many nearby stars would appear as bright as the full Moon does to us. Perhaps here and there a blue horizontal branch star would stand out in contrast against the thousands of nearby yellowish stars and the bright, red giants. Stellar astronomy would thrive; cosmology would be very hard; orbit theory would be very well developed ! (See Asimov (1974) for an interesting exploration of the human side to this scenario).

The simplest model is that stars in globular clusters all formed together, at the same time and from the same material. All the stars in the cluster should therefore contain the same balance of chemical elements. Any difference, in luminosity, temperature or detailed chemical composition, that is seen between stars in a cluster is a function of the different initial masses of the stars and their consequently different evolution. Globular clusters are the proving ground of stellar evolutionary theory and a proper understanding of their physical parameters is therefore vital.

The reader is recommended to consult Madore (1980) and Freeman and Norris (1981) for excellent, if now rather out of date, introductions to the study of globular clusters. IAU Symposium 126 (Grindlay and Philip, 1987) contains more detailed papers covering most current areas of the field and many recent conferences, such as Cacciari and Clementini (1990) and Caputo (1992), have covered specific topics. Peterson (1986) contains a compilation of cluster parameters, together with references to colour-magnitude studies, for over a hundred clusters.

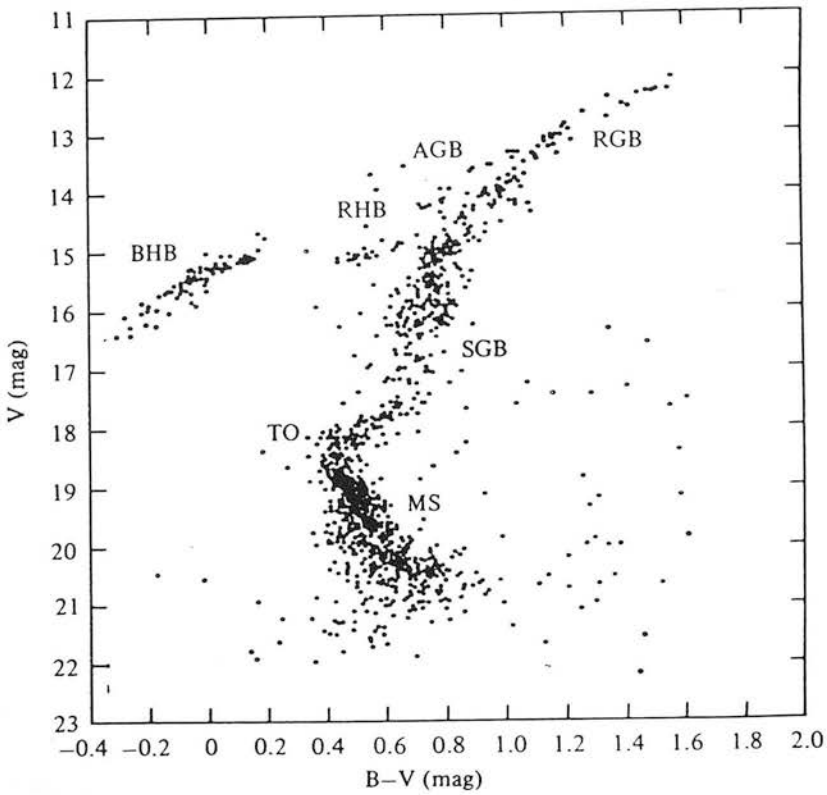

Figure 1: Example globular cluster CMD showing the primary sequences.

main sequence - stars, like the Sun, burning H in the core. The main sequence phase is very long: 9 Gyr for the Sun and longer for the less massive stars seen in globular cluster MSs.

turn-off - once the H in the core is exhausted the core contracts and the outer layers of the star expand, taking the star to the red.

sub-giant branch - H burning continues in a shell outside the core. As this narrows the star moves accross to the base of the RGB.

giant branch - as the star evolves brighter and redder the core continues to heat up until, at the top of the GB the He flash occurs - He ignites in the core and the star moves rapidly on to the horizontal branch.

horizontal branch - core He burning. Lifetime ~25% of main-sequence lifetime.

asymptotic giant branch - as the He core is exhausted it contracts and the envelope expands again, with H and He burning in shells.

instability strip - a region in the CMD where stars contain zones where opacity is near a critical T and pressure. In the middle of the HB stars pass through this phase and are likely to pulsate as RR Lyrae variable stars.

2.1 History

The first telescopic observation of a globular cluster was probably Abraham Ihle's discovery of M22 in 1665, although the naked-eye clusters ω Cen, 47 Tuc, M13 and M4 would have been known since ancient times as 'fuzzy' stars. Charles Messier included many globular clusters in his catalogue of objects-to-avoid-whilst-comet-hunting. Even with his moderate equipment, he could resolve some clusters into individual stars. When the cluster RR Lyraes were discovered at the turn of the century it became possible to work out the distance to the globular clusters by assuming a fixed absolute magnitude for the variables. In 1918 Harlow Shapley found that the clusters formed a spheroidal system and were concentrated towards Scorpius/Sagittarius, and from this he was able to make one of the first estimates of the position and distance of the Galactic Centre. Since that time, the globular clusters have remained very important in the study of the past and present structure of our Galaxy.

Ejnar Hertzsprung and Henry Norris Russell plotted stars on a spectral-type - absolute magnitude (Hertzsprung-Russell) diagram to show that there were different sorts of stars: giants and dwarfs. This diagram is closely related to the temperature-luminosity plane and these studies formed the basis of today's colour-magnitude diagrams (CMDs). In 1944, Baade used the HR diagram to show that the globular cluster stars were rather different from stars in the solar neighbourhood. After the first pioneering studies, CMD work took off in the 1950s (see for instance Arp, Baum and Sandage, 1952; Arp, 1955), bringing a revolution in our understanding of the globular clusters. Figure 1 shows an example (B-V)-V CMD with the primary sequences marked on it.

At first it was thought that the clusters formed a sequence in their CMD morphology that was related to their metal content, with the metal-rich clusters having short red horizontal branches and the metal-poor ones showing long blue and red horizontal branches, with RR Lyrae variables in the instability strip between. However, it soon became clear that things were not so simple, with clusters of the same metallicity having very different horizontal branches. Sidney van den Bergh (1965) posed the 'second parameter problem' - that one or more other parameters beyond metallicity were needed to explain the observed HB structure. Over the intervening years, many parameters and combinations of parameters have been proposed to explain this effect, from age and the abundances of the CNO

elements to rotation, core mass and helium abundance. It seems that a solution is almost as elusive as it was in 1965, with the problem becoming ever more complex as new data become available.

2.2 Observations

See Hesser (1987) for a detailed discussion of the recent advances that the advent of CCDs have brought about in many areas of globular cluster research. Hesser et al (1987) show for instance, the tremendous improvement in precision and sensitivity that has been possible over older photographic and photoelectric studies. However, although CCD studies are usually free from linearity problems, they are still susceptible to calibration errors, as again evidenced by Hesser et al, and as will be seen in subsequent chapters.

2.2.1 CMDs

The theoretical HR diagram is usually a plot of stellar effective temperature against absolute luminosity (T-L). This is the parameter space in which stellar theorists work, whereas the observer will produce a plot of observed colour against magnitude - the colour-magnitude diagram. It is in relating these two diagrams that many of the problems of reconciling theory and observation lie. It is the HR or CM diagram that is the primary tool of those studying the stellar content of globular clusters.

Stellar models can be combined with an initial mass distribution and allowed to evolve to produce an isochrone - a line of constant age representing a set of stars in the temperature-luminosity plane. With an appropriate transformation via stellar model atmospheres this can be converted into the colour-magnitude plane and compared to observations. Isochrones can be matched up to the data to determine the 'best-fit' metallicities and ages. The usual procedure relies on an accurate knowledge of the distance modulus and reddening to the cluster in question.

In the last five years many cluster studies have used either the VandenBerg and Bell (1985) or the Revised Yale isochrones (Green, Demarque and King, 1987) to fit to their data, with great success. Straniero and Chieffi (1991) have recently calculated a comprehensive new set of isochrones and new oxygen-enhanced isochrones, with [O/Fe] varying as a

function of [Fe/H], will soon be available (Bergbusch and VandenBerg (1992)).

2.2.2 Luminosity functions

The luminosity function - the number of stars in a given brightness interval - allows the relative lifetimes of stars in the various evolutionary phases to be estimated from the numbers occupying each branch in the CMD (see, for example, Renzini (1986)).

The LF also allows the mass function to be estimated, with all that this implies for the cluster's formation and evolution (see Spitzer, 1987). Any turn-down of the mass function at small masses would be important because a large fraction of the cluster's mass could be tied up in very faint stars. It would also indicate the least massive objects that can actually burn as stars, testing the theoretical limit for the mass of brown dwarfs. Richer et al (1991) find that the mass function is still increasing at $0.4\,\mathcal{M}_{\odot}$ in their I-band observations and between them Richer et al (1990) and Fahlman et al (1989) presented mass functions for 4 clusters, stating that half the mass of the cluster may be tied up in brown dwarfs. McClure et al (1987) showed for a number of clusters that the mass-function power-law index is correlated with metallicity, with the most metal-rich cluster having the flattest mass functions. However, Richer et al (1991) found no such correlation in their data. Smith and McClure (1987) discuss whether the mass function determines the metallicity or vice versa.

2.2.3 Interesting objects

Apart from the familiar sequences in the CMD, what other interesting objects might be found in a globular cluster ? When such objects are being considered, membership probabilities from kinematical studies like that of Cudworth and Rees (1990) are of paramount importance.

[Fe/H] - the logarithmic number ratio of iron to hydrogen atoms, relative to that in the Sun: $log_{10}(n^{*}_{Fe}n^{\odot}_{H}/n^{*}_{H}n^{\odot}_{Fe})$. Usually taken as a general indicator of metallicity.

[O/Fe] - the oxygen enhancement - analagous to [Fe/H].

Blue stragglers

Blue stragglers are stars that lie above and to the blue of the main sequence turn-off - as if they were main-sequence stars that had not evolved into sub-giants. One of the favourite theories to explain blue stragglers is that they consist of close binaries and that it is the transferring of mass between the components that prolongs their life (see Iben, 1986 for a review). Alternatively some unaccounted physical process may affect only a few percent of stars, extending their main sequence lifetimes (see Renzini and Fusi Pecci, 1988). These binaries may coalesce into single objects (see, for instance, Nemec and Harris, 1987). Blue stragglers have been confirmed in M3 (Chafee and Ables, 1983) and ω Cen (Da Costa, Norris and Villumsen, 1986), with three eclipsing binary system candidates in NGC5466 (Mateo et al, 1990) and good candidates in several other clusters.

Main-sequence binary systems

From radial velocity measurements of giants, Pryor et al (1989) have suggested that the fraction of binaries remaining on the main sequence at the present time should be about 10%. These binaries are likely to be close systems, since the result of collisions in globular clusters is to disrupt distant systems and make tight binaries tighter (Heggie (1975), Hills (1975)). These objects are important in constraining dynamical models of globular cluster formation and evolution, since a large fraction of the cluster's binding energy may be locked up in these systems (see, for example, chapter 7 of Spitzer, 1987).

If there are unresolved companions and binaries in the main sequence, where will they lie ? Simplistically, if two stars of the same, normal, main-sequence type become a binary system, it will have the same colour as a single star but appear three-quarters of a magnitude above the single star sequence. Unresolved red companions will also move stars away from the fiducial line: brighter and redder.

The only clusters where a sequence of equal-mass main-sequence binaries has been found

initial mass function - the number of stars formed per unit mass interval in unit volume.
mass function - the number of stars currently present per unit mass interval. Related to the LF by a mass-luminosity relation.

are the outer halo object E3 (McClure et al, 1985) and NGC288 (see Bolte, 1991). However, there is some evidence for main-sequence binaries in several other clusters, including M92 (Stetson and Harris, 1988) and M30 (Piotto et al, 1990).

White dwarfs

White dwarfs are important because they may account for a significant fraction of a cluster's mass but they are at the limit of present detector sensitivities. Although the population I models are quite well developed, the masses of population II white dwarfs are still uncertain. Some candidates have been found (e.g. Richer and Fahlman, 1988), but as yet none are convincing (see Weidemann, 1990, for a review).

X-ray sources

X-ray sources have been discovered in several clusters, like NGC1851, probably corresponding to low-mass X-ray binaries - a neutron star with an accretion disc and a low-mass companion. Most of these objects are concentrated in the cluster cores, where observations are difficult. With the recent discovery of 10 millisecond pulsars in 47 Tuc (Manchester et al, 1991), nearly half of the known examples of these objects lie in globular clusters.

2.3 The globular cluster system and Galactic structure

In 1958 Baade proposed that the metal-rich clusters lay in a more disk-like distribution than the metal-poor ones. It is now clear that the ~25% of clusters more metal rich than [Fe/H]~-0.8 are kinematically and positionally part of Gilmore and Reid's (1983) thick-disk population (Zinn, 1985). It is possible that the *very* distant, low-luminosity clusters like Pal 3 form a third independent group outside the Galaxy's population II halo (see Zinn, 1987). An understanding of the distribution of metallicity and age within the

white dwarf - cool blue remnants of intermediate mass stars. $\sim 1\,\mathcal{M}_{\odot}$.
neutron star - dense, degenerate star. Perhaps $2\,\mathcal{M}_{\odot}$.
white dwarfs and **neutron stars** are the end products of stellar evolution.

globular cluster system is crucial to models of how the Galaxy formed and how it has evolved since.

Globular clusters can themselves be used as 'standard candles' to measure the distance to external galaxies (see Harris, 1991, for a discussion of the problems involved).

2.4 Ages

The ages of the globular clusters are very important. The oldest clusters constrain the age of the Universe, with important consequences for the value of the Hubble constant, H_o. For example, an age for the Universe of 17 Gyr is consistent with $H_o \leq 60$km/s/Mpc for $\Omega=0$ or 40km/s/Mpc for $\Omega=1$. See Fowler (1987) for a discussion of the age of the observable Universe and the relevant observations. If there is a range of ages amongst the clusters, the Galaxy may have formed slowly, contrary to the Eggen, Lynden-Bell and Sandage (1962) scenario of free-fall collapse.

The most popular method of determining the age of a globular cluster is from the luminosity of the turn-off, usually found by looking at ΔV_{TO-HB}, the luminosity difference between the turn-off and the level of the horizontal branch (see Sandage, 1986). This relative difference is used as an age indicator because the level of the HB is much less sensitive to age than the level of the turn-off. However, the magnitude of the turn-off, V_{TO}, is very hard to determine, since the sequence is almost vertical for almost a magnitude. Also the HB is often not populated at the colour of the MSTO. Normally these difficulties lead to age ranges of ± 3 Gyr, with ± 1 Gyr in exceptional cases (see, for example, Stetson et al 1989). Also, the calibration of the derived turn-off luminosity relies upon the relation between the absolute luminosity of the RR Lyrae stars and the metallicity of the cluster. The gradient $\delta M_V(HB)/\delta[Fe/H]$ is *very* controversial. In a series of papers in the early 1980s, Sandage showed that the RR Lyraes in different clusters could be related by a simple period shift - the 'Sandage Period Shift Effect' (SPSE) - and that this shift was correlated with both the metallicity of the cluster and the absolute magnitude of the variables. Both the SPSE and some main-sequence fitting studies lead to $\delta M_V(HB)/\delta[Fe/H] = 0.37$. When this is used in the models it implies that there is no significant variation in age between the clusters (see Buonanno, Corsi and Fusi Pecci, 1989). On the other hand, some HB models (e.g. Sweigart, Renzini and Tornambé, 1987)

predict no change of luminosity with changing metallicity for HB stars, which would imply a range of about 10 Gyr between the clusters. In the middle ground, the results of Baade-Wesselink analyses of field RR Lyrae stars suggests $\delta M_V(HB)/\delta[Fe/H] \sim 0.20$. Our own study of the log P - K magnitude relation in eight clusters (a revision of the result in Longmore et al 1990) finds a value of 0.20 and Carney, Storm and Jones (1992) believe that they have reconciled all the previous studies to agree on a gradient of 0.15.

With the SPSE gradient, Sandage and Cacciari (1990) find all the clusters to be 19 Gyr old (or 15.5 Gyr if an [O/Fe]=0.6 enhancement is assumed). Carney, Storm and Jones conclude that the age-metallicity relation depends on whether [O/Fe] is correlated with [Fe/H], with the cluster ages ranging from 15 to 20 Gyr if a constant oxygen enhancement is assumed.

2.4.1 Rotation

From the observations of rotational velocity by Peterson (1985) there is clearly a considerable spread in the amount of angular momentum bound up in the rotation of stars in different clusters. Rotation has been invoked at various times to explain the second parameter problem (Norris, 1981), to extend the age scale by up to 30% (Law, 1981), to explain abundance anomalies and to change the masses of variables of a given luminosity. However, Deliyannis, Demarque and Pinsonneault (1989) show from model calculations that rotation probably has a negligible effect on age and composition, although it may be important in determining HB morphology (see Lee, Demarque and Zinn, 1990).

2.5 Chemical content

The overall chemical composition of the globular cluster system varies from near solar to 300x less than solar, with a group of clusters around [Fe/H]=-1.6 and another at -0.5. The metallicity scale of the globular clusters was very controversial during the last decade, particularly at the metal-rich end where different methods gave very different values. This anomaly has probably been explained by Bell (1987) as an error in the spectroscopic studies caused by the presence of unaccounted TiO bands in the stellar spectra. Bell summarizes the various methods that are used to determine the metal content of globular clusters. These vary from high-resolution spectra of single stars, allowing the abundances

of individual elements to be calculated, to integrated photometry such as the large study by Zinn (1980). Of particular interest in globular clusters is the RR Lyrae spectral parameter ΔS, which has proved to be a good metallicity indicator (see Smith, 1984).

2.5.1 Star-to-star variations

In most clusters there are no large-scale compositional variations between stars. The typical observed width of the giant branches imply a possible range of metallicity of Δ[Fe/H]<0.15. However, ω Cen and, to a lesser extent, M22 exhibit a wide range of elemental abundances, with the ω Cen stars ranging over more than one dex (Freeman and Rodgers, 1975; Noble et al, 1991; Lee, 1991). In most clusters CNO element abundance variations are seen, particularly in CN (cyanogen) (see Norris, 1987, and Smith, 1989, for reviews), with many clusters showing bimodal CN distributions (see, for example, Suntzeff and Smith, 1991). Smith (1987) categorized the different classes of abundance variations and proposed a mixture of primordial differences and evolutionary dredge-up of core-processed material to explain them. For instance, Briley et al (1992) find CN abundance variations in the sub-giants of M5, proposing that at least some of the variation must be due to primordial variations.

Another possibility for CN enhancement is the mixing of processed material caused by mass transfer between the components of binary systems, as proposed by Campbell (1986). Some evidence for this comes from the discovery of CH stars in field binaries (McClure, 1984) and from the central concentration of the CN-rich giants in 47 Tuc.

2.6 The remaining problems

The problems that remain to be solved are many. Some of the most interesting are given below.

- The second parameter problem still remains. The detailed structure of the horizontal branch is being modelled and this will help to quantify the effects of subtle compositional variations (see Lee, Demarque and Zinn, 1990).
- What is the range of ages and maximum age amongst the clusters ? The oldest clusters constrain H_o and the range of ages give the rate at which the Galaxy

formed.

- Despite the proposed unification by Carney, Storm and Jones (1992) the Sandage Period Shift Effect and the gradient of the HB luminosity - metallicity relation are likely to remain controversial.

- Are the globular clusters kinematically and chemically the same as the population II halo stars ? In external galaxies the clusters do seem to be different in colour from the stars (Harris, 1987), but in our Galaxy the data are ambiguous (Laird et al, 1987).

The fundamental parameters that must be gleaned from each cluster before they can be used to address these problems are the distance modulus, reddening, metallicity and age. It is these that the present data will help to determine for M4 and M71.

3 Globular clusters and the infra-red

There are two main reasons to observe globular clusters in the infra-red: (a) many clusters are heavily reddened and the extinction at 2 μm is ~10x less than at V and (b) the long baseline afforded by optical-infra-red colour indices allows a good estimate of stellar temperature, allowing more confidence and accuracy in fitting model isochrones.

3.1 (V-K) as a temperature indicator

Stars in a globular cluster may be expected to show a range of effective temperatures from ~10000K for the bluest HB stars to less than 4000K for the reddest stars. For stars with an effective temperature of ~5000K the peak wavelength of emission is around the V-filter (centred near 550nm), while the K-filter is measuring the Rayleigh-Jeans tail of the energy distribution. Figure 2 shows the relative positions of the B, V and K filters in relation to black-body energy distributions of various temperatures. It can be seen that the energy at the K-filter changes in a slow and smooth manner with temperature. The (logarithmic) ratio between the energy in the V and K filters, the (V-K) colour, changes quickly with temperature, more quickly that the (B-V) colour. Figure 3 shows the relation between black-body temperature and colour for both (B-V) and (V-K). Clearly, a photometric

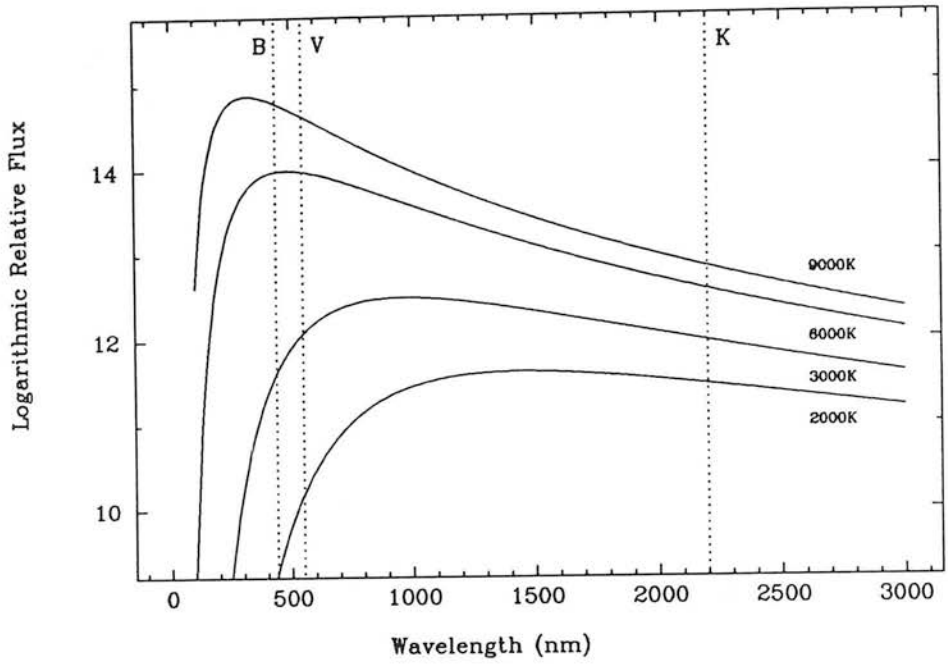

Figure 2: Black-body energy distributions for 9000, 6000, 3000 and 2000K with the central wavelengths of the B, V and K filters overlaid.

error of a given size will produce a much smaller temperature error from (V-K) than from (B-V). For instance, at ~3000K an error of $0^{m}.05$ in (V-K) leads to an uncertainty of ~60K in the derived temperature, whilst the same error in (B-V) leads to a possible range of 200K. (Of course, stellar energy distributions may significantly deviate from those of black-bodies and the filter profiles have been approximated as rectangles, so the diagrams are merely illustrative).

The dominant source of opacity in both the V and K passbands is from the H^- ion, and since the magnitude of its effect is similar in both filters the (V-K) colour is less sensitive to metallicity and gravity changes than comparable optical colours. Also, the effect of TiO absorption in the V-filter is to increase the sensitivity to temperature variations in (V-K) and decrease it in (B-V).

Several studies have attempted to calibrate the (V-K) colour index as a temperature indicator for stars.

- Johnson (1966) - an empirical temperature calibration for population I stars from

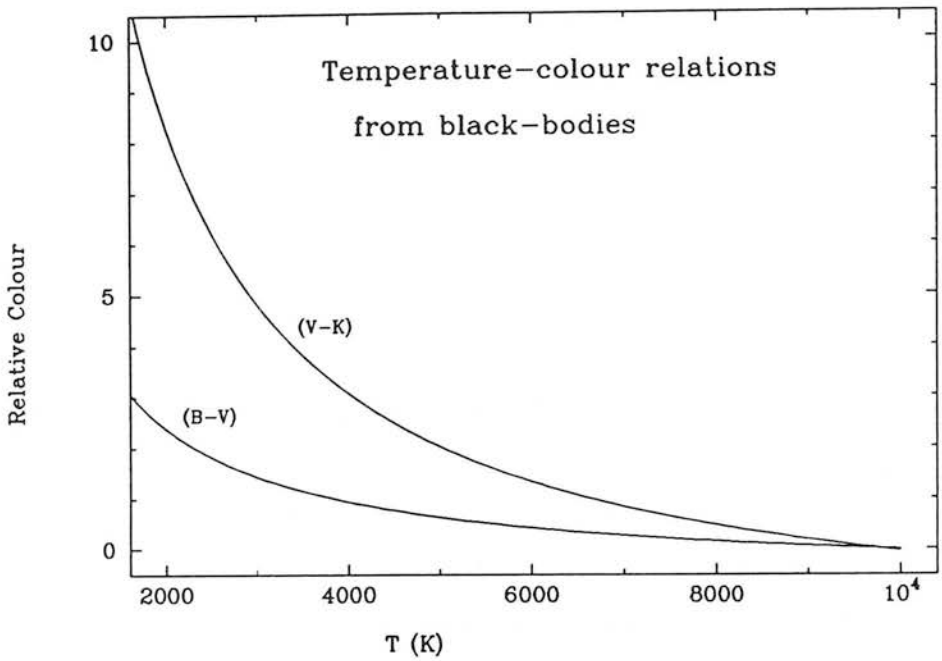

Figure 3: Temperature-colour relations derived from a set of black-bodies.

his extensive database of stellar photometry.

- Persson and Frogel (1980) - showed, from models, that temperatures in the range 3800-5200K derived from (V-K) are ~3.5x less sensitive to photometric errors than temperatures obtained from the (R-I) colour (e.g. ΔT~60K as opposed to ~200K for a colour error of $0^{m}.1$).

- Ridgeway et al (1980) - combined angular diameter measurements and near-IR photometry to calibrate the effective temperatures for late-type field giants.

- Carney (1983) - (based on earlier work by Peterson and Carney) derived temperatures from model fitting to stellar spectrophotometry. He showed that (V-K) is the Johnson colour index least affected by metallicity and gravity, and most sensitive to temperature for F, G and early K stars.

- Fernley (1989) - semi-empirical calibration for stars of all metallicities and gravities in the range 5500<T<10000K based on Kurucz model atmospheres. The models predicted a change of only ~60K for a change of 1 dex in [Fe/H] and a change of ~130K for a change of 1 dex in log g, at 7000K.

- Bell and Gustafsson (1989) - from model atmospheres of main sequence and sub-giant stars. They showed that the scatter in the (V-K)-T diagram was less than in the (B-V)-T diagram for similar observations, because of the greater effects of metallicity and gravity variations on the (B-V) colours.

3.2 History

The use of infra-red photometry to measure stars in globular clusters is relatively recent. Several studies strayed into the photographic IR.

- In the seventies Lloyd-Evans observed a series of cluster in V and I (see, for example, Lloyd-Evans, 1974). He used the (V-I) colour index because it is more sensitive to temperature than (B-V) for the metal-rich M stars that he was observing.

- Alcaino and Liller (1984) obtained UBVRI observations in the cluster M4 - the first globular cluster study to use all five Johnson colours - although they did little to interpret the resulting multitude of CMDs.

- Heasley and Christian (1986), whilst considering their observations of M92, examined the sensitivity of various colour indices to metal content, concluding that both (V-R) and (V-I) are less sensitive to metallicity than (B-V), and that (R-I) might be the least metallicity sensitive index of all in the UBVRI set.

- Richer et al's (1991) recent mass function work has used I-band luminosity functions.

Important near-IR observational studies of stars and globular clusters have included the following.

The first JHKL photometry of globular cluster stars was performed by Glass and Feast (1973), who observed giants and variables in ω Cen and 47 Tuc.

Only two clusters were bright enough to be included in the IRC in 1969, but one of these, IRC -20 385,was so heavily obscured that it had not been discovered in the optical.

Aaronson et al (1978) used integrated $(V-K)_o$ colours as a metallicity indicator for globular clusters and galaxies.

Several studies in the 1970s looked at the use of TiO bands as metallicity indicators. Mould, Stutman and McElroy (1979) used near-IR spectrophotometry to measure the strength of the TiO bands in a number of metal-rich globular cluster giants.

The most important body of work concerning near-IR observations of globular clusters is that of the Cohen, Frogel and Persson group (e.g. Cohen, Frogel and Persson, 1978; Frogel, Cohen and Persson, 1983; Frogel, Persson and Cohen, 1983), who took near-IR photometry of giant stars in 33 clusters in the 1970s and 1980s. They compared their observations to models and used morphological features as metallicity indicators, particularly the $(V\text{-}K)_{o,GB}$ parameter (see box). Similar work by Phillips et al (1986) extended the (V-K)-V CMD of M4 down to the horizontal branch. Before the present study, no globular clusters stars fainter than the horizontal branch had been observed at near-IR wavelengths.

K-band observations have revolutionized Baade-Wesselink studies of field RR Lyrae and Cepheid stars, and were used in 1990 when Liu and Janes applied the method to four RR Lyrae variables in M4. As has already been mentioned, Longmore et al (1990) used K-band observations of RR Lyraes in eight clusters to investigate the distance scale.

Papers by our group (Longmore, Dixon and Guarnieri, 1990, Guarnieri et al, 1990) were the first, and so far the only, studies to show the main sequence in an optical-IR CMD (M71 and M3, respectively).

This thesis will present the deepest yet optical-IR CMDs and two-colour diagrams.

3.3 Aims of this thesis

The aims of the present work may be summarized as follows.

$(V\text{-}K)_{o,GB}$ - the de-reddened (V-K) colour of the giant branch at an absolute magnitude of $M_{K,o}$=-5.5.

integrated light - measurement of most of from the cluster stars in a single aperture.

Baade-Wesselink - a method combining radial velocity and photometric curves to derive absolute physical parameters for pulsating variable stars.

- To show that IR arrays are capable of reliable and accurate photometry.
- To show that images from such arrays can be analysed with profile-fitting software, such as DAOPHOT.
- To derive estimates for the physical parameters of reddening, distance modulus, metallicity and age for M71 and M4.
- To look for main-sequence binaries.
- To show that (V-K) CMDs are less affected by photometric scatter than those using (B-V).

Also, part of the motivation for exploring the new field of optical-IR CMDs and 2CDs was serendipity - to look for unexpected effects.

4 Thesis guide

Chapter 1 discusses the use of IR array images to perform photometry on bright stars. Chapter 2 discusses in detail the reduction of frames taken in globular cluster fields, their analysis with the DAOPHOT profile fitting software and their calibration. Chapter 3 examines the very metal-rich cluster M71 and chapter 4 the obscured cluster M4. A final chapter summarizes the results found and discusses the astrophysical and observational implications of the present work, as well as the future prospects for near-IR studies of globular clusters.

References

Aaronson, M, Cohen, JG, Mould, J & Malkan, M, 1978. Ap.J., **223**, 824.

Alcaino, G & Liller, W, 1984. Ap.J.Suppl., **56**, 19.

Arp, HC, 1955. A.J., **60**, 317.

Arp, HC, Baum, WA & Sandage, AR, 1952. A.J., **57**, 4.

Asimov, I, 1974. *'Nightfall'*. In: *'Nightfall 1'*. Panther Books (St.Albans).

Baade, W, 1944. Ap.J., **100**, 137.

Bell, R.A., 1987. In: *'The Harlow-Shapley Symposium on Globular Cluster Systems in the Galaxy'*, p.79. Eds. Grindlay, JE & Davis Philip, AG. Kluwer Academic Publishers (Dordrecht).

Bolte, M, 1991. Ap.J., **376**, 514.

Briley, MM, Smith, GH, Bell, RA, Oke, JB & Hesser, JE, 1992. Ap.J. (in press).

Buonanno, R, Corsi, CE & Fusi Pecci, F, 1989. A.&A., **216**, 80.

Cacciari, C. & Clementini, G., (eds), 1990. *'Confrontation Between Stellar Pulsation and Evolution'* A.S.P. Conference Series 11, 36. L. Davis Press (San Fransisco).

Campbell, B, 1986. Ap.J., **307**, 750.

Caputo, F, 1992. *'New Results on Standard Candles'* workshop, Trani, Italy 1991. To appear in Mem.Soc.Astr.Ital.

Carney, BW, 1983. A.J., **88**, 623.

Carney, BW, Storm, J & Jones, RV, 1992. Preprint.

Chafee Jr., FH & Ables, HD, 1983. P.A.S.P., **95**, 835.

Cohen, JG, Frogel, JA & Persson, SE, 1978. Ap.J., **222**, 165.

Cudworth, KM & Rees, R, 1990. A.J., **99**, 1491.

Da Costa, GS, Norris, J & Villumsen, JV, 1986. Ap.J., **308**, 743.

Deliyannis, CP, Demarque, P & Pinsonneault, MH, 1989. Ap.J., **347**, L73.

Eggen, OJ, Lynden-Bell, D & Sandage, A, 1962. Ap.J., **136**, 748.

Fahlman, GG, Richer, HB, Searle, L & Thompson, IB, 1989. Ap.J., **343**, L49.

Fernley, JA, 1989. M.N.R.A.S., **239**, 905.

Fowler, WA, 1986. Q.J.R.A.S., **28**, 87.

Freeman, KC & Norris, J, 1981. Ann.Rev., **19**, 319.

Freeman, KC & Rodgers, AW, 1975. Ap.J., **201**, L71.

Frogel, JA, Cohen, JG & Persson, SE, 1983. Ap.J., **275**, 773.

Frogel, JA, Persson, SE & Cohen, JG, 1983. Ap.J.Suppl., **53**, 713.

Gilmore, G & Reid, N, 1983. M.N.R.A.S., **202**, 1025.

Glass, IS & Feast, MW, 1973. M.N.R.A.S., **163**, 245.

Green, EM, Demarque, P & King, CR, 1987. *'The Revised Yale Isochrones and Luminosity Functions'*, Yale University Observatory (New Haven).

Grindlay, JE & Philip, AGD, (eds), 1987. *'The Harlow-Shapley Symposium on Globular Cluster Systems in the Galaxy'*. Reidel (Dordrecht).

Guarnieri, MD, Longmore, AJ, Fusi Pecci, F & Dixon, RI, 1990. Mem.Soc.Astr.Ital., **61**, 143.

Harris, WE, 1987. In: *'The Harlow-Shapley Symposium on Globular Cluster Systems in the Galaxy'*, p.237. Eds. Grindlay, JE & Davis Philip, AG. Kluwer Academic Publishers (Dordrecht).

Harris, WE, 1991. Ann.Rev., **29**, 543.

Heasley, JN & Christian, CA, 1986. Ap.J., **307**, 738.

Heggie, DC, 1975. M.N.R.A.S., **173**, 729.

Hesser, JE, 1987. In: *'The Harlow-Shapley Symposium on Globular Cluster Systems in the Galaxy'*, p.61. Eds. Grindlay, JE & Davis Philip, AG. Kluwer Academic Publishers (Dordrecht).

Hesser, JE, Harris, WE, VandenBerg, DA, Allwright, JWB, Shott, P & Stetson, PB, 1987. P.A.S.P., **99**, 739.

Hills, JG, 1975. A.J., **80**, 1075.

Iben Jr., I, 1986. Mem.Soc.Astr.Ital., **57**, 453.

Johnson, HL, 1964. Bol. Obs. Tonantzintla Tacubaya, **3**, 305.

Johnson, HL, Mitchell, RI, Iriarte, B & Wisniewski, WZ, 1966. Comm. Lunar Planet. Lab., 4, 99.

Laird, JB, Rupin, MP, Carney, BW, Latham, DW & Kurucz, RL, 1987. In: *'The Harlow-Shapley Symposium on Globular Cluster Systems in the Galaxy'*, p.517. Eds. Grindlay, JE & Davis Philip, AG. Kluwer Academic Publishers (Dordrecht).

Law, W-Y, 1981. A.&A., **102**, 178.

Lee, Y-W, 1991. Ap.J., **373**, L43.

Lee, Y-W, Demarque, P & Zinn, R, 1990. Ap.J., **350**, 155.

Liu, T & Janes, KA, 1990. Ap.J., **360**, 561.

Lloyd-Evans, T, 1974. M.N.R.A.S., **167**, 393.

Longmore, AJ, Dixon, RI & Guarnieri, MD, 1990. In: *'Astrophysics with Infra-red Arrays'*,

ed. Elston, R, p.121. Publications of the Astronomical Society of the Pacific (San Fransisco).

Longmore, AJ, Dixon, RI, Skillen, I, Jameson, RF & Fernley, JA, 1990. M.N.R.A.S., **247**, 684.

McClure, RD, 1984. Ap.J., **280**, L31.

McClure, RD, Hesser, WE, Stetson, PB & Stryker, LL, 1985. P.A.S.P., **97**, 665.

McClure, RD, Stetson, PB, Hesser, WE, Smith, GH, Harris, JE & VandenBerg, DA, 1987. In: *'The Harlow-Shapley Symposium on Globular Cluster Systems in the Galaxy'*, p.485. Eds. Grindlay, JE & Davis Philip, AG. Kluwer Academic Publishers (Dordrecht).

McClure, RD, VandenBerg, DA, Smith, GH, Fahlman, GG, Richer, HB, Hesser, JE, Harris, WE, Stetson, PB & Bell, RA, 1986. Ap.J., **307**, L49.

Madore, B, 1980. In: *'Globular Clusters'*, eds. Hanes, D & Madore, B, p.21. Cambridge University Press (Cambridge).

Manchester, RN, Lyne, AG, Robinson, C, D'Amico, N, Bailes, M & Lim, J, 1991. Nature, **352**, 2

Mateo, M, Harris, HC, Nemec, J & Olszewski, EW, 1990. A.J., **100**, 496.

Nemec, JM & Harris, HC, 1987. Ap.J., **316**, 172.

Neugebauer, G & Leighton, RB, 1969. *'Two-micron Sky Survey'*, NASA SP-3047 (IRC).

Mould, J, Stutman, D & McElroy, D, 1979. Ap.J., **228**, 423.

Noble, RG, Dickens, RJ, Buttress, J, Griffiths, WK & Penny, AJ, 1991. M.N.R.A.S., **250**, 314.

Norris, J, 1981. Ap.J., **248**, 177.

Norris, J, 1987. In: *'The Harlow-Shapley Symposium on Globular Cluster Systems in the Galaxy'*, p.93. Eds. Grindlay, JE & Davis Philip, AG. Kluwer Academic Publishers (Dordrecht).

Persson, SE & Frogel, JA, 1980. In: *'Globular Clusters'*, eds. Hanes, D & Madore, B, p.21. Cambridge University Press (Cambridge).

Peterson, CJ, 1986. P.A.S.P., **98**, 1258.

Peterson, RC, 1985. Ap.J., **294**, L35.

Phillips, JP, Martinez Roger, C, Sanchez Magro, C, Lazaro Vilchez, C, 1986. A.&A., **161**, 257.

Piotto, G, King, IR, Capaccioli, M, Ortolani, S & Djorgovski, S, 1990. Ap.J., **350**, 662.

Pryor, C, McClure, RD, Hesser, JE & Fletcher, JM, 1989. In: *'Proceedings of the Workshop on Dynamics of Dense Stellar Systems'*, p.175. Ed. Merritt, D, Cambridge University Press (Cambridge).

Renzini, A, 1986. Mem.Soc.Astr.Ital., **57**, 357.

Renzini, A & Fusi Pecci, F, 1988. Ann.Rev., **26**, 199.

Richer, HB & Fahlman, GG, 1988. Ap.J., **325**, 218.

Richer, HB, Fahlman, GG, Buonanno, R & Fusi Pecci, F, 1990. Ap.J., **359**, L11.

Richer, HB, Fahlman, GG, Buonanno, R, Fusi Pecci, F, Searle, L & Thompson, IB, 1991. Ap.J., **381**, 147.

Ridgeway, ST, Joyce, RR, White, NM & Wing, RF, 1980. Ap.J., **235**, 126.

Sandage, A, 1986. Ann.Rev.A.Ap., **24**, 421.

Sandage, A & Cacciari, C, 1990. Ap.J., **350**, 645.

Shapley, H, 1918. P.A.S.P., **30**, 42.

Smith, GH, 1987. P.A.S.P., **99**, 67.

Smith, GH, 1989. In: *'The Abundance Spread within Globular Clusters: Spectroscopy of Individual Stars.'*, IAU Commission 37, p.63. Eds. Cayrel de Strobel, G, Spite, M & Lloyd-Evans, T. Obs. de Paris-Meudon.

Smith, GH & McClure, RD, 1987. Ap.J., **316**, 206.

Spitzer, L, 1987. *'Dynamical Evolution of Globular Clusters'*, Princeton University Press (Princeton, NJ).

Stetson, PB & Harris, WE, 1988. A.J., **96**, 906.

Stetson, PB, VandenBerg, DA, Bolte, M, Hesser, JE & Smith, GH, 1989. A.J., **97**, 1360.

Straniero, O & Chieffi, A, 1991. Ap.J.Suppl., **76**, 525.

Suntzeff, NB & Smith, VV, 1991. Ap.J., **381**, 160.

Sweigart, AV, Renzini, A & Tornambé, A, 1987. Ap.J., **312**, 762.

van den Bergh, S, 1965. Journ. Roy. Astron. Soc. Canada, **59**, 151.

VandenBerg, DA & Bell, RA, 1985. Ap.J.Suppl., **58**, 561.

Weidemann, V, 1990. *Ann. Rev.*, **28**, 103.

Wheeler, JC, Sneden, C & Truran Jr., JW, 1989. *Ann. Rev.*, **27**, 279.

Zinn, R, 1980. Ap.J.Suppl., **42**, 19.

Zinn, R, 1985. Ap.J., **293**, 424.

Zinn, R, 1987. In *'The Harlow-Shapley Symposium on Globular Cluster Systems in the Galaxy'*, p.37. Eds. Grindlay, JE & Davis Philip, AG. Kluwer Academic Publishers (Dordrecht).

1. Infra-Red Array Photometry

Summary

The photometric accuracy and repeatability of an InSb array in the infrared camera IRCAM is investigated[1]. Measurements of standard stars are described; these were made using the United Kingdom Infrared 3.8m Telescope (UKIRT) over 5 nights in 1988 May, as part of an observational program on globular clusters. Observations were made at wavelengths of 1.25 μm (J) and 2.2 μm (K). The results show clearly that the camera-array combination is capable of a photometric accuracy of better then 1% when the standard star images obtained with short on-chip exposure (0.5 sec) are flat-fielded with long on-chip exposure (7-50 sec) sky flats. Linearity corrections determined in the laboratory were applied to the data and there was no evidence of residual non-linearity of $> 2\%$ over the magnitude range $6^{\rm m}.5$ - $13^{\rm m}.0$. The range of mean nightly zero-points at K in the 5 nights was $0^{\rm m}.03$, showing that both the site and the camera system were very stable over this period. At J the zero-points were less well determined and had twice this range in 3 nights.

1 Introduction

Astronomers with an interest in making observations at near-infrared wavelengths have now had access to infrared arrays on large telescopes for about five years. One of the most productive of these arrays is the 62 x 58 InSb array from SBRC (Santa Barbara Research Center); this array has 3596 pixels compared to the ~250,000 of optical CCDs. Nevertheless for the purposes of imaging this offers such a vast increase in capability over

[1] this chapter is almost identical to 'The Accuracy of Infra-red Photometry with Arrays' - Guarnieri, Dixon and Longmore (1991).

a single pixel that the field has clearly been revolutionized. Thus programs involving studies of galactic star formation regions and nearby galaxies, for example, had already produced spectacular images and interesting science by the time of the conference 'Infrared Astronomy With Arrays' (Wynn-Williams & Becklin 1987) held at the University of Hawaii, Hilo in March 1987. Understandably the results presented were largely qualitative, concentrating on sources found to have an unexpected or peculiar morphology. The potential of these arrays for accurate astronomical photometry was not demonstrated clearly at this time, although laboratory tests and models indicated that if the arrays were operated in strictly controlled conditions an excellent photometric performance could be achieved. However, it remained to be seen if this could be attained at the telescope.

In this study we have investigated the 'on telescope' photometric properties of an SBRC 62 x 58 InSb array + DRO (direct readout) multiplexer in the infrared camera IRCAM, mounted on UKIRT, Mauna Kea, Hawaii. The operation and performance of this camera is described by McLean (1987), McLean (1989) and McLean et al (1989). The latter reference uses recent astronomical observations to illustrate the versatility of operating modes now available with the camera and ancillary equipment.

Ideally a photometric study should be done using whole nights dedicated to the measurement of a range of standards at several near-infrared wavelengths to give independent determinations of zero-points, extinction corrections and colour equations. An attempt was made to do this. In two semesters after the initial commissioning of IRCAM in December 1986, the Panel for the Allocation of Telescope Time awarded a total of 6 nights to the project. Enough data were obtained to ascertain that photometry to better than 5% accuracy was possible, although inexplicably large errors (20%-100%) sometimes occurred. The array installed at that time was a development device, inferior cosmetically and with a higher dark current than later detectors. The project was further hampered by bad weather and by a hardware problem in the array temperature controller, and so the need to determine the photometric performance remained. In May 1988 a large number of observations of standard stars was obtained during a long-term program of infrared photometry of globular cluster stars. This is not as satisfactory as a dedicated study, but enough measurements were made over 5 nights in May 1988 for some useful statistics to be obtained on the photometric performance of IRCAM. As explained below the primary aims of this work did not include determination of colour transformation for the IRCAM

filters. Only J (1.25 μm) and K (2.2 μm) filters were used. In section 2 details of the standards measured and the properties of the filters used are discussed briefly. The raw data are presented in section 3 and data reduction techniques are discussed in section 4. The reduced data are presented in section 5 and the suitability of the instrument for very accurate IR photometry is addressed in section 6.

It should be borne in mind that this investigation concentrates on the measurement of bright stars as indicators of photometric performance (although some relatively faint standards were also observed, providing some information on linearity). Optimization of the signal-to-noise ratio on faint sources was not one of the goals. Consequently this topic is touched on only incidentally.

2 Filters and Standards

It is often assumed that the spectral response of a photometric system is defined solely by the filter. Of course this is not true. Other factors affecting the response include the transmission of lenses and windows, the reflectance of mirrors (primary, secondary and other external mirrors peculiar to an instrument), the reflectance of the dichroic mirror if used, the quantum efficiency of the detector and the transmission of the atmosphere. Mirrors (with the possible exception of a near-IR reflecting dichroic mirror near 1 μm) have a relatively flat spectral characteristic and the other factors (detector response, windows and lenses) are often similar from one system to another (although different anti-reflection (AR) coatings on any of the last three items can seriously compromise this statement). Not all IR photometers employ a dichroic mirror and atmospheric transmission can be very site-dependent at some wavelengths. It appears from the transformations given by Bessell & Brett (1988, hereinafter BB) that at 2.2 μm (K) the differences between the various systems (South African Astronomical Observatory, European Southern Observatory, Mount Stromolo Observatory, Anglo-Australian Observatory (AAO), California Institute of Technology (CIT), Johnson) are very small, always less than 2% and usually zero within measurement errors. The J filter systems (usually referred to as centred at 1.25 μm) are much less uniform, as seen from the range of effective wavelength (1.198 - 1.246 μm) found by BB. The transmission through the J atmospheric windows is worse than that through the H and K bands. Variability of OH airglow in the J window could also contribute to

photometric errors in the J band. The UKIRT J and K spectral transmission profiles are given in figure 1.

In this paper there are insufficient data to allow more than a cursory investigation of colour effects, and so only a brief description is given here of the photometric system. IRCAM is mounted at UKIRT's Cassegrain focus, with IR light reflected into the cryostat via a gold-coated dichroic mirror. After two further reflections by gold-coated optical surfaces the IR light enters the cryostat through a CaF_2 window and is imaged with an AR-coated ZnSe lens onto the AR-coated InSb detector. Spectral reflectances/transmissions/responses of these components are given in McCaughrean (1988). The JHK filters are a standard OCLI (Optical Coating Laboratory Inc.) set identical to those of the AAO system.

A selection of bright near-IR standards from the (unpublished) UKIRT standards list was measured. Most of these are stars taken from the list of Elias et al. (1982) and converted empirically to the natural UKIRT system based on measurements using the photometer UKT9 (an InSb system with two ZnSe lenses, CaF_2 window and JHK filters, with an additional blocking filter of OW1 to remove a long-wavelength leak for the J filter, as in the AAO system). At 2.2 μm no systemic difference was found in the unpublished UKIRT study between the magnitudes of Elias and the natural UKIRT system. This is consistent with the findings of BB with respect to the AAO and CIT systems. Therefore through the K filters the IRCAM, AAO and the UKIRT systems should be very similar. IRCAM lacked a long-wavelength blocking filter at J when these observations were made which could lead to a non-negligible colour term in (J-K).

Three additional fainter standards were observed to check for non-linearity effects; magnitudes for these were from very preliminary results by Zuckerman & Becklin (private communication, 1989) based on measurements using the Infra-Red Telescope Facility (IRTF) and UKIRT single-channel photometer systems. Table 1 lists all the standard stars' names and the initially adopted magnitudes.

3 The Data-Set

The observations were made on the nights of 1988 May 20 - 24 UT on UKIRT using IRCAM in its $0.6\widehat{''}$/pixel mode. As they were made to calibrate measurements of stars in

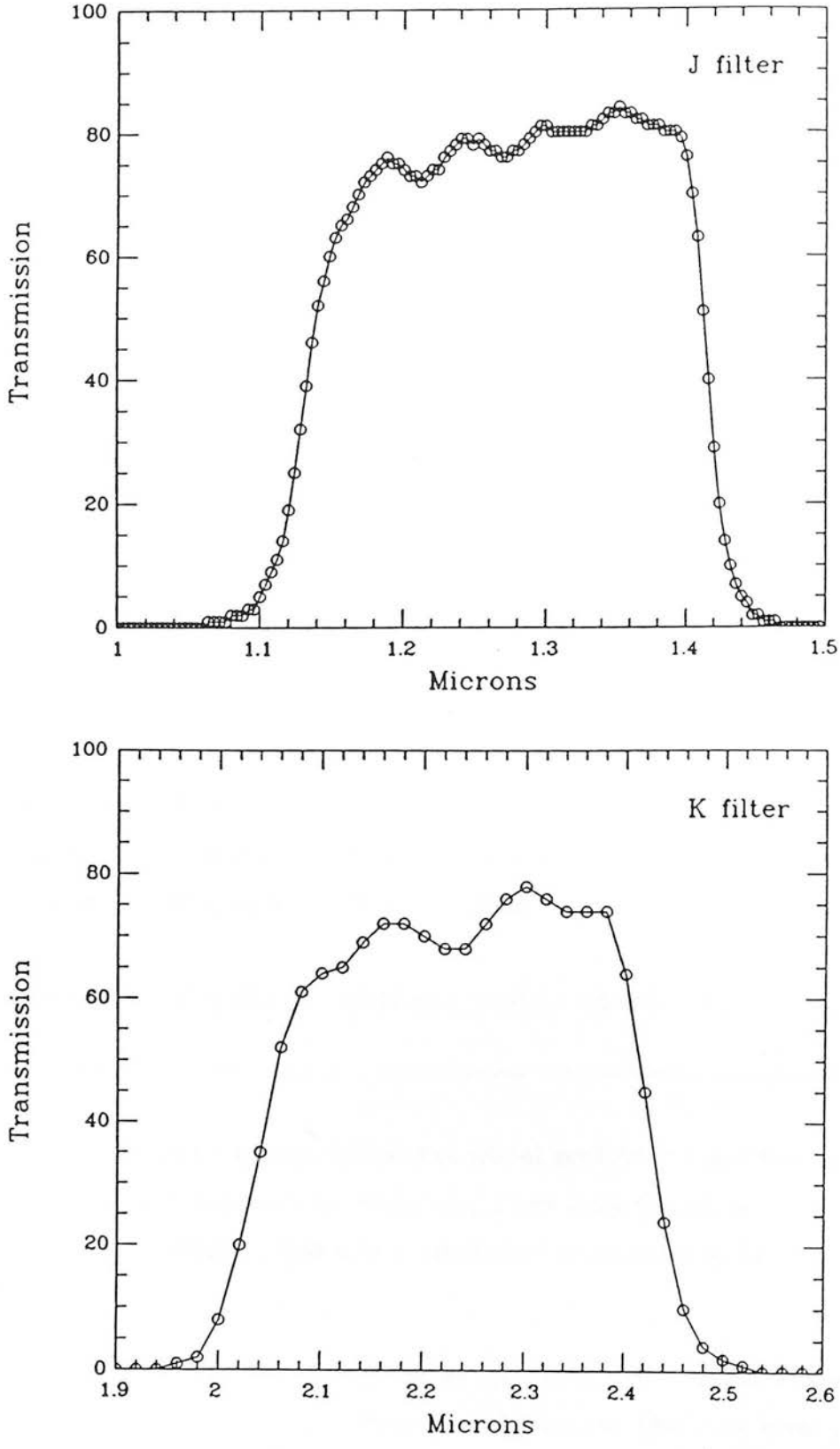

Figure 1: J and K spectral transmission profiles.

Table 1: Standard Stars

Star	Right Ascension	Declination (1950)	J mag.	K mag.	Source of mags.	Errors[a] J and K
GD140	11 34 22.6	30 04 35	12.95	13.15	Z	0.03
HD105601	12 06 56.1	38 54 39	6.819	6.685	E	0.015
M3⋆206	13 39 23	28 42 27	7.82	7.07	L	0.015
GD153	12 54 35.1	22 18 08	14.02	14.28	Z[b]	0.03
HD129653	14 40 38.2	36 58 07	6.984	6.920	E	0.010
HD129655	14 41 11.0	-02 17 38	6.824	6.690	E	0.007
SR3	16 23 07.7	-24 27 26	7.788	6.520	E	0.015
HD161903	17 45 43.3	-01 47 34	7.170	7.020	U	0.007
GL748	19 09 38.0	02 48 36	7.095	6.305	U	0.015
EG141	20 39 41.9	-20 15 21	12.82	12.99	Z[b]	0.03
HD203856	21 21 37.1	39 48 12	6.925	6.860	E	0.010

[a] Errors for GD140, GD153 and EG141 are 0.06 at J and 0.03 at K.

[b] The J magnitude for EG141 and J and K for GD153 have been slightly weighted with new single channel photometry by Longmore & Dixon.

Key to sources: E - Elias et al (1982), U - UKIRT standards,
Z - Zuckerman & Becklin (Private comm., 1989),
L - Longmore et al (in prep.).

globular clusters, large fractions of each night were spent looking at the same cluster. The calibration strategy was to make frequent measurements of a local standard close to the cluster and compare this against at least two other standards over the period of time for which the cluster was observed. If a global reduction of a whole night's data is intended, this is clearly not as satisfactory as having pairs of blue and red stars measured at high and low air mass at regular intervals throughout the night. However at infrared wavelengths the set of standards of appropriate colour and with uniform high accuracy is small and makes such an approach difficult. Experience with the single channel systems has shown that the adopted approach results in photometry repeatable to $\leq 2\%$, consistent with uncertainties in magnitudes and colour equations for the IR standards used.

The bright standards all lie in the range $6^{m}.5$ - $8^{m}.0$ at J and K and can be measured with 0.5 sec on-chip integration without saturation. The data collection procedure with IRCAM is to co-add a number of frames in the Array Data Processor (ADP) before transferring the summed frame to disk. Therefore the information on the individual frames is lost. Typically 50 0.5 sec frames are co-added for a single standard measurement (exposure timings are found to be accurate to $\pm$ 1 msec.). Because we were ourselves uncertain of the photometric properties of the array, each filter measurement consisted of two observations, one at each of two positions on the array. The two positions were usually offset by $5\hat{''}$ N,$5\hat{''}$ E and $5\hat{''}$ S,$5\hat{''}$ W from the centre of the array, although other offsets were tried as additional consistency checks (e.g. $7\hat{''}$ N,$6\hat{''}$ W with $7\hat{''}$ S,$6\hat{''}$ E). Table 2 lists the number of pairs of observations of each star at J and K for each of the 5 nights of observation. The colour range of the standards observed (-0.3<(J-K)<1.3) encompassed the colour range of the vast majority of stars we expected to find in the globular clusters.

The problems associated with flat-fielding bright standards are discussed in section 4. Sky frames with long on-chip exposures (7 sec on-chip x 15 co-adds up to 50 sec x 4 co-adds) were used to flat-field the standard frames (one of the aims of this investigation was to determine whether or not this is a viable method of flat-fielding short exposures). These were either single images of blank sky or the result of median filtering a series of 'jittered' frames. (In our case, jittering consists of taking a set of frames with offsets of 10-30% of the frame size about the central frame. This procedure is used in regions where faint stars contaminate the sky area to such an extent that median filtering is necessary to obtain a flat-field). Bias frames of 129.6 millisec on-chip exposure and 100 co-adds were taken at

Table 2: Numbers of Observations of Standards

	# of pairs of observations (# of different standards)				
Filter	5/20/89	5/21/89	5/22/89	5/23/89	5/24/89
J	0 (0)	0 (0)	7 (3)	17 (6)	8 (5)
K	10 (7)	18 (7)	15 (7)	7 (4)	13 (8)

the beginning, middle and end of the night. Similarly dark frames were taken covering the range of on-chip exposures.

4 Data Reduction

The requirements for reducing IR array data are similar to those which are well-established for the reduction of optical CCD data. Both procedures involve subtracting bias and dark current frames and ratioing with an appropriate flat-field frame, as well as removing or allowing for bad pixels where possible. Important characteristics of a flat-field frame are that the illuminating source has a very similar colour to that dominating the counts in the object frame and that the intensity of the flat-field source is similar to the intensity of the source being flat-fielded. At near IR wavelengths the brightness of the night-sky, which is such a handicap in limiting the on-chip integration times of broad-band measurements, becomes an advantage in flat-fielding. Blank-sky frames are excellent as flat-fields because the dominant source of photons in any deep exposure is also the sky. As exposures are also short compared to deep optical exposures, flat-fields can be taken frequently. This has led to flat-field noise being reduced to $<0.01\%$ of the sky (e.g. Cowie et al 1988). However for bright standards there are a lot more photons from the source than from the sky and it is possible that significant non-linearities could be introduced in the flat-field procedure. (For a detailed explanation of these effects, see McCaughrean 1988). With

the very short on-chip exposures needed to measure bright standards it is not possible to record a sufficient number of photons or electrons to define an accurate flat-field. Thus the question alluded to at the end of section 3 arises - are long on-chip exposures suitable for flat-fielding very short exposures at the same wavelength?

To answer this, all the standard observations have been reduced here using a flat-field or median-filtered combinations of flat-fields taken during the same night. 4 co-adds x 50 sec (7 x 35) on-chip exposures were used for the K (J) observations respectively. In addition some frames were reduced using flat-fields constructed from co-adds of 10 sec on-chip exposures (K) or 7 sec on-chip exposures (J).

At the time of the 1988 May observations a new SBRC detector chip had just been installed in IRCAM. It was pressed into use before all the operating parameters had been fully optimised and was found to be more non-linear than expected[2]. A linearity correction was therefore determined by careful laboratory measurements and has been applied to all the May observations. It was of the form

$$x' = x(1 - 2.308 * 10^{-9}x + 8.689 * 10^{-11}x^2 + 2.281 * 10^{-14}x^3 - 1.687 * 10^{-18}x^4 + 4.287 * 10^{-23}x^5)$$

where x is the count (in photo-electrons/24) after subtraction of a bias frame and x' is the linearity-corrected count. Fortunately this correction appeared to be constant with time and the same for each pixel within experimental error. Therefore the present study automatically tests the success of the linearity correction procedure as part of the assessment of the overall photometric properties.

The full data-reduction procedure was as follows.

1. Normalise all frames to 1 co-add
2. Subtract a bias frame from all frames
3. Apply the appropriate linearity correction to all frames.
4. Prepare flat-field frames from the long on-chip sky exposures, usually by median-filtering 3-6 frames, including a normalization step. On the rare occasions when only 3 sky frames were applicable this approach still provides better bad pixel discrimination than averaging.

[2] A non-linearity of up to 4% is expected in this type of DRO detector (McLean 1989); the larger effect noted here was traced to an incorrect value of a voltage (V_{retruc}) at the operating temperature of 35K.

5. Subtract a dark frame of the relevant exposure time from the flat-field and standard frames.

6. Ratio the standards' frames with selected flat-field frames.

7. Interpolate over bad pixel positions.

The candidate stars' magnitudes were measured on the fully reduced frames using the recently released Starlink package PHOTOM (v1.0 - this package is described in the Starlink User Note SUN/45.2). An aperture is defined (in pixels) in which the measurement is to be made. Two further apertures are then defined in terms of the size of the first one. These additional apertures are used to determine a sky level as the mode of the pixels in the area. We adopted an aperture size of 5 pixels radius ($6\widehat{''}$ diameter) and concentric apertures 1.3 and 2.1 times this size to determine sky levels. These were chosen on the basis of brief trial and error tests involving the comparison of ratios of magnitudes produced using different aperture sizes from 4 to 8 arcsec., to give a good S/N ratio even for the fainter stars while leaving the photometry insensitive to small changes in the seeing. The same parameters were used for every measurement. No significant ghosts were seen in the images and no attempt was made to correct for them. The brightest ghosts in previous data-sets have been observed to be diagonally opposite the parent star image, across the centre of the frame. This means that they will not influence the sky measured in an annulus around the star. Similarly no corrections were made for seeing profile variations, which were judged to be small on the nights concerned. The value of the sky flux was found to vary slowly over the course of a night, changing by up to 10% at K on an average night.

Raw zero-points were calculated from each individual measurement, and then each pair of measurements (see section 3) was averaged. Except for the section on analytical comparison between components of each pair, all references to an 'observation' from now on apply to this average.

5 Results

The data set was very inhomogeneous. On each night it comprised multiple measurements of a few stars and one or two observations of a few others. There were not enough

measurements on a single night to allow automatic solutions for linearity, extinction, colour terms and the variation of zero-point with time. An additional complication was introduced because not all the standards' magnitudes were known to the same level of accuracy. Therefore the results were reduced by hand. Whenever possible extinction coefficients were determined from the data, but if inconsistent numbers were obtained a value was adopted which was consistent with the mean values of the site ($0^{m}.11$/air-mass at J, $0^{m}.06$/air-mass at K). There was no strong evidence for a systematic change of zero-point with time.

All the observations were corrected to an extinction of 1.0 air-mass and the mean zero-point for the night was calculated (an air-mass of 1.0 was used, rather than 0.0, since this involves less extrapolation and no global solutions for air-mass correction were obtained because of the observing procedure described above). The residuals from this mean were found for each observation and the mean residual for every star was calculated, for the whole night and also for the complete set of observations. We have selected the observations from the night of 1988 May 22 to illustrate the results obtained. These are given in tables 3 (K) and 4 (J). The standard deviations of the zero-points and the standard error of the mean zero-point are given at the bottom of each table. Examination of the residuals over the full data set showed that SR3 appeared consistently too faint by $0^{m}.015$ at 2.2μm compared with the value in table 1. The adopted magnitudes were corrected by these amounts and the mean zero points and residuals re-calculated. The corrected values appear in the final column of table 3. The corrections are discussed further in section 6. At 1.25μm there was an indication that SR3 was too bright by $\sim 0^{m}.025$ compared with table 1, but not enough other standards were measured for this to be established unambiguously.

A summary of the final mean residuals for each night appears in table 5. The mean zero-points at the bottom of table 5 have been calculated excluding the fainter stars, GD140, GD153 and EG141, which have large individual errors.

Table 3: K Observations for May 22nd 1988

Star	Air mass	Raw Zp	Mean Zp	Extinction corr. Zp	Final Zp
HD105601	1.10	-20.086	-20.085	-20.090	-20.090
HD105601	1.10	-20.098			
HD105601	1.10	-20.071			
GD140	1.02	-20.129	-20.114	-20.115	-20.115
GD140	1.02	-20.100			
GD153	1.02	-20.187	-20.162	-20.163	-20.163
GD153	1.02	-20.138			
M3⋆206	1.14	-20.130	-20.129	-20.136	-20.136
M3⋆206	1.14	-20.129			
M3⋆206	1.05	-20.110	-20.117	-20.120	-20.120
M3⋆206	1.05	-20.125			
M3⋆206	1.02	-20.115	-20.114	-20.115	-20.115
M3⋆206	1.02	-20.114			
M3⋆206	1.01	-20.129	-20.131	-20.132	-20.132
M3⋆206	1.01	-20.134			
M3⋆206	1.07	-20.114	-20.117	-20.121	-20.121
M3⋆206	1.07	-20.120			
GD140	1.54	-20.106	-20.090	-20.117	-20.117
GD140	1.57	-20.075			
GD153	1.21	-20.186	-20.162	-20.173	-20.173
GD153	1.23	-20.139			
SR3	1.44	-20.050	-20.064	-20.086	-20.101
SR3	1.44	-20.079			
SR3	1.42	-20.090	-20.084	-20.105	-20.120
SR3	1.42	-20.078			
SR3	1.95	-20.069	-20.058	-20.106	-20.121
SR3	1.96	-20.048			
EG141	1.38	-20.143	-20.147	-20.166	-20.166
EG141	1.37	-20.151			
GL748	1.05	-20.105	-20.111	-20.114	-20.114
GL748	1.05	-20.118			
	Mean	-20.112	-20.112	-20.124	-20.127
	Std.dev.	0.033	0.032	0.026	0.024
	Std.err.	0.006	0.008	0.007	0.004

Table 4: J Observations for 1988 May 22nd

Star	Air mass	Raw Zpt	Mean Zpt	Extinction corr.Zpt
SR3	1.42	-21.170	-21.170	-21.215
SR3	1.42	-21.170		
SR3	1.66	-21.118	-21.121	-21.191
SR3	1.66	-21.124		
SR3	1.94	-21.116	-21.114	-21.214
SR3	1.94	-21.112		
EG141	1.40	-21.229	-21.229	-21.271
EG141	1.40	-21.219		
EG141	1.39	-21.238		
GL748	1.06	-21.162	-21.168	-21.174
GL748	1.06	-21.175		
GL748	1.16	-21.152	-21.149	-21.166
GL748	1.16	-21.153		
GL748	1.16	-21.143		
	Mean	-21.163	-21.159	-21.205
	Std.dev.	0.041	0.042	0.038
	Std.err.	0.010	0.017	0.016

Table 5: Residuals for all nights

Star	Date 5/20	5/21	5/22	5/23	5/24	Mean Res.
GD140	-0.027		-0.005		-0.051	-0.028
HD105601	0.014	0.010	0.021		-0.006	0.010
				(0.051)		(0.051)
M3⋆206[a]	-0.040	0.008	-0.014		0.003	-0.011
				(-0.016)	(0.000)	(-0.008)
GD153	0.002	0.086	0.048		0.051	0.037
				(0.009)	(0.010)	(0.010)
HD129653					0.005	0.005
SR3	0.007	0.003	-0.003	0.000	0.000	0.001
			(-0.018)	(-0.032)	(-0.028)	(-0.026)
HD161903		-0.022				-0.022
GL748		0.000	-0.003	-0.014	-0.002	0.005
			(0.019)	(0.001)	(0.028)	(0.016)
EG141	-0.035	0.038	-0.055	-0.048	-0.043	-0.041
			(-0.082)	(-0.126)		(-0.104)
HD203856	-0.002			0.014		0.006
Mn Zpt[b]						
J	—	—	-21.189	-21.154	-21.215	
K	-20.102	-20.123	-20.111	-20.093	-20.105	

NB: Bracketted numbers are for J.

[a]The pair of observations of M3⋆206 on the 20/5 were significantly different so the mean was used at half weight in calculating the nightly zero-point and the residuals.

[b]Mean zero-points exclude GD140, GD153 and EG141.

6 Discussion

6.1 Flat Fields

The count variation as a fraction of the signal was examined in two areas on each of 5 flat fields. It was found to be very consistent for each area, independent of the on-chip integration time, number of co-adds or the number of frames involved in the median filtering exercise. Both areas were centred on the middle of the 62 x 58 array; the first was a 56 x 52 pixel box, the second 28 x 26. In the larger area the standard deviation of a pixel was 6.55 $\pm$ 0.15% of the signal while in the smaller area this figure was 4.4 $\pm$ 0.1%. These numbers are due to the intrinsic shape of the flat-field, coming from the large scale variations due to varying detector element sensitivities across the chip. In the unlikely situation that the shape of the flat-field changes significantly with exposure, errors of up to about the size of the sensitivity variations, i.e. $\sim$6%, could be introduced in the derived photometry. However, in the short-exposure, standard star frames the signal from the sky is very small, so that the intrinsic shape of the flat-field is lost in the read-out noise and in noise introduced by small changes in the dark and bias counts. (We have found that variations of 10% can occur in the bias count during the course of the night, with the count generally being higher at the end of the night. These fluctuations introduce a zero point shift in the dark-subtracted image which also give the appearance of enhanced noise in the short exposure sky pixels after flat-fielding). Thus the pixel-to-pixel noise actually measured in the 'sky' for short exposures was 13.5% of the sky signal. It must be emphasized that this does not reflect on the photometric accuracy of bright sources within such an image, since these contain sufficient counts to flat-field correctly.

6.2 The Photometry

6.2.1 Expected Performance

What photometric performance is to be expected from IRCAM? In his thesis McCaughrean (1988) concludes 'The flat fielding process used seems highly satisfactory, reducing all systematic errors well below noise levels from read noise and shot noise'. However this statement applies to frames ratioed with flat-fields of the same on-chip exposure; it does not necessarily follow that the same success will be achieved on bright standards. The

well size of the SBRC InSb + DRO arrays is $\sim 10^6$ electrons. For integrations in which the sky is allowed to half fill the wells, the Poisson noise expected is ~700 electrons. The read-out noise is ~450 electrons. Expressed as a fraction of the 'signal' such a measurement should allow flat fielding to 0.17% with a single frame if the system is stable. After co-adding and median filtering the error introduced by shot noise in the flat-field should be <0.1% . If the wells are only 10% filled, this limit becomes <0.2% .

McCaughrean investigated the effect of the ~90% filling factor of the InSb array on photometry performed with $0\overset{''}{.}6$ pixels. In $1\overset{''}{}$ seeing the maximum error introduced (the difference between a star centred on a pixel and centred at the corners of 4 pixels) is <0.1% . Combining these uncertainties, we conclude that, for the type of observation we have made, IRCAM should be capable intrinsically of a photometric performance of better than 0.3% accuracy.

6.2.2 Achieved Photometric Performance

This can be assessed by examining the residuals and their deviations in tables 3-5. In table 3 the extinction-corrected zero-point (for the paired observations) has a standard deviation (e) of $0\overset{m}{.}026$ with a range of $0\overset{m}{.}083$ before any allowance is made for errors (or colour terms) in the standards. If the correction of section 5 is applied to SR3, the standard deviation becomes $0\overset{m}{.}024$. In table 4, the corresponding figures are e = $0\overset{m}{.}04$ with a $0\overset{m}{.}105$ range. Figure 2 compares the raw zero-points for one night's data, with the final zero-points after extinction correction and the SR3 adjustment. Such figures are typical of all the nights in May. The mean absolute value of the residuals and the range of the nightly zero-points at 2.2 μm are $0\overset{m}{.}038$ and $0\overset{m}{.}03$ respectively, and at 1.25 μm $0\overset{m}{.}061$ and $0\overset{m}{.}06$ (table 5). This is about the error one would expect from the limited accuracy of the standards alone, without taking into account any noise introduced by seeing and atmospheric transmission changes. Most of these observations comprise pairs of measurements at two positions on the array. We have calculated the mean difference between all the frame pairs taken at positions $5\overset{''}{}$ N,$5\overset{''}{}$ E and $5\overset{''}{}$ S,$5\overset{''}{}$ W (or within $2\overset{''}{}$ of these positions) to look for systematic errors. A difference of 1% $\pm$ 0.3 was found. Comparisons between (the small number of) other areas on the array which were also used showed similar or smaller differences.

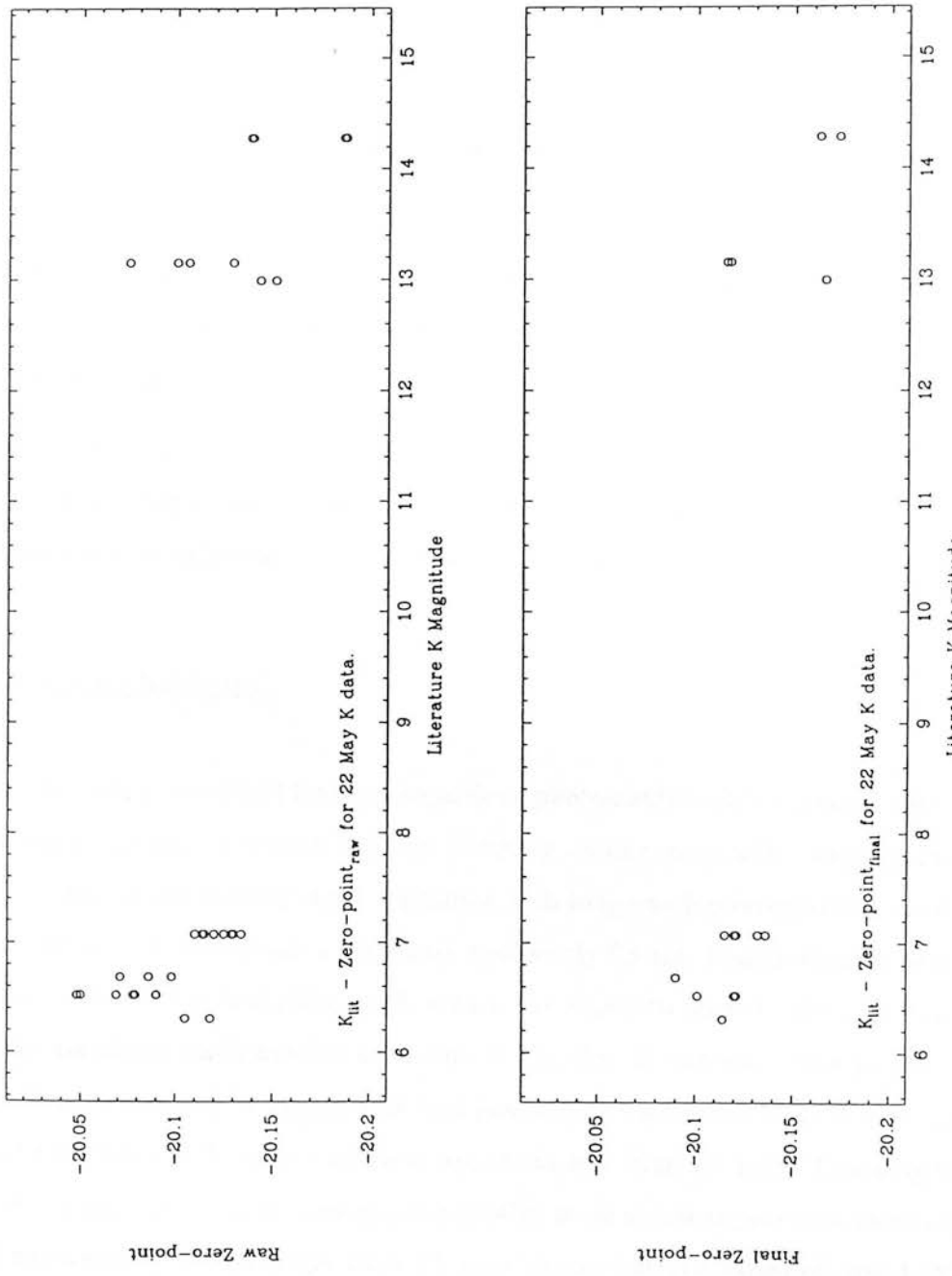

Figure 2: The upper panel is standard literature magnitude vs. raw zero-point for May 22 K data. The lower panel is the standard literature magnitude vs. final zero-point.

The final residuals for the three faint stars GD153, GD140 and EG141 are consistent with the lower precision of the present measurements and the larger uncertainty of the standard magnitudes. These are also the three bluest stars in the sample, allowing additional errors to be introduced if the colour term in (J-K) is significant.

An outstanding question from the early tests was the incidence of frames on which the photometry had inexplicably large errors. In the current data set only one frame was omitted from the analysis, on the basis of a photometric residual more than 5 sigma from the expected value. Close examination of this image showed that a 'glitch' had occurred in the telescope tracking during the exposure, so that a faint extension to the image of $\sim 10''$ in an EW direction was visible.

Brief tests using flat fields taken on different nights, for example May 22nd star frames flat-fielded with May 21st sky frames, showed zero-point changes of less than 1% for the bright stars and up to 7% for the fainter stars.

Finally the effects of ratioing different flat-fields (including frames with similar and with different on-chip integration times) with the standard images was investigated. The mean of the absolute difference was $0^{m}.006$ for both J and K filters, with no systematic effect.

7 Conclusions

The techniques described here are capable of photometry which is limited almost entirely by the observing conditions and the accuracy of the standards. Any systematic error introduced by flat-fielding short exposures with long on-chip integrations are at or below the 1% level. However such a procedure works only for the measurement of bright sources as variations of the dark/bias levels reduce the signal-to-noise in the final data, because of the relatively small number of counts in the sky. If necessary this problem could be significantly reduced by taking dark and bias frames on a much more frequent basis. The effects of ghosts and seeing variations are at the less than 1% level. Linearity corrections based on laboratory measurements and applied to all pixels appear to remove successfully all non-linearity effects larger than 2% over the magnitude range observed (K = $6^{m}.5$ - $13^{m}.0$).

References

Bessell,M.S. & Brett,J.M., 1988. P.A.S.P., **100**, 1134. (BB)

Cowie,L.L., Lilly,S.J., Gardner,J. & McLean,I.S.,1988. Ap.J., **332**, L29.

Elias,J.H., Frogel,J.A.,Matthews,K. & Neugebauer,G., 1982. A.J., **87**, 1029.

Guarnieri, MD, Dixon, RI & Longmore, AJ, 1991. P.A.S.P., **103**, 675.

McCaughrean,M.J., 1988. 'The Astronomical Applications of Infrared Array Detectors', Ph.D. thesis, University of Edinburgh.

McLean,I.S., 1987. In 'Infrared Astronomy with Arrays', eds. Wynn-Williams,C.G. & Becklin,E.E., University of Hawaii, p.180.

McLean,I.S., 1989. In the proceedings of 'ESO Conference on Very Large Telescopes and their Instrumentation', Volume II. Ed. Ulrich,M.H., p.955.

McLean,I.S., Casali, M.M., Aspin, C.A., & Wright, G.S., 1989. In Proceedings of 3rd NASA Ames Infrared Detectors Workshop, ed. C. McCreight, p.183.

Wynn-Williams,C.G. & Becklin,E.E. (Eds.), 1987. Proceedings of the workshop on 'Infrared Astronomy with Arrays', University of Hawaii.

2. Observations and Data Reduction

1 Introduction

Performing imaging observations in a globular cluster field requires a compromise to be made between signal to noise and areal coverage, particularly when using a detector with as small a field as IRCAM. Observing a large area will allow a large number of stars to be measured, so sampling the less common stars in the cluster such as the RGB stars. However, in a given allocation of telescope time observing a small area will allow the fainter objects to be measured, and of course improve the accuracy of the other measurements. The position of the observed field is also important:

- too close to the centre of the cluster and the stars will be so crowded that they will be measurable only at low precision,
- too far out and more field stars than members will be found, and/or each frame will contain few stars, thus wasting the detector,
- too near bright stars means ghosts and saturated images will degrade the photometric measurements.

This thesis discusses observations of two clusters and the approach adopted was to observe both large area strips and small area 'deep' frames. The large areas consist of three strips of 11 frames each. The strips run EW with about 50% overlap between adjacent frames and the three strips overlap by about 10% vertically so that the final mosaics are about 300 x 150 pixels or $180''$ x $90''$. The deep observations are made up of ten frames each taken in a 'jitter' pattern, that is, with frames at offsets of +5, 0 and -5$''$ in each axis from a central frame. The first and last frames are taken at the central position. This procedure builds up high signal-to-noise in the central region whilst moving the images around the image plane to avoid dead array pixels always falling in the same place within an image. These two observing patterns are shown schematically in figure 1.

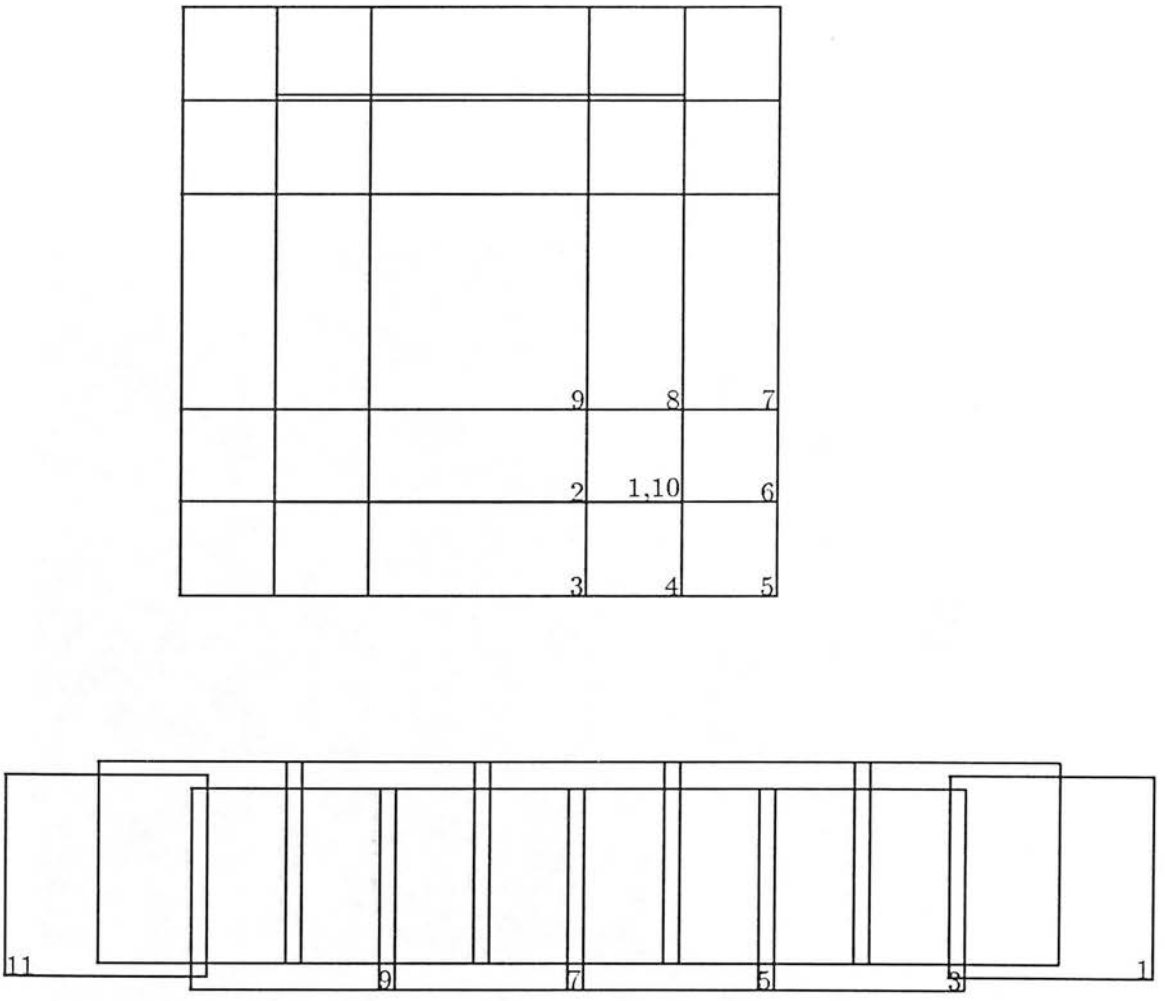

Figure 1: 'Jitter' pattern for deep frame observations and pattern for single strip. Numbers are sequential frame numbers and are placed in the bottom right corner of the frames they refer to. Alternate frames in the strip have been displaced vertically to show the pattern more clearly.

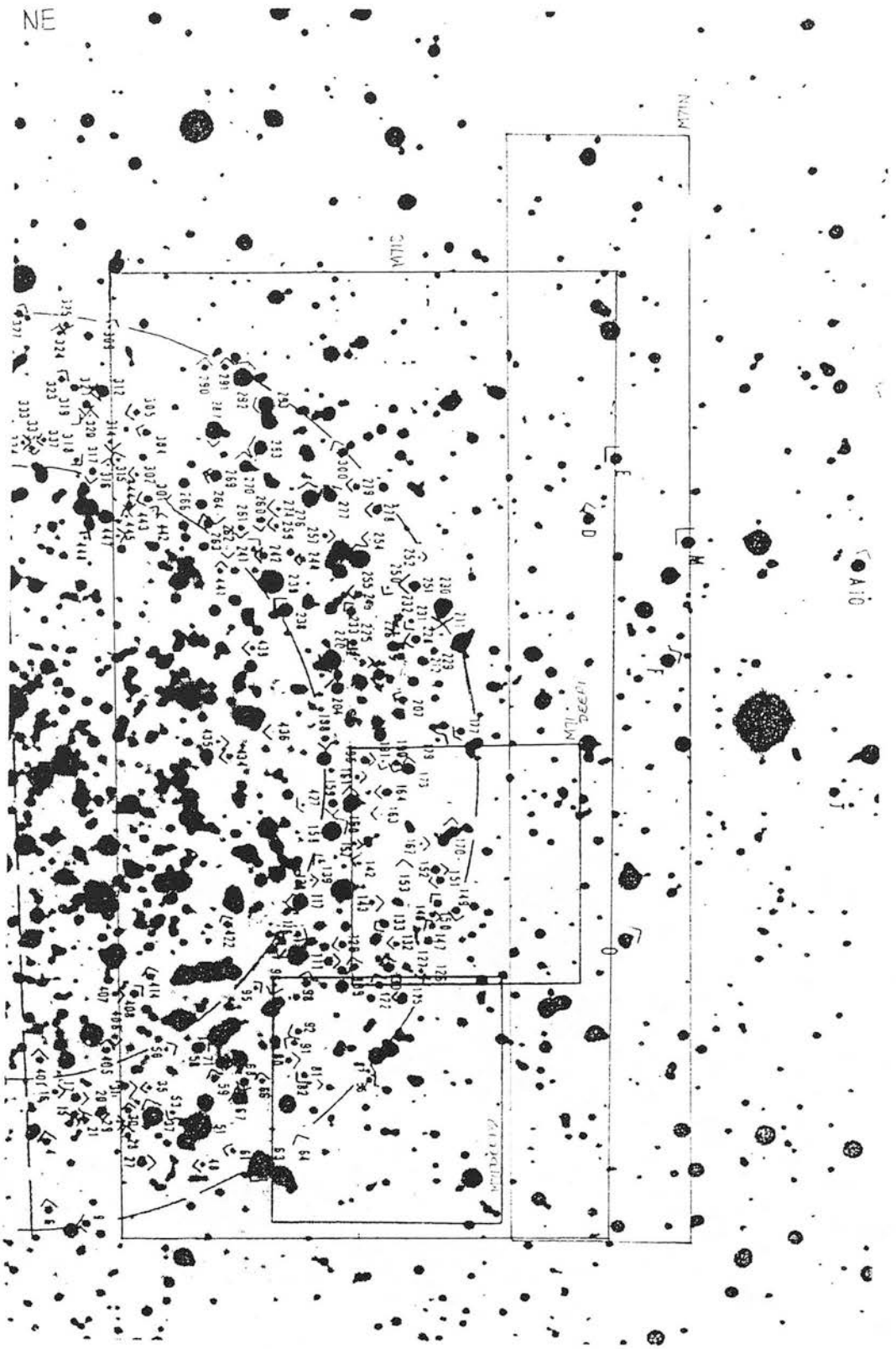

Figure 2: (a) Map of M71 (after Arp and Hartwick, 1971). The present areas of observation are labelled with the names used in table 1.

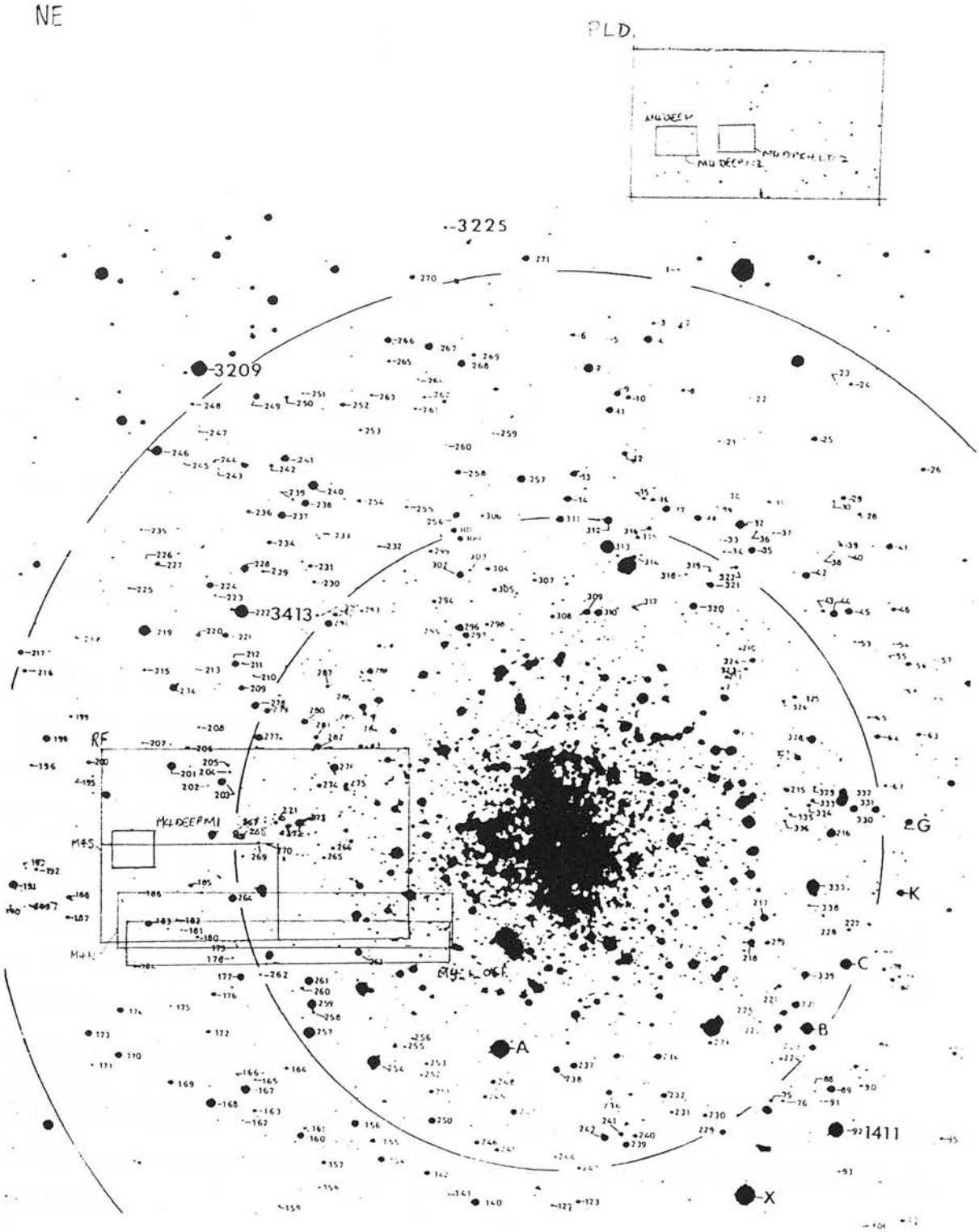

Figure 2: (b) Map of M4 (after Alcaino and Liller, 1984). The Richer and Fahlman (1984) and Penny, Lubenow and Dickens (1987) areas are shown.

Areas were chosen to be within fields for which recent CCD photometry exists so that the IR photometry could be matched up, primarily to allow long baseline indices such as (V-K) to be calculated. Within the CCD areas the IRCAM area was chosen to be clear of very bright stars and not too crowded. The deep frames were additionally chosen to be centred on groups of faint stars to maximise the number of stars observed at good signal-to-noise. Figure 2(a) and 2(b) show the areas chosen in the two clusters as well as the regions covered by optical work.

Clearly the brightest stars will be saturated if exposures are optimised for the fainter sources. Fortunately IR and optical photometry exists for many of the brightest stars in both M71 and M4, so the present work can concentrate on the fainter stars.

This chapter describes the reduction and analysis of the observed frames, including the use of the profile fitting package DAOPHOT, and discusses the zero-point calibration of these data and the associated optical data.

2 Observations

The infra-red camera IRCAM was used on the 3.8m UK Infra-Red Telescope (UKIRT) during the summer of 1988 to take frames of several regions of M71 and M4 at both J ($1.2\,\mu$m) and K ($2.2\,\mu$m). The camera/filter/telescope system has been discussed in the previous chapter (see that discussion for more detailed references).

Three sets of strips were taken which combine to produce a 33 frame mosaic of the central southern half of M71 and in M4 a 33 frame mosaic was located at $\sim 5\widehat{'}$ out to the East of the cluster centre. 'Jitter' observations were made in two areas in M71 and three areas in M4 to provided deep exposures, achieving high signal-to-noise ratios for stars on the main sequences of both clusters.

Tables 1 and 2 list all the K-band observations made in M71 and M4 respectively. Also listed are any pertinent comments from the observing log, such as weather or instrument conditions.

The areas listed in the tables correspond to those shown in figure 2 and can be summarized as follows:

Table 1: **IRCAM M71 images from 1988 May and July**

Sequence name	Container file	frames	exposure	comments
M71N1	20MAY88_2	39-45	2x50 strong wind	
sky		46,47		
sky	21MAY88_2	57-59	3x35	
M71S1		60-70		
sky		71-73		
M71S2		76-86		
sky		87-89		
M71S3	23MAY88_2	87-97	3x35	
M71S1		109-119	8x7	
M71S2		120-130		auto-guider problem at end
sky		83-86,101-104	3x35	
sky		105-108,137-140	8x7	
M71S3	24MAY88_1	110-120	8x7	
sky		106-109,121-122		
M71DEEPM1	07JUL88_1	95-104	4x50	
sky		105-107		wind
M71DEEPM1		125-134		
sky		135-137		54 & 57 no good
M71DEEPM2	10JUL88_1	52-63		poor seeing
sky		64-67		
M71DEEPM2	11JUL88_1	53-62		thin cloud about

Table 2: **IRCAM M4 images from 1988 May and July**

Sequence name	Container file	frames	exposure	comments
M4_1_OFF	20MAY88_1	56-67	2x50	#57 no good
sky		54,55	4x50	
sky		68-72	2x50	stars !
M4N2	20MAY88_2	4-13	2x50	
M4N3		18-28		
sky		2,3,14,15,29-31		
M4S1	21MAY88_1	98-108	2x50	light gusty wind
M4S2		114-124		
M4S5		133-143		
sky		92	10x10	
sky		93-95,97,109-111,125-127,144	2x50	
M4S1	21MAY88_2	5-15	2x50	
M4S2		21-31		
M4S5		37-47		
sky		1,2,16-18,32-34,48,49,51		
M4S1	22MAY88_1	130-140	5x10	
M4S2		141-151		
M4S5		152-162		
M4S5 #11		163	1x50	
sky		125-128,165-168	10x10	
sky		164	1x50	
M4DEEP	24MAY88_1	84-93	4x50	
M4DEEPM1	07JUL88_1	17-26	4x50	
M4DEEPM1		61-70		
sky		27-29		
M4DEEPM2	08JUL88_1	10-20	4x50	gusty wind
M4DPFIELD2		23-34		seeing variable
M4DPFIELD2		37-46		

- M71N1: a test strip to the south of the main strip.
- M71S1,2,3: primary strips taken for large mosaic at deep and shallow exposures. These strips make up the M71DK area and this area lies within the Richer & Fahlman (1988, RF88) optical CCD study area.
- M71DEEPM1,2 jittered frames within large M71 area.
- M4DEEP, M4DEEPM1, M4DEEPM1_2 - jittered frames within the large M4 area.
- M4DEEPM2, M4DPFIELD2, M4DPFIELD2_2 - jittered frames lying within the Penny, Lubenow and Dickens (1987) area.
- M4S1, M4S2, M4S5 (x2) - strips that make up the M4S large mosaic.

Some of the brighter stars in the test strip M71N1 were found to be saturated in the 50 second on-chip exposure time so the shorter integration time of 35sec was chosen for the main mosaic in M71. 50 seconds was found to be usable for the M4 main mosaic.

Sky frames were taken at various (small) offsets from a central sky position, so that the effects of any stars inadvertently included could be minimised by median filtering.

3 Reduction

The preliminary image reduction was performed using the STARLINK computer system with the IRCAM reduction software written by Colin Aspin and Mark McCaughrean (see Aspin (1990)), with additional routines (summarized in appendix B) written by the author.

3.1 Counts on IRCAM frames

The reduction philosophy is based on a knowledge of the various contributions to the count in each pixel that come from the source, the sky, 'dark current' and the bias structure of the detector.

In a frame with an exposure time of n seconds and consisting of p coadds the counts in a pixel are made up of the bias count, the count due to the dark current, the count from

the sky and the count from the source. For a sky frame, an image frame and a dark frame these look like this:

$$F_{sky} = pf_b + npf_d + npf_s$$

$$F_{star} = pf_b + npf_d + npf_s + npf_*$$

$$F_{dark} = pf_b + npf_d$$

where f_b is the bias count in 1 coadd, f_d is the dark count rate, f_s is the sky count rate and f_* is the source count rate. Normalizing to 1 second 1 coadd:

$$F'_{sky} = f_b/n + f_d + f_s$$

$$F'_{star} = f_b/n + f_d + f_s + f_*$$

$$F'_{dark} = f_b/n + f_d$$

Clearly a reduced (dark subtracted and flat-fielded) pixel contains:

$$\frac{F'_{star} - F'_{dark}}{F'_{sky} - F'_{dark}} = \frac{f_s + f_*}{f_s}$$

if the exposure times are the same for the source frame and its dark frame, and for the sky frame and its dark frame. If the exposure times were to be different for the source and dark frames (or sky and dark) an odd fraction of the bias count would be left in the final frames. This is why it is essential to take dark frames of the same exposure time as the source and sky frames throughout the night. If the exposure time is the same for the sky and source frames the same dark frame may be subtracted from both.

Aperture photometry is performed by measuring the counts in a source aperture, C_*, and in a sky aperture, C_s, of the same size. The measured magnitude is:

$$m_* = -2.5log_{10}(C_* - C_s) + zp$$

where zp is the zero-point of the photometry. This is correct on the reduced frames because:

$$C_* - C_s = \Sigma\frac{f_* + f_s}{f_s} - \Sigma\frac{f_s}{f_s},$$

where Σ is the sum of the counts in the pixels in an aperture. In other words, the difference between the total counts in the source aperture and in the sky aperture is just the total normalized counts due to the source, which is what is wanted.

3.2 Strip observations

The reduction procedure used for the large mosaics was similar to that detailed in the last chapter for the bright standards frames. It can be summarized as follows:

- Linearity correction
- Dark subtraction
- Flat-fielding
- Interpolate over bad pixels
- Normalize sky counts to those of first frames
- Find frame offsets
- Shift by fractions (and set edges to zero)
- Mosaic together

These are discussed in the next sections.

3.2.1 Linearity correction

A nearby-in-time bias frame was subtracted from each image to give a bias-free count in each pixel. The frame was normalized to 1 coadd and the appropriate linearity correction was applied to each pixel. Array parameters were changed at the start of 1988 July so that the present data spans two different forms of the linearity correction. Examination finds

no significant difference between fully-reduced final images of the same objects taken in 1988 May and those taken in 1988 July, confirming the success of the linearity correction. Finally the frame was normalized to an exposure time of 1 second.

3.2.2 Dark subtraction

The nearest good dark frame of the same exposure time (also linearity corrected and normalized to 1s 1coadd) was subtracted from the image frame.

3.2.3 Flat-fielding

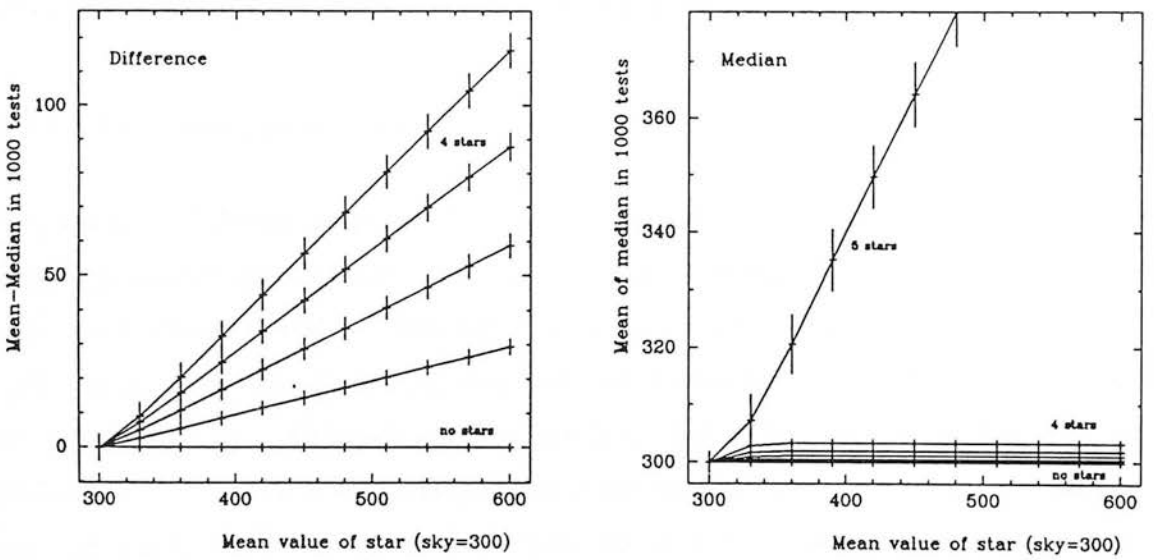

Figure 3: Simulated comparison of the mean and median as estimates of the true sky/flat-field level in a frame.

A flat-field frame was constructed by taking the median filter of all the nearby dark-subtracted sky frames. Median filtering minimises the effect of any stars in the sky frames although it does yield higher flat-field noise than taking a mean frame in the case were there are no stars in the frames.

Figure 3 shows the results of tests were 1000 sets of 10 artificial pixel values were created

from a Gaussian distribution. Larger values were included to represent contaminating stars and the mean and median values, along with their standard deviations, were calculated for each set of values. Group means were calculated for each of the sets of 1000 values. The values of sky level and contamination were chosen to be typical of real frames. The plots show the difference between the mean and the median, and the median as a function of the brightness chosen for the contaminating star and of the number of stars, or bad frames, chosen. Of course, when 50% of the pixels contain stars the median is as bad an estimator of the true sky/flat-field level as the mean, but for <50% stars the median gives a much better estimate.

If few sky frames were available the least crowded image frames were included in the median filtering process. After flat fielding the image was multiplied by the median value of the flat field frame, to restore real count values. (Using a flat field which has been previously normalised to a median of unity is exactly equivalent).

3.2.4 Bad pixel replacement

For each pixel of the array that was known to be permanently 'dead' (i.e. unresponsive to image flux) an interpolation was carried out to replace the 'bad' value with one calculated from the 8 adjacent pixels. There were 21 of these pixels. Where these fell within a stellar image they were instead set to a 'bad' value allowing them to be disregarded at the mosaicing stage. Although marking pixels as bad in this way is the best way to deal with them, since it is then always clear which pixels do not contain real sky/source flux, this was not done for all the 'bad' pixels because of the effect that the bad values have on the centroiding of nearby stellar images and the estimation of sky statistics. More sophisticated centroiding and statistical routines than those used would be able to disregard the pixels marked with the bad value. All bad pixels could then be dealt with in this way, and interpolation would be necessary only for cosmetic reasons.

Each image was inspected and any extra 'bad' pixels (due to cosmic ray hits, electronic glitches or similar) were marked up and similarly interpolated over or set to the 'bad' value. Bad-pixel selection is a fairly subjective process, but once a user is familiar with IRCAM frames it is fairly easy to pick out pixels that are higher or lower than expected from the noise in the sky areas of the frames, but also too sharp to be a stellar profile. In the 0.6

$\widehat{\pi}$/pixel mode differentiating between stars and bad pixels is simple since the stellar profile is visible over several pixels (in average seeing conditions and with the telescope/camera system performing as it did in 1988). A selection effect was in operation during this process because of the way that the images were displayed: bad pixels that were too bright stood out in a bright colour, whilst bad pixels that were too faint were dark. The dark pixels had less contrast from the sky and covered a smaller range of colours than the bright pixels. This under-selection of dark bad pixels is not significant since (a) the DAOPHOT parameters are set to treat as bad any pixel 10 sigma fainter than the sky, (b) only the least deviant pixels will have escaped detection so their contribution to the sky statistics will be insignificant, and (c) dark bad pixels within stellar images show up with excellent contrast and were therefore all spotted and dealt with.

3.2.5 Sky normalization

Each frame was now 'sky-normalized': the median sky value of the frame was compared with that for the first frame in the sequence and the difference was added to the frame. The different values of sky pixels between frames are due to the changing brightness of the sky at K, so a simple additive transformation is appropriate. Had the differences been due to changing gain within the camera/telescope system a multiplicative transformation would have been necessary. If the differences had been due to changes in the atmospheric transmission (i.e. the night was not photometric) a multiplicative transformation would have been necessary based on the brightness of a set of bright non-variable stars within the frame. This type of photometry on non-photometric nights is possible, if difficult, with a camera system (provided calibrating photometry can be obtain in good conditions). For example, for Simon et al (1990) the present author reduced a series of 350 short exposures taken during a lunar occultation of the Galactic Centre; although the observations were taken through drifting cloud, it proved possible to flatten the image backgrounds and normalize each frame to the brightness of the bright source IRS7, so that emergence light-curves could be measured for the other sources in the region. During the same event other telescopes performing single-channel photometry in the same conditions produced nothing useful.

Where a very bright (usually saturated) star appears on a frame the median of the counts in the frame is biased upwards. This means that too much is subtracted from the frame

in the sky-normalization process and the sky in that frame appears too dark relative to the other frames in the final mosaic. Aperture photometry on an area of empty sky in these frames and in the reference frame allows the bright star frame to be normalized correctly.

3.2.6 Determining offsets

When the frames had reached this stage the positional offsets between each frame and the first (central) frame in the sequence was found by using a cursor to select five stars common to both frames. The IRCAM package's CENTROID routine finds the centre of the stellar images and the mean co-ordinate differences give the offsets between the frames. Typically the standard deviation of the mean offset was 0.25 pixels, although it could be as good as 0.05 pixel (which is the limit of the accuracy of the centroiding routine) or as bad as 0.8 pixel. Care must be exercised since the centroiding routine can be confused both by bad pixels and by other nearby stars.

The IRCAM routine SHIFT was used to shift each frame by the appropriate fraction of a pixel to make it an integer number of pixels in offset from the central frame. This routine simply performs two-point linear interpolation in each axis, thus preserving the total flux. Since the shifting process involved an interpolation the resultant frames were slightly smoothed when compared with the pre-shift originals. To ensure that this effect was uniform the central frame was also shifted with the same routine. The shifting process left an edge of unused pixels on each frame, on the side(s) from which the shift was made. These pixels were set to zero so that the mosaicing routine would recognise them as 'bad pixels' and discard them.

The vertical overlap between strips was so small that there were not enough stars in most frames to allow the offset to be determined. The offsets were taken as the mean of the offsets for those few (at least five) stars that could be measured. All the strips run exactly parallel to each other to within the errors of measurement.

Finally all 33 frames were mosaiced together to form the large area images, taking the value zero as a marker of bad pixels.

Although two complete sets of frames were available to make the M4 mosaic these were not combined into one single image but made into two separate M4 mosaics. This was

thought best since the frames were taken in different observing conditions. The profile fitting measurements of the two separate frames were later combined to give one set of data for the region.

3.3 Jitter frames

The reduction procedure for the jittered observations is the same as that for the large area mosaics except that the flat-field was formed from the median filter of all the image frames and whatever sky frames were available. In practise it was found that since the deep areas had been selected to contain no bright stars the median filtered images were sufficiently clear of residual stellar counts to be used as the flat-field in all cases.

The fact that the frames contain mainly the same stars greatly speeds up the determination of the fractional offsets.

3.4 Final frames

The final large mosaics for both clusters are shown in figures 4(a) and 4(b). Figure 4(c) shows maps of the stars found by DAOPHOT in these two mosaics. Figure 5 shows one of the deep frames from M71, together with a map of the stars found.

4 Using DAOPHOT on IRCAM frames

DAOPHOT (Stetson, 1987) is a widely used crowded-field photometry package written at the Dominion Astrophysical Observatory. It was designed to be used on CCD data where pixels scales are typically of the order of $0.2''$/pixel (although Hesser et al's 1987 observations of 47 Tuc were taken at $0.58''$/pixel, comparable with those of IRCAM). DAOPHOT works by attempting to fit a profile, constructed from bright, isolated stars, to the stars on the frame. The fitting takes place simultaneously for each group of up to 60 stars.

Whilst DAOPHOT was used fairly much as recommended to find stars and create the point spread function for each image, the advanced program ALLSTAR was used in preference to DAOPHOT's NSTAR option to actually do the profile fitting. ALLSTAR

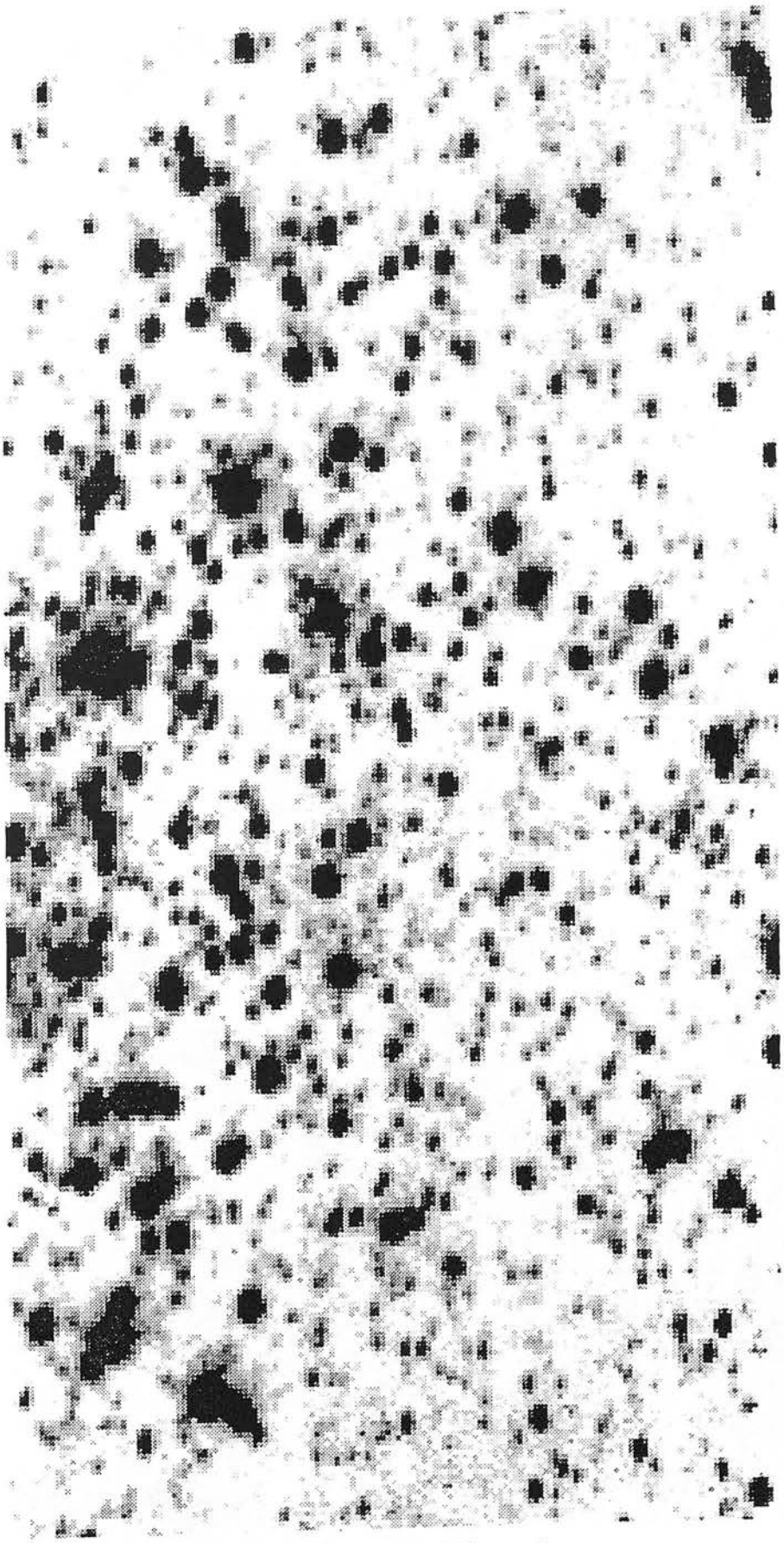

Figure 4: (a) The M71DK mosaic.

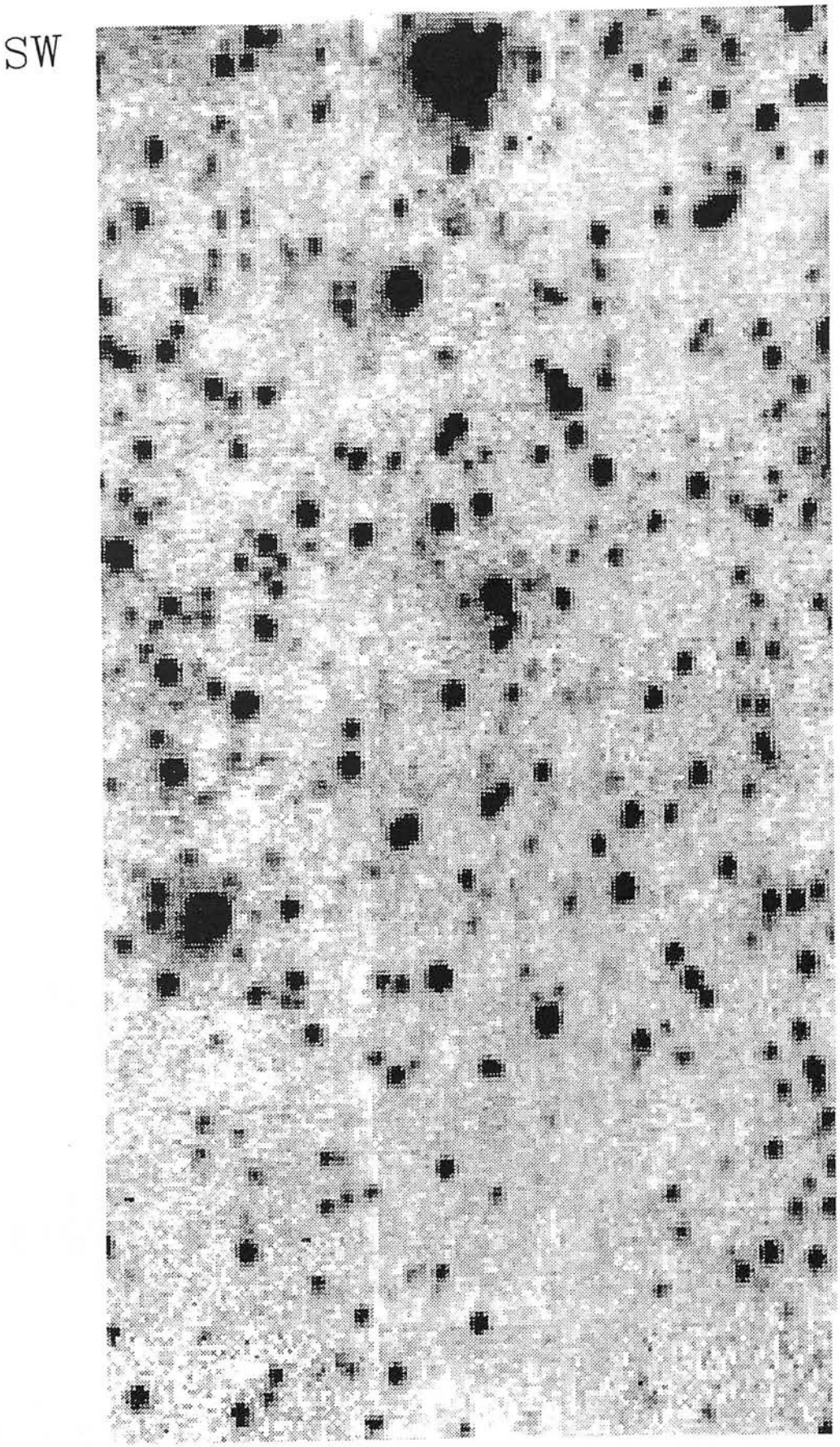

Figure 4: (b) The M4S mosaic.

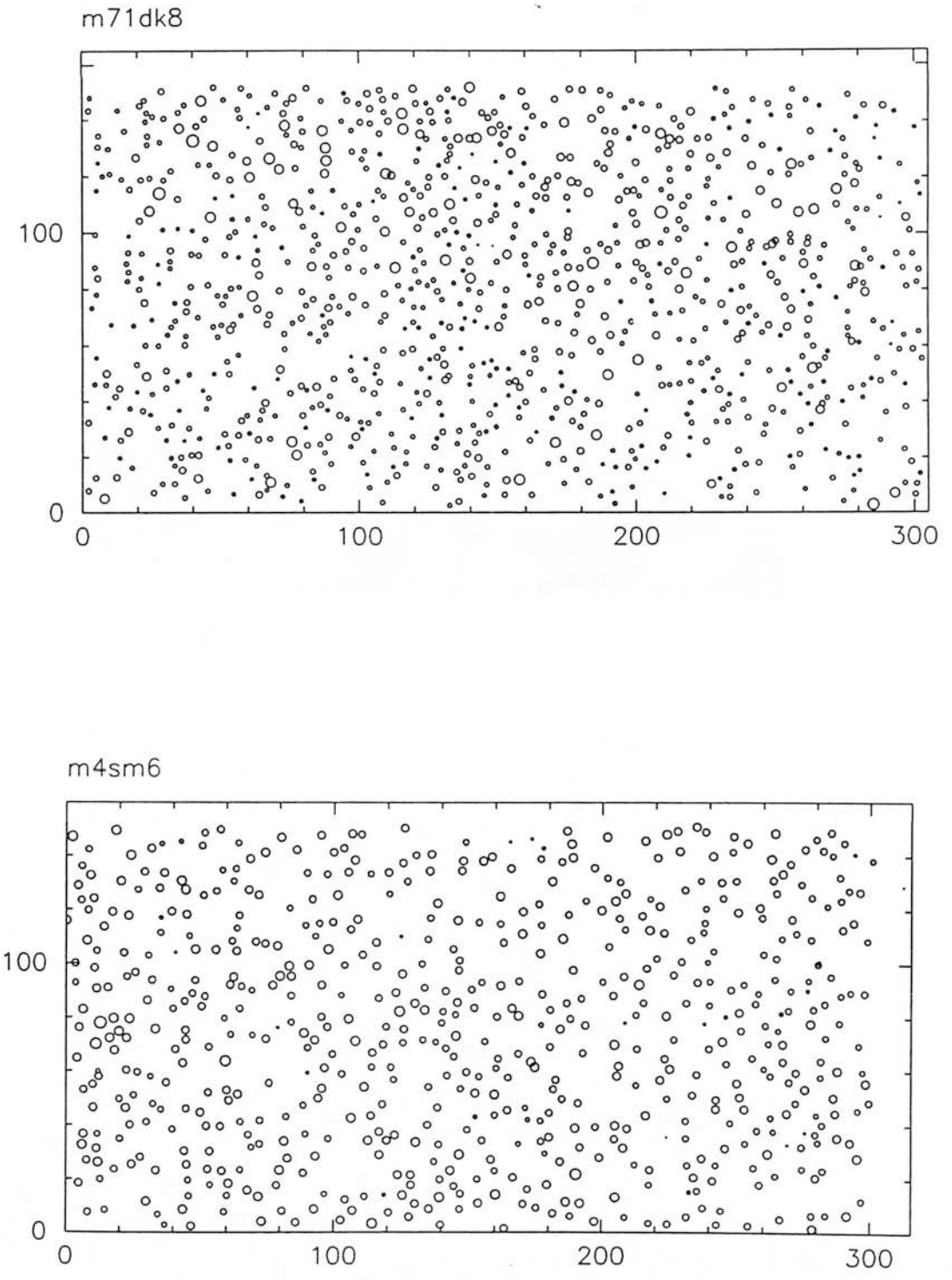

Figure 4: (c) The stars found in M71DK and M4S.

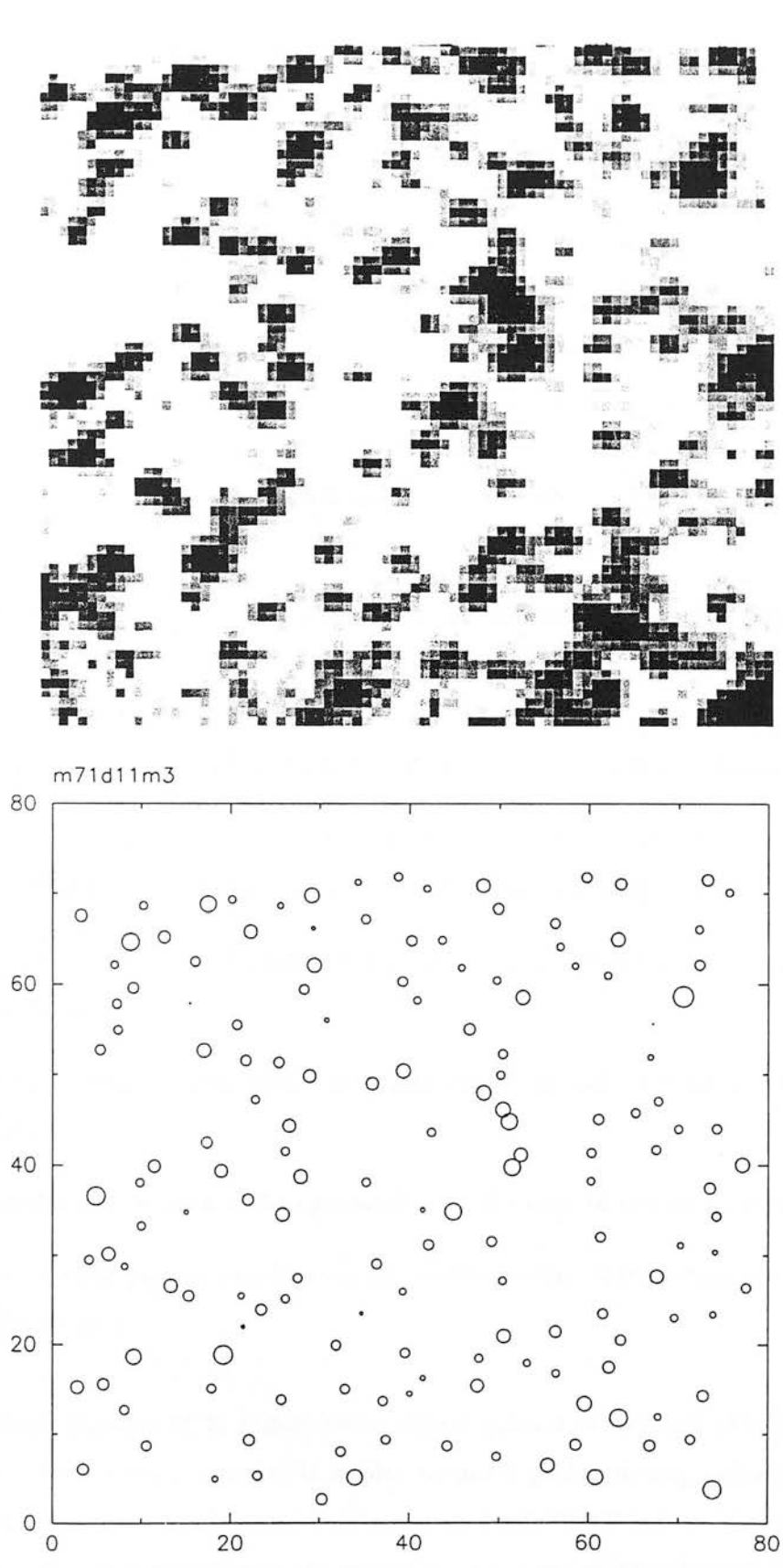

Figure 5: The M71DEEP1_1 image and the stars found therein.

was written by Peter Stetson as a simplified and improved, stand-alone version of NSTAR and SUBSTAR, the profile fitting and star subtraction routines in DAOPHOT. Its major advantages are convenience and speed. With NSTAR the stars in the list to be fitted have to be grouped into collections small enough for NSTAR to work on before the main program does the fitting. With ALLSTAR the chosen fitting radius is successively reduced (if necessary) until each group is small enough, when the group is fitted with the modified radius. This means that the fitting radius is optimised for each group. ALLSTAR comes with a warning that it is a preliminary version and that it should be used with care. Tests quickly showed that the output from the IR frames was just as good from ALLSTAR as from NSTAR. In addition ALLSTAR was faster and easier to use. All the DAOPHOT magnitudes derived from the IR data have been obtained using ALLSTAR.

DAOPHOT measurements of IRCAM frames are expected to be less accurate than comparable optical frames because:

- frames are taken at different times and thus may have different intrinsic profiles;
- the poorer sampling of the stellar profile by the small IRCAM pixels means that DAOPHOT has much less to make a profile from and to fit a profile to;
- the small size of the IRCAM frames mean that there is less sky area to estimate statistics from;
- there are fewer isolated, bright stars from which to make the point spread function (PSF);
- more stars are wasted by being too close to the edge of the frame to be measured;
- the mosaicing process can degrade the stellar profiles, introducing random errors in the photometry.

Even the large mosaics of 33 frames cover only a quarter of the area of a typical, single CCD frame. For these reasons it is harder to use a profile fitting package on IRCAM frames than on optical CCD frames. The use of DAOPHOT will be discussed in some detail in this section, together with the results of some tests of DAOPHOT's and IRCAM's performance.

4.1 Use of DAOPHOT and optimal parameter selection

Various parameters must be provided for DAOPHOT to handle the image data and perform its fitting operations.

The 'maximum good data value' parameter determines at what level bright pixels are determined to be *too* bright. This parameter is set somewhat below saturation so that DAOPHOT and ALLSTAR will not try to fit the saturated cores of very bright stars, which it would otherwise measure as being too faint. This would lead to the fitting of a profile that was too small and leave a large residual wing around the star that would confuse the fits of any nearby stars. The maximum good data value is determined to be the above-bias saturation level thus:

$$MGD = \frac{65000 - 37000}{t_{exp}}$$

This is the difference between the maximum possible value of the data (2^{16}) and the average bias level in a frame divided by the exposure time of the frame. Since all the frames are dark-subtracted and reduced to 1 second 1 co-add this calculation gives (a bit less than) the maximum value it is possible to find in a frame. For a 35 second frame MGD is set to 800 counts and for a 50 second frame MGD is set to 560 counts. Since the sky at K takes up between 200 and 300 of these counts it can be seen that the dynamic range of a 50 second frame is rather small, perhaps 6 magnitudes from the sky to saturation.

Other parameters that are set at the start of a DAOPHOT session are: FWHM, the fitting radius and the PSF radius. The Full Width Half Maximum is used as a starting estimate of the width of the profiles for which the FIND routine searches. The setting of this parameter is not critical and the value FWHM=2 was used throughout, being estimated by examining the profiles of bright stars on several frames. This agrees well with the value found from the widths of the Gaussian component of the PSF created on the frames.

The fitting radius is of course the distance out to which the fit is to be made. The larger the fitting radius the more of the stellar profile is used and so the better the fit, but also the longer it takes and the more stars get included in each group. If any group has more than 60 members the fitting radius has to be reduced. There is some evidence that ALLSTAR tends to reject a large number of stars if the fitting radius is set large. Figure 6

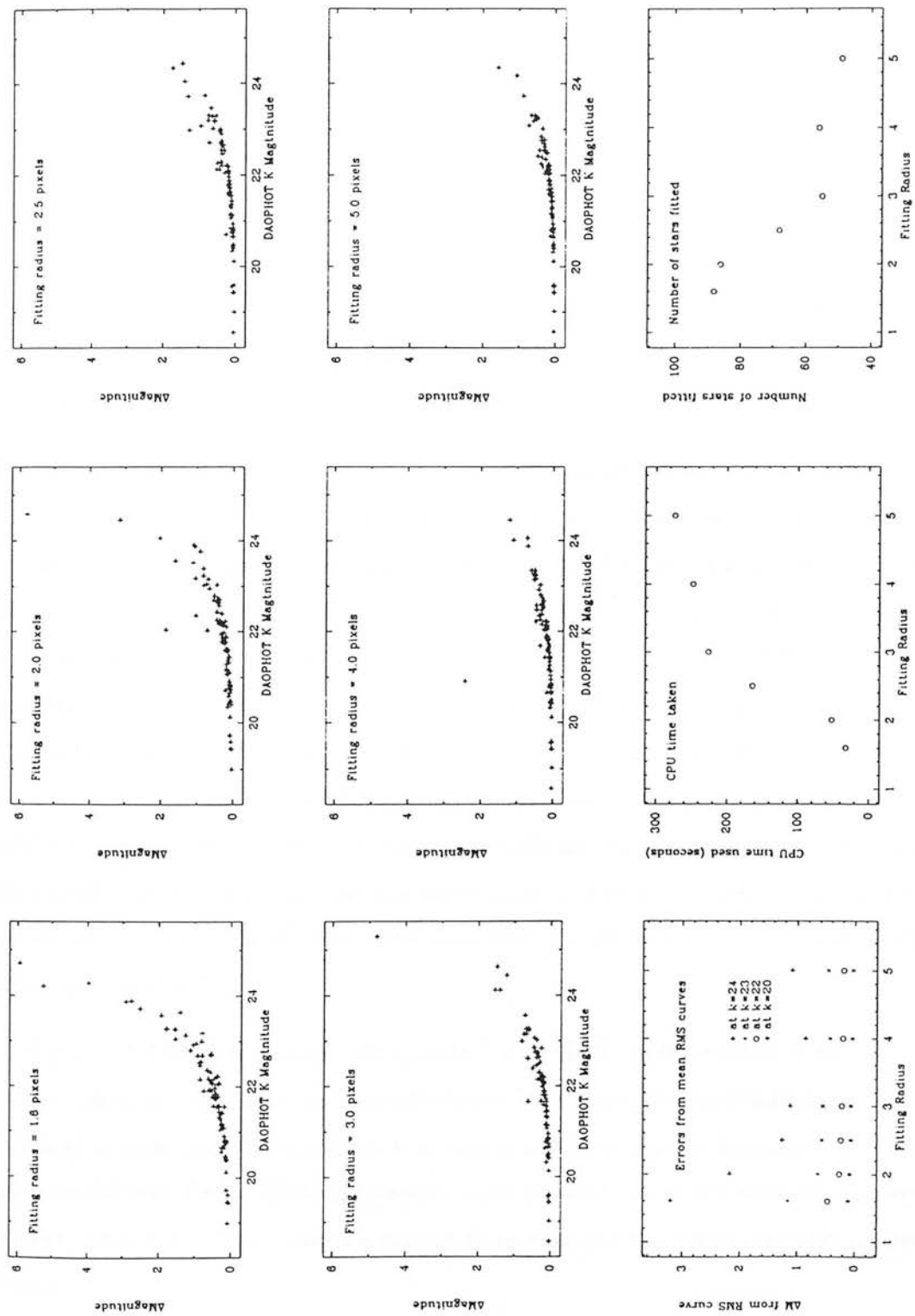

Figure 6: The effect of varying the PSF fitting radius.

shows the RMS plots for the same frame reduced with different fitting radii, together with a figure which summarises these variations by plotting the mean DAOPHOT errors at various instrumental magnitudes as a function of fitting radius and figures showing the CPU time used and the number of stars fitted. The magnitudes plotted are instrumental K magnitudes from DAOPHOT which are ~5 magnitudes larger (more positive) than true magnitudes. Thus k=23 corresponds to K~18. A fitting radius of 2.5 pixels was chosen as a good compromise between speed, accuracy and completeness.

The PSF radius is the distance out to which the profile is defined and is set to 6 pixels based on trial and error tests. If this were set too small bright stars would be seen to have residual haloes in the subtracted frames, too large and the fitting would take an excessively long time.

The routine SKY estimates the mode and standard deviation of the mean of the sky in a frame. The value for rejecting low bad pixels is set to ten standard deviations below the mean. This may seem a wide margin, but the standard deviation of the sky is over-estimated because of contributions from the wings of stars, even though SKY attempts to correct for this. If $3\sigma_{sky}$ is used as the threshold for objects for FIND to record, a large number of stars are missed out which, although faint, are certainly measurable by ALLSTAR. Trail and error experiments found the optimum value of the FIND threshold to be about $1\sigma_{sky}$. The value of σ_{sky} from the final star-subtracted frames is somewhat unreliable because is can easily be biased by residuals left when a bright stars has not subtracted properly. However, for the larger images, where this effect is minimised, the star-subtracted σ_{sky} is somewhat lower than that on the original frame, confirming the choice of a 1σ threshold.

RMS plots (DAOPHOT magnitude against DAOPHOT estimated fitting error) can be used to assess the success of successive iterative fitting procedures, although care must be exercised in these comparisons since it is common for there to be a change in zero-point between different PSFs. This difference is most pronounced at the start of the iterative process, when the PSF is changing rapidly (hopefully for the better) between successive versions.

4.1.1 DAOPHOT sequence.

Although the basic procedure is similar to that recommended by Stetson and other users of DAOPHOT it is worth setting down the exact steps involved in using DAOPHOT on an IRCAM frame. (SKY, FIND, PHOTO, etc are routines within DAOPHOT).

- SKY: estimates the sky value and noise (σ) in the sky over the whole frame
- FIND: searches the frame for peaks above the given threshold value, discarding pixels below the given bad pixel threshold
- PHOTO: performs aperture photometry on the stars found
- PSF: construct a PSF from bright isolated stars on the frame

loop:

- fit (NSTAR/ALLSTAR) the original frame with new PSF (output to ALS/NST file)
- SUBSTAR: subtract all the fitted stars from the original frame
- DAOCURS: mark up any extra stars that are found in the subtracted frame
- edit out PSF stars from ALS/NST file.
- SUBSTAR: subtract out all but the PSF stars
- PSF: construct a new PSF from this subtracted frame

end loop

Caution must be exercised when adding extra stars into the co-ordinate list file as trying to fit something which is actually a residual may cause ALLSTAR to fail to fit both it and the star of which it is a residual. There were usually 8-15 stars making up a final PSF, and as many as 8 iterations were necessary for the PSFs to stop changing between iterations.

4.2 Accuracy, repeatability and completeness

There are a number of questions that need to be answered regarding the best way to get the most out of IRCAM mosaics. For instance, does mosaicing with fractional pixels represent any gain over integer shifts when the resultant smoothing is taken into account ? What internal accuracy can be expected from the DAOPHOT fitting procedure ?

4.2.1 Comparison of 2 independent data sets: part I

Frames 95 and 104 from the set IRCAM_7JUL88_2 are the start and end frames of the first M71DEEP1 mosaic. They are thus nominally centred on the same position and can therefore be compared easily. Figure 7 shows the match in position and magnitude of the two frames and the RMS plot for one of the frames. The RMS plot for the other frame is almost exactly the same. There is a slight zero-point shift in both position and magnitude between the frames. This is quite normal for frames reduced with different PSFs. The frames match in magnitude as well as can be expected, that is, the scatter between the two sets of measurements is the same as the DAOPHOT errors for those measurements. The envelope plotted in figure 7(b) is simply the mean curve through the RMS plot in 7(c).

4.2.2 Comparison of 2 independent data sets: part II

M71DEEP1_1 and M71DEEP1_2 are mosaics of the same small area of M71 made up from two different sets of frames. These provide the ideal opportunity to examine the repeatability of DAOPHOT measurements on IRCAM frames.

For M71DEEP1_1 DAOPHOT's SKY routine found a mean value of 293 and a standard deviation of 0.8 for the sky pixels on the frame. FIND (with a threshold of 2 above the sky and a minimum good data value of 280) listed 99 stars. For M71DEEP1_2 SKY found 304 ± 0.7 and FIND (threshold=2, minimum good data value=290) listed 101 stars. Both frames were measured with ALLSTAR.

The match in figure 8 shows that again the stars match to within their error estimates. The mean difference between the two sets is $0^{m}.17 \pm 0.04$ from all points matched up with a separation of less than 2 pixels. For only the brightest stars (K$\sim$15-16.5) this is reduced

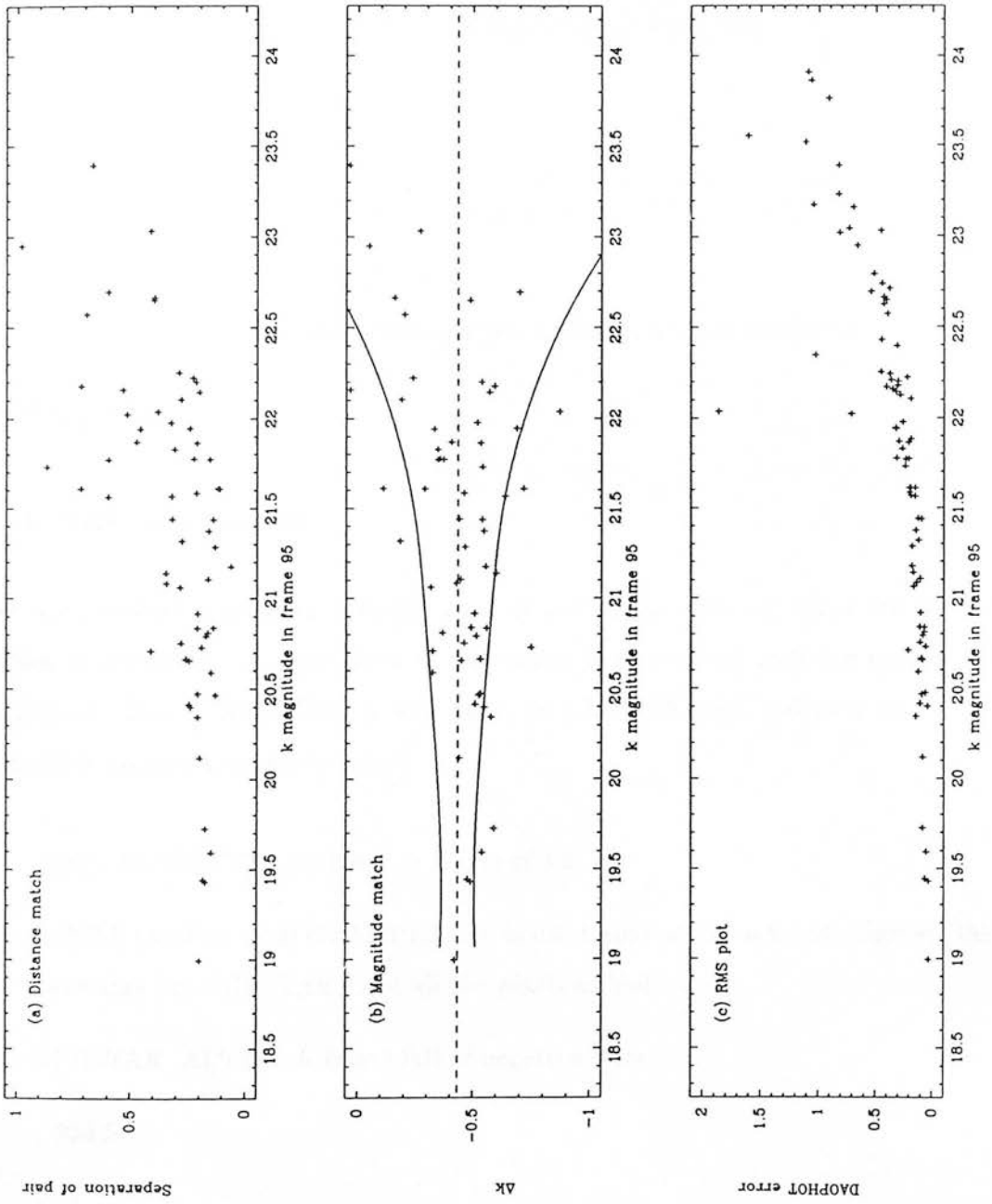

Figure 7: A comparison of frames 95 and 104. The magnitudes are instrumental.

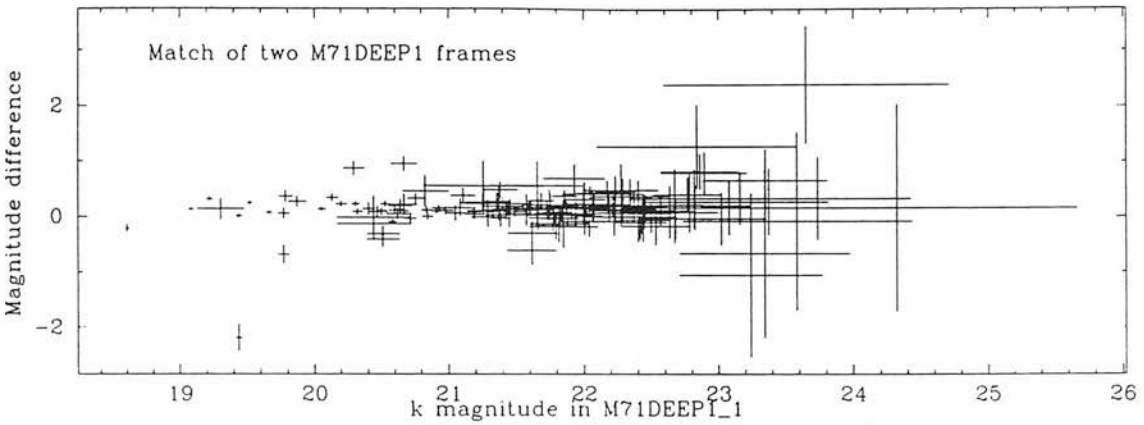

Figure 8: The match between M71DEEP1_1 and M71DEEP1_2.

to 0.028 ± 0.008.

4.2.3 Self measurement

One test involved making an artificial copy of one of the mosaics, using the measured profiles to construct the stars, then re-measuring it to see how well the profiles fitted themselves. Frame M71DEEP1_1 was used, on which 99 stars had been found. The artificial frame was constructed thus:

- divide M71DEEP1_1 by itself → frame of 1's
- x 293.5 (median of M71DEEP1_1) → blank frame at sky level of original (this is necessary lest SUBSTAR treat all the pixels as bad)
- SUBSTAR .ALS list → frame full of negative stars
- - 293.5
- x -1
- + 293.5 → artificial frame with these stars

and then measured to see how well the profiles fitted themselves.

- DAOPHOT

- SKY → 293 with a standard deviation too small to be measurable
- FIND threshold = 2, min good data = 280 (same as for M71DEEP1_1 fit)
  → 92 stars.
- PHOTO
- ALLSTAR

The derived magnitudes can now be compared to those measured on the original image frame. If a fitting radius of 5 pixels is used a non-linearity is apparent: the stars appear too faint in one frame as a function of magnitude, so that the artificial stars with k=24 are $0^{m}.4$ brighter. The RMS deviation from the mean line, i.e. the internal scatter, at k=24 is $\Delta k \sim 0.1$. If a fitting radius of 2.5 pixels is used the difference between the two fits becomes flat with k and $\Delta k=0.25$ at k=24. This is easily explained: the PSF was constructed on the original image frame with the fitting radius set to 2.5 pixels so the magnitude scale will not be linearly related to one measured with twice the fitting radius if a significant intensity-proportional, non-Gaussian, wing is present in the real stellar profiles. Such a wing is only partly dealt with by the scaled residuals component of the DAOPHOT PSF. Some other profile fitting packages make more allowance for this, STARMAN for instance, fits both Lorentzian and wide Gaussian components, as well as an empirical residual table (see Stetson, Davis and Crabtree (1990) for further discussion and references). Also, the fitting radius of 5 provides more pixels to fit to and so the estimated errors on the fits are smaller. For comparison, on the original M71DEEP1_1 frame the average error estimated, with a fitting radius of 2.5, for a star with k=24 was $\Delta k \sim 1.5$. As expected the error introduced in the fitting procedure is much less than the random errors caused by the noise in the data.

4.2.4 Internal errors and completeness

Following on from the last section, the internal errors and completeness of the DAOPHOT reduction can be assessed by adding artificial stars to a frame with the ADDSTARS routine within DAOPHOT. This allows a number of artificial stars, based on a given PSF, to be created over a given magnitude range and added into one of the mosaics at random positions. This frame is then reduced in the normal way and the results compared

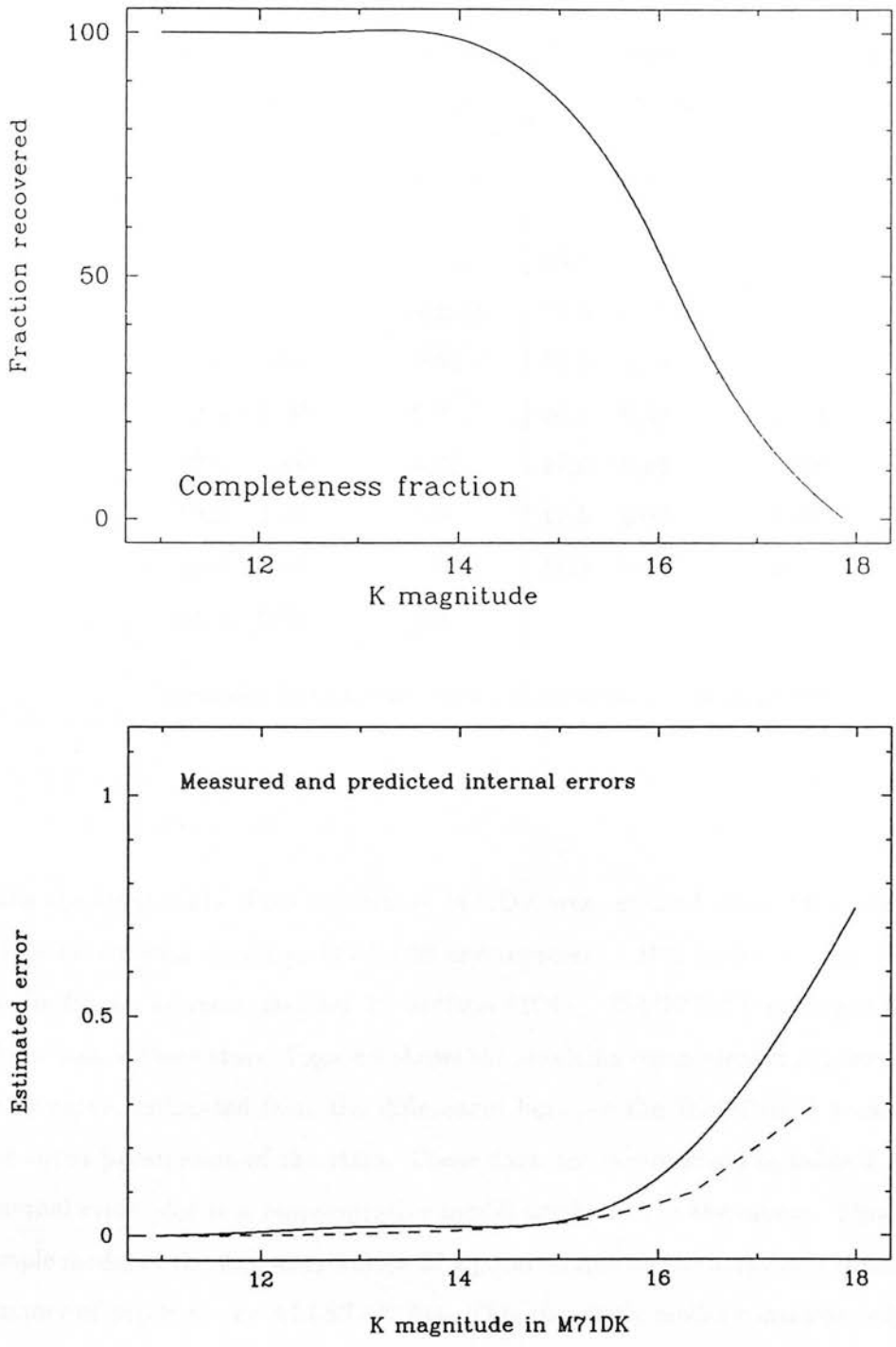

Figure 9: The completeness and internal error curves for M71DK. The dashed line is a model prediction.

Table 3: The internal errors and completeness fractions for M71DK

K	Fraction Recovered	Internal Error	K	Fraction Recovered	Internal Error
11.0	1.00	<0.01	15.0	0.86	0.03
11.5	1.00	<0.01	15.5	0.73	0.06
12.0	1.00	0.01	16.0	0.54	0.13
12.5	1.00	0.0	16.5	0.34	0.22
13.0	1.00	0.02	17.0	0.18	0.38
13.5	1.00	0.0	17.5	0.07	0.55
14.0	0.98	0.02	18.0	0.00	0.75
14.5	0.94	0.0			

with the input stars. Five versions of M71DK were created with 100 extra stars in each. The stars covered the range 11<K<22 and represent a 10% increase in the number of stars in the frame, as recommended by Stetson (1987). DAOPHOT managed to find and fit about half of these stars. Figure 9 shows the resulting completeness curve and the internal error curve, estimated from the differences between the DAOPHOT measurements and the input parameters of the stars. These data are summarized in table 3. Shown in the internal error plot is a representative model prediction of the errors. This is based on a simple model of the flux distribution of a point source on the array and considers the same number of pixels as the ALLSTAR fits. This simplistic model considers only the Poisson $\sqrt{n}$ noise on the dark, sky and star counts and the read-noise of ~450 electrons in each co-add and is thus very much a lower limit of the possible error. Example synthetic star images were considered for pairs of frames consisting of 50 co-adds of 0.5s each. The count rates come from scaled counts measured for an example star of known magnitude, with all

the counts converted into numbers of electrons (1DN (IRCAM Data Number) $\sim$ 24 e^-). For the brighter magnitudes the agreement between model and theory is excellent. The bump in the observed error curve between 12th and 14th magnitudes is almost certainly not real, being an artefact of the small number of stars sampled in this region. For the fainter magnitudes the errors are observed to be larger for a given magnitude than is predicted by the simple model. This is to be expected since, for the fainter magnitudes, the omissions from the model are most significant. These include the seeing and transmission variations that introduce extra noise into the sky, the broadening of the stellar profile by mosaicing errors, sky noise caused by the background of unresolved, faint sources and the intrinsic variations of the bias and dark counts. Either making the function more sharply peaked than observed, or using a larger number of pixels, both of which increase the number of low-level pixels and hence degrade the signal-to-noise, can make the two curves agree very well at all magnitudes. Considering the simplistic nature of the model the present agreement is excellent.

4.2.5 Fractional pixel mosaics - are they worth it ?

When using a program such as DAOPHOT it is important to preserve as much information as possible about the shape of each star throughout the reduction procedure. For instance, smoothing the images to make them look nicer would change the shape of the profiles. The mosaicing routine in the IRCAM reduction package only works with integer pixels, in this case that means that it can only overlap images to the nearest $0.3''$ (half a pixel). DAOPHOT and ALLSTAR are capable of fitting a profile to much greater accuracy than this, so it seems that information is being lost as the images are mosaiced together and any offset smaller than half a pixel contributes to smearing out the profiles. Worse still, this residual offset will be different for different frame combinations so that stars in different parts of a mosaic will have different profiles. This produces random errors in the photometry. The SHIFT routine allows an image to be moved by a fraction of a pixel by re-sampling the image by interpolation. Some tests were performed to see if it was possible to measure the fractional shift between frame sufficiently accurately to make precise fractional mosaicing possible.

The set of frames that go to make up the M71DEEP1 area were reduced normally and also with fractional pixel shifts. A PSF was constructed on each of these two mosaics,

since the fractionally shifted image contained smoothed profiles and would not be fitted properly by the original PSF. Both frames were measured and the results compared. No zero-point shift was evident between the two data-sets but the RMS plot for the 'fractional' frame appears significantly better with $\Delta k \sim 0.3$ at k=23 as compared to 0.6 for the 'normal' frame. The positions of most stars match to within 0.2 pixels between the frames, although ~15% are between 0.2 and 0.5 pixels different. In the (V-K)-K CMD several (5 out of ~100) anomalous stars come back in to agreement with the majority of the data if the fractional-shift data is used instead of the integer-shift data. Clearly, in this case, fractional shifting has been worthwhile.

Another test involved the M4 data. The image-set M4DEEP was reduced as normal and also with all the fractional offsets set to 0.5 in both co-ordinates. This was to investigate whether the fractional offsets were really worth the effort by comparing two frames that had both received the same smoothing through interpolation. The mean difference between the two sets of measurements is -0.002 $\pm$ 0.003 and all the stars are the same on both frames to very much less that their DAOPHOT error estimates.

The conclusion must be that fractional pixel shifts are always worth doing, since it does no harm to attempt them even when the data are not good enough for shifts of less than half a pixel to be meaningful. All the final data have been reduced using fractional shifts.

4.2.6 Reduction artefacts and crowding problems.

One possible cause of systematic or random errors in the final measured numbers from the IRCAM mosaics is broadening of stellar profiles due to incorrect mosaicing. For two frames where incorrect offsets have been used a star may seem too faint because its profile has been broadened, or the twin peaks may be identified as two different stars. The problem is worst for the strip mosaics where each stellar image in the final mosaic contains only two to four images. To examine this problem the M71DK mosaic was divided vertically into five bands, bands 2 and 4 covering the regions of overlap between the three strips that make up M71DK, so that most star images contain contributions from 4 individual frames, and bands 1, 3 and 5 covering areas free of these overlaps, where there are only 2 images in each star. Each band contains between 160 and 220 stars. The resulting CMDs are shown in figure 10.

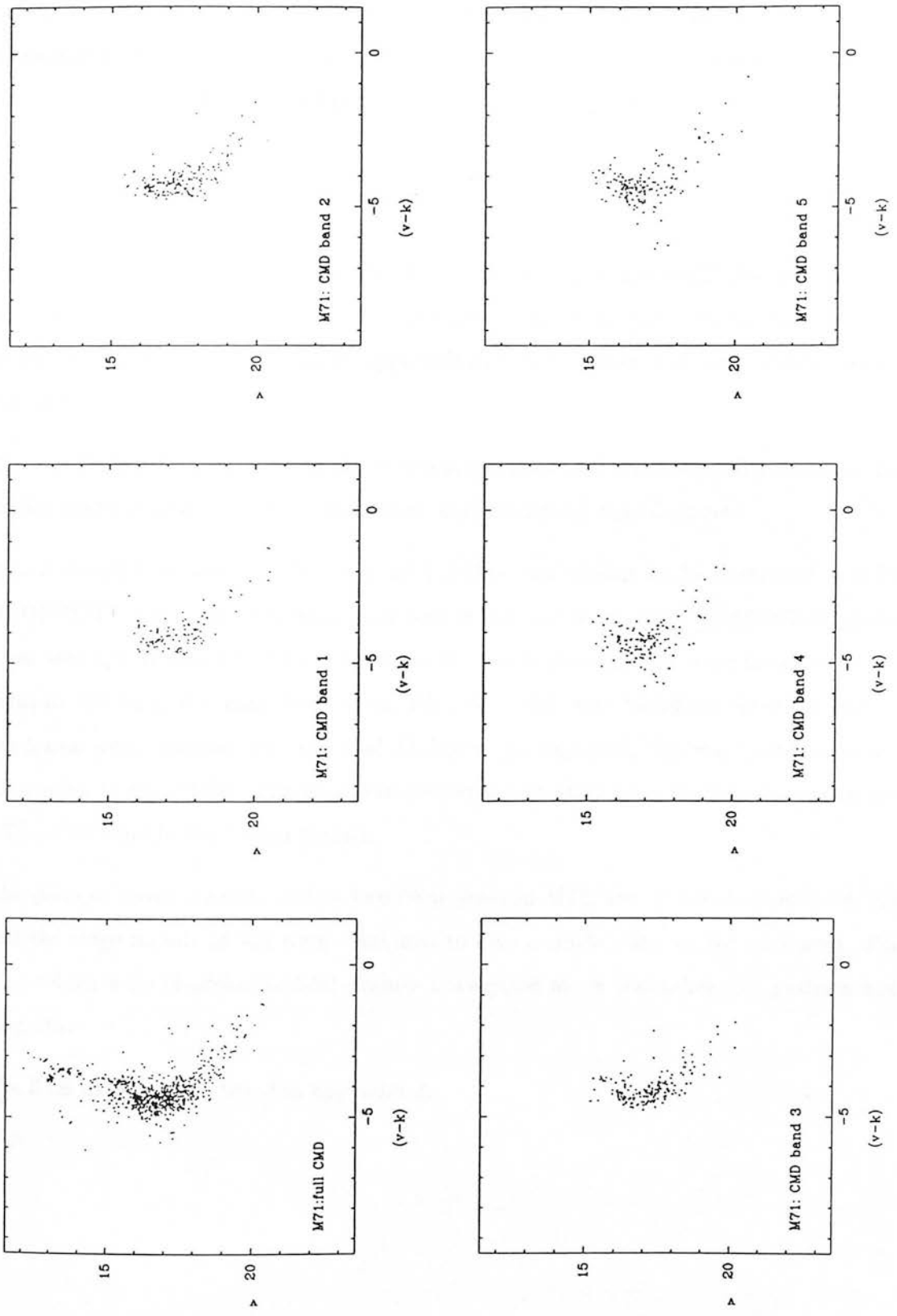

Figure 10: CMDs showing difference between bands. All magnitudes are instrumental.

Examination of the CMDs for these five bands shows that there is no apparent difference between the bands with and without the overlap region. This confirms the success of the mosaicing process. The two bands nearest the cluster centre (4 and 5) show considerable scatter because of crowding and the presence of saturated images.

4.2.7 Final adjustments to the data

The first 'quality filter' applied to the data was to look at the RMS plot and define a curve by hand, similar in shape to the lower envelope of the data, above which all data would be rejected. This is simply an application of the correlation of error with brightness expected in any photometry.

The raw frames for each final image were examined to look for saturated pixels that lay within stellar images. Any such stars were discarded from final data-sets.

It was found that stars on the edge of a frame can appear to be measured well by DAOPHOT, sometimes even when only half of the star is recorded ! DAOPHOT makes some attempt to measure these stars correctly but in general they were found to be deviant in various colour-magnitude plots. All stars within one fitting radius of the edge of the frame were removed from the final ALS files. As expected, this was found to reduce the scatter in the CMDs. The procedure removed $\sim$15 stars from the larger mosaics and $\sim$7% of all stars in the deeper frames.

The pairs of measurements for the two deep areas in M71, two of the deep areas in M4 and the large mosaic in M4 were combined to give a single data set for each area. For stars which were identified in both frames a weighted mean was taken, for position and magnitude.

The final data-sets are listed in appendix A.

5 Constructing CMDs and fiducials

5.1 Matching IR and optical data

All data were put into a standard file format (DAOPHOT ALS/NST) containing star number, x, y position, magnitude and error estimate.

A STARLINK routine, XYFIT, to find a least-squares' six parameter transformation between two sets of stars, was modified to work with DAOPHOT ALS/NST files. This fit allows reflection, rotation, stretch and shear between the coordinates. Other routines were written to display the ALS data as maps, and to match up different ALS files to a given positional tolerance once they had been shifted.

The procedure to match two data sets is as follows:

- Use DAO_MAP to plot stars then cross-identify at least 6 bright ones;
- for these stars change identification numbers of 1st data-set to those of the other;
- run DAO_XYFIT to find the transformation co-efficients;
- use DAO_XYTRAN with these co-efficients to convert 1st set co-ords to 2nd set ones;
- use DAO_COMBINE to match the two sets to a given pixel tolerance;
- plot magnitude and distance residuals and select good stars.

Having been through this procedure once it is possible to iterate by choosing all the stars that fit to, say, 1 pixel and using XYFIT again with those stars. The procedure converges rapidly, although for small data sets 6 iterations were often required to achieve the desired level of constancy.

For the final matching of two data-sets a maximum good separation was found from the distance residual plot of the match (as in figure 7). In all cases a value was apparent below which most separations clumped. This value was between 1.5 and 2.0 pixels in all cases (i.e. $\sim 1\hat{''}$). The data were also examined for multiple matches. A routine (DAO_DOUBLES) automatically displayed the regions from both images around any

stars that were matched with more than one star in the other data-set. The user could then decide which star was the correct match, or simply to reject both matches. It was found to be quite common for two close stars in one data set to be identified as one star in the other data, with a position approximately determined by the intensity-weighted mean of the two stars' positions. Naturally this was most commonly a pair in the optical data matching with a single star in the IR data, since the smaller pixels in the optical data allow better source separation. In these cases the matches were both rejected.

5.2 Fiducials

Fiducial sequences for the main sequences were calculated in the manner advocated by Hesser et al (1989) in their optical work on 47 Tuc. Taking a set magnitude increment the mean and standard deviation of the colour of all the stars in each magnitude interval was calculated all the way down the main sequence. Any star greater than a given colour difference from the mean was rejected as a field star. After recalculation of the mean and standard deviation any star more than the given number of standard deviations from the mean was rejected. The mean magnitude of the remaining stars was calculated and the resulting fiducial point recorded as the mean colour and magnitude, both with standard deviations. The stars not rejected were also recorded. Figure 11 shows an original CMD, the fiducial points derived from it and the stars that make up the fiducial sequence. This sequence has been constructed by considering the data in $0^{\rm m}.25$ bins, rejecting field stars at $0^{\rm m}.6$ from the mean colour and cutting the data at 2.5σ. Some magnitude bins contain very few stars and are discarded for isochrone fitting purposes. There is a small bias in operation in that if the distribution of stars is such that there are many more near either the top or the bottom of a magnitude interval, and the real sequence is a curve, the fiducial point will be biased away from the correct line. If the real sequence is a straight line the bias takes place along this line so the solution is to chose the magnitude increment to be small enough that the fiducial is approximately straight through each interval. It is ironic but perhaps the ultimate test of this fitting procedure is that the derived fiducials agree with the best fit line drawn by eye through the data. The reader may wish to perform this experiment with the data in figure 11.

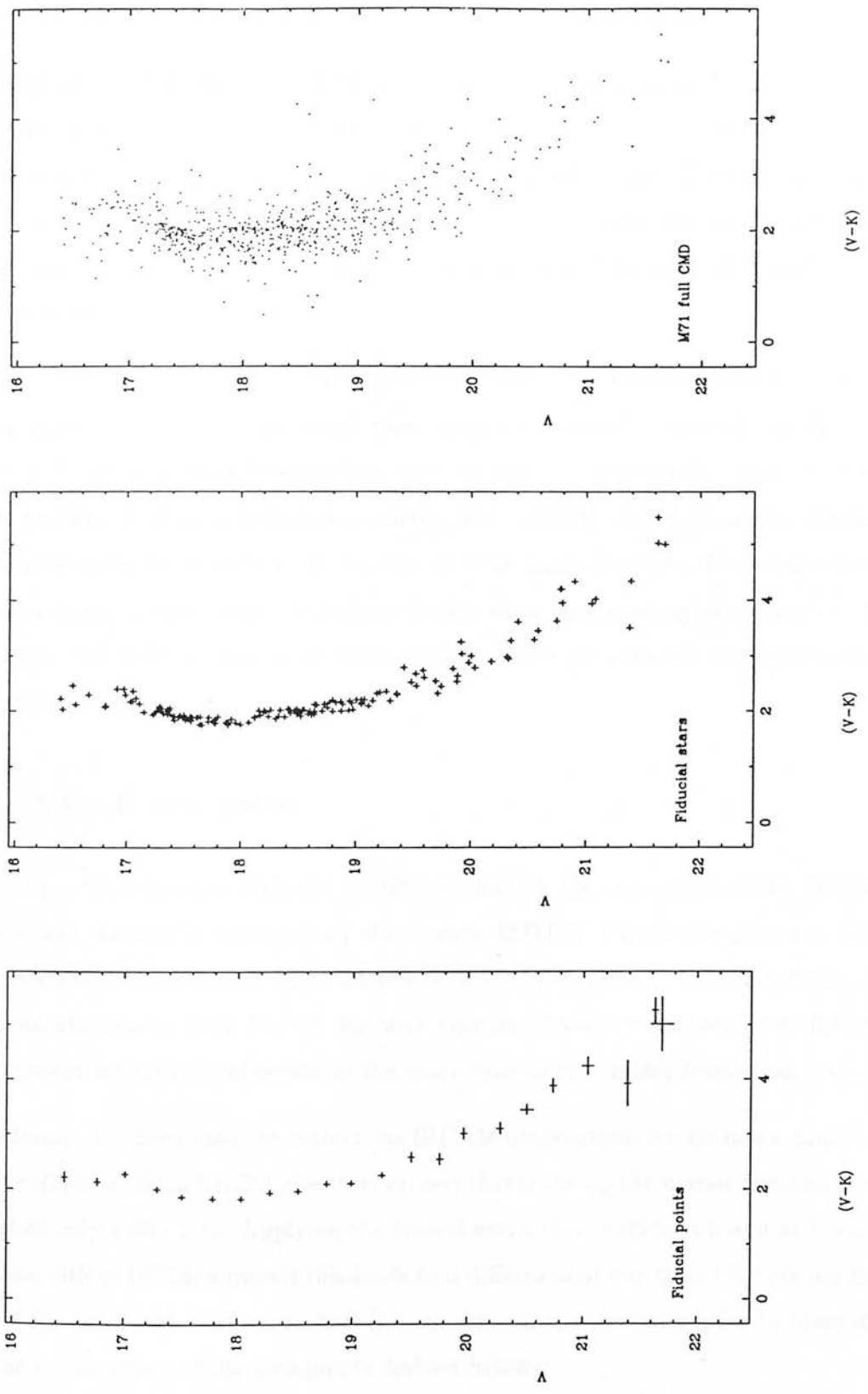

Figure 11: Fiducial sequence for M71, together with the original data and the stars that make up the fiducial.

6 Zero-points

Having reduced the data to final frames and measured them using DAOPHOT it is time to calibrate the derived K magnitudes. It was shown in the last chapter that IRCAM photometry is free of non-linearity over a wide magnitude range. The calibrating data for the two clusters are insufficient to test this further. The calibration of both the present K photometry and past studies at K and V is discussed for both M71 and M4 in the following sections.

Calibration of near-IR photometry is generally more difficult than is the case for optical data, since the standards are much more sparsely distributed around the sky and are often only accurate to 1% themselves (see chapter 1). For cluster work there is very little previous K-band photometry available, and certainly no reliable sequences covering a wide range in magnitude, as is the case at V in many clusters. The small size of the IR frames means that there are likely to be few stars with existing photometry included, whereas a CCD frame may allow inclusion of a cluster photometric sequence in the area of interest.

6.1 M71: K Zero-points

There are two ways to tackle the problem of finding the zero-point of the DAOPHOT magnitudes found for the stars on the mosaic M71DK. Firstly the previous infra-red observations of stars within the field can be used. This includes specially-taken single-channel photometry from UKIRT for both clusters. Secondly the zero-point found from the standards that were observed at the same time as the cluster frames can be used.

No attempt has been made to correct the IRCAM observations for air-mass. Since M71 is very well placed from UKIRT the observations that make up the mosaic cover an air-mass range of only 1.00 - 1.10. Applying the typical extinction coefficient found at UKIRT for K observations ($0^{m}.06$/airmass) this leads to a difference of less than 1% between frames. The 6-7% total extinction correction (i.e. to zero air-mass) that applies to these data is left as a component of the zero-points derived below.

6.1.1 Comparison with Previous Photometry

Frogel, Persson and Cohen (1979, FPC79) presented JHK photometry for 25 giant in the region of M71. These stars can be used to calibrate the IRCAM K photometry through aperture photometry on the M71DK mosaic. The relations presented by Bessell and Brett (1988) show that there is no practical difference between their CTIO system and the present UKIRT system (see chapter 1 for further discussion).

6.1.1.1 FCP79 stars N and C

FPC79 stars N and C are just to the south of the large mosaic M71DK but lie on the M71N1 test strip, 7 2x50s frames in an EW mosaic. Examination of the raw frames of this strip showed that 3 central pixels of star N were saturated in frame 41 of the second container file of the night of 1988 May 20 and that there were no saturated pixels in or near star C which appears in frames 42 and 43. Twelve bright stars were selected in the overlap region between M71DK and M71N1. The STARLINK aperture photometry package PHOTOM (see chapter 1) was used with a 12 pixel ($\sim 7\widehat{''}$) aperture to measure these stars in both frames. The sky was taken as the average of the same 5 areas on both frames. The two sets were found to be the same within the PHOTOM error estimates for all but one star, which only just exceeds this match. The results, listed in table 4 and illustrated in figure 12(i)-(iii), were also compared to the measurements of the same stars made using DAOPHOT on M71DK.

The correlation between the two sets of PHOTOM numbers is good, but in the plots of DAOPHOT magnitudes against PHOTOM stars K and L lie off the relation. Both these stars have nearby companions which have caused the centroiding procedure in PHOTOM to miss the centre of the star. DAOPHOT has not had any problems since the companion stars are fitted at the same time. Also crowding contamination is becoming important at these fainter magnitudes. The relative zero-points in table 4 have a weighted mean of 24.77 ± 0.02 when stars K and L are excluded.

FPC79 used apertures of $7.5\widehat{''}$ and $10\widehat{''}$ for their measurements and selected the reference beam location to be as free of stars are possible. These measures should be directly comparable to the PHOTOM measurements made here. Using the correlation of M71N1 PHOTOM k with M71DK DAOPHOT k, k for FPC79's stars N and C can be found and

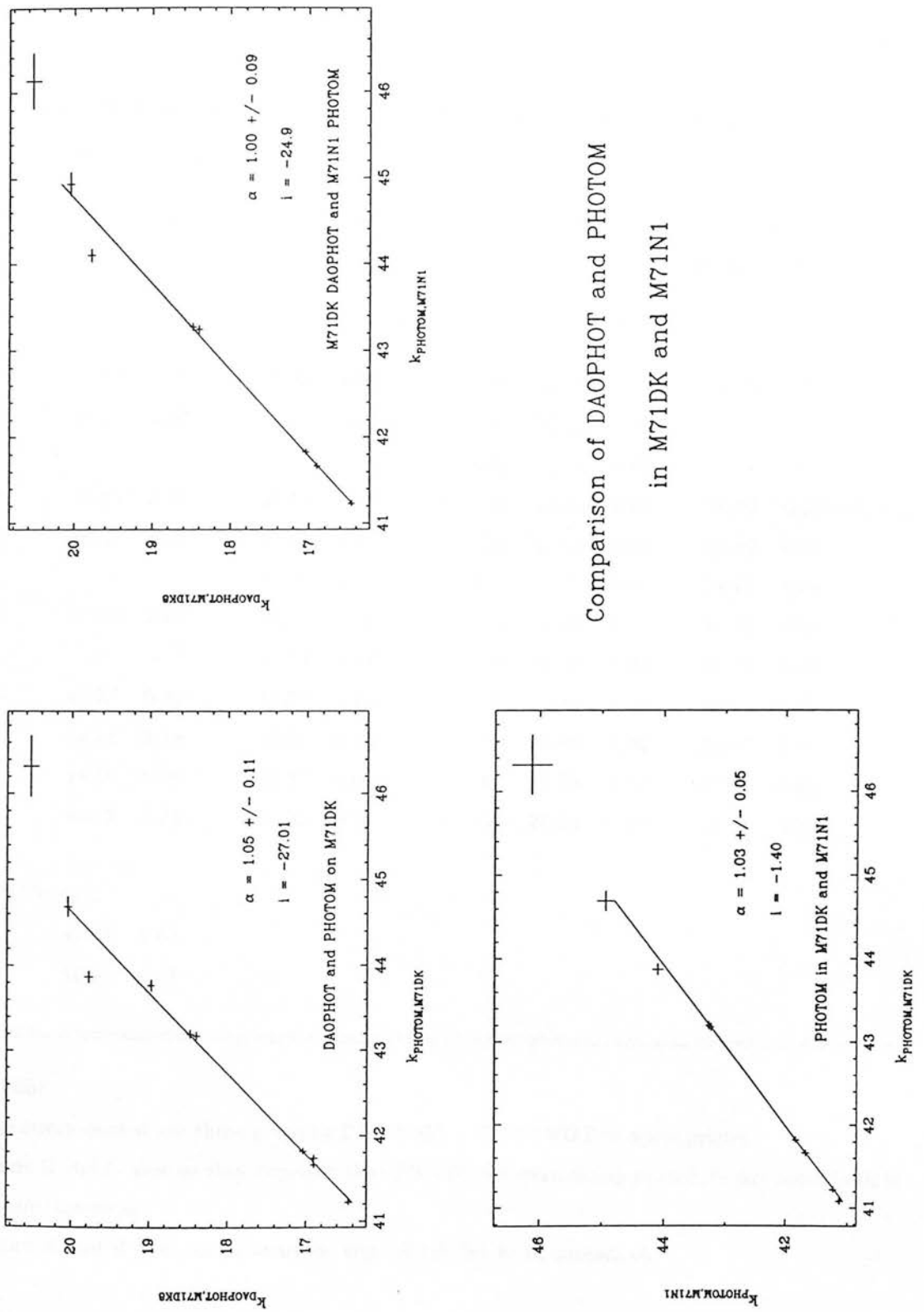

Figure 12: Using DAOPHOT and PHOTOM on M71DK and M71N1.

Table 4: Match of PHOTOM in M71DK and M71N1 and DAOPHOT in M71DK

Star	PHOTOM M71N1		PHOTOM M71DK		DAOPHOT			Relative zero-point	
	k	err	k	err	no.	k	err	M71DK	(PH-DAO)
A	41.67	0.02	41.66	0.02	37	16.90	0.03	24.76	0.04
B	(41.13	0.02	41.08	0.02)	84	17.15	0.04	—	–
C	(			)	109	16.82	0.05	—	–
D	41.23	0.01	41.22	0.02	45	16.46	0.02	24.76	0.03
E	41.83	0.03	41.82	0.03	105	17.04	0.04	24.78	0.05
F	—	—	41.74	0.03	121	16.90	0.02	24.84	0.04
G	43.24	0.05	43.18	0.05	34	18.40	0.02	24.78	0.05
H	—	—	43.77	0.07	116	18.98	0.04	24.79	0.08
I	43.27	0.05	43.20	0.05	42	18.48	0.04	24.72	0.06
J	44.94	0.14	44.69	0.12	48	20.05	0.06	24.64	0.13
K	44.10	0.08	43.87	0.07	83	19.78	0.05	24.09	0.09
L	46.13	0.32	46.32	0.36	39	20.54	0.10	24.78	0.37
FPC79 stars									
C	41.41	0.02							
N	40.39	0.01							

NOTES:

i) the errors quoted are those given by PHOTOM or DAOPHOT as appropriate;

ii) stars B and C were so close together that PHOTOM's centroiding procedure put them both in the same aperture;

iii) stars F and H were too close to the edge of M71N1 to be measured.

Table 5: Zero-points from FPC photometry, part 1

Star	FPC79 K		k(DAOPHOT,M71DK)		Zero-point	
C	11.58	0.03	16.51	0.02	4.93	0.03
N	10.51	0.03	15.49	0.02	4.98	0.03

hence zero-points for k. The FPC79 and present magnitudes of the two stars are given in table 5, along with the resultant zero-point estimates.

The errors in the derived M71DK magnitudes of the two stars are estimated from the goodness of fit in the bright region of the correlation (k<17.5).

Knowing that the image of star N is saturated it is expected to appear fainter than it should, which means the zero-point will be larger. Fortunately, this is what is found !

This is not the complete story however; star C has a nearby companion that is included in the larger aperture and on the edge of the smaller one. Using DAOPHOT to do a preliminary fit to the stars in this frame it is possible to subtract out all the stars around star C. Simple aperture photometry on the original frame and on the cleaned frame give a contamination correction for the FPC79 magnitude. (PHOTOM cannot be used since it finds a sky estimator from the mode of the pixels in the sky aperture, thus eliminating all but the worst contamination).

The results of the photometry are given in table 6. The PSF from the M71DK frame was used to fit these stars and the RMS plot and the final subtractions were judged to be adequate in the region of interest. The agreement of the photometry from the cleaned frame to 1% and 2% for the two sky apertures shows this to be reasonable. The increase of 2-3% seen between the aperture sizes may have some contribution from the wings of the stellar profile of star C, but is mainly due to the residual of the companion star.

Table 6: Establishing contamination corrections in M71N1

	normal frame		subtracted frame	
	6 pixel	8 pixel	6 pixel	8 pixel
sky #1	41.29	40.95	41.37	41.36
sky #2	41.40	41.05	41.38	41.34

Note: sky #1 was chosen as the best nearby sky area and sky #2 as the worst, with two faint stars visible in it.

Unfortunately, Frogel (private communication, 1991) no longer has a record of the aperture sizes, or chop amplitude or direction used for his photometry in 1977. This leaves a range of possibilities. The best possible case is where they used the 7.5 $\widehat{''}$ aperture for all the stars and were able to select the cleanest pieces of sky for the reference beams. In the worst case they would have used the 10$\widehat{''}$ aperture, including companion stars, or selected a contaminated sky. Of course contamination in both main and reference beams could lead to partial cancellation of these errors.

In the best case contamination corrections are 0.08 and 0.41 for the small and large apertures respectively. From table 6 it can be seen that choosing the wrong sky could lead to an error of up to 0.10, choosing the wrong aperture to an error of 0.35. This is a rather sad state of affairs, which means that for the worst case of sky contamination FPC79 may have measured a magnitude 0.02 too faint and for the worst case of main beam contamination they may have been 0.41 too bright. In the best case their K magnitude for star C would have been 0.08 too bright due to the companion star on the edge of the main beam. The PHOTOM result and zero-point in table 5 are for this 'best case', but if FPC79 were unlucky in their choices the zero-point could be as low as 4.59 or as high as 5.04. To summarize, the contamination-corrected zero-point for FPC79 star C is 4.85, but a large error estimate of $\pm$ 0.25 must be assigned to cover all likely possibilities.

6.1.1.2 FPC79 stars 18, 19 and 21

FPC79 stars #18, 19 and 21 are within the M71DK mosaic. Unfortunately analysis of the original raw frames shows that #21 is saturated on the two frames that it appears on. During the same observing run that produced M71DK the same area was observed at a shallower exposure (8 co-adds of 7s) and these frames have been combined to produce the mosaic M71SK. On these frames #21 is not saturated. Thus, in order to use #21 as a calibrator for M71DK it is necessary to relate the magnitude scales of the two mosaics.

DAOPHOT was run on the shallow mosaic, initially using the PSF found on M71DK, and then with a PSF derived from stars on the frame. The DAOPHOT photometry is a poor match to M71DK at faint magnitudes but has measured the brighter stars well. The measured magnitudes match well for the magnitude range of interest, and a simple straight line regression was fitted (see figure 13). The measured value of k_{M71SK} for #21 was converted to the M71DK scale via this regression.

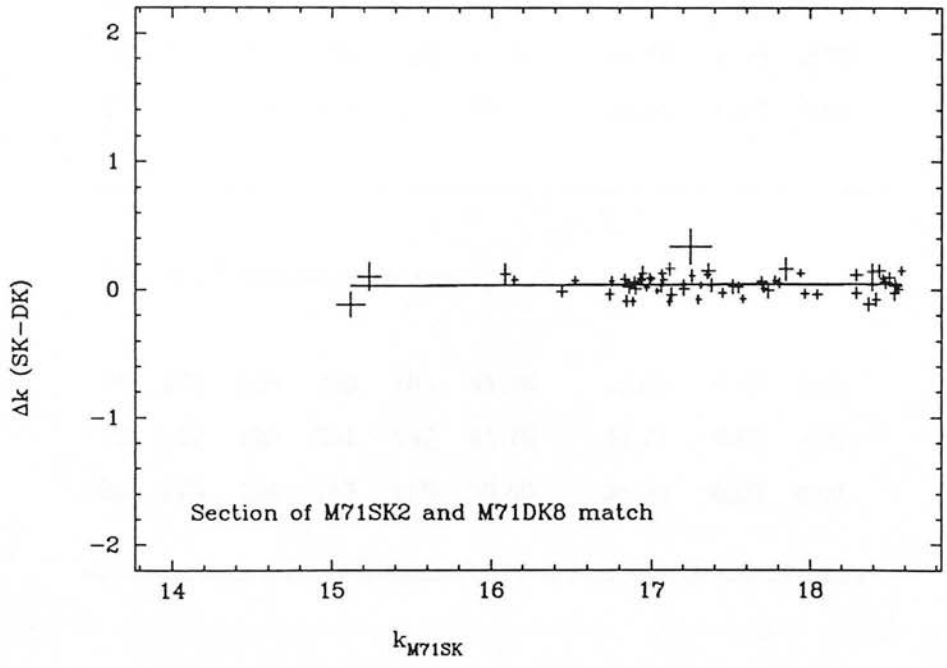

Figure 13: Magnitude match between M71DK and M71SK.

Again contamination corrections were calculated by performing simple aperture photometry on the stars in the original frames and in frames with all the nearby stars removed. These results are given in table 7.

The errors are estimates coming from measurements made with PHOTOM on the clean frame. This time the contamination corrections must be applied to the FPC79 magnitudes before the zero-point is calculated since a comparison is being attempted between aperture photometry and profile fitting photometry. The results are in table 8.

Table 7: Contamination corrections for FPC stars on M71DK

	star		sky		k	k		
	x	y	x	y	M71DK	clean	Diff	err
$12^{\widehat{m}}$ pixel diameter aperture								
18	273	116	284	102	41.39	41.60	0.21	0.04
19	257	125	252	138	41.66	41.66	0.00	0.03
21	174	134	158	121	39.52	39.55	0.03	0.01
$16^{\widehat{m}}$ pixel diameter aperture								
18	273	116	283	103	41.16	41.64	0.48	0.03
19	257	125	251	137	41.79	41.77	-0.02	0.03
21	175	134	155	118	39.50	39.52	0.02	0.01

The errors on k′ are estimated from the RMS deviation of the straight line fit to the bright star data. The derived k'_{DK}-magnitudes of stars 18 and 19 can be compared with the magnitudes actually measured in M71DK. The k′ and k for these stars agree within their errors ($2\,\sigma$).

Table 8: Calibration of star 21 on M71DK

FPC79#	DK#	SK#	x_{DK}	y_{DK}	k_{DK}	err	k_{SK}	err	k'_{DK}	err
18	551	551	273	116	16.93	0.03	16.86	0.02	16.80	0.08
19	591	591	257	125	16.98	0.03	16.91	0.03	16.85	0.08
21	—	628	175	134	—	—	14.57	0.14	14.62	0.08

Table 9 lists the k magnitudes of the three stars on the M71DK scale and the zero-points derived from the M71SK and M71DK frames.

Table 9: Corrected magnitudes and zero-points for FPC stars

FPC79#	K_{FPC79}	err	$K_{7.8}^{corr}$	err	K_{10}^{corr}	err	$Z_{7.8}$	err	Z_{10}	err
18	11.55	0.03	11.76	0.05	12.03	0.04	5.17	0.06	4.90	0.05
19	11.94	0.03	11.94	0.04	11.92	0.04	5.04	0.05	5.06	0.05
21	9.54	0.03	9.57	0.03	9.56	0.03	5.05	0.09	5.06	0.09

Stars 19 and 21 give very consistent results, albeit with rather large errors.

The measurements of star 18 obviously contain some unaccounted error, although the weighted mean of the results for the two apertures is 5.01. The errors quoted for the contamination corrections in table 7 are formal errors and do not take into account the large variations that can arise from a small positional offset of the aperture if a contaminating source lies on the edge of the photometric aperture. From the measurements in table 7

it can be seen that one likely possibility is that a contaminating source is partly within the $7.8\widehat{''}$ aperture and fully included in the $10\widehat{''}$ aperture. Thus the likely errors for the photometry of star 18 are larger than those quoted.

6.1.1.3 UKT9 Calibration Observations

Two bright stars that lie within the M71DK mosaic were observed with the single channel bolometer system UKT9 on UKIRT in 1989 June. Observations were made through the $7.8\widehat{''}$ and $12.4\widehat{''}$ apertures. The reduced, air-mass-corrected magnitudes are shown in table 10.

Table 10: UKT9 Observations

Star	$K_{12.4}^{UKT9}$		$K_{7.8}^{UKT9}$		M71DK8#	k(M71DK8)	
A	14.239	0.03	14.20	0.08	227	19.02	0.03
B	11.832	0.03	11.88	0.04	231	17.00	0.01

Again cleaned images were made with all but these two stars subtracted and photometry was performed on M71DK and the cleaned images to work out contamination corrections using the appropriate aperture sizes and good skies. These results are summarized in table 11.

6.1.2 Zero-point from standards observed with IRCAM.

In chapter 1 the standard stars observed during the 1988 May observing run were used to investigate the photometric accuracy and repeatability of IRCAM. PHOTOM was used to measure the bright standards from the UKIRT standards list and three additional faint standards. To use the zero-points derived there, PHOTOM must be calibrated against

Table 11: Zero-points from UKT9 observations

Star	Corr(12.4″)		Corr(7.8″)		K(12.4″,cor)		K(7.8″,cor)		Zpt(12.4″)		Zpt(7.8″)	
A	0.35	0.10	-0.03	0.11	14.59	0.10	14.17	0.11	4.43	0.10	4.85	0.11
B	0.13	0.04	0.07	0.04	11.96	0.04	11.95	0.04	5.04	0.04	5.05	0.04

DAOPHOT magnitudes for stars on M71DK. Using SUBSTAR all but 12 bright, isolated stars were subtracted from the M71DK frame and PHOTOM was performed on these stars using the same parameters of aperture size and sky area as in chapter 1. (N.B. PHOTOM magnitudes differ by 50.0 between chapter 1 and this chapter (for consistency with Guarnieri, Dixon and Longmore, 1991). For convenience, 50.0 has been added to all chapter 1 PHOTOM zero-points and magnitudes quoted here). Table 12 contains the comparison between the PHOTOM and DAOPHOT measurements.

The relative zero-points are shown in figure 14, plotted against magnitude in M71DK. There is no evidence that the residuals from the mean relative zero-point are correlated with position, colour, crowding of the images or position on or off a strip boundary.

A brief consistency check was made by reducing from scratch two frames of the bright standard GL748 taken on the 1988 May 22 and using PHOTOM to measure the stars. The zero-points for these frames came out to within better than 1% of those quoted in chapter 1. Since the bias, dark and sky frames used were not necessarily the same for the two independent reductions this is a encouraging result.

The results for table 4 give a mean relative zero-point which is 0.03 ± 0.02 smaller. This is in the sense that for a given DAOPHOT magnitude the PHOTOM magnitude for the same star will be brighter. This is expected since the PHOTOM magnitudes in table 4 were taken using a 7″ aperture, which includes more of any residual wing component of the stellar profiles. This difference is comparable to that between single-channel photometry with these two aperture sizes.

Table 12: Output of match of PHOTOM and ALS files

Star		M71DK8		PHOTOM		Δk	
	no.	k	err	k	err		err
A	496	16.96	0.04	41.73	0.02	-24.78	0.04
B	480	17.28	0.02	42.00	0.03	-24.72	0.03
C	405	16.75	0.03	41.59	0.02	-24.84	0.03
D	433	18.37	0.02	43.21	0.05	-24.83	0.05
E	121	16.90	0.02	41.75	0.03	-24.85	0.03
F	219	16.92	0.01	41.69	0.02	-24.77	0.03
G	243	16.90	0.02	41.68	0.02	-24.79	0.03
H	448	16.94	0.02	41.72	0.02	-24.78	0.03
I	591	16.98	0.03	41.76	0.03	-24.78	0.04
J	409	17.20	0.04	42.06	0.03	-24.86	0.05
K	231	17.00	0.01	41.82	0.03	-24.82	0.03
L	212	18.25	0.05	43.17	0.05	-24.92	0.07
					Weighted mean	-24.80	
					Standard error of mean		0.01

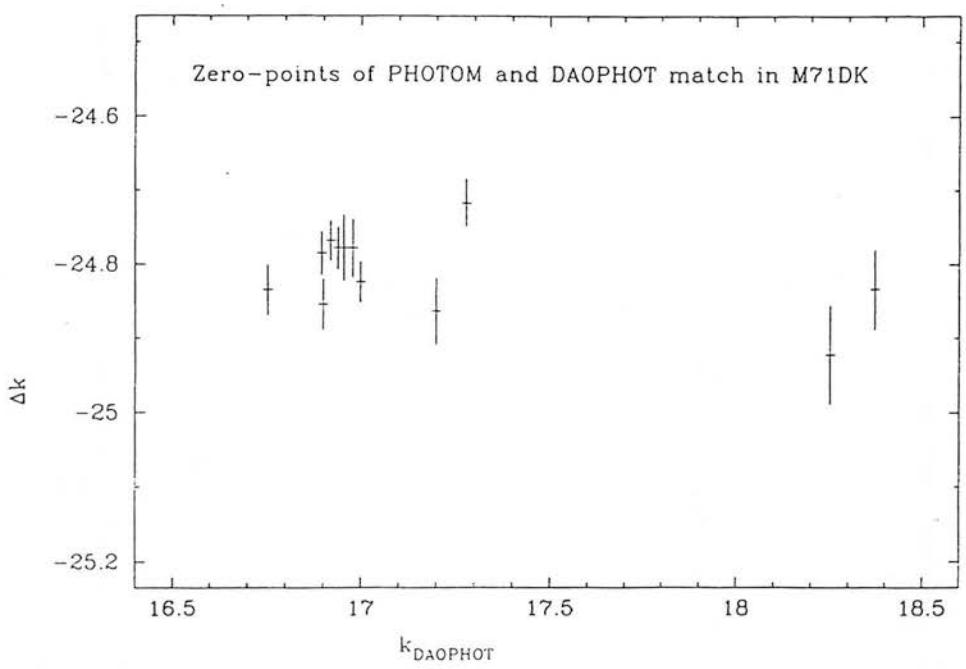

Figure 14: Matching DAOPHOT and PHOTOM in M71DK.

The frames that make up M71DK were taken on the nights of 1988 May 20/21 and 22/23. The frames of M71 were taken towards the end of the night, so the residuals from the zero-points given in chapter 1 were examined to see if there was a trend with time of observation. No clear evidence was found for such a trend, so the mean zero-points for the whole night were used. chapter 1 gives zero-points of 29.877 and 29.907 respectively for these nights so the zero-point for the mosaic as a whole is 29.892 ± 0.015. The chapter 1 magnitudes have been reduced to an air-mass of 1.0, whereas the FPC79 stars used above have been reduced to the more normal 0.0 air-mass. Using the mean air-mass coefficient of chapter 1 of $0^{m}.06$/air-mass the zero-point applicable to the mosaic becomes 29.83 ± 0.02.

Thus the zero-air-mass zero-point for DAOPHOT magnitudes in M71DK8 derived from PHOTOM measurements of standard star frames and bright stars on M71DK is (29.83 ± 0.02) + (-24.80 ± 0.01) = 5.03 ± 0.02.

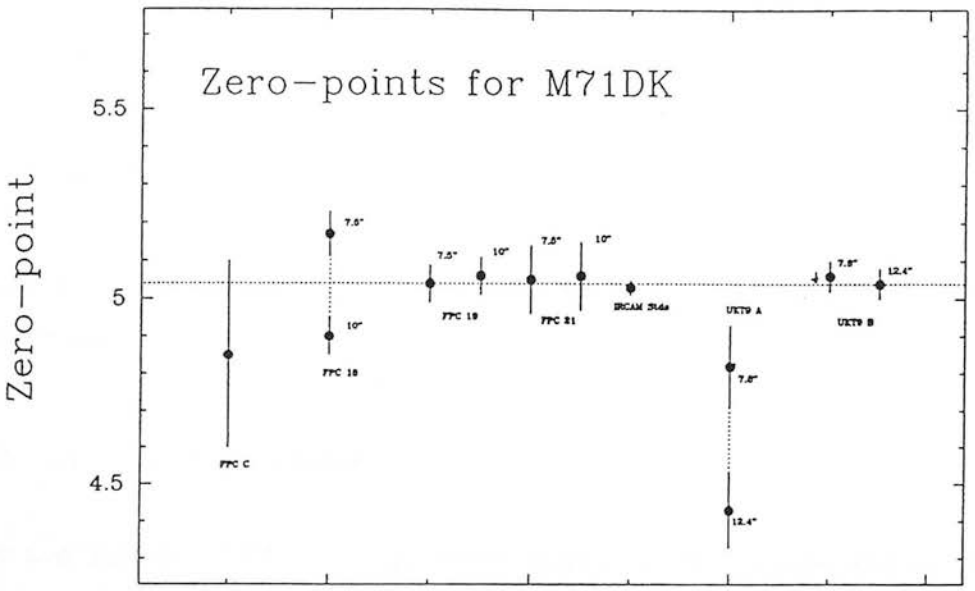

Figure 15: Zero-point estimates for M71.

6.1.3 Final Zero-point

All the zero-points derived above are shown in figure 15. UKT9 star A was excluded from determining the mean. The weighted mean of the points is 5.04 ± 0.02. (Since there are two estimates for some stars, because of the possibility of different apertures being used, these measurements were used at half weight). This is the final zero-point for the M71DK frame and agrees well with the quoted UKIRT/IRCAM zero-point at the time of the observations.

6.1.4 Matching the Deep Images to M71DK

Both the DEEP1 and DEEP2 regions are contained within the M71DK region so it is a simple matter to calculate the relative zero-points of the K data. For each of the four DEEP mosaics a co-ordinate transformation is derived which allows the DEEP and DK magnitudes to be matched up. All the sets match well and the mean zero-points are:

$$K = k_{D11} - (5.16 \pm 0.03) \qquad n = 55$$

$$K = k_{D12} - (5.02 \pm 0.02) \qquad n = 86$$

$$K = k_{D21} - (5.33 \pm 0.02) \qquad n = 83$$

$$K = k_{D22} - (5.65 \pm 0.03) \qquad n = 44$$

These were found in the range $19 \leq k_{DK} \leq 22$, as errors begin to dominate at fainter magnitudes.

6.2 M71: V Zero-points

Arp and Hartwick (1971, AH71) performed photo-electric and photographic photometry for most of the southern half of the cluster down to V $\sim$ 18.5. Cuffey (1973) observed a sequence of standard stars in 1964 as part of a study of the cluster. Cudworth (1985, Cud85) re-observed some of the photo-electric standards from both these studies to characterize the zero-point discrepancy between the two. He also performed photographic photometry from a collection of 25 plates covering most of the cluster. Cudworth's careful analysis of the previous work and his meticulous work on his own data lead to great confidence that his photometry is very close to standard B and V. For this reason all V magnitudes used in this study have been reduced to the Cudworth zero-point. Zdanavičius (1986) took BVRI observations of six giants in M71, finding V magnitudes the same as AH71.

The AH71 data were matched up with the IR images by hand: the IR image was displayed, an AH71 star identified from their finding chart and the cursor used to find its co-ordinates on the IR frame.

6.2.1 Comparing Cudworth and Arp & Hartwick

Cud85 presented BV photometry and membership probabilities from radial velocity and proper motion studies for over 350 stars in M71. The M71DK field was found to lie in the range 100 $\leq$ x $\leq$ -100, 0 $\leq$ y $\leq$ -120 in Cudworth's cluster-centric co-ordinates. All Cudworth's stars in this range were extracted from his Table IV and converted into DAOPHOT ALS format so that they could be matched up to the IR and RF88 data. The following notation was used to preserve Cudworth's naming scheme: stars of the

form KC-n became 3n (e.g. KC-321 is 3321), stars common to AH71 Cudworth called 1-n and 2-n which became 1n and 2n respectively. Stars which did not fit in were I, Y, A3, C and Z which became 4000 - 4005.

Cud85 found a zero-point difference of ΔV (AH-Cud) = 0.057 $\pm$ 0.007 from his photoelectric photometry. Matching up those stars common to both AH71 and Cud85 that lie within the M71DK area produces the correlation in figure 16. The mean zero-point of these data is -0.051 $\pm$ 0.006. The slight slope gives a relation:

$V_{Cud} = 1.03V_{AH} - 0.509$ 0.0509

There is no evidence for a colour term.

It is interesting to note that FPC79 used AH71's V magnitudes in their study of the M71 giants, so that this work may be re-interpreted using the re-calibrated V data.

6.2.2 Comparing AH71 and RF88 data

Matching the AH71 stars with those in the RF88 data gives the correlation seen in figure 17. Since the AH71 data cuts off at V $\sim$ 18.8 the turn-down in the plot is expected, since only those stars which are scattered brighter are detected at the plate limit. The dotted line shows the mean value of ΔV for all the stars with V < 18.0. All of the AH71 data with V>18.2 have been discarded in subsequent discussion since they are unreliable and mainly duplicated in the RF88 data. No convincing evidence was found for a colour term in the relation between the two data sets. Unfortunately the Cud85 and RF88 data sets only overlap for 12 stars at the faint end of the Cud85 data. Considering the small number and poor quality of these data it was decided to use the calibration derived via the AH71 data, which overlaps both Cud85 and RF88 well. Since the Cud85 stars were so sparse they were matched to the RF88 and AH71 data through their common identifications with the IR data. The mean zero-point correction of 1.314 $\pm$ 0.006, shown in the figure, was applied to the RF88 data to bring it on to the AH71 scale. The correction of -0.057 derived above was then applied to bring this data on to the Cudworth scale.

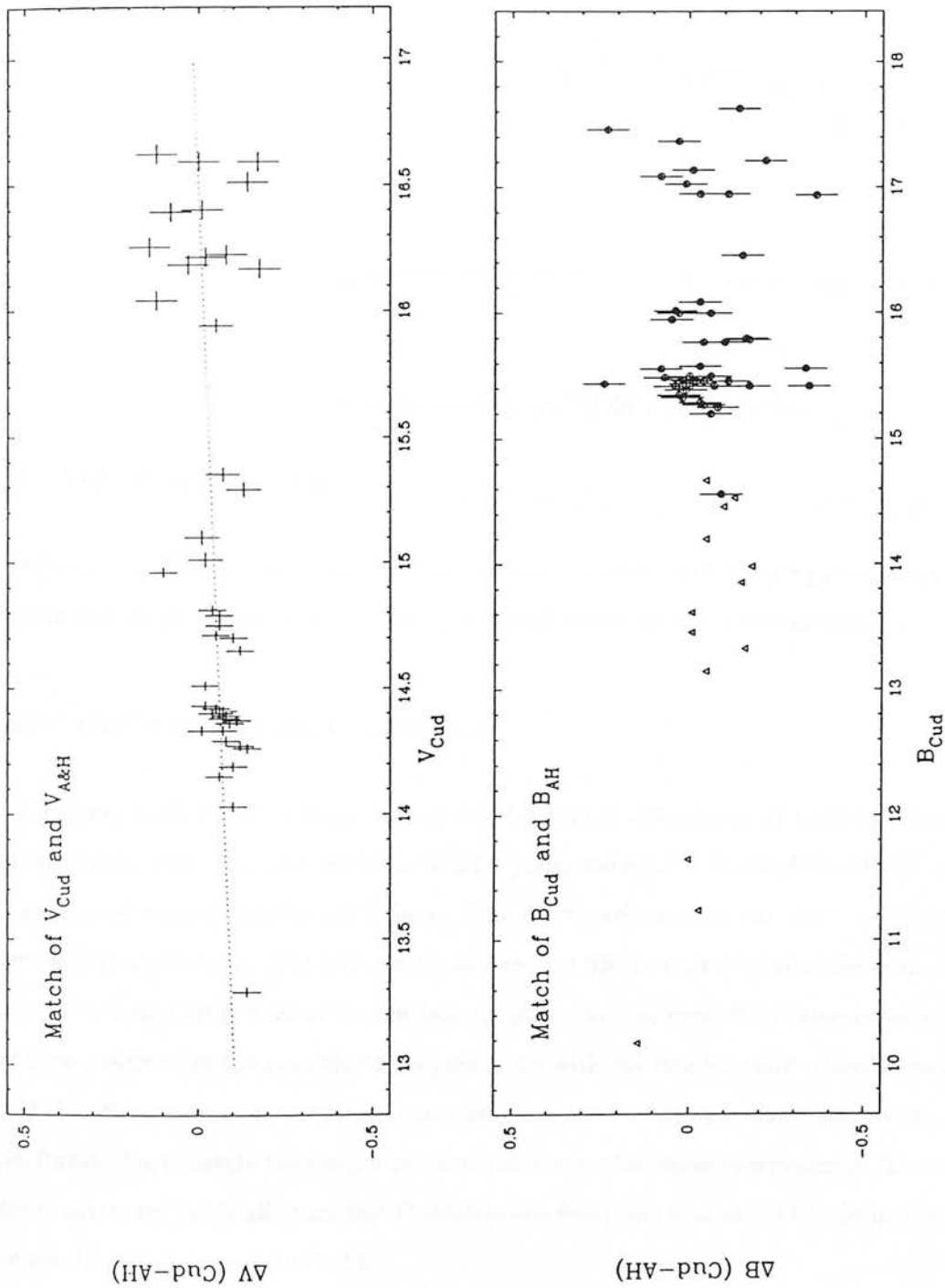

Figure 16: Matching Cud85 and AH71 V and B magnitudes.

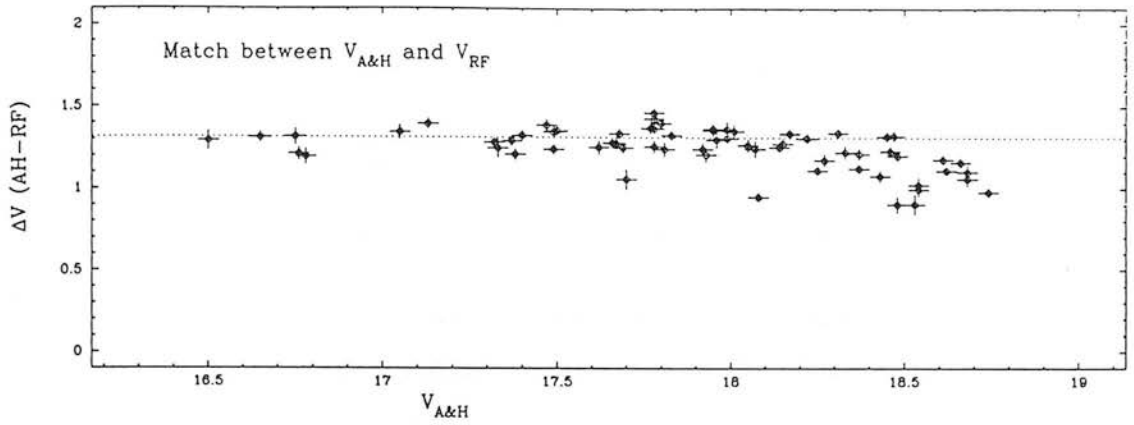

Figure 17: Matching AH71 and RF88 V magnitudes.

6.3 M4: K zero-points

As with the M71 data the UKIRT standards observations and UKT9 photometry of two stars in the large mosaic area can be used to calibrate the M4 photometry.

6.3.1 UKT9 calibration observations

Two bright, fairly isolated stars, which will be simply designated B and C, lying in the M4 large area were observed with the UKT9 photometer at K through the 12.4$\widehat{''}$ and 7.8 $\widehat{''}$ apertures respectively in 1989 June. The observations with the 7.8$\widehat{''}$ aperture have been zero-pointed using only a single observation of SR-3, after applying the correction to this star's K-magnitude noted in the last chapter. An appropriately large error estimate has been assigned to the resulting zero-point. As with the similar calibration observations for M71 a contamination correction must be calculated from aperture photometry on the M4S frame. Fortunately the chop direction was known for these observations. Two frames were constructed with all stars but B subtracted from one and all but C from the other. The results are shown in table 13.

6.3.2 IRCAM standards

As before all but a number of bright isolated stars were subtracted from the M4S frame and aperture photometry was performed using PHOTOM. The resulting mean difference

Table 13: Zero-points from UKT9 observations

	K_{UKT9}	K_{corr}	Zero-point
B	13.11 ± 0.02	13.13 ± 0.06	5.12 ± 0.06
C	15.32 ± 0.09	15.23 ± 0.17	4.99 ± 0.18

between DAOPHOT and PHOTOM for 20 stars was -24.84 ± 0.01, leading to an air-mass corrected zero-point of 4.97 ± 0.02.

The three DAOPHOT zero-point results are shown in figure 18 together with the mean value, 4.99 ± 0.02. The value derived from the aperture photometry of star B is 2σ from the mean. This highlights the difficulty of aperture photometry in crowded fields, even when contamination corrections are possible. It is also possible that the star is variable.

6.4 M4: V Zero-points

Fortunately Cudworth has also studied M4 (Cudworth and Rees 1990, CR90). Clementini (1987) found that the BV photometry of Lee (1977), Cacciari (1979) and Alcaino and Liller (1984, AL84) all agreed well (although she only measured three stars in common with AL84). The Alcaino, Liller and Alvarado (1988, ALA88) and CR90 studies also appear to agree well. The discrepancy in Lloyd-Evans' 1977 photometry is discussed in the M4 chapter. Richer and Fahlman (1984, RF84) do not provide a listing of their photometry but their main-sequence fiducial curve matches that of ALA88 (figure 19; see also VandenBerg and Bell 1985). The IR photometry of Frogel, Persson and Cohen (1983) uses UBV mainly from Lee. Using the values of B and V from CR90 makes little difference.

The present K photometry is matched to the stars in AL84, which were not listed with

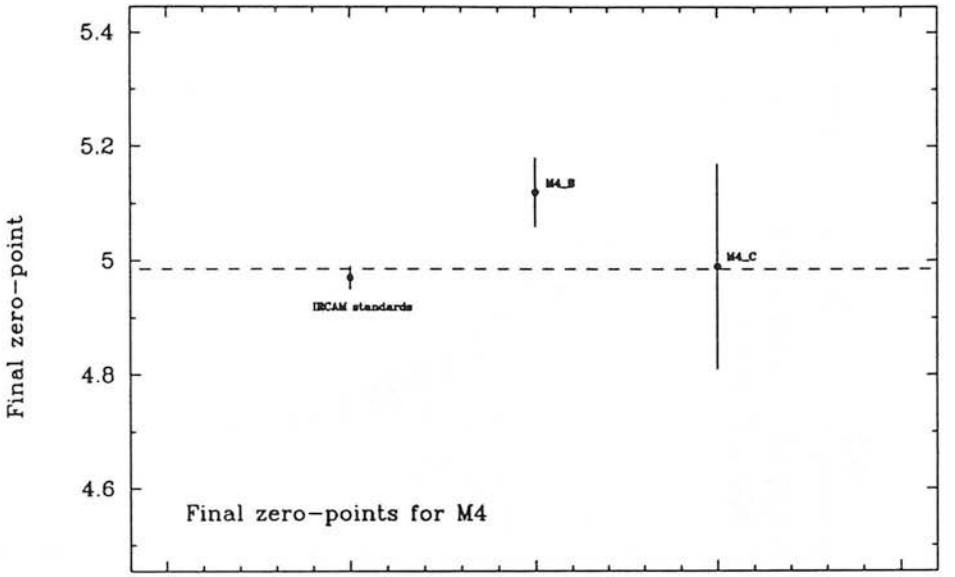

Figure 18: Zero-point estimates for M4.

positions and so were identified on their finding chart and matched to the IR images, with the co-ordinates being taken from the IR data. It is possible that a zero-point problem exists with the AL84 data for the fainter stars. Figure 19 shows the main-sequence fiducials of AL84, RF84 and ALA88, both as published and with an 18% decrease in V in the AL84 data. Clearly the fiducials match better in the region of the turn-off with this shift included. This will be discussed further in chapter 4 where these V magnitudes are used. The colour of the turn-off agrees, within the errors, between the studies, which implies that the AL84 B magnitudes contain a similar zero-point error.

7 Concluding remarks

This chapter has discussed the optimum data reduction of IRCAM mosaic frames, their analysis with DAOPHOT and the calibration of the K data and the previous optical work. Having thus set the scene, the results arising from these frames are discussed in the next two chapters.

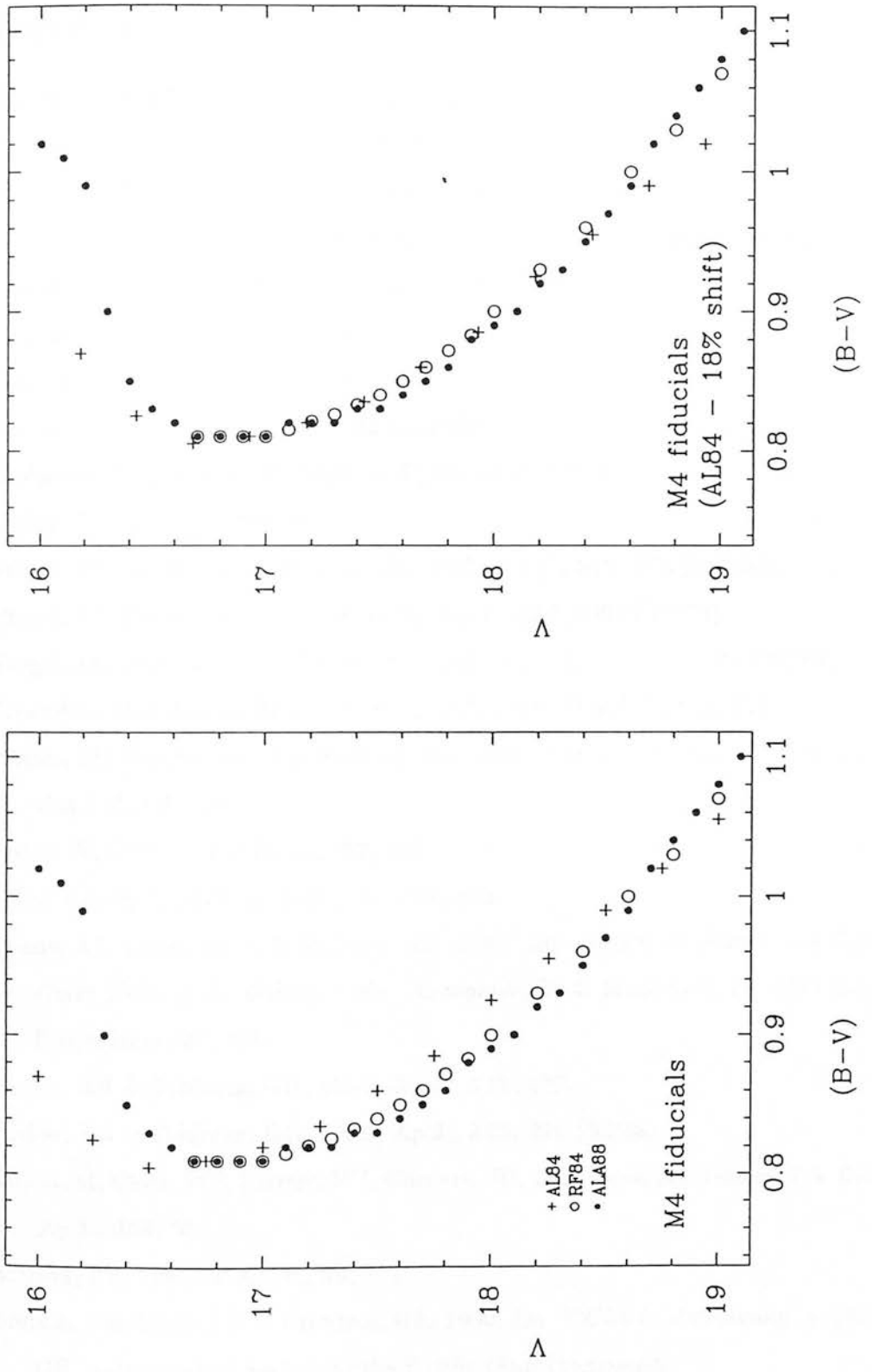

Figure 19: Comparison of the fiducial main-sequences for M4.

References

Alcaino, G & Liller, W, 1984. Ap.J.Suppl., **56**, 19 (AL84).

Alcaino, G, Liller, W & Alvarado, F, 1988. Ap.J., **330**, 569.

Arp, HC & Hartwick, FDA, 1971. Ap.J., **167**, 499 (AH71).

Aspin, C, 1990. *Starlink User Note 41.2*, Starlink Project, Rutherford Appleton Labs.

Bessell, MS & Brett, JM, 1988. P.A.S.P., **100**, 1134.

Cacciari, C., 1979. A.J., **84**, 1542.

Clementini, G, 1987. P.A.S.P., **99**, 637.

Cudworth, KM, 1985. A.J., **90**, 65 (Cud85).

Cudworth, KM & Rees, R, 1990. A.J., **99**, 1491 (CR90).

Cuffey, J, 1973. A.J., **78**, 408.

Frogel, JA, Cohen, JG & Persson, SE, 1983. Ap.J., **275**, 773 (FCP83).

Frogel, JA, Persson, & Cohen, J, 1979. Ap.J., **227**, 499 (FPC79).

Frogel, JA, Persson, SE & Cohen, JG, 1983. Ap.J.Suppl., **53**, 713 (FPC83).

Guarnieri, MD, Dixon, RI & Longmore, AJ, 1991. P.A.S.P., **103**, 675.

Hesser, JE, Harris, WE, VandenBerg, DA, Allwright, JWB, Shott, P & Stetson, PB, 1987. P.A.S.P., **99**, 739.

Lee, S-W, 1977. A.&A.Suppl., **27**, 367.

Lloyd-Evans, T, 1977. M.N.R.A.S., **178**, 353.

Penny, AJ, Lubenow, A & Dickens, RJ, 1987. In: *'Stellar Evolution and Dynamics in the Outer Halo of the Galaxy.'*, eds. Azzopardi, M & Matteucci, F., ESO Conf. Workshop Proceedings, **27**, 401.

Richer, HB & Fahlman, GG, 1984. Ap.J., **277**, 227.

Richer, HB & Fahlman, GG, 1988. Ap.J., **325**, 218 (RF88).

Simon, M, Chen, WP, Forrest, WJ, Garnett, JD, Longmore, AJ, Gauer, T & Dixon, RI. 1990. Ap.J., **360**, 95.

Stetson, PB, 1987. P.A.S.P., **99**, 191.

Stetson, PB, Davis, LE & Crabtree, DR, 1990. In: *'CCDs in Astronomy'*, p.289. Ed. Jacoby, GH. Astronomical Society of the Pacific (San Francisco).

VandenBerg, D.A. & Bell, R.A., 1985. Ap.J.Suppl., **58**, 561.

Zdanavičius, K, 1986. Vilniaus Astron Obs Bull, **74**, 3.

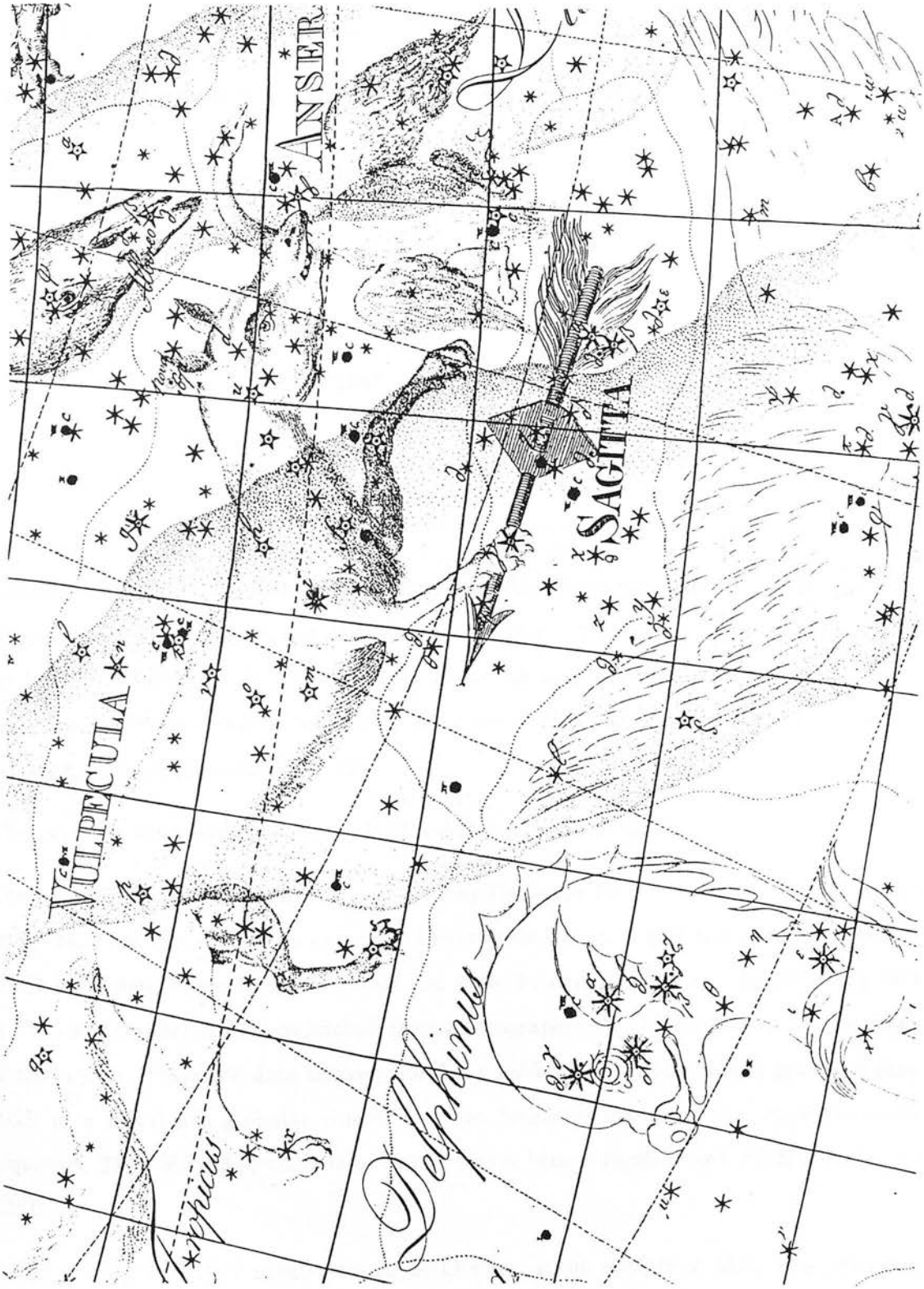

The constellation of Sagitta from Bode's 'Uranographia' (1801).

3. The Globular Cluster M71 Sagittae

1 Introduction

M71 Sge ≡ NGC6838 ≡ C1951 + 186		
$\alpha = 19^h51^m.5$	$\delta = +18°39'$	(1950.0)
$\ell^{II} = 57°$	$b^{II} = -4.6°$	

Located in the small summer constellation of Sagitta, the Arrow, M71 is a diffuse cluster lying in the Milky Way about 10° North of Altair. The first noted observation was by Koehler at Dresden in 1775 who recorded: *'A very pale nebulous patch in Sagitta ...'* (Jones, 1991). It was subsequently included as the 71st object in Messier's famous catalogue of 1781 (see Burnham 1977).

The available photometric data for M71 are summarized in table 1.

The first CMD study of M71 was presented by Cuffey in 1959. Because of its sparseness many believed that M71 was an open cluster rather than a globular cluster. Cuffey's CMD only went down to the HB and did little to end the debate. In 1971 Arp and Hartwick (hereafter AH71) published their photographic and photo-electric observations of the cluster. Their BV data showed the short red horizontal branch and gently sloping RGB of a metal-rich globular cluster and the brightest magnitude or so of the main sequence. They identified what they thought were blue stragglers and AGB stars in the CMD.

Cuffey (1973) took UBV measurements of 13 stars in the vicinity of M71, as a precursor to a further CMD study that has never been published.

Frogel, Persson and Cohen (1979, FPC79) performed single-channel photo-electric photometry on the brightest cluster stars at J, H and K. Combining these with the AH71 V magnitudes they derived physical parameters for the cluster giants.

Cudworth (1985, Cud85) examined the cluster on a collection of plates, primarily to find proper motions for the stars to derive kinematic membership probabilities. In addition he discussed the earlier studies and their zero-point errors.

Table 1: M71 available data

Wavelength	Max*	Min*	Number of stars	Source
U	17	25	11000	RF88
U	9.5	22	48	AH71
U	9.5	16.5	13	Cuffey 1973
B	13	19.5	330	AH71
B	10	15.5	13	Cuffey 1973
B	12	18	350	Cud85
V	12	18.5	330	AH71
V	10	14	13	Cuffey 1973
V	12	17	350	Cud85
V	16	24	11000	RF88
J	8	13	25	FPC79
H	7	12	25	FPC79
K	11	18	1000	this study
K	7	12	25	FPC79

* The magnitude ranges are approximate.

Richer and Fahlman (1988, RF88) presented (U-V)-U CMDs from their UBV CCD observations in a search for white dwarfs.

Together with 47 Tuc, M71 has been one of the crucial calibrators of the high end of the metallicity scale. It is therefore strange that this cluster has been studied so infrequently

and that even the value of its reddening is still poorly determined. M71 is often linked with 47 Tuc since the two have very similar optical CMD morphologies (see, for example, Heasley and Christian 1991), with many authors suggesting that the two clusters have almost identical metallicities, and possibly ages.

In section 2 the standard parameters of reddening, metallicity, distance modulus and age are reviewed from the previous work in the literature. A brief discussion is also made of differential reddening and the value of R, the ratio of total-to-selective absorption. In section 3 the best available photometric data are collected together to form colour-magnitude and two-colour diagrams. Section 4 contains a discussion of IR isochrones and attempts to fit these to the present data. In section 5 a detailed comparison is made with similar optical-IR data for the metal-rich cluster 47 Tuc. This is followed by a very brief discussion of the prospects of fitting a sequence of sub-dwarfs to the main sequence data to obtain a distance estimate. Finally the two-colour diagrams are compared with model predictions.

2 Standard parameters for M71

The next sections summarize the major previous works on M71, with re-interpretations of their results where appropriate. The zero-point problems of previous studies were discussed in chapter 2.

2.1 Reddening

AH71 addressed the problem of deriving the reddening to M71 in two ways. First, they superposed Tifft's 1963 CMD of 47 Tuc onto their M71 data and concluded that there was a (B-V) differential reddening of 0.28 between the two clusters. Using a value of E(B-V) of 0.03 for 47 Tuc, they concluded that E(B-V)=0.31 $\pm$ 0.02. However, Dickens and Rolland (1972) note that Tifft's sub-giant branch has been shown to be too blue. Both this and the 1% blueward zero-point shift in AH71's (B-V) colour, found necessary by Cud85, reduce the derived E(B-V).

AH71 also compared a nearby field star to standard Johnson colours to derive a reddening of E(B-V)=0.31.

Dickens and Rolland matched AH71's CMD for M71 with their new CMD for M107, also a very metal-rich cluster. They found a differential reddening of 0.07 leading to E(B-V)=0.21 for M71 from their E(B-V)=0.28 for M107. However, Longmore et al (1990, hereafter LDSJF90) find a 'mid-range' value of E(B-V)=0.335 for M107 from the literature. This is close to the E(B-V)=0.32 of Sandage and Roques (1984), who included a re-examination of the Dickens and Rolland data in their reddening determination. Using this, and applying the shift of 0.01 to the blue to the AH71 data, gives a value of E(B-V)=0.275 for M71.

It would be possible to follow the method of Sandage and Roques and use the AH71 UBV data for the giant stars to find the reddening from the two-colour (B-V)-(U-B) diagram by estimating a value of $\delta(\text{U-B})_{0.6}$, the UV excess at $(\text{B-V})_o$=0.6, appropriate to the chosen value of metallicity. AH71 used this diagram in the opposite way: they assumed a reddening and measured the UV excess, deducing a relative metallicity. However, given the zero-point problem that exists with both B and V, it seems unwise to put much faith in U, which Cud85 unfortunately did not re-examine.

Burstein and McDonald's 1975 compilation of cluster parameters took a simple average of the Dickens and Rolland and AH71 results, giving a fortuitous value of 0.27 $\pm$ 0.03, which was used by many authors in subsequent multi-cluster studies.

Kron and Guetter (1976) used six-colour photometry of integrated light to derive various parameters for a number of clusters, including E(B-V)=0.20 for M71. In an attempt to assess their consistency, their reddenings can be compared to those of Zinn (1980a) which are also derived from integrated-light measurements and find E(B-V)=0.26 for M71. Reddenings for 37 clusters were compared but, although the Kron and Guetter values were on average 0.039 $\pm$ 0.007 higher than Zinn's, no other significant correlation of ΔE(B-V) was found with reddening, metallicity (from Zinn) or horizontal branch morphology, as represented by Zinn's (1980b) B/(B+R) parameter. A correlation with HB morphology might be expected if the changing ratio of red to blue HB stars was affecting the two filter systems differently. It would seem that the Kron and Guetter reddenings are as good as those found by Zinn. Whilst their value for M71 represents one extreme of the differences between the two data sets it cannot be seen as anomalous.

FPC79 used Cuffey's 1973 photometry of three stars that they believed to be bright main-

sequence stars (blue stragglers) to find a reddening correction of E(B-V)=0.3 from the standard (B-V)-(U-B) diagram for main sequence stars. Cud85 found that one of these stars (Cuffey's star 6) was not a member and that Cuffey's (B-V) colours were all 0.02 too blue. After this correction, the two cluster stars best fit the two-colour diagram at E(B-V)=0.34. This seems a very unreliable number, derived as it is from only two stars and using unchecked U photometry. Also no allowance has been made for a UV excess in the fitting procedure. If the stars really are blue stragglers they may be expected to have anomalous colours, particularly if they consist of close binaries.

Janulis and Straižys (1984) used Vilnius photometry to determine reddenings and distances for 96 stars in the direction of M71, concluding that galactic extinction ranges from E(B-V)=0.12 to 0.32 along this line of sight. Tabulating previous integrated-light reddening estimates for M71, they found an average of E(B-V)=0.29 $\pm$ 0.05.

Cud85 superimposed a 47 Tuc CMD, matching the two clusters at the horizontal branch and RGB to derive a differential reddening of 0.23 $\pm$ 0.02. Using Hesser et al's (1987, hereafter HHVASS87) reddening of 0.04 $\pm$ 0.01 for 47 Tuc, this gives E(B-V)=0.27 $\pm$ 0.02 for M71.

RF88 found E(B-V)=0.28 from their two-colour (B-V)-(U-B) diagram. Although there may be some calibration problems with their magnitudes, the value of $\delta(\text{U-B})_{0.6}$=0.11 that they found from the same diagram corresponds to [Fe/H]=-1 using Butler's (1975) calibration. This is consistent with the value that will be found in section 2.4.

Clearly, a re-examination of the older results shows them to be consistent with the more recent estimates of E(B-V). Taking a mean weighted by the quoted error estimates of the results of Cud85, RF88, Janulis and Straižys, Kron and Guetter and the revised Dickens and Rolland value leads to E(B-V)=0.27 $\pm$ 0.02. If the Kron & Guetter estimate is discounted, the value becomes E(B-V)= 0.274 $\pm$ 0.005. The adopted value for the reddening to M71 is therefore taken to be E(B-V)=0.27 $\pm$ 0.02.

2.2 The value of R

In the next chapter it is shown that there is a convincing body of evidence that points to the value of R, the ratio of total-to-selective absorption, being $\sim$ 4 along the line of

sight to M4. A high value of R has been suggested before and is not unexpected, since the cluster lies behind the Sco-Oph dark cloud complex. However, no-one has suggested that the value of R towards M71 is anomalous. In this chapter both the fits of isochrones and the comparison of the IR-optical data with that for another cluster suggest that a value of R lower than standard, between 2 and 2.5, might be appropriate. The case for M4 is fairly clear, with a good body of data that can be re-interpreted in the light of the revised value of R, but for M71 the data are of lesser quantity and quality.

Is a value of R=2.5 possible ? Certainly the ice-grain models of Whittet and van Breda (1978) extend down to R=2 and fit the data they have for higher R well. However, there are few stars observed to have R less than 3.

One study that may support a lowered value of R is that of RF88. They plotted field DA white dwarf sequences in their (U-V)-V CMD and found that the white dwarf candidates in the cluster lay $\sim 0^{\rm m}.5$ fainter. Changing to R$\sim$2.4 makes all of the candidates lie within their errors of the field lines. There is, however, no theoretical evidence to say that the cluster white dwarfs should be the same as the field ones.

Putting R to a lower value in the multi-cluster study of Frogel, Persson and Cohen (1983) moves M71 away from the regressions in most of their plots, making M71 an anomalous cluster when before it appeared quite normal. The improvement in the position of M4 in these same plots is an important piece of evidence in the argument in favour of R$\sim$4 for that cluster (see next chapter).

In summary it seems unlikely that the value of R is significantly lower than normal in the direction of M71.

2.3 Differential reddening

In any highly reddened cluster there is the possibility that the extinction across the face of the cluster is non-uniform, due to patchiness in the distribution of absorbing material along the lines of sight. It was probably Cuffey in 1959 who first suggested that the photometry of the M71 giant stars contained more scatter than was expected from the internal errors of measurement. Janulis and Straižys (1984) discussed differential reddening, concluding that, if it existed, it amounted to less than ΔE(B-V)=0.1. Cud85

examined the observed width of the RGB and placed an upper limit on any differential reddening present of $0^{m}.05$ in (B-V).

2.4 Metallicity

Table 2 contains a summary of the determinations of [Fe/H] that have appeared in the literature. The following sections discuss those results that may be in error or are changed by using the adopted value of E(B-V).

AH71 used the UV excess, from the Hyades fiducial sequence, of four main sequence stars with photo-electric photometry to derive [Fe/H]= -0.35 ± 0.20. The UV excess of sub-giants and giants gave [Fe/H]= -0.23 ± 0.22. Correcting the photometry as per Cud85 and using the reddening adopted above, these stars can be re-fitted to the Hyades locus. This reduces δ(U-B) by 0.01 for the main-sequence points and increases it to 0.04 ± 0.04 for the giants. Using the same relations as AH71, these correspond to [Fe/H]=-0.30 ± 0.20 and -0.27 ± 0.20. However, see, for example, Ryan (1989) for comments on the accuracy, or rather lack of it, of $\delta(\text{U-B})_{0.6}$ as a metallicity indicator. Also the zero-point of the U observations must be regarded as suspect.

Butler (1975) measured Preston's ΔS parameter for AH71's star Z to find [Fe/H]=-0.04. Unfortunately, Cud85 found a membership probability of 0% for this star.

Canterna (1975) does not list which stars were measured, nor the individual measurements, so no correction can be made in the light of Cud85's membership probabilities.

Bell and Gustafsson (1983) revised their zero-point to agree better with the Searle and Zinn scale, quoting [Fe/H]=-0.5 ± 0.25 for M71. However, they note that the abundance could have been over-estimated by 0.5 dex, due to an opacity source missing from the models, making [Fe/H]=-1.0.

Frogel, Cohen and Persson (1983 FCP83) assumed [Fe/H]=-0.75 for M71 and used it as a calibrating cluster for their [Fe/H]-$(\text{V-K})_{o,GB}$ relation, where $(\text{V-K})_{o,GB}$ is the de-reddened (V-K) colour of the giant branch at $M_{K,o}$=-5.5. Putting their measured $(\text{V-K})_{o,GB}$ back into their derived relationship produced [Fe/H]=-0.60. A revised $(\text{V-K})_{o,GB}$ of 3.81 ± 0.06 may be found from the best fit E(V-K) reddening and distance modulus found later in this chapter, which produce [Fe/H]=-0.77 ± 0.09 from the same relationship, consistent

Table 2: Metallicity estimates for M71

Study	[Fe/H]	error	method
Arp & Hartwick 1971	-0.35	0.20	UV excess of ms stars
"	-0.23	0.22	UV excess of giants
Butler 1975	-0.04	—	ΔS measurement of star Z
Canterna 1975	-0.3	0.3	4-colour Washington giant photometry
Searle & Zinn 1978	-0.22	0.07	spectral scans of giants
Cohen 1980	-1.38	—	high dispersion spectroscopy
Zinn 1980a	-0.36	0.08	integrated light photometry
Bell & Gustafsson 1982	-0.6	—	re-working Searle & Zinn data
"	-0.9	—	best estimate from previous work
Bell & Gustafsson 1983	-0.5	0.25	revised version of Searle & Zinn
Bessell 1983	-0.57	0.25	high resolution spectroscopy
Cohen 1983	-0.81	0.1	high resolution spectroscopy
Frogel, Persson & Cohen 1983	-0.60		[Fe/H]-$(V\text{-}K)_{o,GB}$ relation
Pilachowski et al 1983a	-1.07	0.25	high resolution spectroscopy
"	-0.7	0.2	high resolution spectroscopy
Pilachowski et al 1983b	-1.35	0.3	high resolution spectroscopy
Geisler 1984	-1.04	—	4-colour Washington photometry
Zinn 1985	-0.58	—	revision of earlier result
Bell 1987	-0.4	—	from $(J\text{-}K)_o$
Zdanavičius 1987	-0.44	0.10	Vilnius photometry of 6 giants

with their input assumption.

Zdanavičius (1987) reported on Vilnius photometry for six stars. These were the same six stars observed in the UBVRI system by the same author (Zdanavičius (1986 and 1991, private communication)) so three of them are not cluster members. Both papers used E(B-V)=0.30, but this only makes a few hundredths difference to the derived [Fe/H].

Faced with such a range of metallicity estimates it is hard to give even a mean value. As Bell (1987) discusses, it seems that part of the reason that there is such large range of estimates available for the most metal-rich clusters is the presence of unsuspected TiO absorption in their spectra. In high-dispersion spectroscopic analyses the resulting depression of the continuum is not modelled by spectral synthesis programs, with the result that the equivalent widths of lines are under-estimated, leading to too low a value of [Fe/H]. It is also possible for the TiO bands to blend with the lines being measured, leading to too high a value of [Fe/H].

A simple mean of all the values in Bell (1987) gives a value for [Fe/H] of -0.73. A simple mean of the values listed here (except for Butler's and taking the revised value for FCP83) comes to [Fe/H]=-0.66 $\pm$ 0.35. If the high dispersion spectroscopic results were regarded as suspect the mean of the other results would be 0.51 $\pm$ 0.26. A value of [Fe/H]=-0.7 $\pm$ 0.4 is adopted here.

(Amusing aside: a plot of publication date against [Fe/H] shows that the metallicity of M71 has decreased by $\sim$0.7 dex over the past two decades. Extrapolation shows that it should presently stand at -1.0. No weight whatsoever is given to this result !)

2.5 Distance modulus

Table 3 contains a list of previous determinations of the distance modulus of M71, together with a revised estimate using the adopted E(B-V) where appropriate.

VandenBerg (1983, VB83) used $(m\text{-}M)_V$=13.40 and E(B-V)=0.27 to overlay isochrones onto the AH71 data. VandenBerg and Bell (1985, hereafter VBB85) state that these isochrones are $0^m.1$ too faint in M_V. This means that $(m\text{-}M)_o$=12.68 would produce a match similar to that found by VB83. Since $(m\text{-}M)_o$ was not a free parameter in the isochrone fitting, this value is not included in the table.

Table 3: Distance modulus estimates for M71

Study	$(m-M)_o$	error	$(m-M)'_o$	error	method
AH71	13.07	0.21	12.88	0.25	UV excess of ms stars
FPC79	13.0	0.2	—	—	UV excess of ms stars
"	12.9	—	—	—	assuming $M_{V,o,HB}=0.8$
Cud85	12.8	0.3	—	—	assuming $M_{V,o,HB}=0.8 \pm 0.2$
RF88	12.86	—	12.89	—	fitting sub-dwarfs
LDSJF90	—	—	12.8	0.2	log P - $M_{K,o}$ relation

Although M71 is too metal rich to contain any RR Lyrae variables, the $M_{V,o}(RR)_{-0.3}$ - [Fe/H] relation from LDSJF90 can be used to determine $M_{V,HB}$ and hence the distance modulus from Cudworth's $m_{V,HB}=14.42$. Using a revised version of the relation with R=3.8 for M107 and M4 gives $M_{V,o}(RR)_{-0.3}=0.8 \pm 0.1$ and $(m-M)_o=12.8 \pm 0.2$.

Apart from the VB83 result these values all agree surprisingly well. Assigning error estimates to those values that do not have them, a weighted mean of these (revised) results gives $(m-M)_o = 12.88 \pm 0.09$ (formal error). This corresponds to a distance of 3770 ± 120 pc.

2.6 Age

AH71 used a version of the Iben and Rood (1970) formula to get an age of $7.63^{+3.1}_{-2.3}$ Gyr. VB83 fitted his new isochrones to the AH71 data to find an age of 15 Gyr, although VBB85 state that all ages derived from these isochrones should be extended by about 10%, making ~17 Gyr. Another estimate comes from Hatzidimitriou's (1991) work on the (B-R) colour difference between the mean RHB and the RGB at the HB level. Her calibration is based on Galactic and Magellanic Cloud open and globular clusters and her

result for M71 is an age of 12 ± 2 Gyr. Heasley and Christian (1991) found 16 Gyr from fitting the Hesser et al 1987 isochrones to their preliminary (B-V)-V CMD, although this result awaits confirmation from the larger and better data set on which they are currently working (Heasley 1991, private communication).

Of these results only that of Hatzidimitriou comes from a large, well-calibrated sample. It will be interesting to see Heasley and Christian's final estimate of the age of M71.

The simple mean of all these results (apart from that of AH71) of 15 ± 2 Gyr is adopted.

2.7 Summary

The adopted parameters for M71, taken from the literature and made as consistent with each other as possible, are:

$$E(B\text{-}V)=0.27 \pm 0.02 \qquad t=15 \pm 2 \text{ Gyr}$$
$$(m\text{-}M)_o=12.88 \pm 0.09 \qquad [Fe/H]=-0.7 \pm 0.4$$

The error estimates are a reasonable reflection of the spread in the reported estimates.

3 The colour-magnitude and two-colour diagrams

The present data.

In this section the data are brought together to construct the colour-magnitude and two-colour diagrams. In addition the observed width of the main-sequence is analyzed.

The data available for constructing CMDs and 2CDs were summarized in table 1. The zero-point problems were discussed in the last chapter. Membership probabilities are available only for those stars in Cud85, which includes most of the FPC79 stars. A proper calibration was unavailable for the U data of RF88. Although RF88 do mention B-band photometry, this is believed to contain a linearity problem and so has proven impossible to calibrate properly. It is not listed in table 1.

The IR data of FPC79 were taken using the CTIO filter system, but Bessell and Brett

(1988) show that there is no difference between this and the standard Johnson system at the 2% level.

3.1 The colour-magnitude diagrams

Figure 1 shows the (B-V)-V, (V-K)-V and (V-K)-K CMDs for M71, constructed from the data listed in table 1. The diagrams containing (V-K) are the deepest IR-optical CMDs yet constructed, with an appreciable number of stars, for any globular cluster.

The (B-V)-V CMD uses all the data of AH71 and Cud85 that lie in the M71DK area, regardless of membership probability. One magnitude of the main sequence is visible, as are the bright giants and the horizontal branch. The large scatter in the middle section is due mainly to the large errors on the faintest Cud85 data.

The (V-K)-V CMD shows all the stars measured with DAOPHOT errors smaller than $0^m.5$ in the M71DK mosaic which have been matched up with V magnitudes from AH71, Cud85 or RF88. These data stretch from the faintest stars to just above the horizontal branch. In addition, the FPC79 giant observations are shown, using their K-band magnitudes with the AH71 V magnitudes, corrected to the Cud85 scale. The morphology of the plot is very similar to that of the (B-V)-V plot and bears a close resemblance to AH71's original CMD both in shape and photometric depth.

In comparison with the (B-V)-V diagram for the same region, it can be seen that the HB has become far more tightly defined, the GB is somewhat tighter and a clump in the GB half a magnitude below the level of the HB has become apparent. All the points brighter than V$\sim$15 use the same V magnitudes in both plots, so that the improved tightness of the various sequences is due purely to the change from (B-V) to (V-K). This is of course due to the expansion of the colour axis - since (V-K) is two or three times as sensitive to temperature as (B-V) (see Fernley 1989), the errors of measurement in a range of (V-K) will be only half as dispersive as in (B-V). The GB clump is very interesting and is similar to one seen in the 47 Tuc CMD of HHVASS87. This will be discussed further in the section comparing the two clusters. The diagonal cut-off due to the K data is obvious in the faint, blue corner of the diagram.

The (V-K)-K CMD, whilst containing the same information as the (V-K)-V diagram,

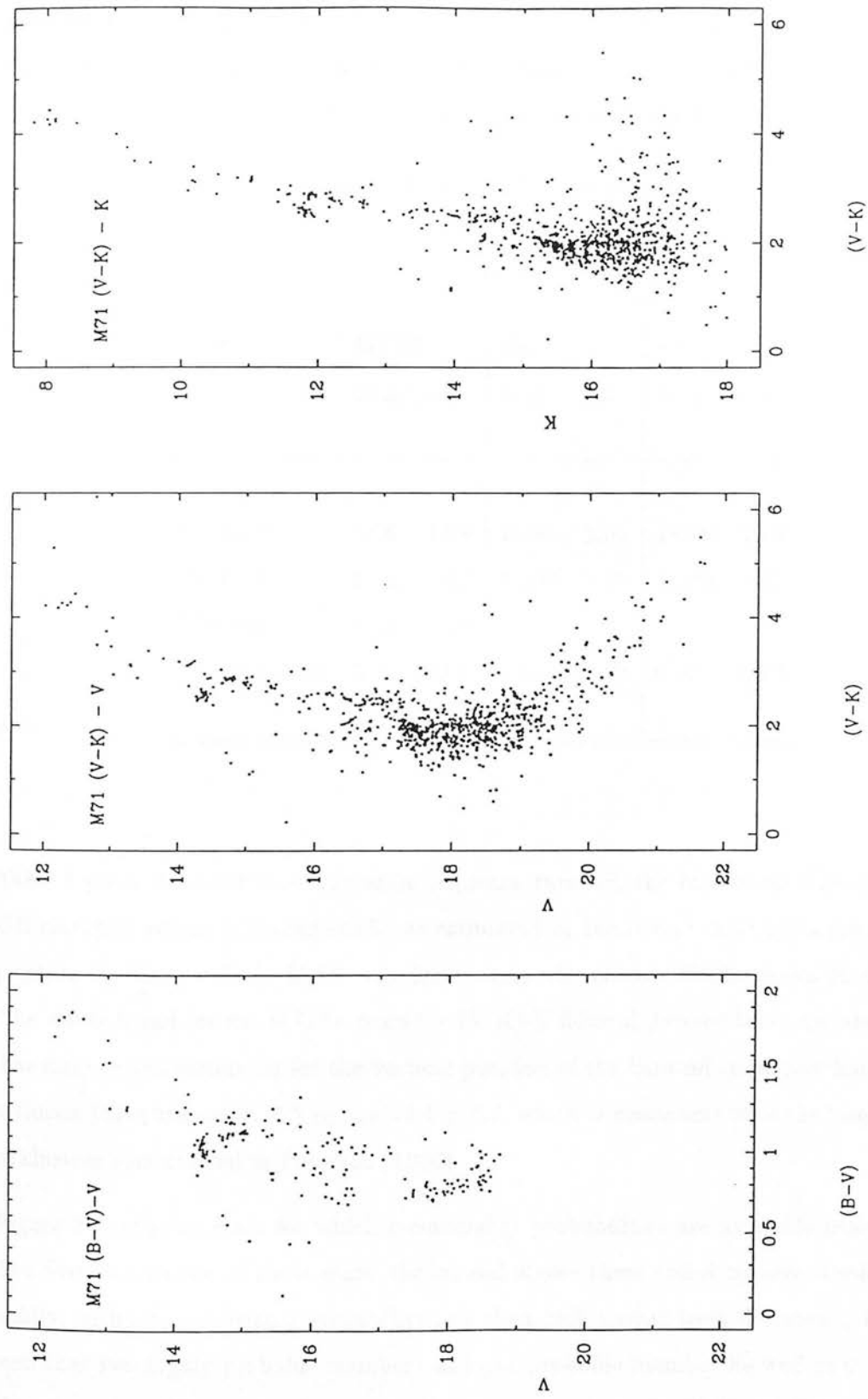

Figure 1: The (B-V)-V, (V-K)-V and (V-K)-K CMDs for M71DK, using all available data.

looks rather different. The RG stars cover a wider range in K, the HB is almost at the same level as the GB clump and the transition between the main sequence turn-off and the base of the GB has become steeper. The clumps and upper GB appear even better defined. The cut-off in the present K data is obvious at K~17.5.

Table 4: Measured CMD parameters

Diagram	MSTO		HB		GB clump	
	mag	col	mag	col	mag	col
(V-K)-V	17.6	1.94	14.40	2.54	14.80	2.89
(V-K)-K	15.9	1.96	11.80	2.56	11.93	2.87
Fiducial	17.9	1.80	—	—	—	—
Typical error	0.3	0.04	0.01	0.02	0.01	0.02

Table 4 gives the position of the main-sequence turn-off, the horizontal branch and the GB clump in colour and magnitude, as estimated in the two (V-K) CMDs (the turn-off position for the (V-K)-K CMD was found from the cleaner CMD shown in figure 6). The values found for the MSTO, from the (V-K)-V fiducial derived later, are also shown. The large errors estimated for the vertical position of the turn-off show how hard it is to estimate this parameter. $\Delta V_{TO-HB}=3.4 \pm 0.2$, which is consistent with the large sample of clusters summarized in Peterson (1986).

Figure 2 shows the stars for which membership probabilities are available from Cud85. The first plot shows all these stars, the second shows them coded by membership probability, with all stars with a probability less than 20% having been discarded. It can be seen that two highly probable members and one probable member lie well to the blue of the other stars. These stars lie in a similar position in Cud85's (B-V)-V CMD. They will be discussed in section 3.2 on the two-colour diagrams.

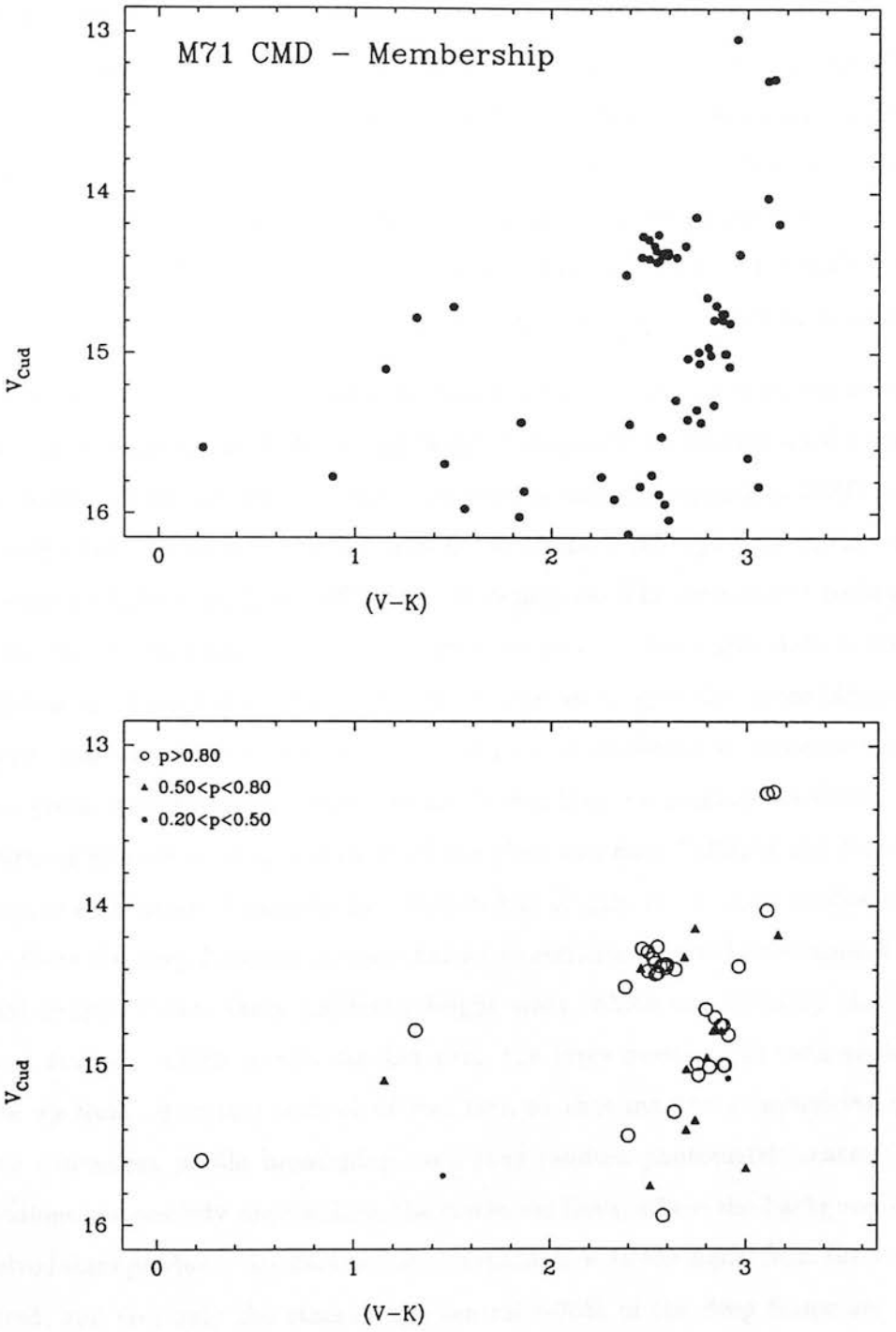

Figure 2: The (V-K)-V CMD for stars with membership probabilities from Cud85. The upper plot shows all the stars with an estimate of membership probability; the lower plot shows those stars with p>0.2.

What interesting objects might be found in the CMD ? Due to M71's position near the plane of the Galaxy, many field stars are expected to contaminate the CMDs. The existence of main-sequence binary stars is discussed in section 3.1.1. RF88 discovered several cataclysmic variable (CV) candidates in M71. Driuker, Fahlman and Richer (1989) and Machin et al (1990) conducted follow-up studies, which concluded that at least the brightest candidates are single, field white dwarf stars. Unfortunately CVs would be too faint and too blue to be detected in the K images. Also Machin et al concluded that, due to the cluster's sparseness, there is only a 1 in 3 chance of any CVs forming in M71.

In addition to the large mosaic, pairs of deeper mosaics were taken in two areas of the cluster. Figure 3 shows the (V-K)-V and (V-K)-K diagrams for the combined pairs of deep frames, together with the FPC79 data. Comparison with the large-area CMD in figure 1 shows very similar structure, with the deep-frame CMDs reaching a little further down the main sequence before the K cut-off begins to dominate. The ratio of the total exposure times for the central portion of the deep mosaics and the large-area data is 2000/210s. In addition the deep-frame sets have been paired up to give 19x more integration on each star. Naïvely this corresponds to a four-fold improvement in signal-to-noise: that is, for a given error the deep frames should be reaching 1.5 magnitudes fainter. In fact the practical difference, judged from the RMS plots and final CMDs of the data (see last chapter), is only about 1 magnitude. This deficit of gain in accuracy is due to several effects: (i) in the deep frames it is *much* harder to construct a good point spread function (see last chapter) since there are fewer bright stars, which are probably close to each other, in the area which is ~8x smaller than the large mosaic; (ii) each stellar image is made up from 10 frames instead of just two, so that inaccurate mosaicing produces position dependent profile broadening, and thus random photometric scatter; (iii) the observations are possibly approaching the confusion limit, where the background of faint unresolved stars produces sky fluctuations comparable with the signal from the stars being measured, and (iv) only the stars in the central ~30% of the deep frame are in all 10 frames, receiving the full integration, the rest receiving successively less, 10x less for the small regions at the four corners. Thus, whilst the deep mosaics do indeed go deeper than the large mosaics, the signal-to-noise improvement is not as great as might be predicted.

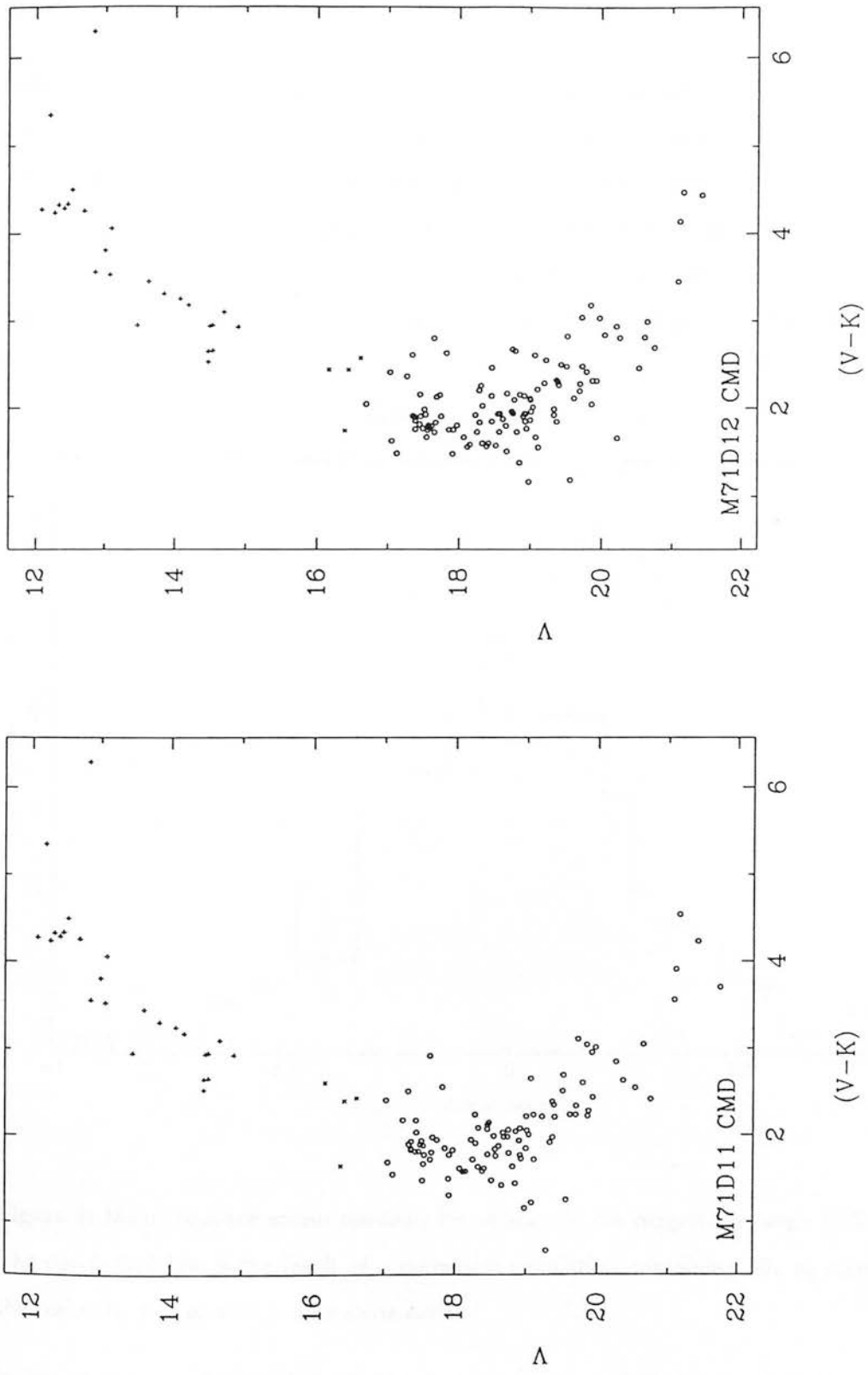

Figure 3: The deep-frame CMDs, with the giant branch observations of FPC79.

3.1.1 Main-sequence morphology

When a fiducial sequence is constructed in the CMD (see the last chapter and section 4 of this chapter), it is possible to examine the horizontal (colour) structure of the main-sequence stars. The solid line in figure 4 shows the histogram of the residuals from the mean in each $0^{m}.25$ vertical (magnitude) bin of all stars in the interval 17.3<V<19.6. This interval covers the main sequence stars from the turn-off to the faintest data for which a fiducial can be constructed, with a dispersion in colour of less than $0^{m}.1$.

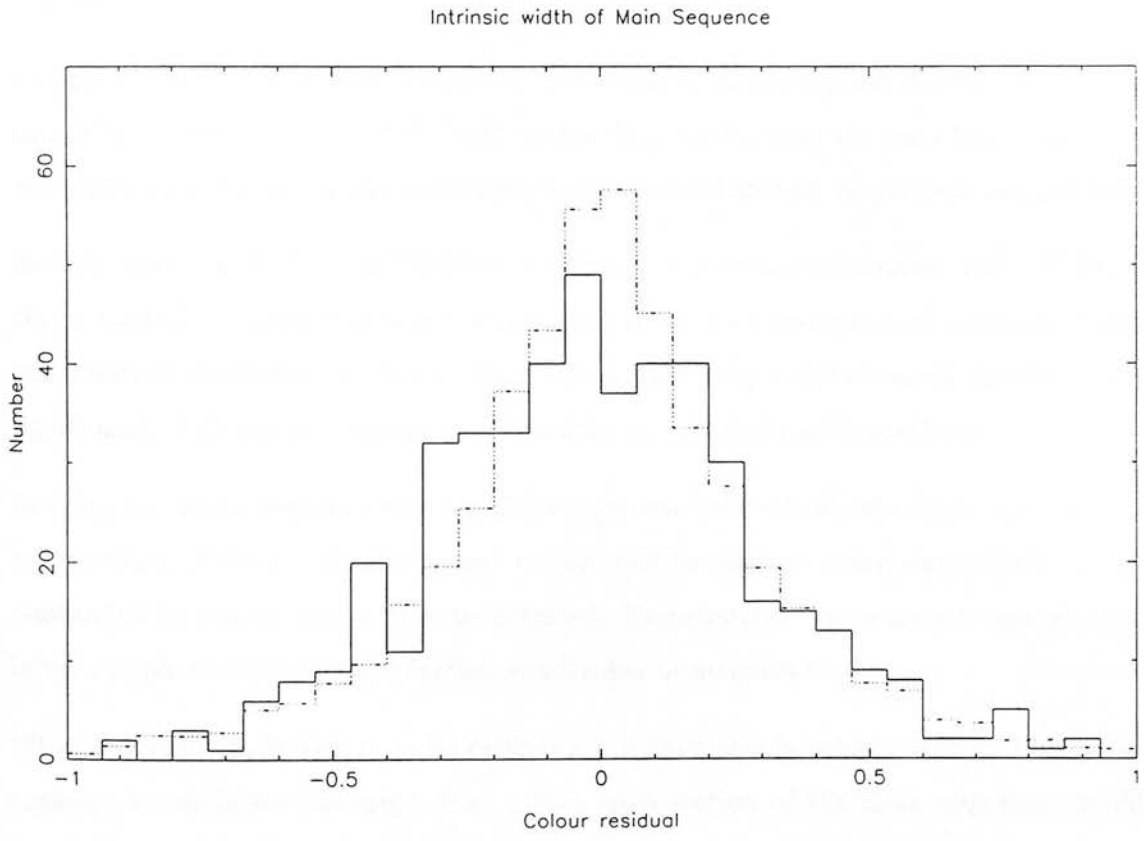

Figure 4: Main sequence colour residuals for all stars in the magnitude range 17.3<V<19.6. The dot-dashed line is the result of a numerical simulation containing 10x as many stars as the real data, but plotted on the same scale.

In both Stetson and Harris's (1988) M92 observations and Piotto et al's (1990) M30 data an excess of stars is seen to the red of the main-sequence fiducial line. Both studies concluded that at least part of this excess was due to binaries. Stetson and Harris suggested that, because of the crowding and pixel scale of their observations, between 2 and 10% of

main sequence stars might be unresolved pairs (that is, visual rather than physical binaries). However, they failed to show that this was the case from measured image roundness parameters, which might be expected to give away close multiple images.

It was mentioned in the last chapter that in the reduction of the IR data, stars were sometimes identified as a single star whilst appearing as two images in the V data. Since these multiple cross-identifications were all rejected, there should be few, if any, such objects left in the present data. The stellar profiles are sufficiently well sampled in the optical data that, given the normal atmospheric seeing, all pairs that can be separated will have been.

In figure 4 there is an excess of stars in the central $0^{m}.5$, making the distribution appear rather flat topped. The (V-K)-V CMDs for the deep frames show the same broad shoulders and something of a red excess, although there are less stars and so the data are less clear.

In their study of 47 Tuc, HHVASS87 performed a similar examination and concluded that a Gaussian distribution was a satisfactory fit to their histogram of residuals. Using the standard procedures in Fisher (1963) shows that the present observed distribution is significantly different in shape from a Gaussian at the 99% confidence level.

Dividing the main sequence into smaller magnitude intervals should show that, for the fainter stars, there is a significant red excess, due to the increasing importance of contamination by sources too faint to be detected. Unfortunately there are not enough stars in the sample to allow it to be further subdivided in magnitude.

What residual distribution is to be expected ? If each star is subject only to Poissonian counting errors in its measured flux, a thin cross-section of the main sequence should resemble a Gaussian distribution. However, a cross-section over a range of magnitude will be a sum of such Gaussians, with increasing width as the stars become fainter. This will produce a distribution that is more centrally peaked than a single Gaussian.

The dot-dashed line in figure 4 is a synthetic distribution of stars over the same range as the observations. This has been generated so that for each real star in the data there are 10 synthetic stars drawn randomly from a Gaussian distribution, with a width appropriate to stars of that K magnitude, as determined from the artificial star experiments discussed in chapter 2. The standard deviation of the Gaussian, σ, is obtained from the deviation in these experiments, δ, by assuming that δ is the probable error so that $\sigma = \delta/0.6745$

(as stated in Stetson and Harris, 1988). The synthetic distribution is plotted so that it is directly comparable with the observations and is a good match to the observations except that the real data show broader 'shoulders' at -0.25 and 0.25 in colour. However, a Kolmogorov-Smirnov test shows that the two distributions cannot be said to be different at more than the 80% level of confidence. If the (small) errors in the V magnitudes were also included, the synthetic distribution would be broadened and fit the observations even better. It must also be remembered that the (unknown) field star distribution is still affecting the observed colour residuals.

The simplest hypothesis, that the stars in the main sequence form a simple, unique sequence in colour and magnitude that is broadened by simple Poissonian counting errors, is therefore acceptable.

Were the observed shoulders to prove to be real, they could be due to the existence of a secondary sequence of stars, consisting of binaries and unresolved pairs of stars, running parallel to the main sequence, confusing the calculation of the mean in the fiducial calculations, and broadening and flattening the central region.

3.2 The two-colour diagram

Using the present K magnitudes and the B and V magnitudes of Cud85, and including stars from FPC79, the (V-K) - (B-V) diagram shown in figure 5 was constructed for those stars with membership probabilities greater that 50%. The stars using the FPC79 K magnitudes match up well to those using the present ones.

Three stars (Cud85's KC-234, KC-268 and AH71's I-255) are much bluer than the rest of the data (KC-234 is so blue that it is not plotted in figure 5). These are the stars mentioned in section 3.1 and appearing as blue straggler candidates in figure 2. In the next chapter, the dereddened two-colour data for M4 and M71 are overlaid in figure 14. In that diagram the three very blue stars are plotted without any de-reddening and are found to lie on the line defined by the two sets of cluster stars; indeed, if they were de-reddened by the same amount as the cluster data, they would all shift off the cluster relation. Star KC-234 lies above the cluster line (redder in (B-V)). Although this star has two close, bright companions, and is therefore unlikely to be as precisely measured as other stars of similar brightness, it lies off the cluster locus in the correct sense and by

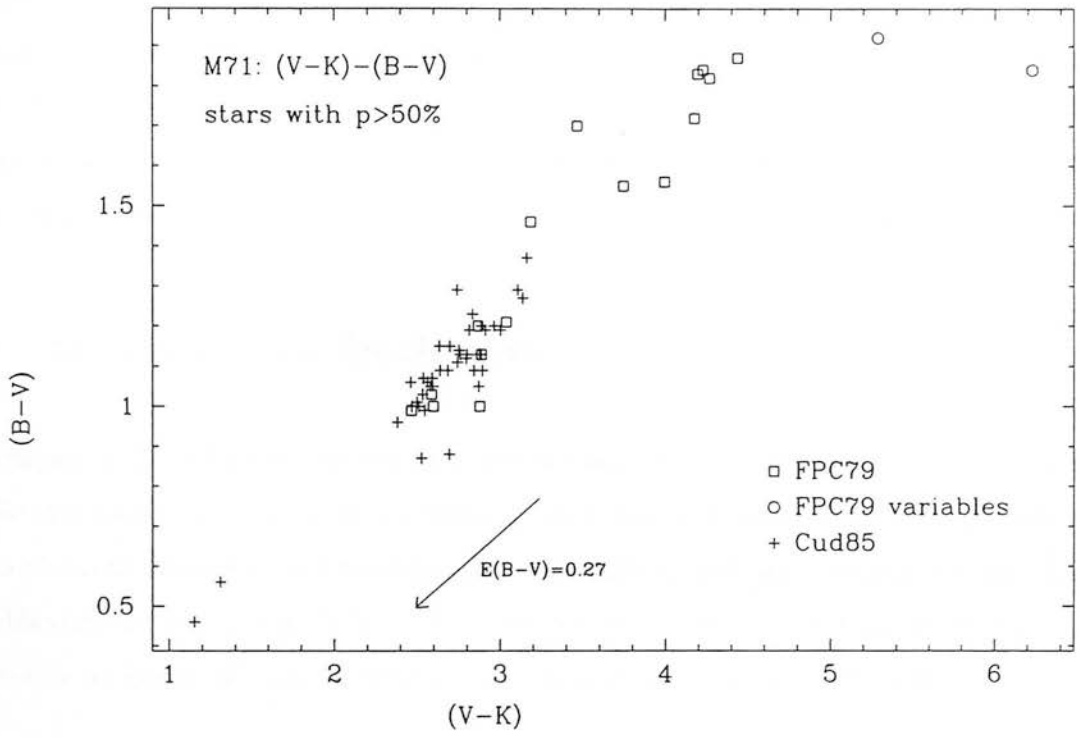

Figure 5: The (V-K)-(B-V) diagram for M71 for stars with more than 50% probability of being cluster members.

approximately the correct amount to be a field star of solar metallicity.

The kinematics of M71 are not sufficiently different from the local disc galactic dynamics for the field star separation to be completely successful. (Thus M71 is a good example of the metallicity population separation of the globular clusters, with those clusters with [Fe/H]>-0.8 being governed by thick-disc-like dynamics (Zinn, 1985)). It is easily possible that these three stars are field stars whose peculiar velocities make them appear to be cluster members. If this is so and the stars suffer little extinction, then KC-268 and I-255 have the same intrinsic colours as the RHB and MSTO stars in M71. In figure 1 they appear 2.5-$4^{m}.0$ brighter than the MSTO so that if they are sub-dwarfs this corresponds to a distance from us of 0.6-1.2kpc or 20-30% of the distance to M71 (thus the assumption of small reddening could be true).

It seems highly probably that all three of these objects are field stars.

3.3 Summary

The colour-magnitude and two-colour diagrams have been constructed from the available data. They can now be compared to the predictions of stellar models and to observations of other clusters. In addition, three blue-straggler candidates have been shown to be consistent with being field stars. No significant fraction of binary stars has been detected on the main sequence.

4 Matching with isochrones

Comparing CMD data to isochrones is now a common-place procedure in optical studies. The isochrones are now so well developed that they can match very well the shape of the observed sequences and reliably predict metallicity and age, and confirm the chosen reddening and distance modulus. This is not to say that they are not mis-used also. Until recently no isochrones were available that included the K band in any detail.

The fitting procedure adopted here is simply to find the offsets in colour and magnitude that allow a metallicity-family of isochrones to fit to the shape of the observations. In this way E(B-V) and $(m\text{-}M)_o$ are found as part of the fitting procedure. If the models provide accurate predictions, the best-fitting isochrone will produce values for the reddening and distance modulus that are consistent with the adopted values, lending greater weight to the derived metallicity and age. The reddening data of Martin and Whittet (1990, MW90) are used to derive colour excess ratios.

The only comprehensive set of isochrones covering the IR-optical passbands is that of Bell (1992) which is based on the calculations of Bergbusch and VandenBerg (1991). (These IR isochrones will henceforth be referred to as the BBVB isochrones). Roger Bell has kindly provided machine readable versions of these ahead of publication. The isochrones cover 10 metallicities in the range -0.48 $\geq$ [Fe/H] $\geq$ -2.26, with ages of 8, 10, 12, 14, 16 and 18 Gyr and with [O/Fe] varying as a function of [Fe/H] (as listed in table 5).

These isochrones are still somewhat preliminary. Bell's comparison, in the T_{eff}-(V-K) diagram, with the Saxner and Hammarbäck (1985, SH85) F dwarfs ((V-K) coming from the observations of Johnson et al (1966)) and the stars common to the IR photometry of Glass (1974a,b), and the IR flux-method work of Bell and Gustafsson (1983), suggests

that the calculated isochrones are $\sim 0^{m}.12$ too red. Since the major features in the (V-K)-V CMD agree very well in magnitude with the comparable Straniero & Chieffi (1991, hereafter SC91) (B-V)-V isochrones, this translates into making the K magnitude $0^{m}.12$ fainter. The situation is somewhat more complex, in that the colour-shift necessary to reconcile observations and theory is itself a function of colour. Clearly this is rather disappointing and will be discussed a little further in section 7.

In the following sections the isochrones have been used as supplied, with subsequent discussion of the effects of zero-point changes on the derived parameters. Since $(m\text{-}M)_o$ and reddening are left as free parameters in the adopted fitting procedure, changing the colour and magnitude zero-points of the isochrones changes the derived $(m\text{-}M)_o$ and reddening, but does not affect the best-fit metallicity and age.

The M71 data were matched to these isochrones in both the (V-K)-V and (V-K)-K diagrams. Clearly these two diagrams contain the same information, but their different morphologies may bring out features in one that are less easily seen in the other, so that the isochrones may be easier to fit in one than the other. Also, simply having two goes at fitting the same data will hopefully reduce the random errors in the derived parameters.

First the best data were selected. The data for the deep and large areas that used the RF88 Vs were combined, so that every star that was measured in more than one frame was taken as the weighted mean of the measurements. A fiducial sequence was then constructed as discussed in the last chapter. The data were binned at $0^{m}.25$ intervals in the magnitude axis and any star was rejected as a field star if it lay more than $0^{m}.6$ from the mean point. The data were then cut at 2.5σ from the mean in each bin. This procedure reduced the data from over 600 stars down less than 200. The data at the bottom of the magnitude range are not reliable since (a) they have large error estimates, (b) they are so sparse that the fiducial means were not reliably determined and (c) they are biased towards the red in (V-K) by the cut-off in the K observations.

The stars with Cud85 V magnitudes for which he found a membership probability greater than 50% make up the SGB and some of the HB and GB. The remaining GB and HB data are those of FPC79 for which p>50%.

This is the best IR-optical CMD data for use in isochrone fitting that can be derived from the available observations. The (V-K)-V and (V-K)-K CMDs are shown in figure 6.

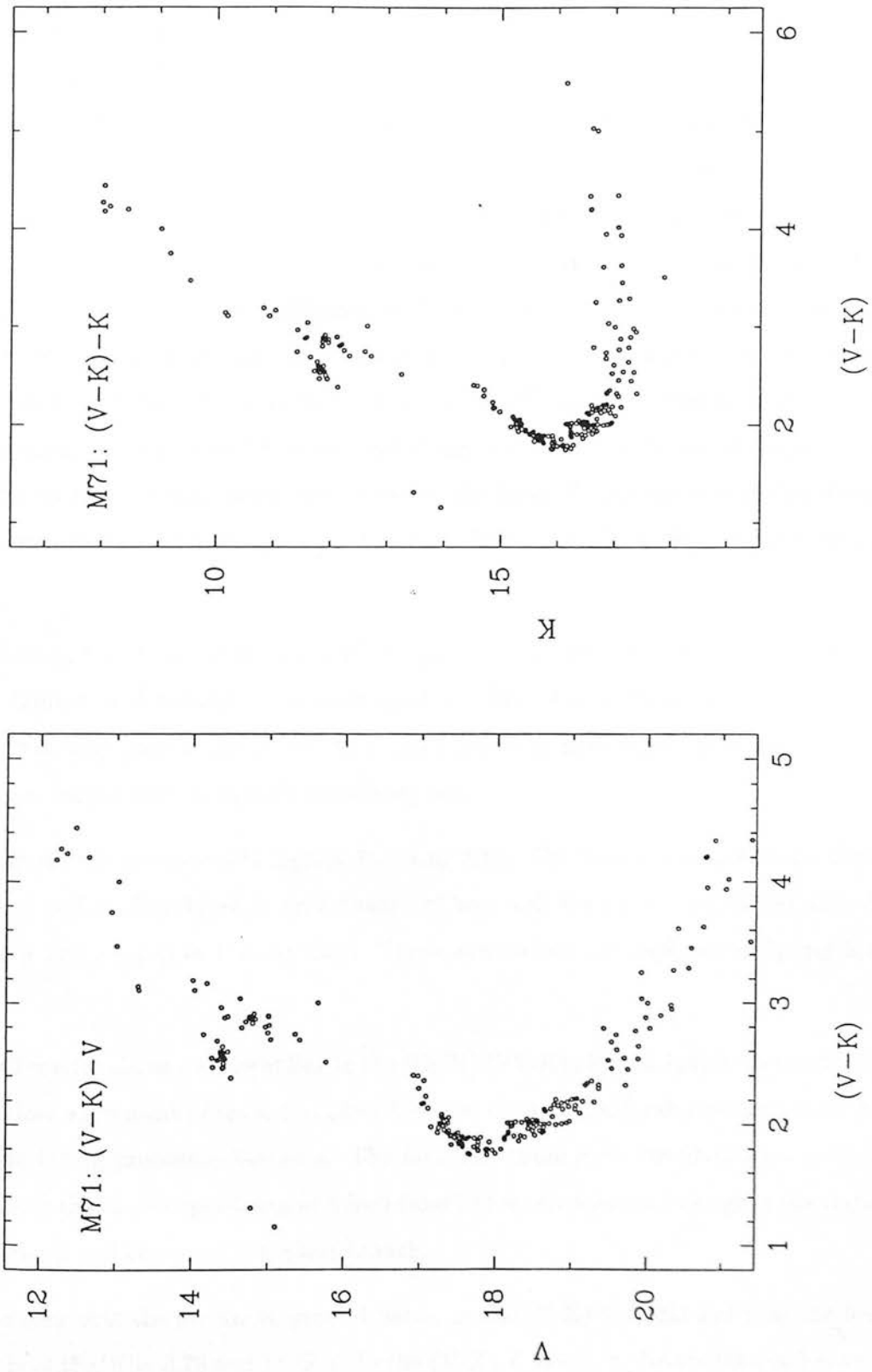

Figure 6: 'Best' (V-K)-V and (V-K)-K CMDs for isochrone fitting.

These data were fitted for every combination of age and metallicity, allowing $(m\text{-}M)_o$ and E(B-V) to vary freely. The fitting was done by eye. It might seem more appropriate to devise a statistical fitting technique based on the deviation of all the observed points from each isochrone. This would make the systematic fitting errors more uniform. However, examination of the data shows that a simple fit of this kind would be inappropriate, since all the stars in the HB region would have to be removed lest they bias the fit. The GB is already sparse enough without removing further stars. Also, the small clump at the base of the giant branch ((V-K)$\sim$2.5) would have to be given low weight because its fiducial position was calculated from a small number of stars. The errors on individual stars could be convolved in some way with the errors in the calculation of each fiducial point, but there is still a great deal of leeway in the choice of 'good' and 'bad' stars and clumps and in the assigning of weights to these stars and clumps. This process is just as subjective as fitting the data by eye and so was not explored. No form of automated isochrone fitting has been reported in the literature and the results below entirely justify the use of fitting by eye.

Whilst fitting, the clump at the base of the giant branch was considered at low weight and the faintest and reddest stars were ignored. The observational data were shifted arbitrarily in both axes to get a best fit to each family of isochrones. It was found that there was a unique best fit to each metallicity set.

The isochrone fits are shown in figures 7(a) and 7(b). The fitting parameters are listed in tables 5 and 6. Also listed is an estimate of how well the isochrones fit the data on the scale A (very good) to F (very bad). These parameters are displayed in figures 8(a) and 8(b).

The small scatter about a straight line in the [Fe/H]-E(V-K) plots in figures 8(a) and 8(b), and the close agreement of these two plots between the two CMDs shows how consistent the by-eye fitting procedure has been. The fact that these plots are fitted by a straight line confirms the small dependence of colour (and hence temperature) on age in the region of the turn-off and the lower sub-giant branch.

It can be seen that the fits are in general better in the (V-K)-V CMD and that the best fit of all is at [Fe/H]=-0.78 and 13 Gyr. In the (V-K)-V diagram, discrimination between metallicities is rather easy with the top of the giant branch matching the theoretical

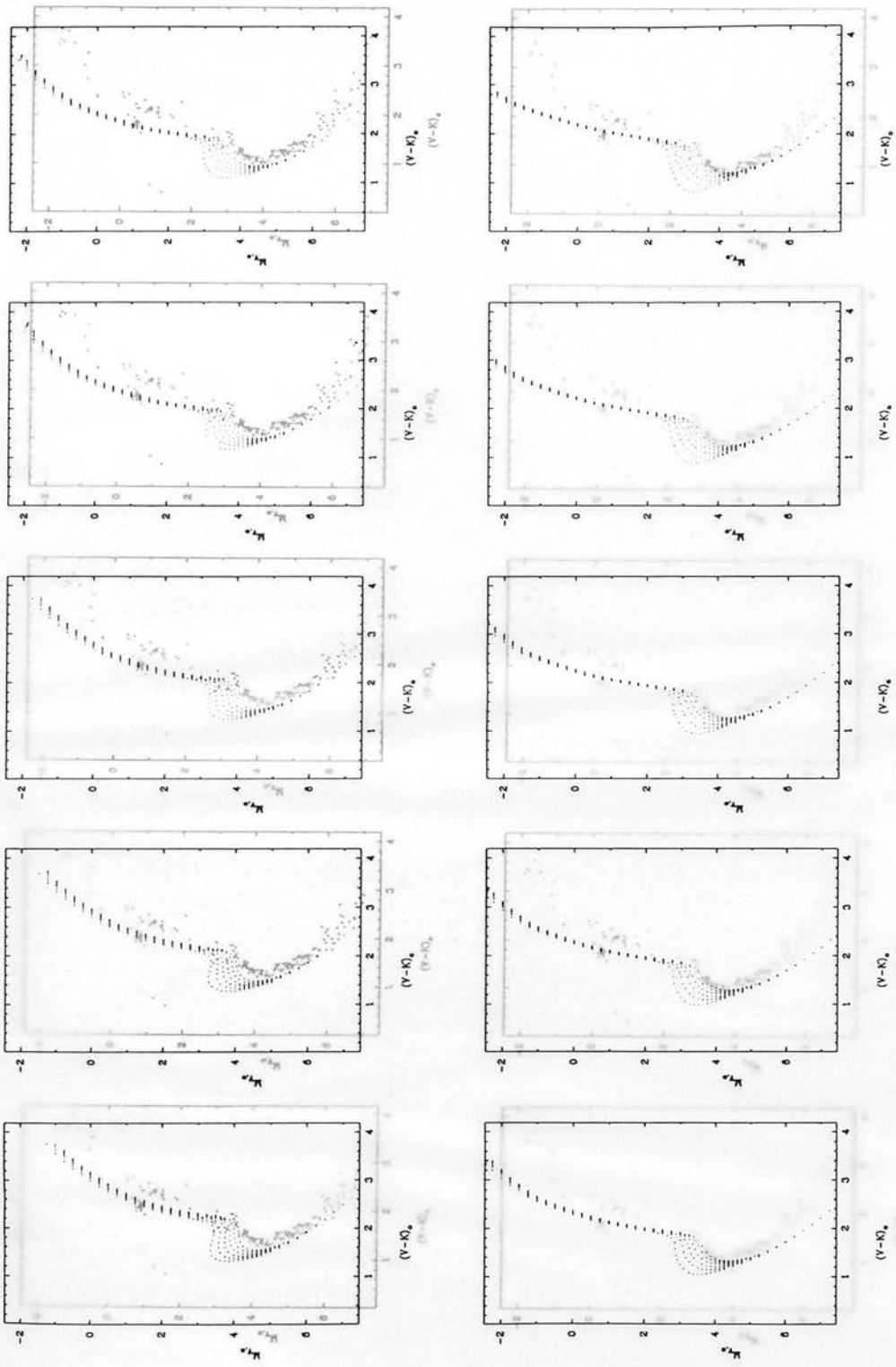

Figure 7: (a) Isochrone fits to the (V-K)-V CMD. The actual fitting procedure took place on full-size plots.

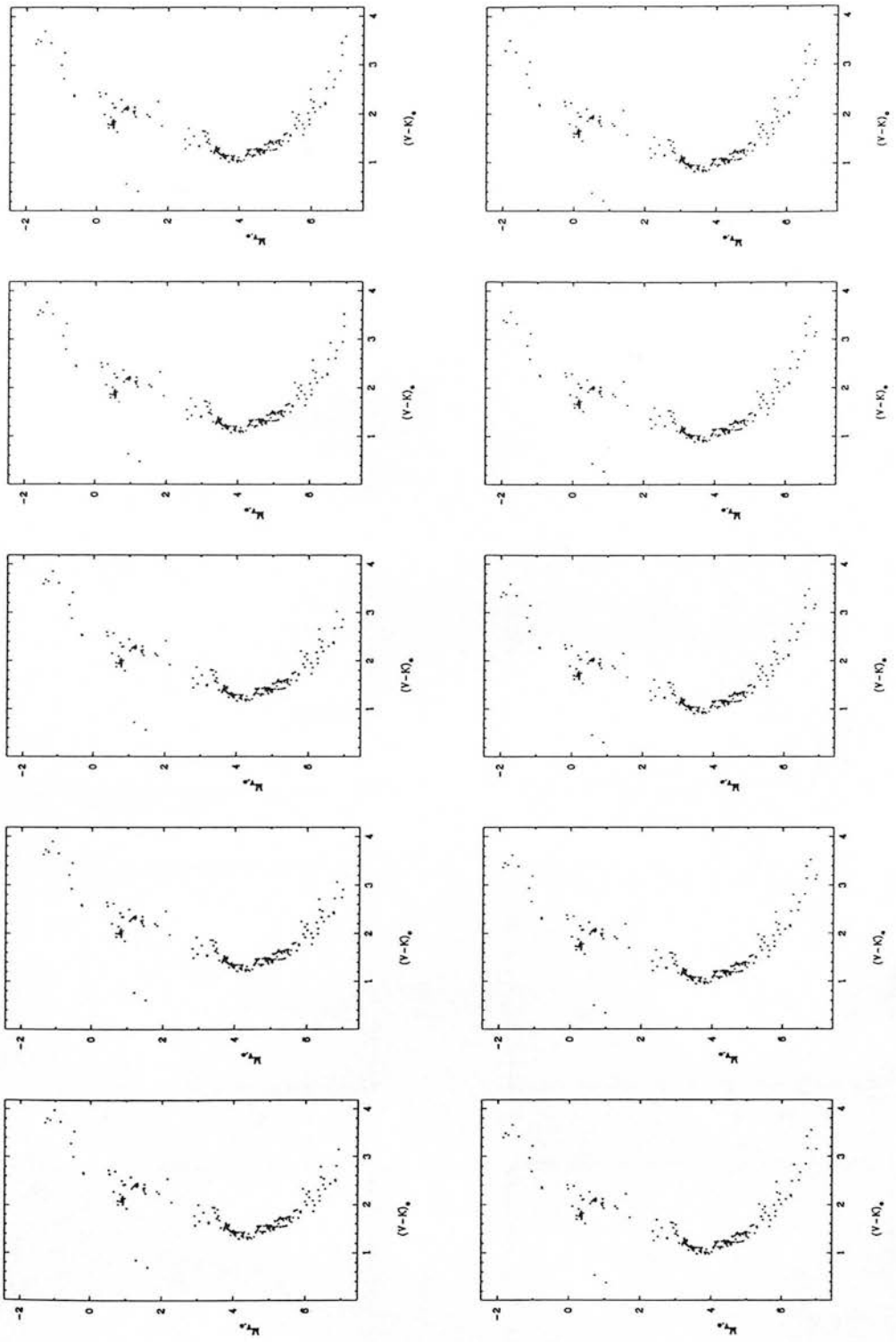

Figure 7: (a) Isochrone fits to the (V-K)-V CMD. The actual fitting procedure took place on full-size plots.

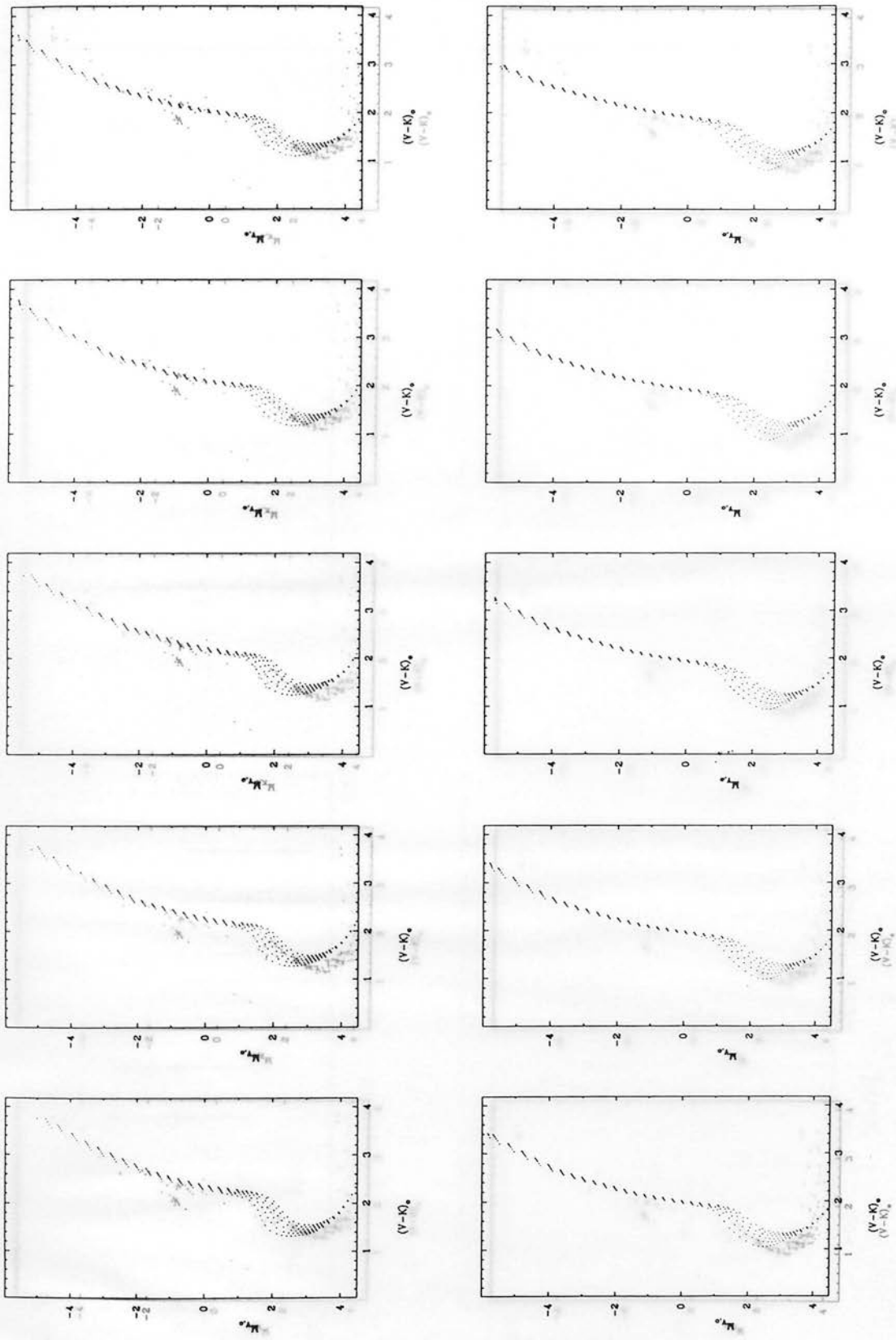

Figure 7: (b) Isochrone fits to the (V-K)-K CMD.

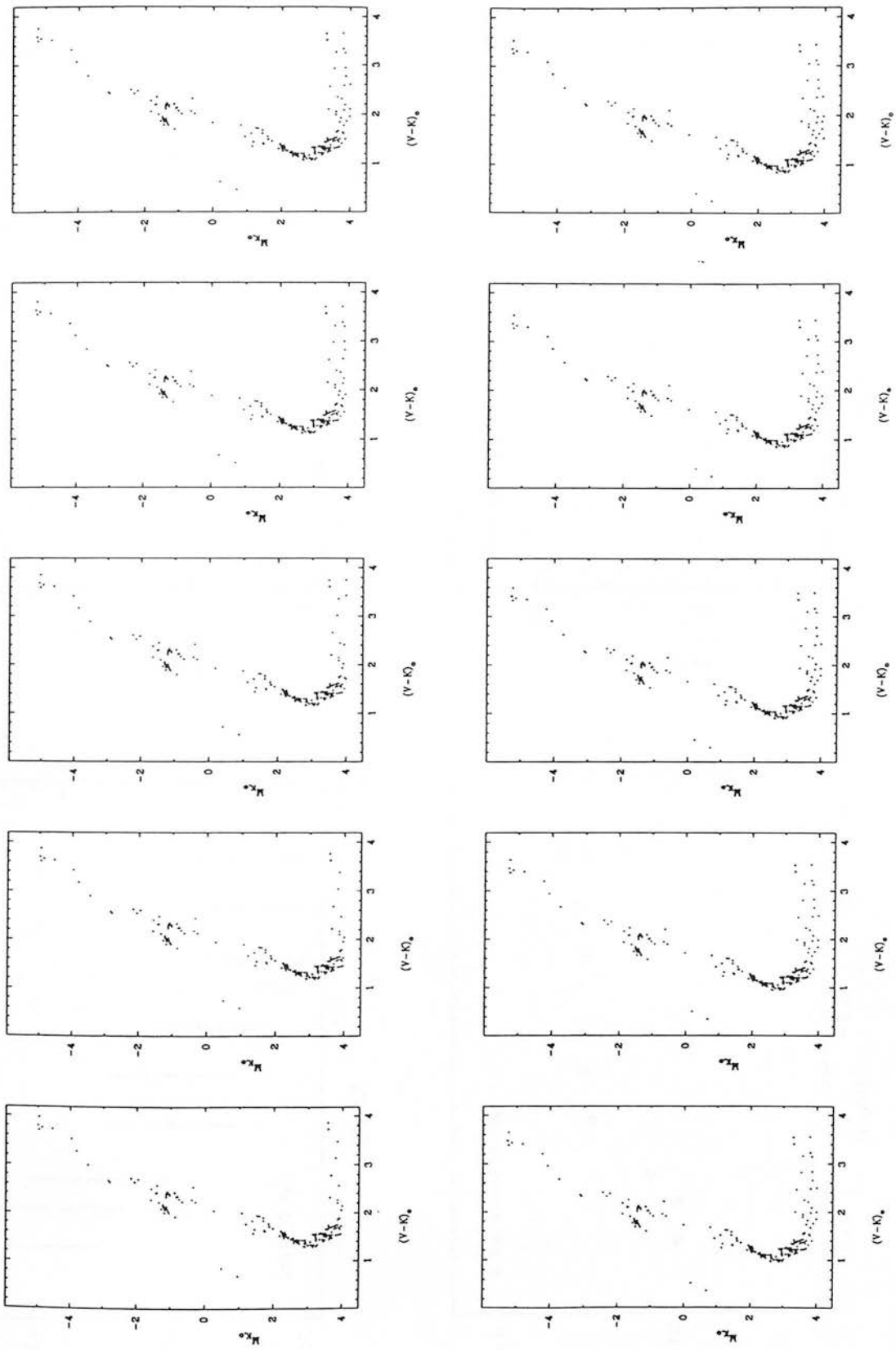

Figure 7: (b) Isochrone fits to the (V-K)-K CMD.

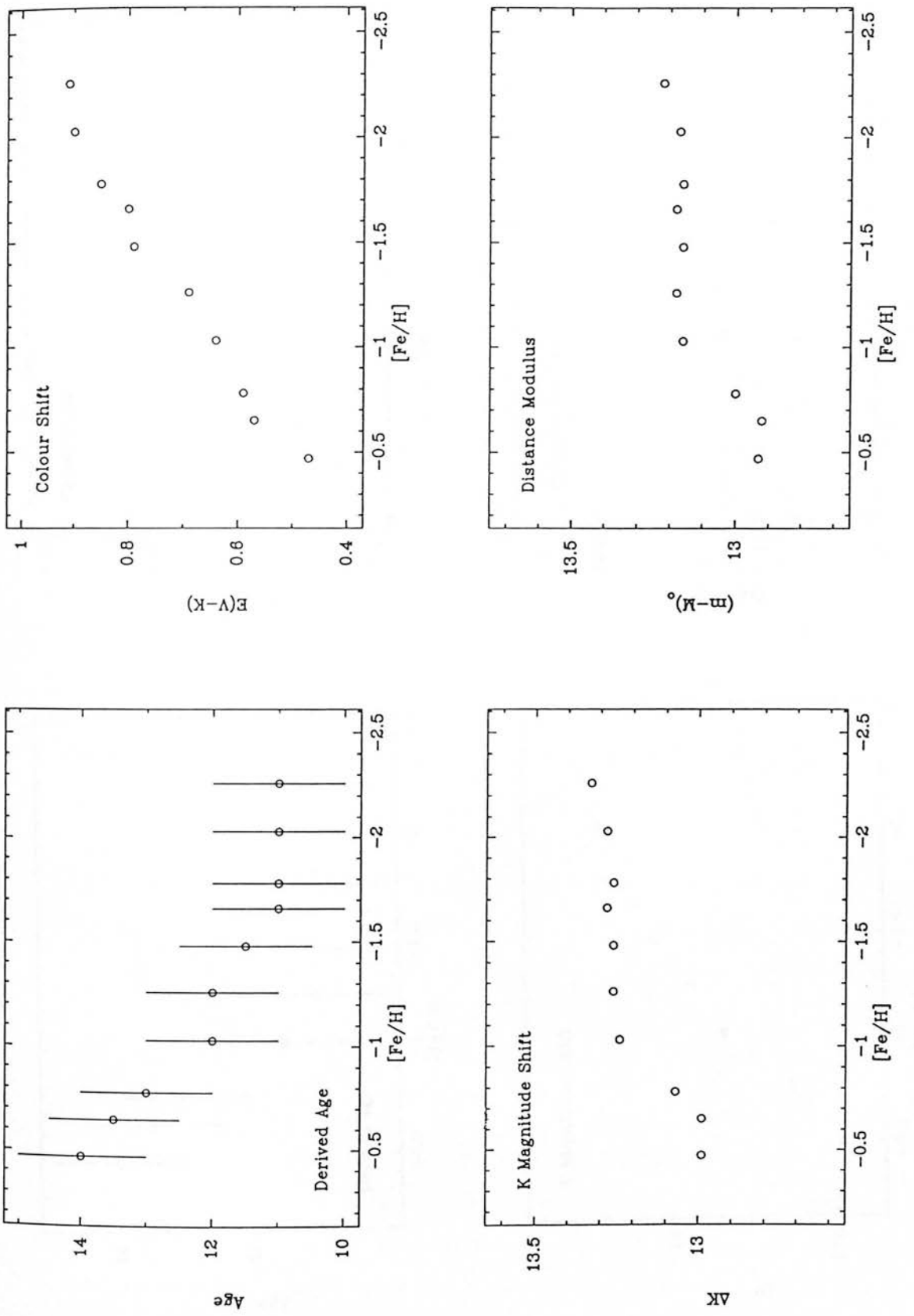

Figure 8: (a) Fitting parameters from (V-K)-V fits.

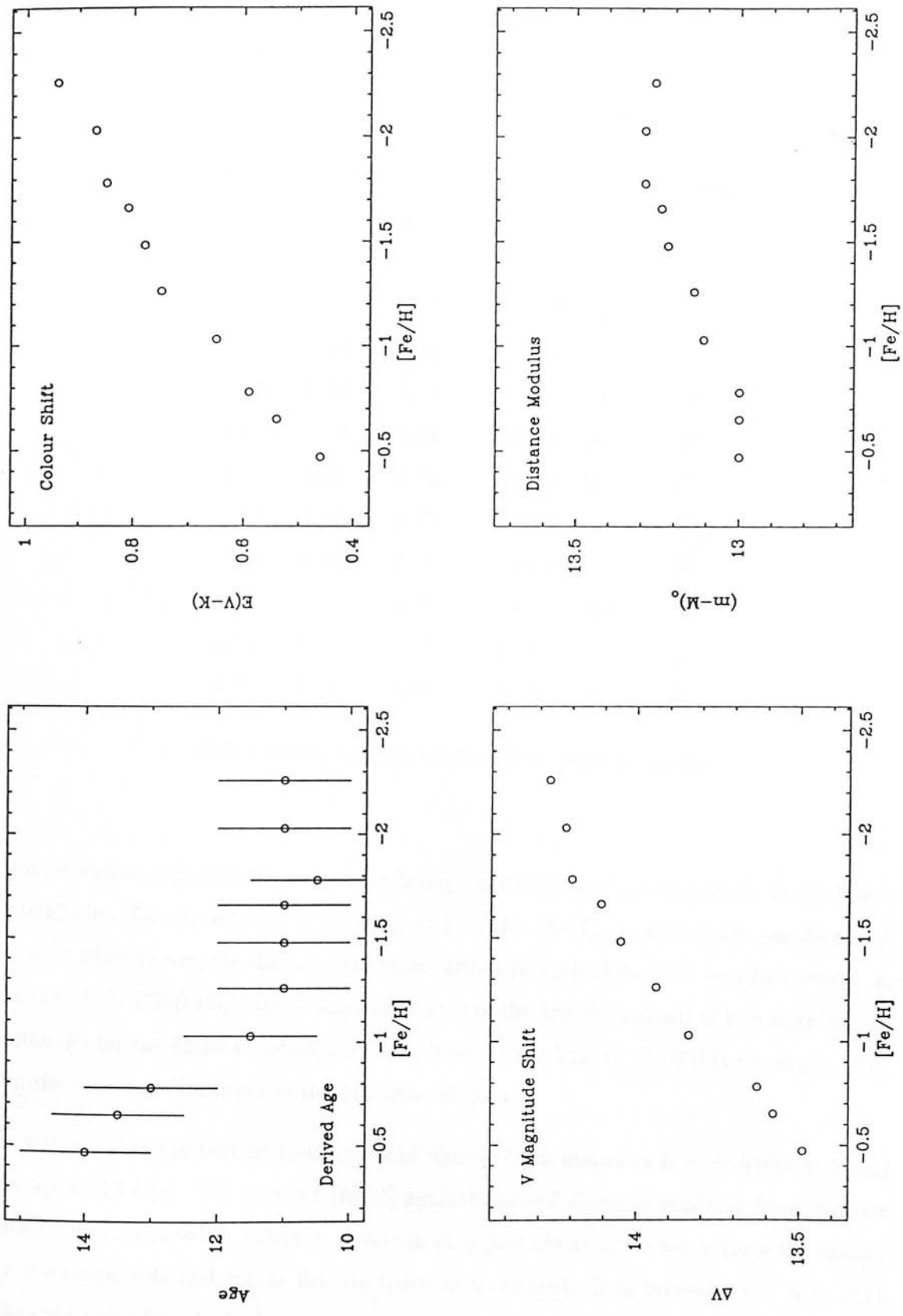

Figure 8: (b) Fitting parameters from (V-K)-K fits.

Table 5: Best-fit parameters for (V-K)-V CMD

[Fe/H]	[O/Fe]	Δ(V-K)	ΔV	Age	Quality
-0.47	0.23	0.46	13.49	14	C
-0.65	0.30	0.54	13.58	13.5	C
-0.78	0.39	0.59	13.63	13	B
-1.03	0.50	0.68	13.84	11.5	C
-1.26	0.55	0.75	13.94	11	C
-1.48	0.60	0.78	14.05	11	D
-1.66	0.63	0.81	14.11	11	D
-1.78	0.66	0.85	14.20	10.5	D
-2.03	0.70	0.87	14.22	11	D
-2.26	0.75	0.94	14.27	11	D

curves well at high metallicities whilst being too red by nearly a magnitude at the lowest metallicity. This correlation is the basis of FPC79's $(V\text{-}K)_{o,GB}$ metallicity parameter. A similar effect is seen for the faint MS stars, although these data have very low weight. In the (V-K)-K CMD there is the same mismatch of the brightest giants at low metallicities, although for the highest metallicities the clump at the base of the GB is too bright to fit on the same age isochrone as the MS turn-off data.

It appears that the best fit to the present data in both diagrams is at [Fe/H]=-0.78 and an age of 13 Gyr. The plots of [Fe/H] against derived distance modulus from the two diagrams are somewhat different, although they just about agree when the RMS scatter in the magnitude and colour fits are taken into account. It is interesting to note that the only point for which the two agree exactly is at [Fe/H]=-0.78, when $(m\text{-}M)_o$=13.00. Setting [Fe/H] to -0.78 gives a reddening to M71 of E(V-K)=0.59, which corresponds to

Table 6: Best-fit parameters for (V-K)-K CMD

[Fe/H]	[O/Fe]	Δ(V-K)	ΔK	Age	Quality
-0.47	0.23	0.47	12.99	14	C
-0.65	0.30	0.57	12.99	13.5	C
-0.78	0.39	0.59	13.07	13	C
-1.03	0.50	0.64	13.24	12	D
-1.26	0.55	0.69	13.26	12	D
-1.48	0.60	0.79	13.26	11.5	E
-1.66	0.63	0.80	13.28	11	E
-1.78	0.66	0.85	13.26	11	D
-2.03	0.70	0.90	13.28	11	E
-2.26	0.75	0.91	13.33	11	E

E(B-V)=0.21 if R=3.05.

To make E(V-K) agree with the standard value of E(B-V), either [Fe/H] would have to be much lower than the best-fit value of -0.78, R would have to be lowered, or the isochrones would have to be wrong. The K zero-points of the observations are fairly secure since the isochrones match up so well to both the FPC79 and the present data, which are almost entirely independently calibrated. A value of [Fe/H] as low as -1.45 (for which E(V-K) comes out as expected) is rather improbable, being lower than any of the wide range of estimates in the literature.

To make the value of E(V-K) consistent with E(B-V)=0.27, R would have to be 2.4 (extrapolating from the data of MW90). The adopted distance modulus would then increase to $(m\text{-}M)_o$=13.06 and the value from the fits above would be 13.01. These two values could easily be made to agree exactly by increasing [Fe/H] to -0.85. However, it

has already been shown that R is unlikely to be this low.

Introducing the isochrone zero-point shifts mentioned at the start of this section increases all the reddenings by $\Delta(\Delta(V\text{-}K))=0.12$ and makes the ΔK_s $0^m.12$ smaller. This changes the values of derived distance modulus and reddening for the best-fit age and metallicity to those listed in table 7. Clearly, these derived values of reddening and distance modulus are in excellent agreement with those derived from the literature in section 2. This confirms the zero-point calibration of the model K magnitudes and gives added weight to the derived age and metallicity.

Table 7: Revised best-fit parameters for t=13 Gyr and [Fe/H]=-0.78.

Diagram	E(V-K)	$E(B\text{-}V)_{equiv}$	Δm	$(m\text{-}M)_o$
(V-K)-V	0.71	0.26	13.63	12.84
(V-K)-K	0.71	0.26	12.95	12.86

The final best-fit parameters, together with (somewhat subjective) error estimates, are:

$(m\text{-}M)_o=12.85 \pm 0.15$ $\quad$ $t=13 \pm 1$ Gyr

$E(B\text{-}V)=0.26 \pm 0.03$ $\quad$ $[Fe/H]=-0.78 \pm 0.3$

The age and [Fe/H] derived are consistent with previous work. Both the VB83 and Heasley and Christian (1991) age determinations use isochrones which do not include any oxygen enhancement and since the BBVB isochrones do include an [O/Fe] enhancement they are expected to predict younger ages. VandenBerg (1985) suggests that an oxygen enhancement of [O/Fe]=0.5 will produce ages about 10% younger than a similar solar-scaled model. The present result thus corresponds to ~14 Gyr for unenhanced isochrones and lies between Hatzidimitriou's (1991) 12 ± 2 Gyr and the 16-17 Gyr of VB83 (revised) and Heasley and Christian's 16 Gyr.

A gratifying confirmation of the consistency of these results comes from the [Fe/H]-$(V\text{-}K)_{o,GB}$ relation of Frogel, Cohen and Persson (1983). As mentioned before, using their value of $(V\text{-}K)_{o,GB}$=4.00 from E(B-V)=0.25 and $(m\text{-}M)_o$=12.90, they found [Fe/H]=-0.60 for M71 from the mean relation through their clusters, even though it was one of their calibrating clusters with an assumed metallicity of -0.75. Using the presently derived values of E(V-K) and $(m\text{-}M)_K$, $(V\text{-}K)_{o,GB}$ can be remeasured, with a small extrapolation, to be 3.81 $\pm$ 0.06, which puts M71 right onto the mean line with [Fe/H]=-0.77. The [Fe/H]-$(V\text{-}K)_o$ relation is purely empirical, so this 'consistent' agreement with the results of isochrone fitting is very pleasing.

The present results show:

- the 12% correction to the model K-fluxes is appropriate;
- the present collection of data is consistent with the adopted values of reddening, distance modulus, age and metallicity;
- the present procedure of fitting (by eye) the best-shaped isochrone to the data is successful.

In addition, the $(V\text{-}K)_{o,GB}$ metallicity calibration shows that the reddening, distance modulus and metallicity are mutually-consistent. The derived distance modulus is the most precise single estimate of this parameter ever made for M71, although it may be in error because of systematic errors in the isochrones.

4.1 Differential reddening

Using one of the BBVB (V-K),V isochrones it is possible to select a portion of the main sequence where the photometric errors are relatively small and calculate a colour residual from the isochrone for each star. These residuals can be plotted against position in the frame as a reddening map of the area. This procedure finds no significant deviation, but the data are only sufficient to distinguish variations of $0^m.3$ from the mean. Any variation present is already known to be smaller than this.

5 Comparing the CMDs with 47 Tuc

The M71 observations are compared with similar data in 47 Tuc.

Comparing the CMD morphologies of two clusters is potentially very useful because it allows parameters such as metallicity and age to be examined without having to assume values of reddening and distance modulus.

Buckley and Longmore's (1992) K data for 47 Tuc from the Anglo-Australian Telescope's IR camera, IRIS, have been used to construct CMDs to compare the two clusters and particularly to examine the values of reddening and distance modulus to M71. M71 and 47 Tuc have similar morphologies in their optical CMDs, hence the use of the 47 Tuc optical CMD, by AH71 and Cud85, to derive differential reddening and distance modulus to M71. The data are used in the same way here but these parameters can be derived independently from the different CM diagrams that are possible with the BVK data available. For each cluster the same stars were used in all plots, with the V data for 47 Tuc coming from HHVASS87.

The reddening to 47 Tuc is small and fairly well determined: the values in the literature range from E(B-V)=0.0 to 0.08, with recent work favouring 0.04 (see discussion in HHVASS87 and Straniero and Chieffi, 1991). A value of E(B-V)=0.04 $\pm$ 0.01 was used to de-redden the 47 Tuc data in all three diagrams. There is no evidence to suppose that R is not standard in 47 Tuc, since it lies well away from the galactic plane ($b^{II} = -50$) and its reddening is small.

As well as the shifts in colour and magnitude due to the different reddenings and distance moduli of the two clusters, shifts and shape changes will also be caused by age and abundance differences, so the question arises of which features to match up in the CMDs. Table 8 lists the shifts in colour and magnitude and the implied reddenings and distance moduli, resulting from various matching attempts. The shifts are given relative to the de-reddened 47 Tuc data, so, for example, ΔV=0.52 means that the M71 points have been shifted $0^{m}.52$ fainter to match up with the 47 Tuc points. $E(B\text{-}V)_{equiv}$ and $\Delta(m\text{-}M)_o$ have been calculated assuming R=3.05 and E(V-K)/E(B-V)=2.77. Also tabulated is the distance modulus derived under the assumption of a constant E(B-V)=0.27 for M71.

As a first attempt the two clusters were matched-up at the horizontal branches.

Table 8: Parameters from various matches between 47 Tuc and M71 CMDs.

ΔV	Δ(V-K)	E(B-V)$_{equiv}$	Δ(m-M)$_o$	ΔV_{HB}	ΔV_{flat}	(m-M)$_o$	(m-M)$_{o,0.27}$
Nominal offsets							
0.42	0.75	0.27*	0.40	0.0	0.26	12.88*	12.88*
Matched at HB							
0.42	0.64	0.23	0.28	0.0	0.20	13.00	12.88
Matched at MSTO							
0.22	0.64	0.23	0.48	0.20	0.0	12.80	12.68
'Self consistent' match							
0.51	0.39	0.14	-0.08	-0.02	0.10	13.36	12.97

* by definition the same as the adopted value.

Δ is in the sense 47 Tuc - M71.

5.1 Matching the horizontal branches

The dependence of the HB luminosity on metallicity is controversial (see, for example, Carney, Storm and Jones, 1991). If the full Sandage Period Shift Effect is valid $\delta M_{V,HB}/\delta$[Fe/H] may be as large as 0.4, whereas if some HB models are to be believed all horizontal branches have the same luminosity (e.g. Sweigart, Renzini and Tornambé, 1987). By first assuming that the latter is true the two clusters' horizontal branches are matched into coincidence (figure 9).

An HB fiducial was first drawn by eye for each cluster in the (B-V)-V, (V-K)-V and (V-K)-K diagrams. The HB data for 47 Tuc are rather sparse, comprising only 10 stars.

The M71 data were arbitrarily shifted in colour and magnitude until the two fiducials coincided. Trial and error determined the range of parameters that gave a sufficiently good match. The parameters that are directly measured from the various colour-magnitude combinations are Δ(B-V) and ΔK, and two values each of Δ(V-K) and ΔV. The magnitude shift necessary to bring the two lines together is a combination of the reddening of M71 and the difference in distance modulus between the two clusters, $\Delta(m\text{-}M)_o$. If values of R and E(V-K)/E(B-V) are assumed, the reddening in (V-K) can be converted to a value of E(B-V) and the measured ΔK and ΔV can be used to calculate a value for $\Delta(m\text{-}M)_o$ corrected for the derived reddening. Obviously the reddenings derived from different colours should be the same when correctly converted onto a common scale and the distance moduli derived at different wavelengths must also be the same.

Table 9: Matching parameters between M71 and 47 Tuc

Diagram	$\Delta(colour)$	$\Delta(mag)$	$E(B\text{-}V)^{M71}_{equiv}$	A_λ	$\Delta(m\text{-}M)_o$
(V-K)-V	-0.57 ± 0.13	-0.405 ± 0.065	0.21 ± 0.05	0.63 ± 0.14	0.23 ± 0.15
(B-V)-V	-0.28 ± 0.06	-0.50 ± 0.11	0.28 ± 0.06	0.86 ± 0.18	0.36 ± 0.21
(V-K)-K	-0.57 ± 0.11	0.18 ± 0.11	0.21 ± 0.04	0.07 ± 0.01	0.25 ± 0.11

Δ is in the sense: 47 Tuc - M71.

The results of the matching process are given in table 9. The error estimates in the table include the fitting margin, the zero-point error estimates in the colours and magnitudes and the error in the distance modulus of 47 Tuc.

The E(B-V) and $\Delta(m\text{-}M)_o$ values are all the same within the errors and the weighted means are $\overline{E(B-V)}$= 0.23 ± 0.02 and $\overline{\Delta(m-M)_o}$=0.26 ± 0.03. Taking HHVASS87's value of $(m\text{-}M)_o$=13.28 for 47 Tuc leads to $(m\text{-}M)_o$=13.02 for M71.

The equivalent E(B-V) colour excesses would agree if R= 2.25 ± 0.6 for M71. To reconcile the differential distance moduli R would have to be 2.6 ± 0.9, which would make $\overline{\Delta(m-M)_o}$= 0.23 ± 0.11 (formal errors on graphical solution). HHVASS87 state that

their colours may be $0^m.01$-$0^m.02$ too blue in (B-V), which would reduce Δ(B-V). If this were an error in V only, it would increase both values of Δ(V-K) by 0.01-0.02 and make $\Delta(m\text{-}M)_o$ smaller (more positive) by the same amount.

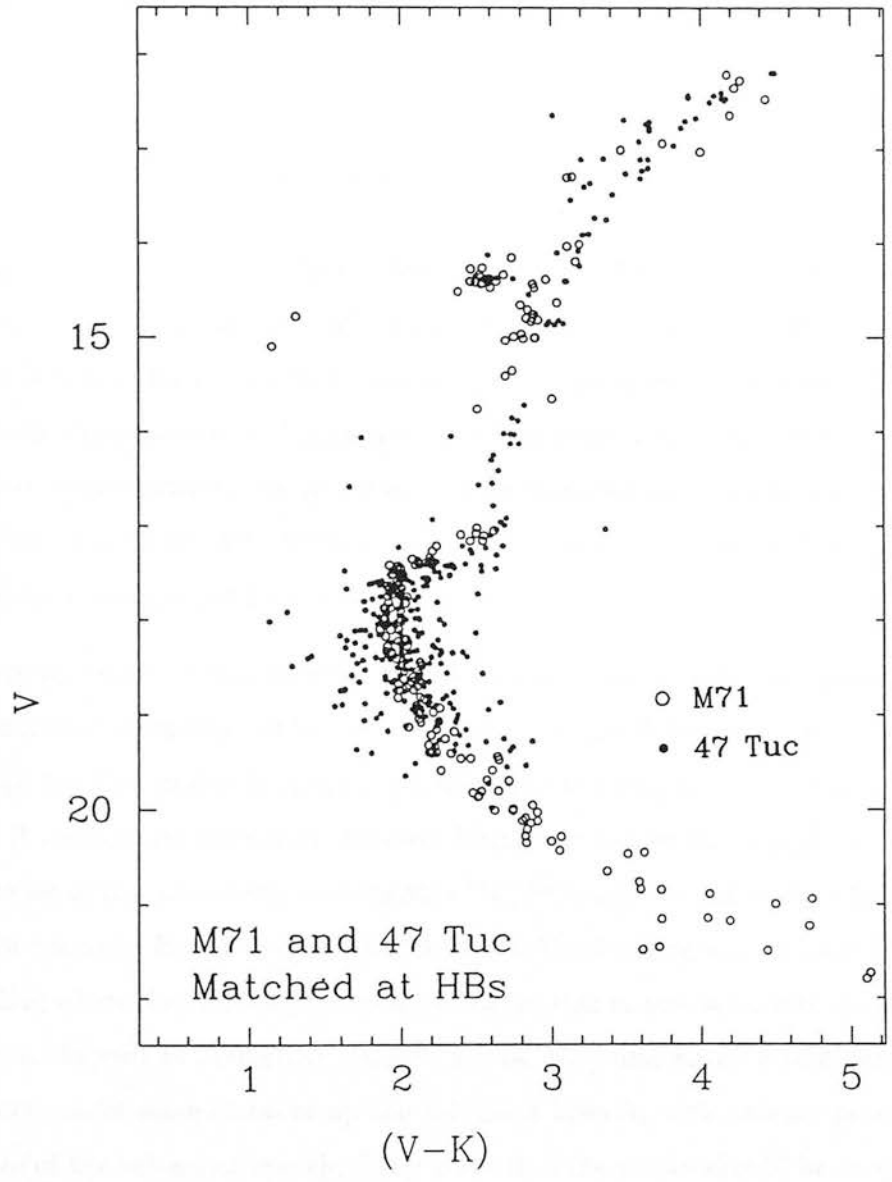

Figure 9: (V-K)-V CMDs for M71 and 47 Tuc with HBs matched.

Clearly, these results are not consistent with the adopted E(B-V)=0.27 and $(m\text{-}M)_o$=12.88. That is to say $\delta M_{o,HB}/\delta$[Fe/H]=0 does not produce consistent results.

It is not possible to give a 'best-fit' solution without assuming some functional dependence of the HB magnitude and colour on metallicity and age. Considering only the (B-V)-V CMD, if $\delta M_{V,HB}/\delta$[Fe/H] = 0.20 (as in LDSJF90) and the HB luminosity is largely independent of age, the distance modulus of M71 comes out to be 12.99 if [Fe/H] is taken

as -0.78 for M71 and -0.65 for 47 Tuc. If the colours of the 47 Tuc data *are* in error by ~2% and E(B-V)=0.27 for M71, $(m\text{-}M)_o$ becomes 12.92, which is very close to the expected value. The difference in metallicity is so small, and so many ifs are involved, that no conclusion can be drawn as to the validity of the chosen gradient for the [Fe/H]-$M_{V,HB}$ relation.

5.2 The giant branch clump

The aggregation of stars $0^m.5$ in V below the HB in M71 was noted earlier. A similar clump is also seen in the 47 Tuc data, albeit only represented by five stars in the (V-K)-V CMD. Whilst it is easy for the eye to be drawn by a chance grouping of stars, and thus to read too much significance into clumps and groups of stars in a CMD, there is evidence that a clump in approximately this location is to be expected from theoretical calculations. As Fusi-Pecci et al (1990, FFCRB90) say: ' ... the identification of the "bump" in a number of clusters is not merely a piece of filigree in globular cluster arcana.'

This clump/bump is caused when the H-burning shell of the stars passes through the compositional discontinuity left behind by the earlier RGB phase, when the convective envelope reached so deeply into the interior that it dredged up material from the region where H abundances have been affected during the H-core burning phase. This is a possible cause of the anomalous and variable $^{12}C/^{13}C$ ratios found in globular cluster giants (see, for example, Bell, Briley and Smith 1990). VandenBerg and Smith (1988) performed modelling where they allowed the envelope of the star to penetrate into the core-processed material. As well as predicting $^{12}C/^{13}C$ ratios, they also found a foldback in their evolutionary tracks some distance up the sub-giant branch, with another possible clump at the base of the sub-giant branch. They state that the clump should be overpopulated by a factor of 5 with respect to other regions of the giant branch. They also state that there is no evidence for such a clump in the HHVASS87 luminosity function of 47 Tuc, but this is because their predicted clump is two magnitudes fainter than the real one. The SGB base clump is also interesting because there is a clump seen here, albeit represented by only a few stars, in the M71 CMD.

The SC91 (B-V)-V isochrones also contain just such a clump, a foldback in the isochrones where stars briefly decrease in brightness on their way up the giant branch, close to the

level of the HB. FFCRB90 modelled this clump and proposed the difference between its V magnitude and that of the HB, $\Delta M_V^{HB}_{clump}$, as a metallicity indicator. They calibrated this using 11 representative clusters including 47 Tuc and M107 at the metal-rich end. Measuring $\Delta M_V^{HB}_{clump}$ for M71 gives 0.4, which corresponds to Z=0.0033 or [Fe/H]=-0.78. This result is in excellent agreement with that found from the isochrone fitting to the present data and with the literature values summarized in section 2. SC91 give an equation to find the absolute V magnitude of the clump as a function of age and metallicity. The FFCRB90 predictions of $M_{V,o,clump}$ are very similar for their chosen age of 15 Gyr and Y=0.23.

Using $M_{V,clump}$ as a standard candle, FFCRB90 find a slope in the [Fe/H]-$M_{V,HB}$ relation between 0.0 and 0.2, depending upon their input conditions. Although they have made some assumptions, such as a common age for all the clusters, and their models are somewhat out of date, the agreement of this gradient with the revised LDSJF90 gradient gives confidence in the relative, if not absolute, accuracy of their models.

Another relative, rather than absolute, parameter can be derived by looking at the magnitude difference between the clump and the mid-point of the flattish section joining the MSTO to the base of the GB. Measuring this difference in the SC91 Z=0.002, 0.004 and 0.006 ([Fe/H]=-1.04, -0.74 and -0.56 respectively) families of isochrones produces the following approximate relation:

$$\Delta V_{flat-clump} = -0.0184[Fe/H]t + 0.0212t - 0.245[Fe/H] + 2.369$$

This means that, for example, the separation is ~3 magnitudes for Z=0.004 ([Fe/H]=-0.74) and t=12 Gyr.

Unfortunately, ΔV_{f-c} is measured as 2.6 for 47 Tuc and 2.48 for M71. These cannot be reproduced with any reasonable choice of [Fe/H] or age. Also, using the HHVASS87 best-fit parameters from their isochrone fitting puts the clump at M_V=1.15, whereas the SC91 isochrones predict it to be at 0.77. Thus the clumps seen are not exactly those from the SC91 isochrones, or else the isochrones are wrong in that the real clump occurs somewhat fainter than predicted. FFCRB90 found their clump predictions to be $\sim 0^m.4$ too bright. This is just about the correct size to reconcile the observed values of ΔV_{f-c}. Putting in this shift and t=13.5 Gyr and [Fe/H]=-0.78 for 47 Tuc (from HHVASS87) then predicts

ΔV_{f-c}=2.62. The measured values imply an age difference of ~6 Gyr between the two clusters, if the metallicities are the same, with M71 the younger. Conversely, if the clusters are both the same age their metallicities would have to be different by ~0.5 dex, with 47 Tuc the more metal poor. The error on the difference between the two values of ΔV_{f-c}, $\Delta(\Delta V_{f-c})$, is almost $0^m.1$ because of the quality of the photometry. This means that for Δ[Fe/H]=0 Δt~6±6, or for Δ[Fe/H]=0.5 Δt~0±3.5. These error estimates are purely from the measurement errors and cannot include any systematic errors in the theoretical calculations.

Some previous work shows that 47 Tuc is likely to be more metal rich than M71 (see Bell 1987, for example), although Zinn (1985) found [Fe/H]=-0.58 and -0.71 for M71 and 47 Tuc respectively. For 47 Tuc HHVASS87 found the best fitting isochrone to be [Fe/H]=-0.65 with an age of 13.5 ± 0.5 Gyr. Dorman, VandenBerg and Laskarides (1989) fitted model HBs to the same data and concluded that [Fe/H]=-0.65 with $(m-M)_o$=13.31. The metallicity would be slightly lower if a correction is made for the small colour zero-point error found in the VBB85 models, although this may be cancelled out by a similar zero-point error in the HHVASS87 (B-V) colour (see the end of section 5). SC91 refitted the same CMD with their new isochrones to find [M/H]=-0.63 and t=12 ± 1 Gyr with $(m-M)_o$=13.30. Bell (1992) finds $(m-M)_o$=13.33 from unpublished HB evolutionary tracks supplied by Dorman (an improvement on those in Dorman, VandenBerg and Laskarides, 1989). Bell preferred [Fe/H]=-0.78 to fit Buckley and Longmore's IR data with a similar age to Hesser et al. The isochrone fitting earlier in this chapter shows that M71 is likely to be only 500 ± 1000 Myr younger than the HHVASS87 result. Such a result of Δ[Fe/H]=0 and Δt=0.5 Gyr is just possible within the errors of measurement. If Heasley and Christian (1991) are correct in saying that M71 is ~3 Gyr older than 47 Tuc the metallicity difference would need to be Δ[Fe/H]=-0.95 ± 0.5, which is rather unlikely.

Brown et al (1990) found [O/Fe]=0.4 for 47 Tuc, whilst Gratton (1987) found 0.69 ± 0.06 for M71. From VandenBerg and Stetson (1991) this difference would lead to a colour difference of only 0.01 in (B-V). The effect on the (V-K) colour is likely to be similarly small. Performing simple tests with the MARCS model atmosphere program finds no difference in B,V or K fluxes between [O/Fe] of 0.4 and 0.7 for an otherwise normal [Fe/H]=-1.0 model.

In summary, the differential measurement ΔV_{f-c} within the CMD can provide information

on the metallicity and age differences between two clusters. The observed values of ΔV_{f-c}

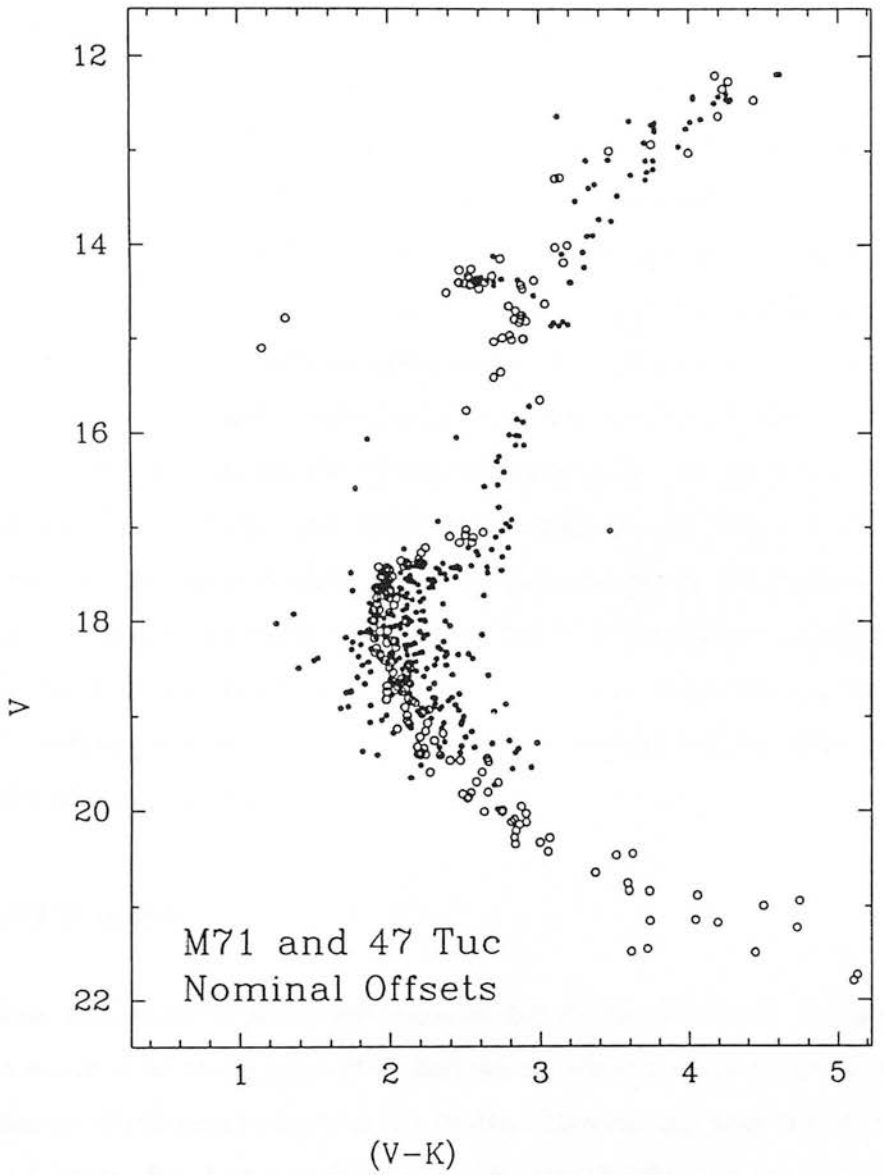

Figure 10: (V-K)-V CMDs for M71 and 47 Tuc matched with nominal offsets.

for 47 Tuc and M71 do not agree in size with the theoretical predictions of the SC91 isochrones, but it seems likely that they will have the predicted dependence on age and metallicity and could be calibrated observationally. In a CMD with (V-K) as the colour the clump is likely to be more tightly defined than in one using (B-V), so that ΔV_{f-c} is likely to be measured more precisely in the optical-infra-red CMD. In this particular case the usefulness of this measurement is limited by the photometric scatter in the data and the small number of stars in the clumps. The difference between the ΔV_{f-c}s for the two clusters, $\Delta(\Delta V_{f-c})$, will be used again in section 5.5.

5.3 Nominal match

Using Bell's distance modulus for 47 Tuc and the adopted value for M71 gives an expected value of $\Delta(m\text{-}M)_o$=0.37. If the Hesser et al value is used, the expected value becomes 0.42 $\pm$ 0.1. The adopted M71 reddening of E(B-V)=0.27 corresponds to E(V-K)=0.75 $\pm$ 0.06. Figure 10 shows the two CMDs overlaid with these nominal offsets. Clearly they do not match well in colour. The MSTO region is bluer in M71 and the 'flat' region is brighter, suggesting that M71 is either considerably younger than 47 Tuc or that it is more metal poor. The giant branch of M71 is considerably bluer (by $0^m.28$) than that of 47 Tuc, suggesting a larger difference in metallicity, since the giant branch does not change much with age. On the other hand, the horizontal branches lie on top of one another in V, indicating that the two clusters are of the same metallicity to $\pm\sim$0.2 dex. This agreement of the HBs is to be expected since many of the estimates of the distance modulus to M71 started by assuming a value of $M_{V,o}$(HB) based on the cluster's assumed metallicity (although the RF88 sub-dwarf fit for M71 gives a similar answer for $(m\text{-}M)_o$). Since 47 Tuc is of a similar metallicity, it is to be expected that the nominal offsets between the clusters should make the HBs agree.

5.4 MSTO match

VandenBerg, Bolte and Stetson (1990) suggest that clusters which are of similar metallicity can be matched up at the turn-off so that the age difference can be estimated from the colour difference between the bases of the RGBs, although they note that their technique is not so successful for clusters more metal rich than [Fe/H]=-1.2 (see also VandenBerg and Stetson (1991) for calculations regarding the effects of [O/Fe] variations). Although it is fairly easy to match M71 and 47 Tuc at their turn-offs (figure 11), the lack of stars measured on the lower GB for M71 means that the two cannot be compared until $\sim 0^m.5$ below the HBs, where the colour difference is Δ(V-K)=0.15, in the sense that the GB of M71 is bluer. Heasley and Christian (1991) found the GB of M71 to be bluer, relative to the MSTO, than that of 47 Tuc, implying that M71 is older, if their metallicities are the same. It is possible to measure this difference in the BBVB isochrones as a function of age and metallicity. Looking at just the [Fe/H]= -0.65, -0.78 and -1.03 families of isochrones

gives the (V-K) colour difference between the MSTO and the giant branch at $M_{V,o}$=1 as:

$$\Delta(V-K)_{TO-GB1} = -0.008t + 0.47[Fe/H] + 1.54 \quad (1)$$

At the extremes, M71 could be 20 Gyr older than 47 Tuc or M71 could be 0.3 dex more metal poor.

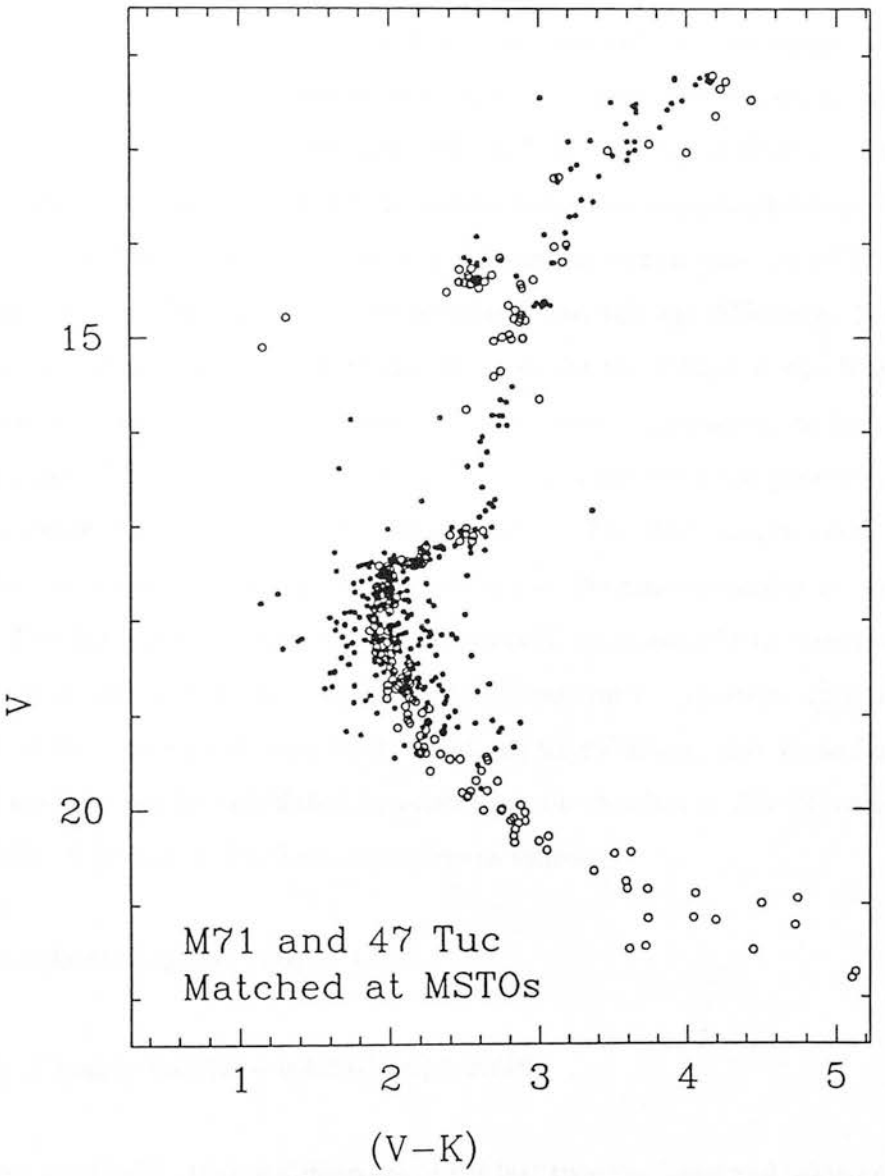

Figure 11: (V-K)-V CMDs for M71 and 47 Tuc with the main sequences matched.

5.5 'Self-consistent' match

The preceeding sections lead on to the possibility of finding a 'self-consistent' fit between the clusters, that is the colour-magnitude shift combination that yields the most self-consistent set of parameters. This approach has not been tried before and gets around the problems of using previous, possibly incorrect, reddenings and distance moduli and negates any zero-point errors in either data set, because the colour and magnitude shifts are solved for as part of the fitting procedure. In principle this technique will lead to better determinations of the parameters that determine the match between the two CMDs. There are four parameters to determine: ΔV, Δ(V-K), the age difference, Δt, and the metallicity difference, Δ[Fe/H]. Thus four measurements are required between the CMDs to solve for these. The difference of the ΔV_{f-c} measurements is one. $\Delta(\Delta V_{f-c})$=0.12 in this case and is dependant on both the metallicity and the age differences between the clusters. A second measurement that can be made on the CMDs is the V magnitude difference between the two 'flat' sections ΔV_f. An obvious parameter to look at is the magnitude separation of the two HBs, ΔV_{HB}, since so much work has gone into its study (see, for example, Carney, Storm and Jones, 1991). The final measurement has also already been discussed, $\Delta(V\text{-}K)_{GB1}$, the separation of the giant branches at $\sim 0^m.5$ below the HBs. The last three parameters are illustrated schematically in figure 13, which shows two isochrones as representative of the CMD data for two clusters. $\Delta(V\text{-}K)_{GB1}$ has been taken to be measured at $M_{V,o}$=1.0. Relations for $(V\text{-}K)_{GB1}$ and V_f as functions of metallicity and age can be calculated by measuring the families of BBVB isochrones for [Fe/H]= -0.65, -0.78 and -1.03. The results are as follows:

$$V_f = 0.0663t + 0.590[Fe/H] + 3.255$$

$$(V - K)_{GB1} = 0.0111t + 0.608[Fe/H] + 2.778$$

Measuring up the CMDs, taking differences in the last two equations and taking $\delta M_V(HB)$ = 0.20 δ[Fe/H] from LDSJF90, it is possible to produce the necessary four simultaneous equations. Unfortunately the equation for $\Delta(\Delta V_{f-c})$ contains a cross-term in [Fe/H] and t, so that these must be estimated for one of the clusters to start with. Starting with [Fe/H]=-0.65 and t=13.5 Gyr for 47 Tuc and solving the equations gives the values of ΔV and Δ(V-K) given in table 8 and:

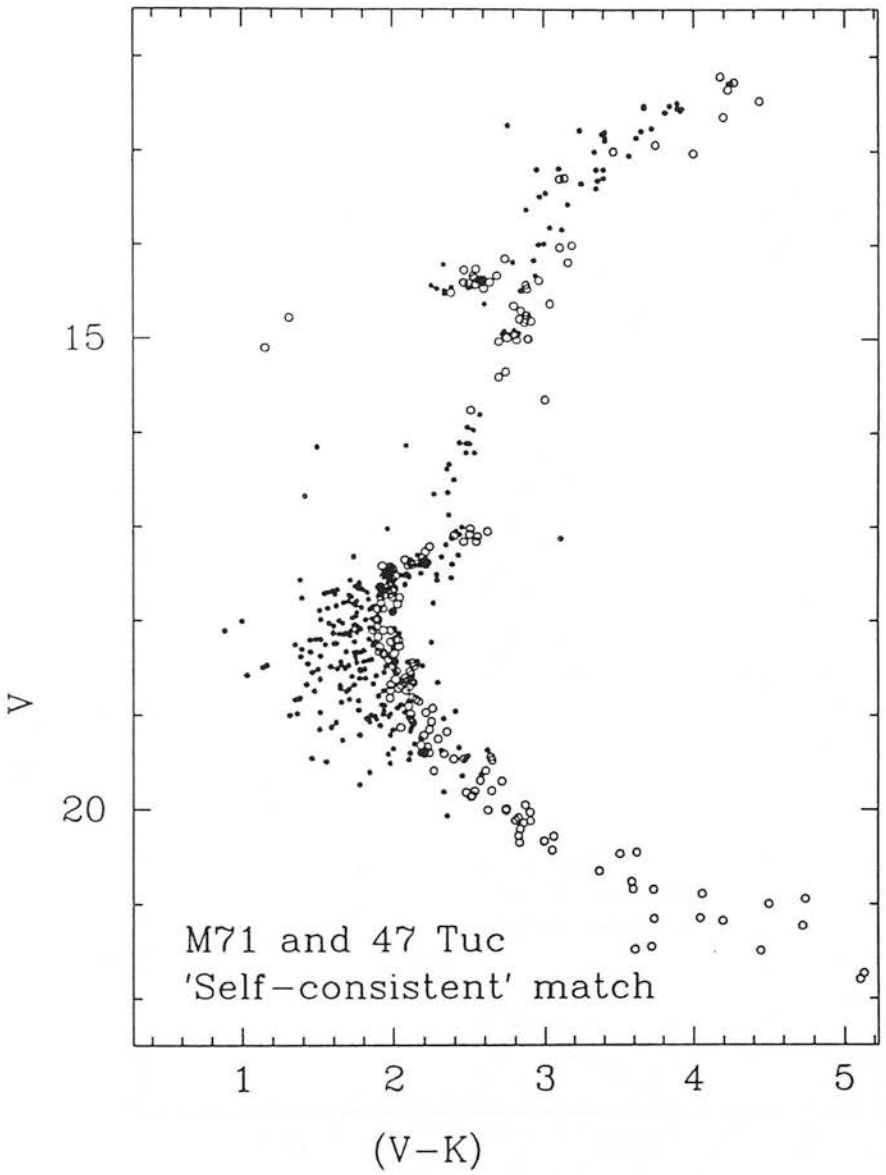

Figure 12: (V-K)-V CMDs for M71 and 47 Tuc: 'self-consistent' match.

Δt	2.34
Δ[Fe/H]	-0.09
$\Delta(V\text{-}K)_{GB1}$	-0.03

That is to say that the HBs and GBs are matched-up close together whilst the flat regions are 10% apart in V. This result is shown in figure 12. The result that M71 is 0.10 dex more metal-rich than 47 Tuc agrees well with Zinn (1985). That it is also 2 Gyr younger is in direct contradiction to the result of Heasley and Christian (1991), although

they note that their results are only preliminary. Heasley (1991, private communication)

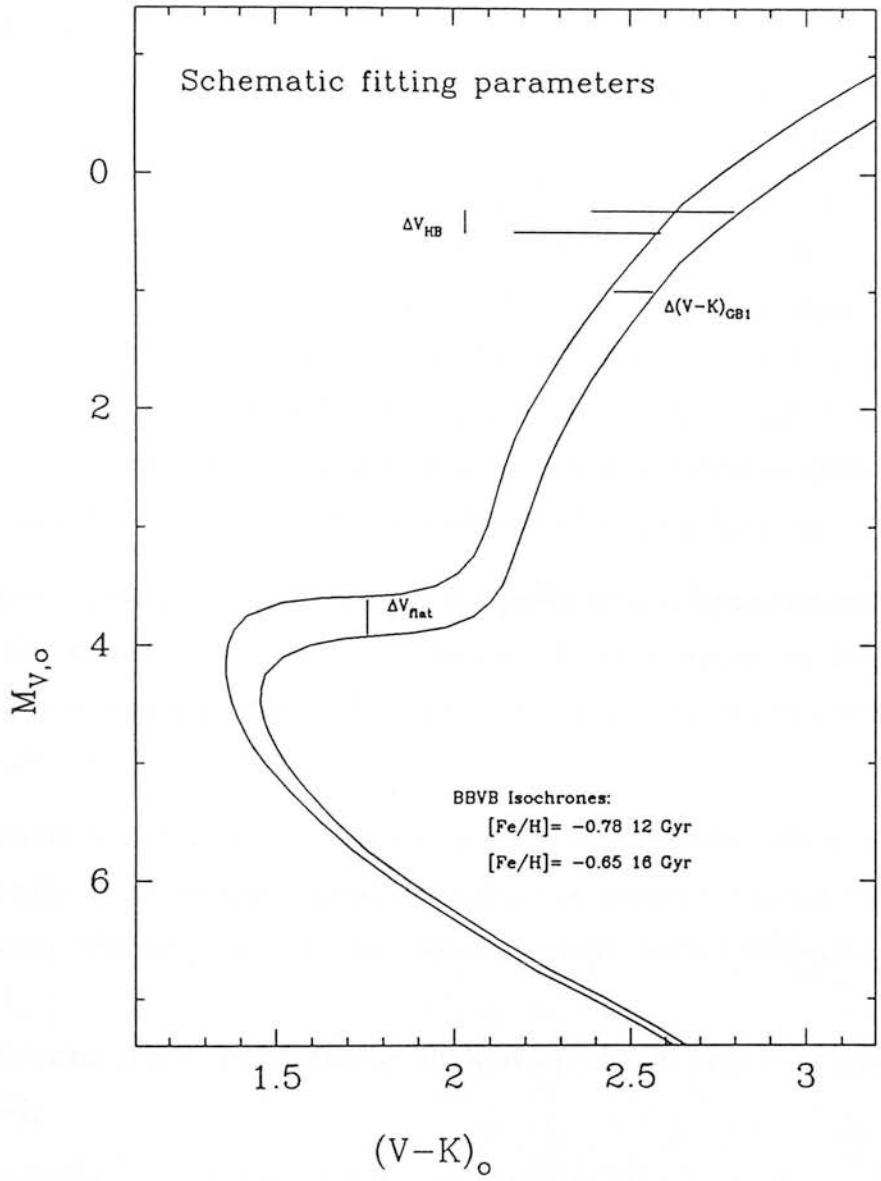

Figure 13: Schematic (V-K)-V CMD showing matching parameters.

states that the zero-point calibrations were somewhat uncertain in this study and that another group has found a result that suggests that there is no difference between the two clusters. The differential colour difference between the TO and the GB (equation (1)) has not been used in this analysis and can therefore be used as a check on the answers. Putting in the present values of Δt and Δ[Fe/H] gives $\Delta(\Delta(V\text{-}K)_{TO-GB1})\sim 0$ rather than the measured 0.15. Also, the derived reddening for M71 is much lower than expected. If, for some reason, the expected reddening of E(B-V)=0.27 is appropriate the derived distance modulus to M71 comes out only $0^m.1$ larger than the adopted value. Clearly the

procedure has not been successful in producing a self-consistent fit.

The zero-points of the 47 Tuc data in both V and K are somewhat uncertain. HHVASS87 state that their colour could be too blue by up to $0^{m}.02$. This seems quite likely to be the case considering what SC91 found when they compared the HHVASS87 fiducial sequence with those from Alcaino and Liller (1987) and Buonanno, Corsi and Fusi Pecci (1989). The latter study in particular found the turn-off region and base of the sub-giant branch to be redder (by $0^{m}.04$) and fainter than the HHVASS87 data. Buckley and Longmore (1992) assign a rather pessimistic zero-point error of ± 0.1 to their K photometry. Even combining these possible errors it is not possible to reconcile the derived reddening with the expected value. Again a value of R close to 2 or a significant deviation from the normal form of the extinction law would be required to make these agree.

Experimenting with the possible errors in the gradients and original separations measured on the CMDs shows the sensitivity of the method. For example, the range of possible error on the original magnitude difference between the two HBs allows a range of Δ[Fe/H] from -0.32 to 0.14.

Although the present results are dominated by the uncertainties in the coefficients of the relationships, it is interesting to judge the effects of varying the inputs. Experimenting with a range of input parameters has little effect on the derived differential parameters:

- increasing [Fe/H] for 47 Tuc to -1.0 increases ΔV by only $0^{m}.01$ and Δ(V-K) by 0.02;
- varying the age of 47 Tuc between 12 and 15 Gyr has no significant effect;
- increasing $\delta M_V(HB)/\delta$[Fe/H] to 0.40 decreases ΔV by $0^{m}.03$ and increases Δ(V-K) by 0.01.

In summary, this 'self-consistent' approach shows much promise, but the present results are of little significance because of the (lack of) quality of the data and the uncertainties in the relations derived from the SC91 isochrones, particularly that for $\Delta(\Delta V_{f-c})$. A more sophisticated analysis could include the effects of HB evolution and varying CNO element abundances, once these have been modelled better, and could be calibrated against good quality, homogeneous isochrone fitting. Had the M71 (B-V)-V CMD been of better qual-

ity, it would have been possible to include matching parameters between the M71 and 47 Tuc optical CMDs in the fitting procedure.

5.6 Summary of comparison with 47 Tuc

Several approaches have been explored to match the CMDs of M71 and 47 Tuc.

Matching the clusters only at the HBs, is not very useful because a gradient must be assumed for the $M_{V,o}$(HB)-[Fe/H] relation before a relative reddening and distance modulus can be derived. This gradient is controversial enough, but the situation will be much worse when the observations become precise enough to have to take into account age and CNO abundance differences.

The clump on the giant branch is certainly real and corresponds to the clump modelled by FFCRB90. Their [Fe/H]-$\Delta M_V^{HB}_{clump}$ relation gives a metallicity of -0.78 for M71, although the absolute position of the clump is wrong in the models.

A new differential measurement is ΔV_{f-c}, which has been measured in the SC91 isochrones and may be used as a metallicity and age indicator, and $\Delta(\Delta V_{f-c})$ may be used in comparisons of clusters.

The prospect of a 'self-consistent' match is interesting, this is potentially the way to maximise the use of the data available for two clusters, although it is dependent on model-derived relations. The present data are not sufficiently precise to produce meaningful answers.

Both the M71 and 47 Tuc data, and the isochrone-derived relationships, lack sufficient precision to draw any conclusion other than that the observations are consistent with the adopted ages, metallicities, reddenings and distance moduli for the two clusters.

6 Sub-dwarf fit

Laird, Carney and Latham (1988) published IR photometry for seven nearby metal-poor sub-dwarfs that are often used to fit main sequence observations. Discarding one that they found to be deviant and one that SC91 note to be deviant it was attempted to estimate both E(V-K) and $(m-M)_o$ from the (V-K)-V CMD. Four of the sub-dwarfs are

so faint that they match up with the very poor data at the bottom of the CMD which are biased to the red by the K cut-off. Thus only a very rough fit was possible, the solutions being $(m\text{-}M)_V=13.40 \pm 0.4$ and $E(V\text{-}K)=0.60 \pm 0.2$ when no Lutz-Kelker (LK) corrections were used. When the full Lutz-Kelker corrections were used $(m\text{-}M)_V$ became 13.50 ± 0.4. The errors are so large that these results are not of much use. In the (V-K)-K CMD it is not possible to make any attempt at fitting but if the cluster data are shifted to the nominal positions, with $E(V\text{-}K)=0.75$ and $(m\text{-}M)_o=12.88$, the main sequence data overlays the bright sub-dwarf and the four fainter ones are too faint to match. Because these results are so uncertain no attempt has been made to correct for the metallicity difference between the cluster and the sub-dwarfs ($\sim$0.7 dex) or to decide the extent to which the LK corrections should be applied (corrections in full, at half size or not at all, have been suggested by various authors). The most that can be said is that the sub-dwarf fits are not inconsistent with the nominal values of $(m\text{-}M)_o$ and E(B-V). Longer integrations in deep frames, would be needed to use these sub-dwarfs to find the distance to this cluster.

7 Matching the two-colour diagram with models

The two-colour diagram allows the observations to be compared to models and to fiducial sequences from field star observations without the need to know the distance of the cluster. Model lines allow physical parameters such as mass, radius and temperature to be estimated for individual stars. How well a set of isochrones fit the 2CD data can be used to judge the metallicity of the cluster. The (V-K)-(B-V) 2CD constructed earlier is used in this section.

7.1 The models

The only appreciable set of recent models providing (V-K) colours are those of Bell and Gustafsson (1989, BG89) which cover the range $4000 \leq T_{eff} \leq 6500$K, $0.75 \leq \log g \leq 4.5$ and $0.0 \leq [Fe/H] \leq -3.0$. These are the models, together with the additional but consistent calculations for $T_{eff}=6500$ and 7000K and $\log g = 3.75$ and 4.5 in Bell (1992), which were used to produce the IR colours of the BBVB isochrones, and are thus, presumably, responsible for the $0^m.12$ zero-point shift found necessary in (V-K) in those

isochrones, as mentioned in section 4.

Elias et al (1989) attempted to match observed and synthetic J, H, K and L′ magnitudes for four metal-poor sub-dwarfs with colours in the range $1.2 \leq (V\text{-}K) \leq 1.4$. Whilst they found good agreement between the stars the absolute calibration of the fluxes, relative to Vega, appeared to be out by more than $0^{m}.1$ at H, K and L′, in the sense that the stars were not as bright as the models predicted. Since the optical models agree so well with the observations this again points to a calibration or filter profile error in the IR colours or to missing opacity in the model calculations. At K the zero-point shift was $0^{m}.13 \pm 0.03$.

To reconcile the mis-match that they found between theory and observation in the (V-K)-(J-K) diagram for high metallicity stars BG89 proposed temperature-dependent colour shifts in V, K or J, stating that the shift in V was far less likely, because of the excellent agreement found already between observations and model optical colours. The proposed shift in K ranged from 0.07 at (V-K)=1.6 to 0.15 at (V-K)=3.3, the mean of which is $0^{m}.13$.

Applying the (V-K) colour-dependent corrections from BG89 to the T_{eff}-(V-K) data in Bell (1992) shifts the model predictions into good agreement with the SH85 F dwarfs (although they are cooler than the BG89 data and the corrections are extrapolated and small). Adding in those additional dwarfs for which Koorneef (1983) provides (V-K) colours confirms the position of the Johnson et al (1966) colours and makes it appear that a simple shift of $0^{m}.11$ would best match theory and observation. However, using the colour-dependent shift causes the models to agree with the Glass giant observations at the hot end but disagree by $0^{m}.15$ at the cool end, where no correction appeared necessary in the first place (although, simply choosing a different set of gravities for these stars can shift the model line into or out of agreement with the stars). Without access to all the data and a full knowledge of the input physics of the models, applying any sophisticated colour correction to the model calculations cannot be justified. It seems most likely that the optical colours from the various models are correct and that the IR colours are wrong. Errors in the CO abundance or the H^{-} absorption coefficients are likely candidates for the source of this error (see discussion in BG89). In the following discussion the (V-K) colours have been shifted to be $0^{m}.12$ bluer, in agreement with Bell (1992) and the isochrone fitting in section 4. It should be borne in mind that, particularly at the cool

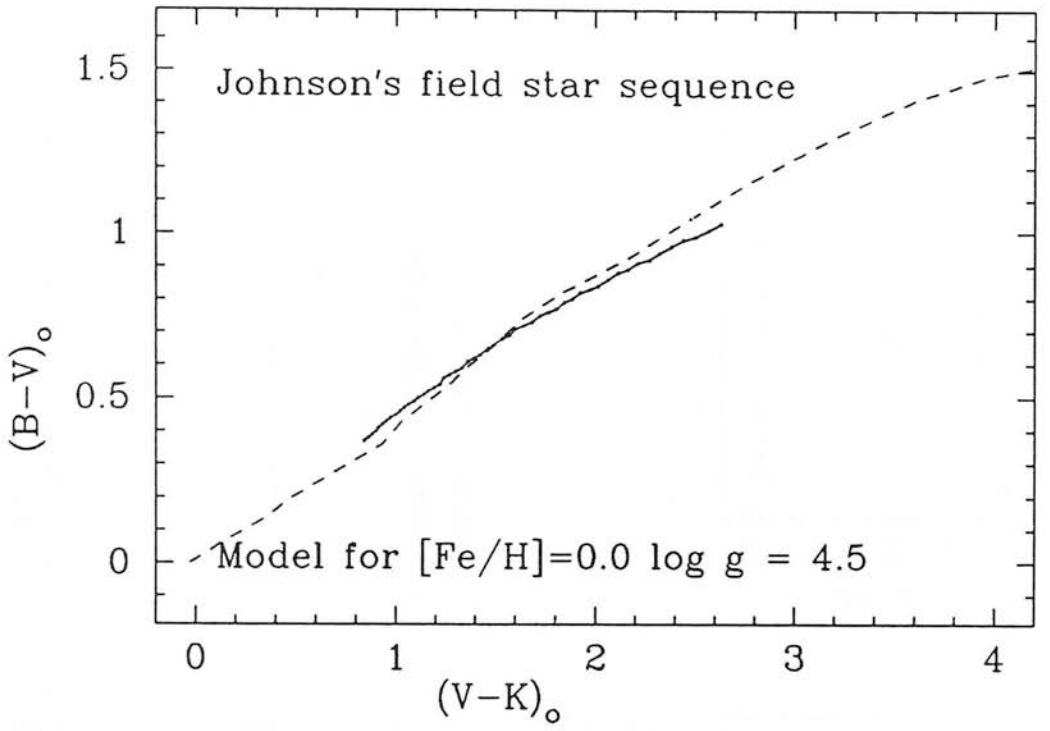

Figure 14: The solar abundance, log g=4.5 model compared to the main sequence field star observations of Johnson (1966) (dashed line).

end, this may produce colours of as much as $0^m.1$ too blue in (V-K).

In order to create a set of two-colour model curves it is necessary to match up the BG89 model IR colours with optical colours from similar models. Bell and Gustafsson (1978, BG78) contains model UBV colour calculations for giant stars and VBB85 contains similar colours for dwarfs. Unfortunately there is a calibration difference between the two studies so that where the two overlap at log g=3.0 and $4500 \leq T_{eff} \leq 6000$ K the VBB85 model (B-V) colours are 5% bluer. The difference has only a very small dependence on temperature, so all of the VBB85 data were shifted to the red by this amount. At the same time a small correction in V was made for the effects of TiO absorption in the coolest metal-rich models, as suggested in BG89. Intermediate values were interpolated within the available data. The normalisation to the BG78 data was chosen because it is the redder of the two and missing opacity in calculations will make the models bluer. For instance, BG89

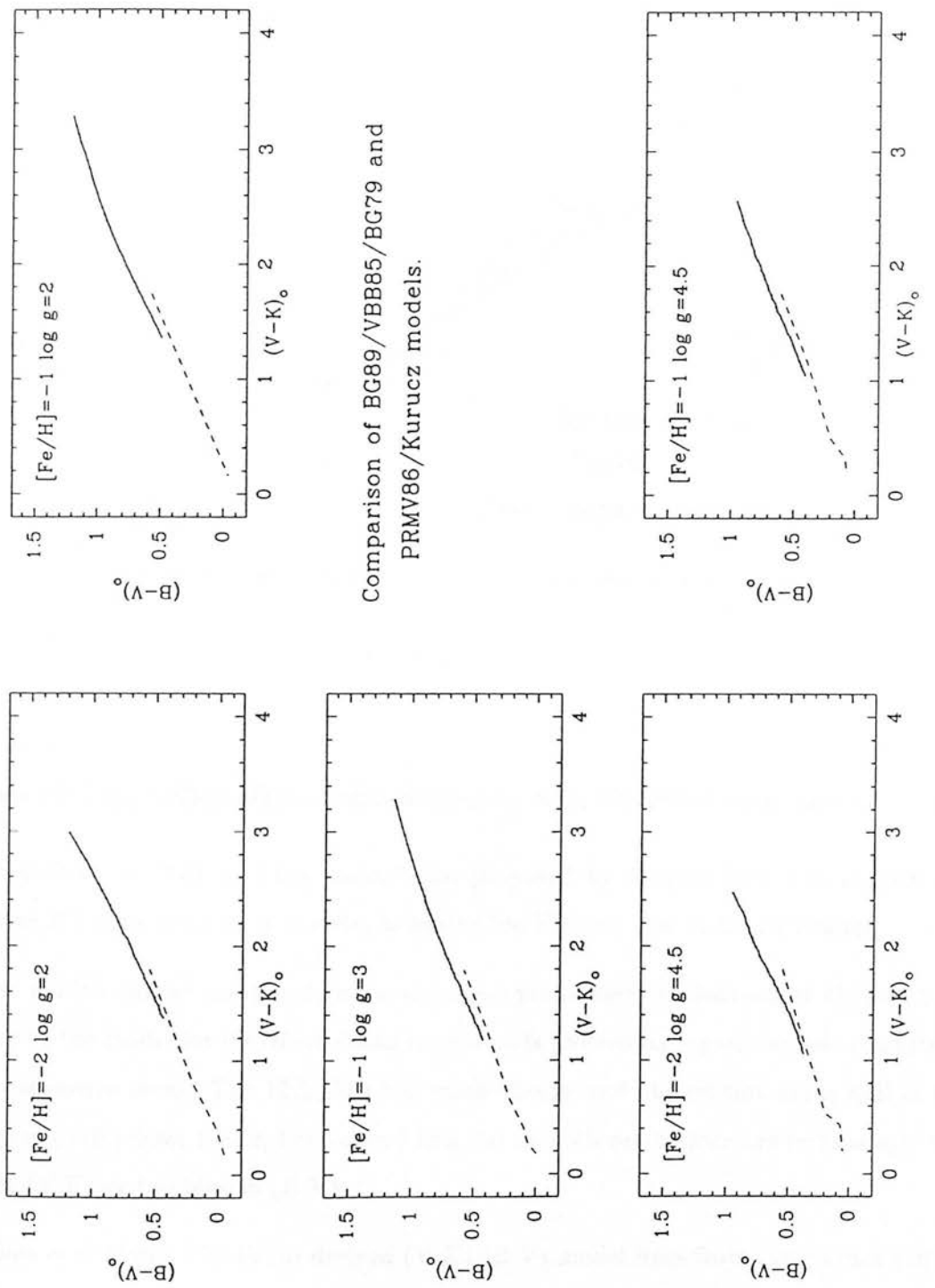

Figure 15: Comparing the BG89/VBB85/BG78 and PRMV86 models in the (V-K)-(B-V) two colour diagram.

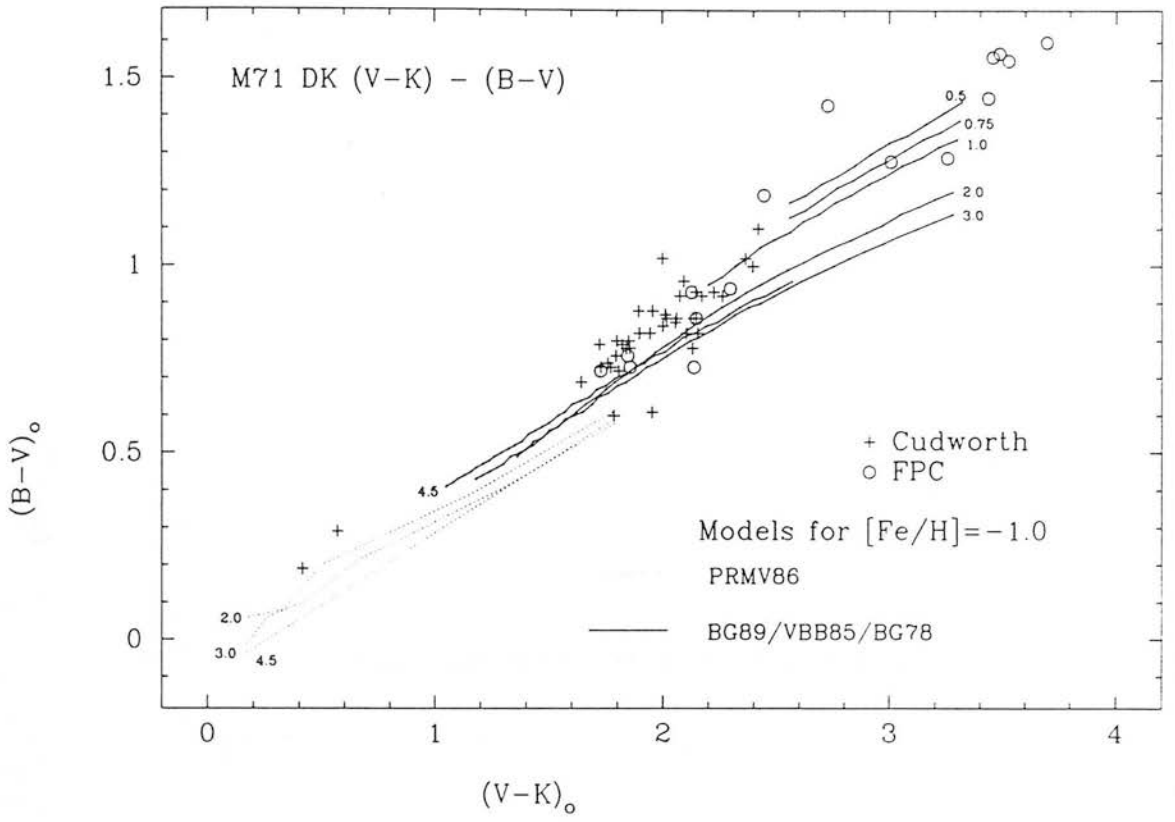

Figure 16: The (V-K)-(B-V) two-colour diagram for M71, with model tracks for [Fe/H]=-1.0.

showed that the 'veil' of weak metal lines, proposed by Magain (1983) to explain the missing UV opacity in solar models, increases the K fluxes due to backwarming.

These models can be compared to the extensive photometry of Johnson et al (1966). In figure 14 the model for [Fe/H]=0.0 and log g=4.5 is plotted on top of the Johnson (1966) main sequence locus. The 12% shift has made theory and observation agree well in the range of (V-K) from 1 to 2, but beyond this the model's predictions are increasingly too red in (V-K) or too blue in (B-V).

Phillips et al (1986, PRMV86) derived (V-K)-(B-V) model lines from the Kurucz (1979) population II models as part of their investigation of the HB of M4. It should be noted that these models are very coarse in the infra-red with the nearest points to the K filter being at 1.8 and 2.7 μm. These model lines are plotted together with the BG89/VBB85/BG78 (BGVB) models in figure 15. At first sight it appears that the 12% blueward shift in (V-K) is in error - the two sets of models would match fairly well in the region of overlap

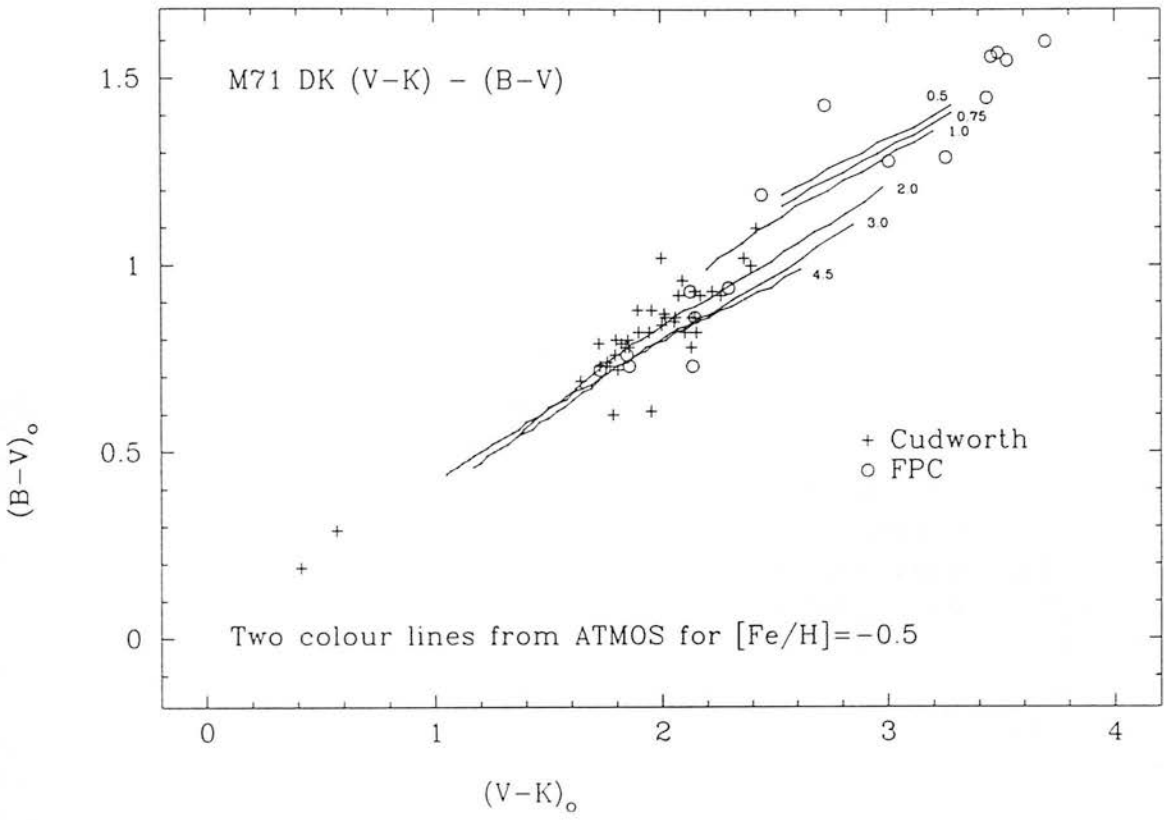

Figure 17: The (V-K)-(B-V) two-colour diagram for M71, with model tracks for [Fe/H]=-0.5.

if the BGVB models had not been shifted. However PRMV86 note that their models appear too blue in (B-V) (or too red in (V-K)) for the cooler stars. Comparing their solar abundance, log g=4.5 model to Johnson's (1966) field star observations shows that, whilst the two match well for the hot stars, a $\sim$ 20% blueward shift in (V-K) would be needed at the reddest model point ((V-K)=1.6) to reconcile model and observation. PRMV86 found their M4 HB observations to be well fitted for high (V-K) and badly fitted for low (V-K). It will be shown in the next chapter that the opposite is more likely to be true - it is the RHB stars that are not fitted by the models. This is then consistent with the sense of the error in the solar abundance model. Thus, it seems likely that the Kurucz models are affected by a similar problem to those of BG89. The PRMV86 models are used unmodified in the subsequent fitting but it should be borne in mind that they are probably in error for the cooler stars. These models are discussed a little further in the next chapter in relation to the M4 data.

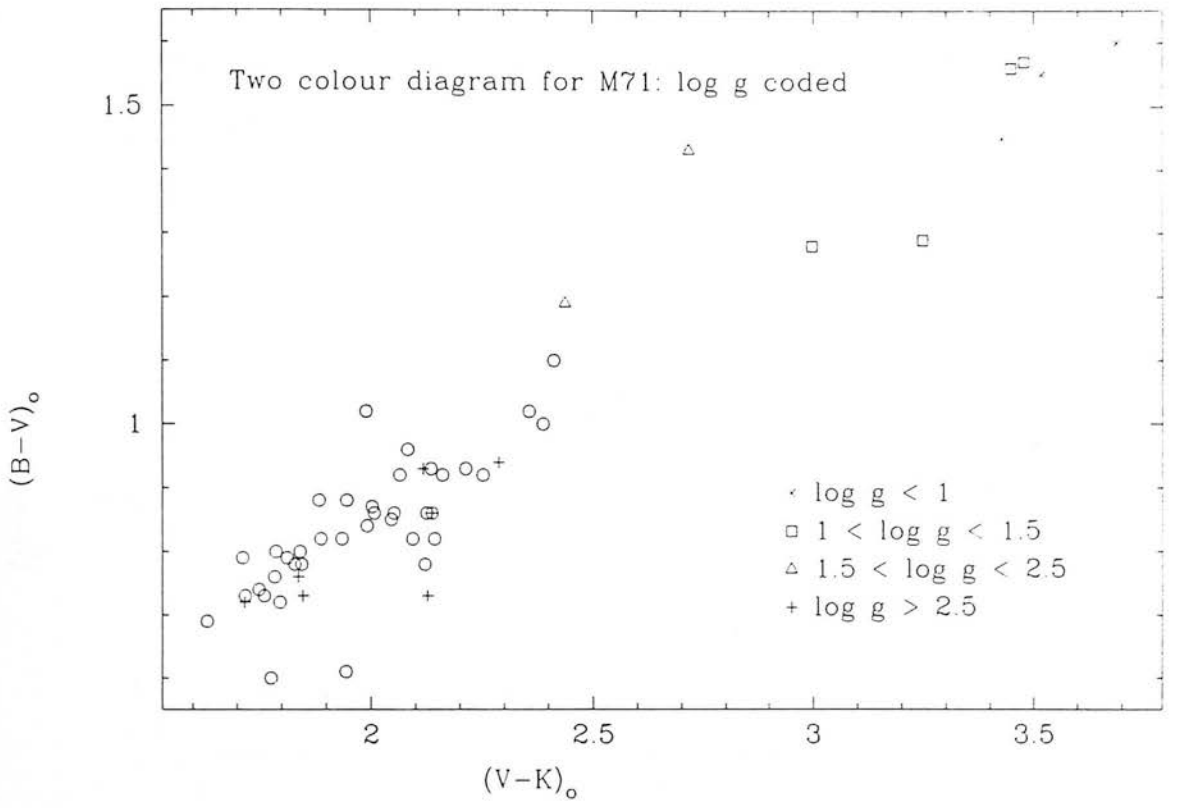

Figure 18: The (V-K)-(B-V) two-colour diagram for M71, stars coded for log g as derived by FPC79. The circles are the data from Cud85 for which no gravity information is available.

Figure 16 shows the (V-K)-(B-V) data for all stars with p> 50%, apart from one of the three probable field stars mentioned earlier. Also shown are the BGVB model lines for [Fe/H]=-1.0 and log g=4.5, 3, 2, 1, 0.75 and 0.5 and the PRMV86 models for log g = 2, 3 and 4.5.

Figure 17 shows the same data with models for [Fe/H]=-0.5 plotted.

Figure 18 shows the stars coded according to the value of log g found by FPC79.

It must be remembered that the errors in the colours are quite large (typically ±0.07 in (V-K) and ±0.05 in (B-V)) and that bright giants may show larger scatter than can be due purely to photometric errors.

For comparison figure 19 shows the Johnson (1966) fiducial lines for his observations of field main-sequence and giant stars. Of course, there are no main sequence stars plotted

for M71, since no B photometry is available.

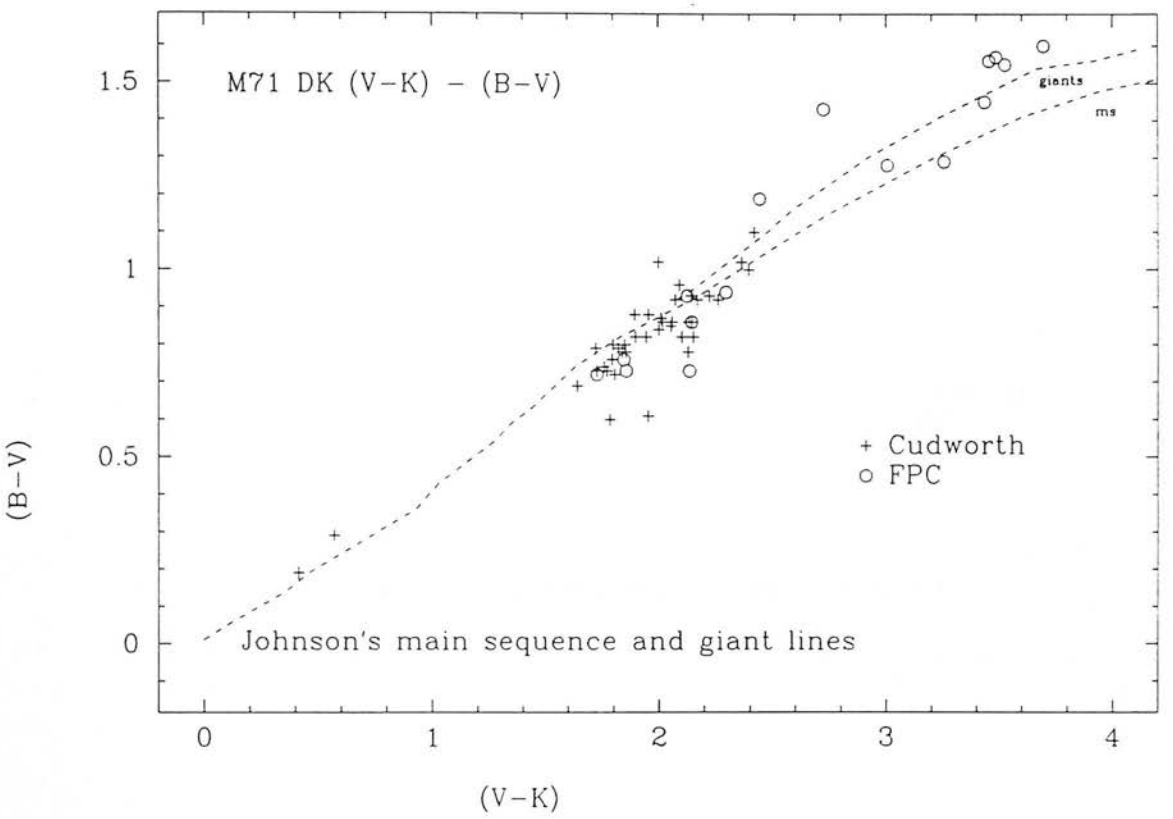

Figure 19: The (V-K)-(B-V) two-colour diagram showing Johnson's field main-sequence and giant lines.

Clearly the models do not exactly reproduce the FPC79 parameters, indeed the higher gravity stars are redder in (B-V), whereas the models suggest that they ought to be bluer. However, FPC79 used the rather unrealistic assumption of $\mathcal{M}$=1 $\mathcal{M}_{\odot}$ for all their stars in the calculation of log g. On the whole, the models fit well, particularly those for [Fe/H]=-0.5. The HB stars cluster about log g=2, which is in reasonable agreement with the values used by HHVASS87 in their HB modelling of 47 Tuc. The giants, although rather scattered, also agree well with the gravities derived from the appropriate SC91 isochrone. It appears that the gravities might agree even better with the expected values if [Fe/H]=-0.3.

In figure 20 five stars with log g derived from their high dispersion spectra are plotted together with the [Fe/H]=-0.5 models. The four stars that come from FPC79 were mea-

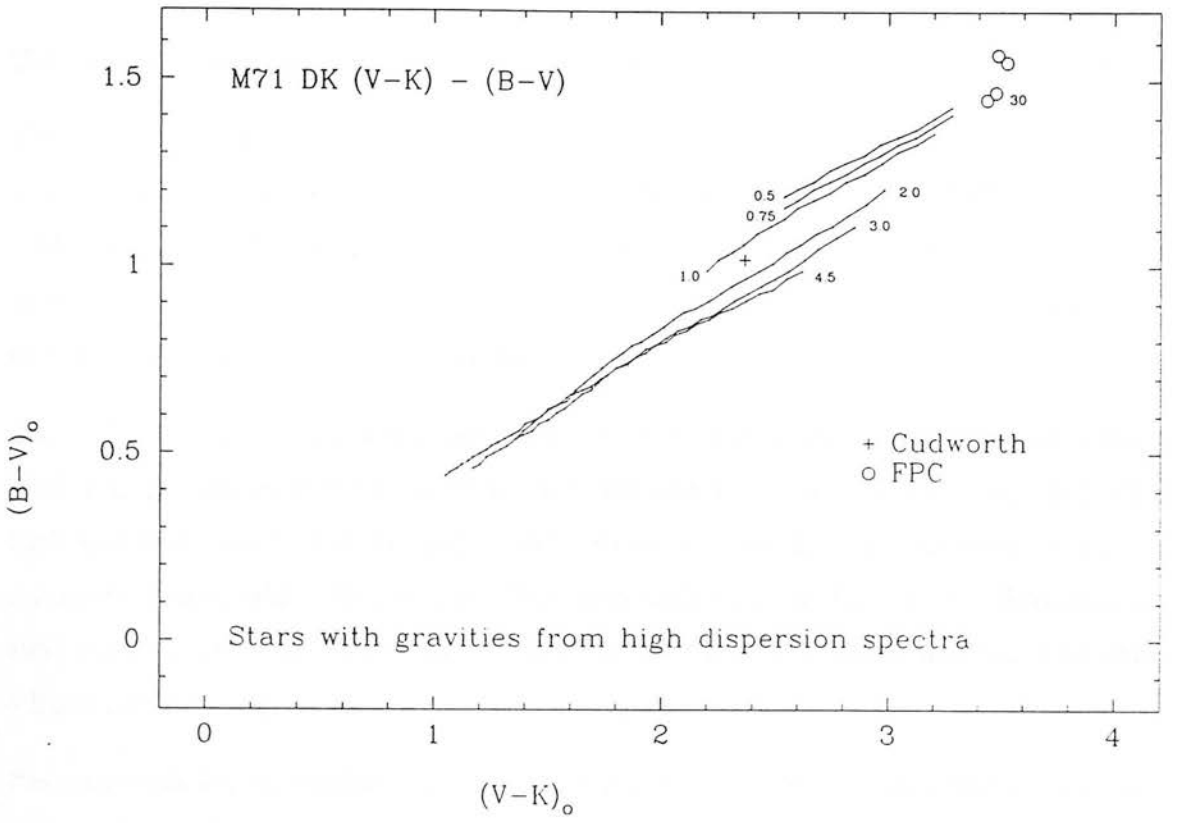

Figure 20: The (V-K)-(B-V) two-colour diagram for five M71 stars with spectroscopic determinations of effective gravity. The models for [Fe/H]=-0.5 are shown for comparison.

sured by Cohen (1980) (two were re-evaluated by Pilachowski, Sneden and Wallerstein in 1983, who found the same log g). For one of these, labelled as star 30 in the figure and not shown in other plots because Cud85 contains no membership information for it, they found log g=0.7, whilst for the other three log g=0.8. Pilachowski and Sneden (1987) found log g=1.6 for the star plotted as a cross in the figure. The latter is in excellent agreement with the models. Of the other four stars the models would seem to predict gravities which are correct for two of them and too small for the other two, however this involves extrapolation. As already discussed the models are most likely to be wrong for the reddest stars and in the sense seen in this case. Additionally taking into account the likely photometric errors in the stars, the present agreement between model and observations is certainly satisfactory.

8 Concluding remarks

This chapter considered K magnitude observations of the metal-rich globular cluster M71.

The previous work on M71 has been reviewed and revised with the conclusion that the best 'literature' parameters for this cluster are: $(m\text{-}M)_o$=12.88 ± 0.09, E(B-V)=0.27 ± 0.02, [Fe/H]=-0.7 ± 0.4 and t=15 ± 2 Gyr. A discussion of the value of R, the ratio of total-to-selective absorption, concluded that there was no strong evidence to suppose that the value was different from the normal 3.05.

The self-consistency of these parameters can be judged from two trials. A revised value of $(V\text{-}K)_{o,GB}$, measured from the (V-K)-K CMD with the adopted $(m\text{-}M)_o$ and E(B-V), leads to a 'consistent' value of [Fe/H]=-0.77 through the Frogel, Cohen and Persson (1983) calibration. Also, taking the mean $M_V(TO)$ from table 4 and [Fe/H]=-0.78 in Buonanno's 1986 equation (1), relating age to metallicity and turn-off luminosity and based on the VBB85 isochrones, gives an age of 12 Gyr for M71.

Previous work has constrained the size of any differential reddening that may be present across the face of the cluster and the present data cannot improve upon this.

The available data were gathered together to form the most complete (V-K)-V and (V-K)-K CMDs and also the 'best-for-fitting' (V-K)-V and (V-K)-K CMDs.

The (V-K)-(B-V) two-colour diagram was constructed from those giant and HB stars with a high membership probability. Three stars were found likely to be field stars, despite their apparent kinematic similarity to the cluster stars.

Examining the colour cross-section of the main-sequence stars showed indications of an excess similar to that expected from a population of binaries and stars with close companions. There were insufficient stars for this to be statistically significant.

The new BBVB isochrones were discussed and fitted to the (V-K)-V and (V-K)-K CMDs with the following 'best-fit' results: $(m\text{-}M)_o$=12.85 ± 0.15, E(B-V)=0.26 ± 0.03, [Fe/H]=-0.78 ± 0.3 and t=13 ± 1 Gyr. The isochrones match the shape of the observed CMDs well and the derived parameters are in excellent agreement with the adopted values. Clearly the 12% colour shift applied to the isochrones is appropriate at least to first order.

Since the derived parameters are independent of the adopted parameters, revised adopted

parameters may be calculated:

$$E(B\text{-}V)=0.266 \pm 0.015 \quad t=14.5 \pm 2 \text{ Gyr}$$
$$(m\text{-}M)_o=12.87 \pm 0.07 \quad [Fe/H]=-0.7 \pm 0.4$$

The range of estimates is so large for [Fe/H] that the adopted value is left unchanged. These are the most accurate estimates of the cluster parameters ever published.

A sequence of sub-dwarfs with known parallaxes could not be usefully fitted to the present data, because it does not go quite deep enough.

An attempt was made to match the CMDs of M71 and 47 Tuc. This proved difficult, both because of the lack of quality of the data and the uncertainties in relations derived from models. With the two clusters registered at their nominal offsets, various indicators were found to give contradictory signals about the age and metallicity differences between the two clusters. Potentially the most useful way to match the two clusters together was to find the colour and magnitude offsets which made such indicators give the most self-consistent pair of age and metallicity. In the present case this approach was not very successful, again being dominated by the observational and theoretical uncertainties.

The clump observed in the giant branch was compared to models by both FFCRB90 and SC91. FFCRB90's metallicity calibration of the V magnitude difference between the clump and HB, gave a metallicity consistent with the adopted value. Although there is a disagreement on the absolute magnitude of the clump, the differential measurement ΔV_{f-c} was examined as an age and metallicity indicator.

Finally the data were compared to (V-K)-(B-V) model colours constructed from several previous works. In general the models fitted the data well, with a good match to the previous spectroscopic values of gravity.

This chapter has been an exploration of what can be done with IR imaging data in a globular cluster. Clearly, the IR-optical CMD is just as useful as a purely optical one for determining cluster parameters, now that the relevant isochrones are available. Indeed, more information has been derived from the isochrone fitting than is usually the case with optical data. The use of (V-K) as the CMD colour reduces the photometric scatter in the

sequences and the IR has a distinct advantage in a cluster like M71 which suffers nearly a magnitude of extinction in the V-band.

References

Alcaino, G & Liller, W, 1987. Ap.J., **319**, 304.

Arp, HC & Hartwick, FDA, 1971. Ap.J., **167**, 499 (AH71).

Bell, R.A., 1987. In: *'The Harlow-Shapley Symposium on Globular Cluster Systems in the Galaxy'*, p.79. Eds. Grindlay, JE & Davis Philip, AG. Kluwer Academic Publishers (Dordrecht).

Bell, R.A., 1992. Submitted to M.N.R.A.S.

Bell,RA, Briley, MM & Smith, GH, 1990. A.J., **100**, 187.

Bell, RA & Gustafsson, B, 1978. A.&A.Suppl., **34**, 229 (BG78).

Bell, RA & Gustafsson, B, 1982. Ap.J., **255**, 122.

Bell, RA & Gustafsson, B, 1983. M.N.R.A.S., **204**, 249.

Bell, RA & Gustafsson, B, 1989. M.N.R.A.S., **236**, 653 (BG89).

Bergbusch, PA & VandenBerg, DA, 1991. Preprint (not seen).

Bessell, MS, 1983. P.A.S.P., **95**, 94.

Bessell, MS & Brett, JM, 1988. P.A.S.P., **100**, 1134.

Blackwell, DE, Booth, AJ, Petford, AD, Leggett, SK, Mountain, CM & Selby, MJ, 1986. M.N.R.A.S., **221**, 427.

Blackwell, DE, Petford, AD, Arribas, S, Haddock, DJ & Selby, MJ, 1990. A.&A., **232**, 396.

Brown, JA, Wallerstein, G & Oke, JB, 1990. A.J., **100**, 1561.

Buckley, DRV & Longmore, AJ, 1992. In preparation.

Buonanno, R, 1986. Mem. Soc. Astr. Ital., **57**, 333.

Buonanno, R, Corsi, CE & Fusi Pecci, F, 1989. A.&A., **216**, 80.

Burnham, R, 1977. *'The Celestial Handbook'*, Dover (New York).

Burstein, D & McDonald, LH, 1975. A.J., **80**, 17.

Butler, D, 1975. Ap.J., **200**, 68.

Canterna, R, 1975. Ap.J.Lett., **200**, L63.

Caputo, F, 19???. A.&A., **189**, 70.

Carney, B, 1979. Ap.J., **233**, 211.

Carney, B, Strom, J & Jones, RV, 1991. Preprint.

Cohen, JG, 1980. Ap.J., **241**, 981.

Cohen, JG, 1983. Ap.J., **270**, 654.

Cudworth, KM, 1985. A.J., **90**, 65 (Cud85).

Cuffey, J, 1959. *Sky and Telescope*, **19**, 93.

Cuffey, J, 1973. A.J., **78**, 408.

Dickens, RJ & Rolland, A, 1972. M.N.R.A.S., **160**, 37.

Dorman, B, VandenBerg, DA & Laskarides, PG, 1989. Ap.J., **343**, 750.

Driuker, GA, Fahlman, GG & Richer, HB, 1989. Ap.J., **342**, L27.

Elias, JH, Bell, RA, Matthews, K & Neugebauer, G, 1989. P.A.S.P., **101**, 1121.

Fernley, JA, 1989. M.N.R.A.S., **239**, 905.

Ferraro, FR, Clementini, G, Fusi-Pecci, F & Buonanno, R, 1991. M.N.R.A.S., **252**, 357.

Fisher, RA, 1963. 'Statistical Methods for Research Workers' Chapter 3 (13^{th} edn.). Oliver & Boyd (Edinburgh).

Frogel, JA, Cohen, JG & Persson, SE, 1983. Ap.J., **275**, 773 (FCP83).

Frogel, JA, Persson, SE & Cohen, JG, 1979. Ap.J., **227**, 499 (FPC79).

Fusi-Pecci, F, Ferraro, FR, Crocker, DA, Rood, RT & Buonanno, R, 1990. A.&A., **238**, 95 (FFCRB90).

Geisler, D, 1984. Ap.J.Lett., **287**, L85.

Glass, IS, 1974a. MNASSA, **33**, 54.

Glass, IS, 1974b. MNASSA, **33**, 71.

Gratton, G, 1987. A.&A., **177**, 177.

Gustafsson, B & Bell, RA, 1979. A.&A., **74**, 313.

Hatzidimitriou, D, 1991. M.N.R.A.S., **251**, 545.

Heasley, JN & Christian, CA, 1991. In: *'The Formation and Evolution of Star Clusters.'*, p.266. Ed. Janes, K. Astronomical Society of the Pacific (San Francisco).

Heggie, DC, 1975. M.N.R.A.S., **173**, 729.

Hesser, JE, Harris, WE, VandenBerg, DA, Allwright, JWB, Shott, P & Stetson, PB, 1987. P.A.S.P., **99**, 739 (HHVASS87).

Hills, JG, 1975. A.J., **80**, 1075.

Iben, I & Rood, RT, 1970. Ap.J., **159**, 605.

Janulis, R & Straižys, V, 1984. Astron & Space Science, **100**, 95.

Johnson, HL, 1966. Ann. Rev. Astron Astrophys, **4**, 143.

Johnson, HL, Mitchell, RI, Iriarte, B & Wisniewski, WZ, 1966. Comm. Lunar Planet. Lab., **4**, 99.

Jones, KG, 1991. *'Messier's Nebulae and Star Clusters.'* Cambridge University Press (Cambridge).

Koorneef, J, 1983. A.&A.Suppl., **51**, 489.

Kron, GE & Guetter, HH, 1976. A.J., **81**, 817.

Kurucz, RL, 1979. Ap.J.Suppl., **40**, 1.

Laird, JB, Carney, BW & Latham, DW, 1988. A.J., **95**, 1843.

Longmore, AJ, Dixon, RI, Skillen, I, Jameson, RF & Fernley, JA, 1990. M.N.R.A.S., **247**, 684 (LDSJF90).

Machin, G, Allington-Smith, J, Callanan, PJ, Charles, PA, Hassall, BJM, Mason, KO, Mukai, K, Naylor, T, Smale, AP & van Paradijs, J, 1990. M.N.R.A.S., **242**, 9p.

Magain, P, 1983. A.&A., **122**, 225.

Martin, PG & Whittet, DCB, 1990. M.N.R.A.S., **357**, 113 (MW90).

Nemec, JM & Harris, HC, 1987. Ap.J., **316**, 172.

Peterson, CJ, 1986. P.A.S.P., **98**, 1258.

Phillips, JP, Martinez Roger, C, Sanchez Magro, C, Lazaro Vilchez, C, 1986. A.&A., **161**, 257 (PRMV86).

Pilachowski, CA, Olszewski, EW & Odell, A, 1983a. P.A.S.P., **95**, 713.

Pilachowski, CA & Sneden, C, 1987. I.A.U. Symposium 126, p.497.

Pilachowski, CA, Sneden, C & Wallerstein, G, 1983b. Ap.J.Suppl., **52**, 241.

Piotto, G, King, IR, Capaccioli, M, Ortolani, S & Djorgovski, S, 1990. Ap.J., **350**, 662.

Pryor, C, McClure, RD, Hesser, JE & Fletcher, JM, 1989. '*Proceedings of the Workshop on Dynamics of Dense Stellar Systems*', 175. Ed. Merritt, D, Cambridge University Press (Cambridge).

Richer, HB & Fahlman, GG, 1988. Ap.J., **325**, 218 (RF88).

Ryan, SG, 1989. A.J., **98**, 1693.

Sandage, A & Roques, P, 1984. A.J., **89**, 1166.

Saxner, M & Hammarbäck, G, 1985. A.&A., **151**, 372 (SH85).

Searle & Zinn, 1978. Ap.J., **225**, 357.

Spitzer, L, 1987. '*Dynamical Evolution of Globular Clusters*', Ch.7, Princeton University Press (Princeton, NJ).

Stetson, PB & Harris, WE, 1988. A.J., **96**, 906.

Straniero, O & Chieffi, A, 1991. Ap.J.Suppl., **76**, 525 (SC91).

Sweigart, AV, Renzini, A & Tornambé, A, 1987. Ap.J., **312**, 762.

Tifft 1963 M.N.R.A.S., **126**, 209.

VandenBerg, DA, 1983. Ap.J.Suppl., **51**, 29 (VB83).

VandenBerg, DA, 1985. In '*ESO Workshop on the Production and Distribution of CNO Ele-*

ments', eds. Danziger, IJ, Matteucci, F & Kjär, K, p.73. ESO (Garching bei München).

VandenBerg, DA & Bell, RA, 1985. Ap.J.Suppl., **58**, 561 (VBB85).

VandenBerg, DA, Bolte, M & Stetson, PB, 1990. A.J., **100**, 445.

VandenBerg, DA & Smith, GH, 1988. P.A.S.P., **100**, 314.

VandenBerg, DA & Stetson, PB, 1991. A.J., **102**, 1043.

Whittet, DCB & van Breda, IG, 1978. A.&A., **66**, 57.

Zdanavičius, K, 1986. Vilniaus Astron Obs Bull, **74**, 3.

Zdanavičius, K, 1987. In *'The Harlow-Shapley Symposium on Globular Cluster Systems in the Galaxy'*, p.515. Eds. Grindlay, JE & Davis Philip, AG. Kluwer Academic Publishers (Dordrecht).

Zinn, R, 1980a. Ap.J.Suppl., **42**, 19.

Zinn, R, 1980b. Ap.J., **241**, 602.

Zinn, R, 1985. Ap.J., **293**, 424.

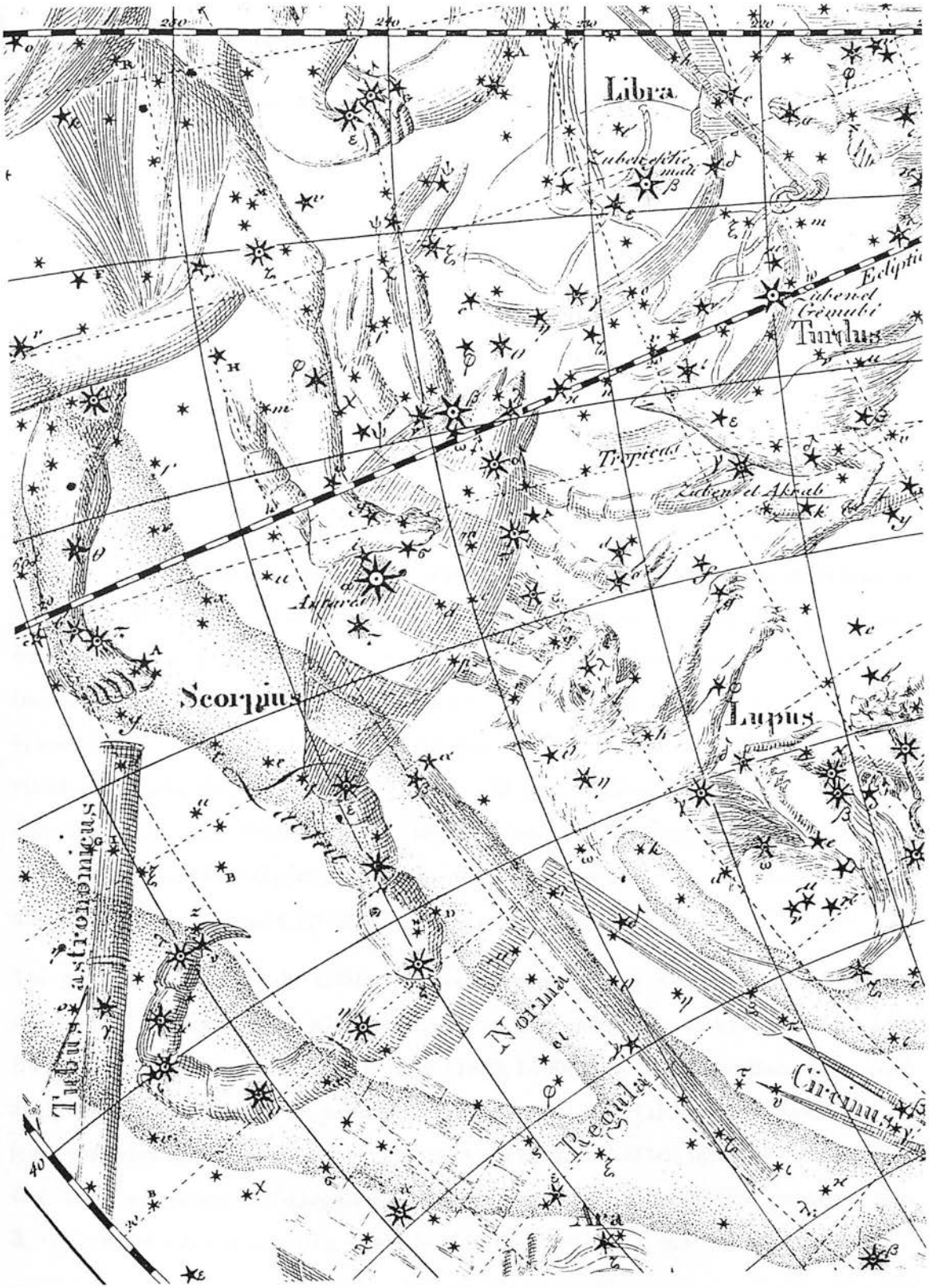

The constellation of Scorpius from Bode's 'Uranographia' (1801).

4. The Globular Cluster M4 Scorpii

M4 Sco ≡ NGC6121 ≡ C1620-720

$\alpha = 16^h20^m.5$ $\quad \delta = -26°24'$ (1950.0)

$\ell^{II} = 351°.0$ $\quad b^{II} = 16°.0$

1 Introduction

At less than 2kpc from the Sun, M4 is probably our closest globular cluster, lying near the bright star Antares, in the heart of the Scorpion. At visible wavelengths this is not obvious because the cluster suffers nearly a magnitude and a half of extinction as the light from its stars pass through the Sco-Oph dark cloud complex. At IR wavelengths this extinction is reduced by a factor of 10 and if we had eyes sensitive to 2 μm wavelengths, M4 would stand out as a bright, fuzzy object of 2nd or 3rd magnitude next to the cluster of young stars that would be revealed within the dark cloud. (This brightness estimate comes from the integrated (V-K)-[Fe/H] relation of Aaronson et al (1978) and the integrated V magnitude given in Norton (1978)).

The previous studies of the cluster are well summarized in Alcaino and Liller (1984, hereafter AL84), since when Alcaino, Liller and Alvarado (1988, ALA88) have presented BVI CCD observations and Liu and Janes (1990, LJ90) have performed Baade-Wesselink analysis on four of the cluster variables. Cudworth and Rees (1990, CR90) examined the issue of cluster membership and Longmore et al (1990, LDSJF90) included the cluster in their study of the log P-K-magnitude relation. Both LJ90 and LDSJF90 proposed that R, the ratio of total-to-selective, might be 4 in the direction of M4.

The uncertainty in E(B-V) for M4 has been a major block to studies of what is otherwise an attractive target, owing to its proximity to the Sun and its sparseness. This has meant, for instance, that the RR Lyraes have not been studied in anything like the detail of those in M3 or M15. Also the range of possible input parameters to isochrone studies has led

to a wide range of estimates of the age and metallicity of the cluster (see, for instance, VandenBerg and Bell (1985, VBB85)).

This chapter is similar in structure to the last, with an additional discussion of the luminosity function derived from the present K data. Having achieved good results with both the isochrones and two-colour models in the last chapter, they may be used here with some confidence, to derive parameters for M4.

Section 2 reviews the cluster parameters derived in previous studies, including a full discussion of the very important question of the values of R and E(B-V) towards M4. Section 3 presents the current data, together with previous optical and IR data. In section 4 the BBVB isochrones (see Bell (1992) and section 4 of the last chapter) are matched to the CMDs and in section 5 the cluster's CMD is compared with that of M71. In section 6 model calculations are matched with the two-colour diagram. Section 7 sees a brief examination of the cluster's luminosity function and attempts to compare it to the previously published LF.

2 Standard parameters for M4

What are the best, current estimates of reddening, metallicity, distance modulus and age for M4 ?

The following sections review the previous work in the literature. Where possible the results are re-appraised in the light of a value of R closer to 4 than to the more normal 3.

2.1 Reddening and the value of R

It has long been known that the reddening to M4 is higher than expected from its position in the galaxy because its line of sight passes through the Sco-Oph dark cloud complex. In addition, as early as 1939 Greenstein suggested that there might be differential reddening across the face of the cluster. This was confirmed and constrained by subsequent studies and finally quantified by CR90 as an E-W gradient, as part of their study of cluster membership. LJ90 and LDSJF90 suggested that R might be closer to 4 than 3, especially since R=3.9 in regions of the ρ Oph dark cloud (Whittet and van Breda, 1980).

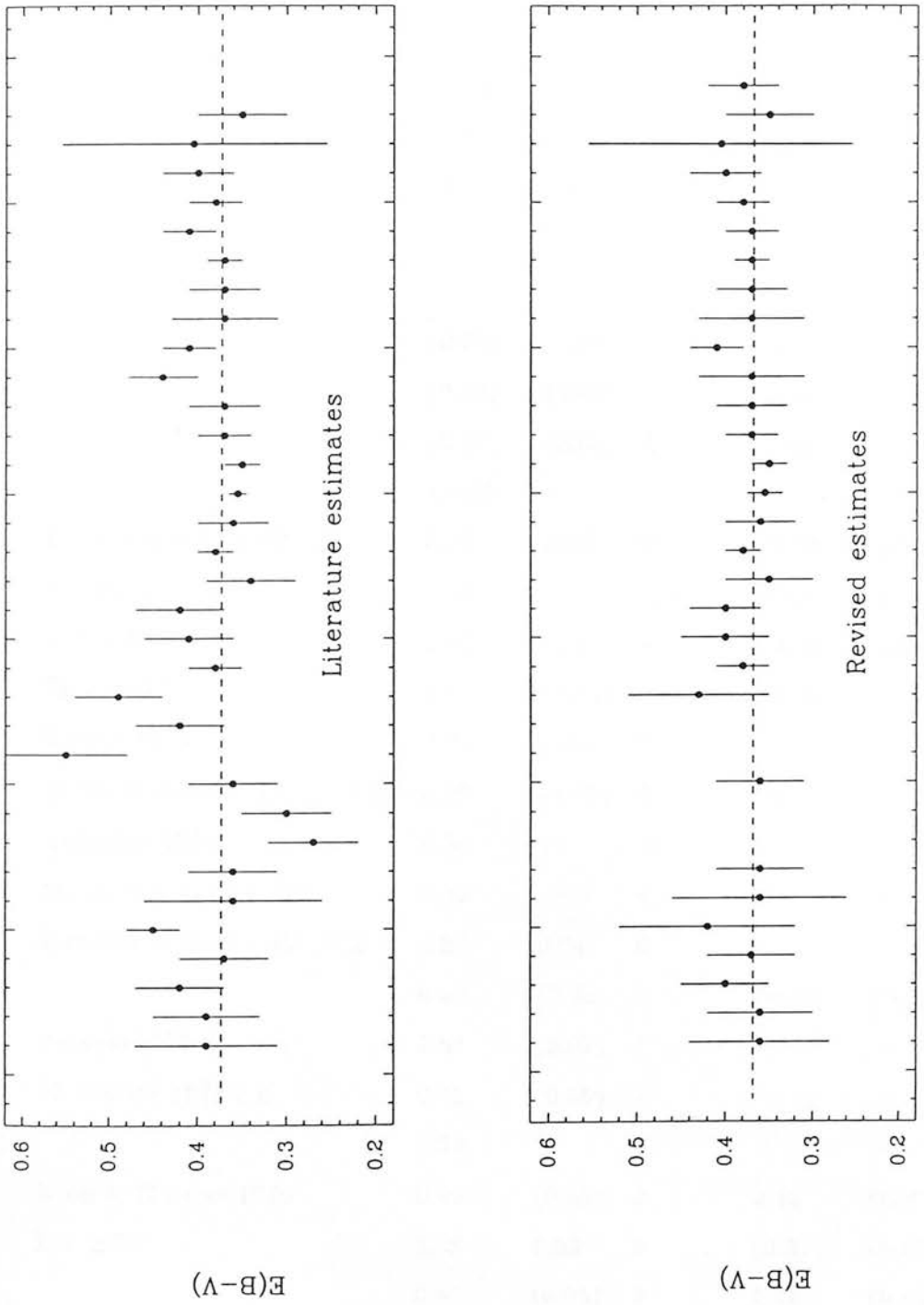

Figure 1: Reddening estimates to M4. The upper plot shows all of the estimates from the literature, whilst the lower plot shows those values which can be revised under the assumption that R=4. The estimates are plotted in the same order as they are listed in table 1.

Table 1: Reddening Estimates to M4

	Author	Quoted E(B-V)	σ	Method	Revised E(B-V)	σ	Notes	
	(1)	(2)	(3)	(4)	(5)	(6)	(7)	
(	Greenstein 1939	(0.39)	(0.08)	1	0.36	(0.08)	1	)
(		(0.39)	(0.06)	2	0.36	(0.06)	1	)
(		(0.42)	(0.05)	3	0.40	(0.05)	1	)
(		<0.52	—	4	—	—	1	)
	Kron & Mayall 1960	0.37	0.05	2	(0.37)	(0.05)		
	Newell 1970	0.45	0.03	4,5	0.42	0.1	2	
	Philip 1971	0.36	(0.1)	4,5	(0.36)	(0.1)	3	
	Eggen 1972	0.36	(0.05)	4	(0.36)	(0.05)	4	
	Racine 1973	0.27	0.05	2	—	—	2	
	Harris & van den Bergh 1974	0.30	(0.05)	2	—	—	5,6	
(	Kukarkin 1974	0.36	—	6	—	—		)
(	Mironov & Samus 1974	0.34	—	4	—	—		)
(	Burstein & McDonald 1975	0.37	0.04	6	—	—		)
		0.36	(0.05)	2	(0.36)	(0.05)		
(	Alcaino 1975	0.55	(0.07)	7	—	—	7	)
	Moshkalev 1975 a,b	0.42	(0.05)	7	—	—	8,9	
(		0.34	—	4	—	—	9	)
	Kron & Guetter 1976	0.49	(0.05)	2	0.43	0.08	10	
	Lee 1977	0.38	0.03	8	(0.38)	(0.03)	11	
		0.41	(0.05)	9	0.40	(0.05)		
	Lloyd-Evans 1977	0.42	(0.05)	9	0.40	0.04	12,13	
	Sturch 1977	0.34	(0.05)	10	0.35	0.05	14,15	
	Cacciari 1979	0.38	0.02	4	(0.38)	(0.02)		
		0.36	(0.04)	9	(0.36)	(0.04)		
		0.355	0.01	10	(0.355)	0.02	14	
		0.35	0.02	11	(0.35)	(0.02)		

	Zinn 1980	0.37	0.03	2	(0.37)	(0.03)	
	Sandage 1981	(0.37)	(0.04)	3	(0.37)	(0.04)	
	Alcaino & Liller 1984	0.44	0.04	8	0.37	0.06	
		(0.41)	(0.03)	12	(0.41)	(0.03)	
	Richer & Fahlman 1984	0.37	0.06	8	(0.37)	(0.06)	
	de Bruijn & Lub 1987	0.37	0.04	3	(0.37)	(0.04)	
	Caputo 1987	(0.37)	(0.02)	3	(0.37)	(0.02)	
	Alcaino et al 1988	0.41	0.03	12	0.37	(0.03)	16
	Kadla et al 1989	0.38	0.03	3	(0.38)	(0.03)	
(	Sarajedini & King 1989	0.40	—	12	—	—	)
	Cudworth & Rees 1990	0.40	0.04	9	(0.40)	(0.04)	
(	LDSJF90	0.405	0.15	6	(0.405)	(0.15)	)
	Sandage 1990	0.35	0.05	3	(0.35)	(0.05)	
		—	—	9	0.38	0.04	
	Mean*	0.373	0.006 n=28		0.368	0.006 n=26	

* weighted by the error estimates and excluding Greenstein's values, compilations and values for which an error estimate cannot be assigned.

() around a whole row indicate that the estimates have not been used in the calculation of either mean.

() in columns 2 or 3 indicate an estimate from the information in the reference, since the value has not been explicitly stated.

() in columns 5 or 6 indicate a value that is unchanged by the revised parameters.

— indicates that there is insufficient information to calculate or re-calculate the quantity.

Key to methods

1. Star counts
2. Integrated colours
3. Colours of RR Lyraes

4. Colours of BHB stars
5. Spectra & model atmospheres
6. Compilation of previous work.
7. Colours of GB stars
8. Colours of field stars
9. Colours of edges of instability strip
10. UV excess for RR Lyrae stars (Sturch 1966)
11. [Fe/H] of RR Lyraes
12. Isochrone fit

Notes to table 1:

1. Greenstein's colour excess in his red index is hard to calibrate against E(B-V). Using the same approximate relation as Newell (1970) gives the values in column 2. The values in column 5 have been reduced by a factor derived from the reddening data of MW90. None of the values is included in the means.

2. Matching up the Greenstein and Lee numbering systems shows, from CR90, that three of the stars observed by Newell are not members. The revised result excludes these stars and includes corrections for CR90's reddening gradient, which make only a 1% difference in E(B-V). The value of E(B-V)/E(nb), where E(nb) is the colour excess in Newell's narrow band colour, is smaller for higher R values, which will bring down the value of E(B-V). Because it is not possible to accurately re-calculate the colour-excess ratio the error estimate for the revised value has been doubled.

3. Philip's result has had an arbitrary, large error estimate assigned since little information is available on its derivation.

4. This estimate combines the Newell and Philip data with new, unpublished photometry. It is included at full weight in the mean.

5. Harris & van den Bergh seem to have used essentially the same data and the same relationship as Racine (1973) to derive this value. The two estimates have been included in the mean at half weight.

6. It seems likely that fitting the integrated broad-band colours to the standard relationship for a group of globular clusters, as Harris & van den Bergh did, will give an

anomalous result since it is well documented that M4 has a sparsely populated upper giant branch and a well populated BHB.

7. Alcaino matched the lower giant branch of M4 with other clusters including M3, M13 and M15. No allowance was made for the metallicity or age differences between these clusters. Measurements on the Straniero and Chieffi (1991, SC91) isochrones show that for the M15 comparison, for example, a correction of up to $0^m.1$ (in the sense of reducing E(B-V)) might be appropriate due to metallicity difference. This is still not enough to explain such a large value of E(B-V), although it does show that the basic method is flawed. It is interesting to note that although Alcaino has written two subsequent papers on M4, he has never referred to this high estimate of the reddening and has only mentioned the photographic data from this paper in passing. Also CR90 noted a small colour-dependent difference between this data and their own. For these reasons this estimate of reddening was not included in the mean.

8. Moshkalev compared $(B\text{-}V)_{o,g}$, the $(B\text{-}V)_o$ colour of the giant branch at the level of the horizontal branch, between M4 and the un-reddened cluster M3 to get E(B-V). This seems a very unreliable method since no allowance was (or could) be made for the clusters' differing metallicities and ages.

9. The English translation of Moshkalev's paper is missing a crucial two lines which mean that this reference has been misquoted as having found E(B-V)=0.34 by the method discussed in note 8. In fact, as listed in the present table, Moshkalev found E(B-V)=0.42 from the colour of the GB, and E(B-V)=0.34 from the colours of the blue horizontal branch stars, following the method of Mironov and Samus (1974).

10. Interpolation between wavelengths in the MW90 data allows a revised conversion between Kron & Guetter's narrow-band colour excess and E(B-V). The error estimate has been increased because the same interpolation for R=3.05 does not reproduce their own original conversion well, that is, the interpolation does not produce a very consistent result.

11. Lee also made another estimate of E(B-V)=0.31 $\pm$ 0.03 from the colours of BHB and field stars but he considered this value unreasonable and the method flawed and so disregarded it. The value has not been included in either mean.

12. The revised estimate uses the more recent M3 photometry of Sandage & Katem

(1982) in matching the red edges of the HB.

13. Comparing Lloyd-Evans' photometry with that of CR90 shows ΔV(LE-CR)=0.07 $\pm$ 0.02 and Δ(B-V)=0.00 $\pm$ 0.01.

14. Sturch's 1966 calibration of RR Lyrae UV excess with E(B-V), which is used by both Sturch (1977) and Cacciari (1979), used E(U-B)/E(B-V)=0.72, which is correct for R$\sim$4.0 (MW90).

15. The quoted value is Cacciari's 1979 re-evaluation of Sturch's data.

16. Figure 2 shows ALA88's (B-V)-V fiducials fitted to the SC91 isochrones. ALA88 found best fit parameters of E(B-V)=0.41, $(m\text{-}M)_V$=12.7, Z=0.001 and an age of 17 $\pm$ 1.5 Gyr. The upper plots show the fiducials plotted at ALA88's E(B-V) and distance modulus for Z=0.0008, 0.001 and 0.002 and ages of 10, 12, 14, 16, 18 and 20 Gyr. It can be seen that none of these is a good fit. The lower panels show the data fitted to the same isochrones by allowing both E(B-V) and $(m\text{-}M)_V$ as free parameters. The best fit is found at Z=0.001 ([Fe/H]=-1.35), E(B-V)=0.37, $(m\text{-}M)_V$=12.6 and an age of 18 Gyr. As with the VBB85 isochrones used by ALA88 the lower main sequence is redder than the isochrones, although the fit is excellent for the brighter stars.

Table 1 contains a summary of the various reddening estimates, together with error estimates, from the M4 literature, as well as a revised estimate if R is assumed to be 4.0, where such a calculation is possible. The table is followed by notes and a detailed discussion of a few important references, with particular regard to determining the value of R. The values in the table are plotted in figure 1. Whilst the weighted means at the end of the table are not significantly different, it is clear from the figure that the revised values contain less scatter, although, of course, part of this is simply because some estimates, which have been shown to be flawed, have been discarded.

The important result is that *R=4 is at least as good as R=3* when used in the interpretation of the previous reddening estimates. The discussion that follows the table aims to show that R=4 is actually *better*.

As in previous chapters, A_K/E(B-V) and E(V-K)/E(B-V) are taken from the data of

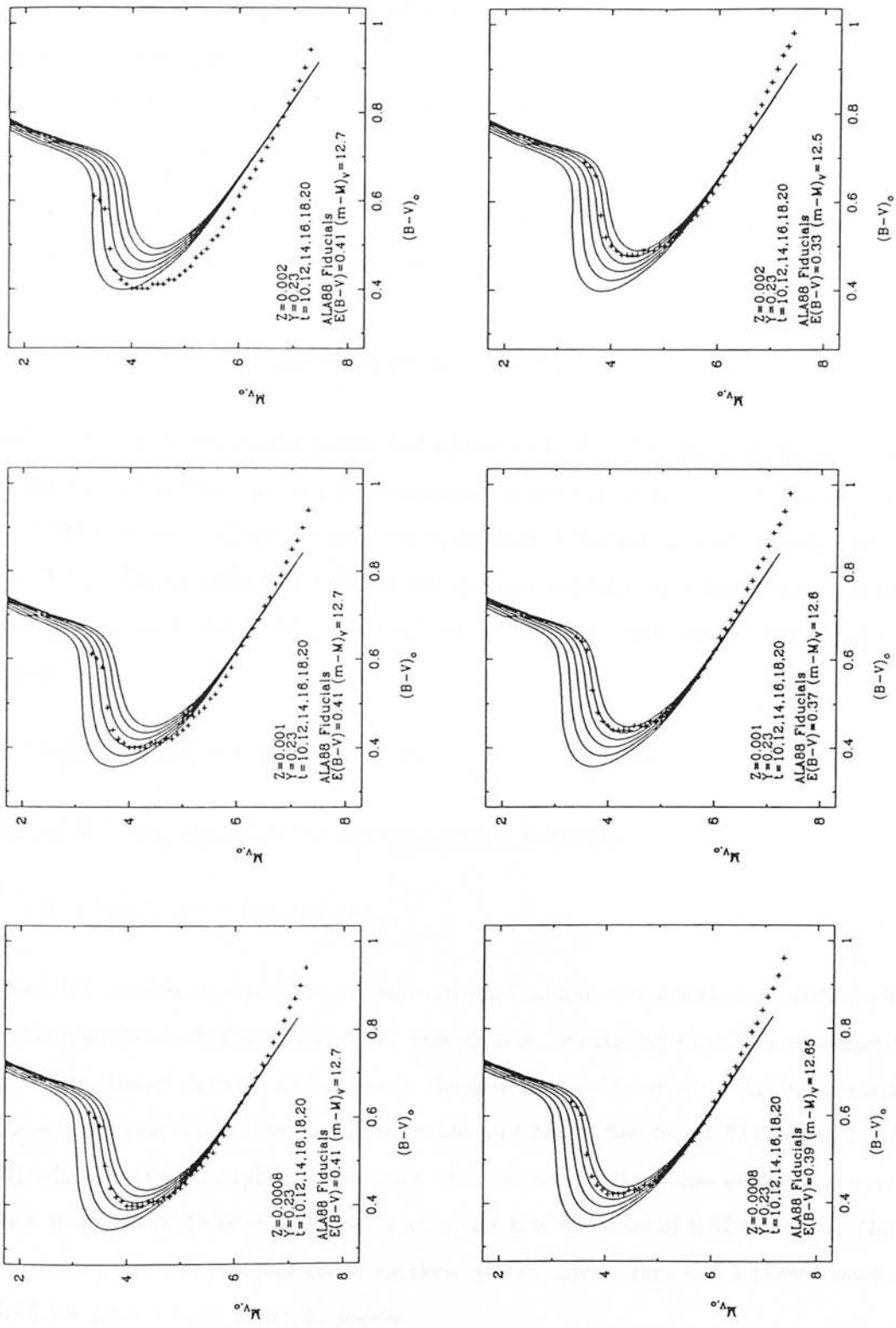

Figure 2: Fitting the ALA88 data to the Straniero and Chieffi isochrones. The upper plots show the data at the offsets that ALA88 determined.

Martin and Whittet (1990, hereafter MW90). These agree well with the extensive observations of Herbst et al (1982) and the data of Cardelli, Clayton and Mathis (1989, CCM89). The observations in Whittet and van Breda (1978) show that the relations are linear between R=3 and 4.

Some of these studies and other works can provide further information, particularly on the value of R, and these are discussed in the next sections.

2.1.1 Caputo's theoretical work on the RR Lyraes

Caputo (1987) used the Sturch (1977) and Cacciari (1979) UBV observations of the cluster's RR Lyraes to find T_{eff} and the bolometric correction from (B-V) by interpolating in the VBB85 models. Caputo's aim was to conduct a 'self-consistent' investigation and she used this T_{eff} to derive the value of the distance modulus as a function of the likely [Fe/H], stellar mass and E(B-V), through the van Albada and Baker (1971) pulsation equation:

$$logP = 11.497 + 0.84log\frac{L}{L_{\odot}} - 0.68log\frac{\mathcal{M}}{\mathcal{M}_{\odot}} - 3.48logT_{eff}$$

Caputo et al (1984) examined the mass-luminosity parameter,

$$A = logL/L_{\odot} - 0.81log\mathcal{M}/\mathcal{M}_{\odot},$$

and used HB models to show that it was a strong function of the helium abundance but almost independent of [Fe/H] and CNO abundances. Assuming that Y is constant for the globular cluster system, Caputo used the observed value of A for M3 to constrain the pulsation equation for the variables in M4 and M15. She found E(B-V)=0.37 and [Fe/H]=-1.1 for M4. Completing Caputo's 'self-consistent' discussion gives an apparent distance modulus of 12.76 $\pm$ 0.02 and a mass for the variables of $0.63\pm0.01\,\mathcal{M}_{\odot}$ (both formal errors). An independent check on these values comes from Lub's (1986) work on the field RR Lyraes from which he found:

$$M_V(RR) = 0.37 - 2.03log\mathcal{M}/\mathcal{M}_{\odot} + 0.20[Fe/H]$$

Substituting in [Fe/H]=-1.1, $\mathcal{M}/\mathcal{M}_{\odot}$=0.63 and the mean V magnitude of the variables observed by Sturch and Cacciari, $< m_V(RR) >$=13.35 $\pm$ 0.16 gives $(m\text{-}M)_V$=12.79 $\pm$ 0.16.

Although the value is rather uncertain it agrees well with that found above, confirming the self-consistency of the derived parameters.

If R=3.05, the true distance modulus, $(m\text{-}M)_o$, is 11.63, or if R were 4.0, $(m\text{-}M)_o$ would be 11.28. The adopted value of R is used only at the last and does not affect the derived $(m\text{-}M)_V$. If, however, (V-K) is used instead of (B-V) to calculate the temperature, the value of R comes in through the ratio E(V-K)/E(B-V) used to de-redden the observed colour. The $m(RR)_{V,-0.3}$ and $m(RR)_{K,-0.3}$ from LDSJF90 can be employed to find an average temperature through the form of Fernley's (1989) (V-K)-T_{eff} calibration used in that paper:

$$log T_{eff} = 3.954 - 0.132(V - K)_o$$

This temperature can be used with $\mathcal{M}$=0.63 $\mathcal{M}_\odot$, E(B-V)=0.37 and [Fe/H]=-1.1 to derive a distance modulus, interpolating in the VBB85 models to find the bolometric correction, BC. (The derived T_{eff} and BC agree well with those from table 9 of LJ90, which is based on unpublished and corrected Kurucz atmospheres for $\mathcal{M}$=0.6 $\mathcal{M}_\odot$ and [Fe/H]=-1.3, and with the approximation to the BC in equation (3) of LDSJF90).

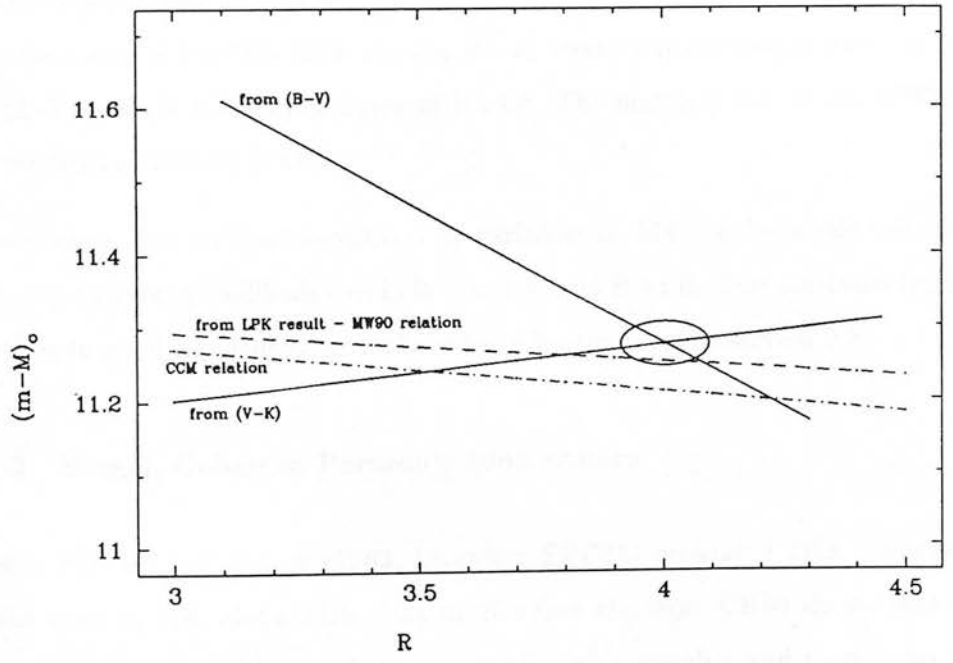

Figure 3: The relation between R and distance modulus for Caputo's data (see text).

Again, the procedure gives a range of values of $(m\text{-}M)_o$ depending on the value of R assumed. Since the dependence of $(m\text{-}M)_o$ on R is different according to whether (B-V) or (V-K) is used as the input to the models, it is possible to plot the two solution sets on an R - $(m\text{-}M)_o$ diagram. This is shown in figure 3. The two procedures are consistent with each other where the two lines intersect, giving values of R=4.0 $\pm$ 0.09 and $(m\text{-}M)_o$=11.28 $\pm$ 0.03 (the calculated (formal) errors in the $(m\text{-}M)_o$ values for both (V-K) and (B-V) temperatures produce the plotted 1σ error ellipse of possible intersections).

The value of $(m\text{-}M)_o$ from the log P - K relation (from LDSJF90) can also be compared to these results but the value of A_K/A_V is dependent on the value of E(V-K)/E(B-V) chosen. From MW90, a simple linear interpolation to R=4.0 gives A_K/A_V=0.097. Using the same functional form of the relation between A_K/A_V and R as CCM89:

$$\frac{A_K}{A_V} = a + \frac{b}{R_V},$$

but with the data of MW90 gives the same value of 0.097 with a=0.1130 and b=-0.0641. The distance modulus derived from the log P - K relation is then $(m\text{-}M)_o$=11.25 $\pm$ 0.05 for R=4.0. Using CCM89's values of a=0.1615 and b=-0.1483 would give A_K/A_V=0.124 and $(m\text{-}M)_o$=11.21 at R=4.0. The solution sets possible from the log P - K relation value and the CCM89 and MW90 reddening relations are also plotted on figure 3. It can be seen that the value of $(m\text{-}M)_o$ from the log P - K relation is consistent with the values from the (B-V) and (V-K) temperatures at R=4.0. The match is best if the MW90 version of the reddening relation is used.

In summary, the BVK observations of variables in M4 can be made self-consistent by choosing an average reddening of E(B-V)=0.37 and R=4.0. This produces $(m\text{-}M)_o$=11.25, which is in good agreement with the value adopted later in section 2.3.

2.1.2 Frogel, Cohen & Persson's 1983 papers

Frogel, Persson and Cohen (1983, hereafter FPC83) presented JHK observations of 26 bright stars in M4, along with stars in 25 other clusters. CR90 shows that 23 of these stars are highly probable members, one star is not a member and there is no information concerning the other two stars.

Another paper by the same group, Frogel, Cohen and Persson (1983, FCP83), discussed

the metallicity scale in relation to their observations in 33 clusters. The morphological parameters that they used were $(V\text{-}K)_{o,GB}$, the $(V\text{-}K)_o$ GB colour at $M_{K,o}$=-5.5; $(J\text{-}K)_{o,GB}$, the $(J\text{-}K)_o$ colour at the same absolute magnitude; $M_{K,o}(GB)$, the absolute GB K-magnitude at $(V\text{-}K)_o$=3.0, and log $T_{eff}(GB)$, the temperature of a star at $M_{bol,o}$=-3.0. All these parameters are changed by changing the value of R.

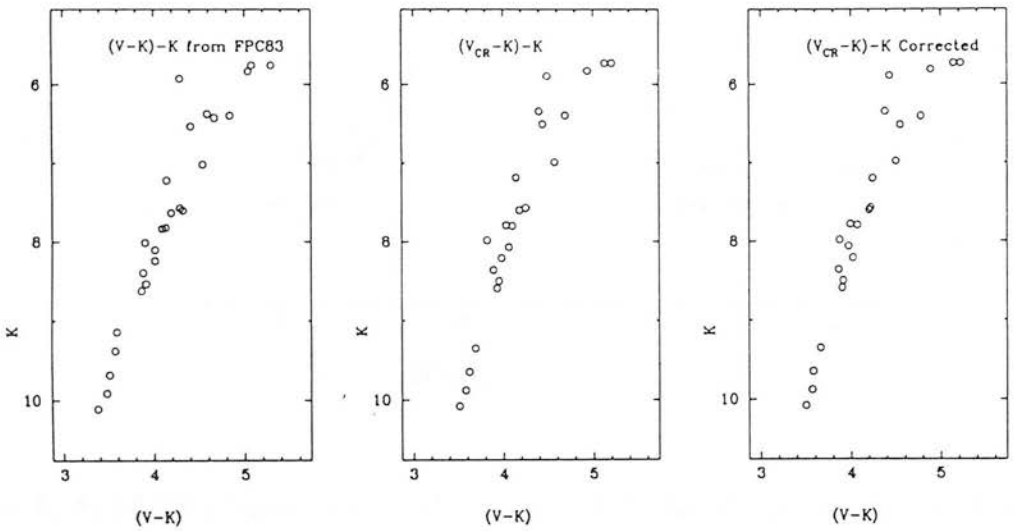

Figure 4: Using CR90 V magnitudes and reddening corrections for the FCP83 giant observations. The plots show a) the giants as FPC83 plotted them, b) with the V magnitudes replaced by those of CR90 and c) with V and K magnitudes corrected for the CR90 reddening gradient.

FCP83 took UBV magnitudes for their stars from Lee (1977) and Eggen (1972). Using the V magnitudes of CR90 instead produces little change, as shown in figure 4. Also shown are the same data after application of the CR90 reddening gradient. Even though the stars cover a quite large range in RA (about $400^{\widehat{n}}$ either side of the centre) this diagram shows little or no improvement over the uncorrected diagram. Since $\Delta E(V\text{-}K)=3.61\Delta E(B\text{-}V)$ for R=4, some of the stars have been shifted by up $0^m.3$ in (V-K), although the shift in K is $\leq 0^m.01$. This lack of improvement is partly because there appears to be real intrinsic scatter amongst the brightest giants (also seen in Cudworth's optical CMD) and partly because the CR90 gradient is more useful as a statistical correction to a large data-set, rather than for a small data-set where the small-scale patchiness of the obscuration dominates.

FPC83 examined their cluster stars in various colour-colour and colour-magnitude plots.

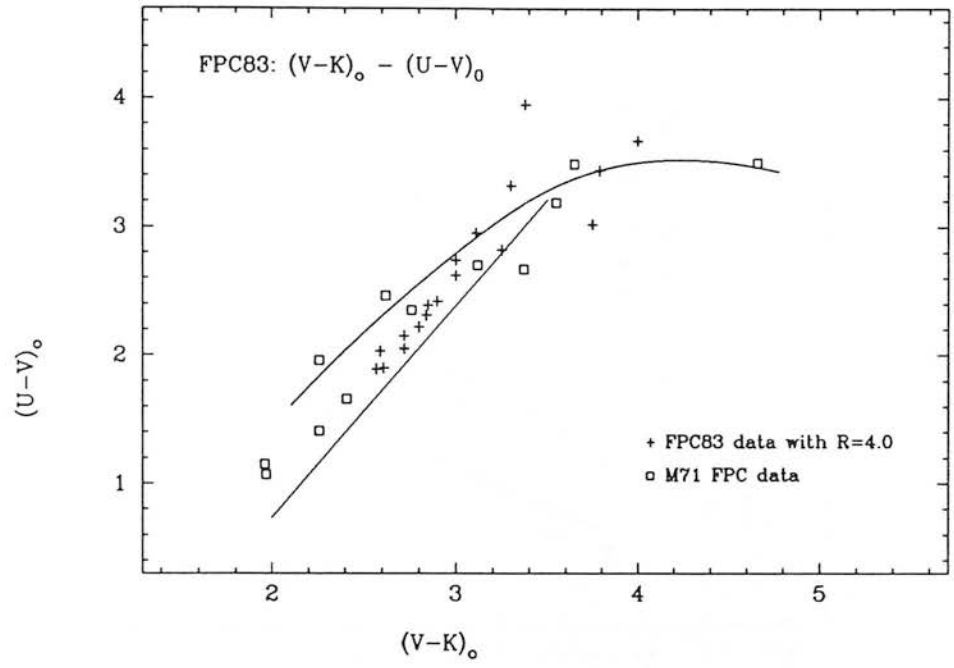

Figure 5: As FCP83's figure 1a but with R=4.0 for M4. The straight line is the fiducial for M3/M13/M92 and the curve is for field giants.

In the $(V\text{-}K)_o$-$(U\text{-}V)_o$ plot (their figure 1a) they found the M4 stars to lie redward of their expected position and proposed an increase in E(B-V) of $0^m.1$ to $0^m.46$. This was based on the assumption that the M4 stars should lie with the intermediate-metallicity clusters near the M3/M13/M92 fiducial line that they found in their earlier work (Cohen, Frogel and Persson, 1978). Varying the value of R allows the original E(B-V)=0.36 to be used and the data to fit the fiducial line. The best fit of the M4 stars to the M3/M13/M92 line is achieved at R=3.7. However, if M4 is more metal rich than these clusters, the stars will lie to the blue of the line. Figure 5 is analogous to FCP83's figure 1a, but shows the M4 data de-reddened under the assumption that R=4.0. The Frogel, Persson and Cohen (1979) M71 data are also shown, as is the M3/M13/M92 fiducial line and the field giant curve. It is clear that M4 is a good fit and indicates a metallicity approaching [Fe/H]=-1, an estimate consistent with, for instance, [Fe/H]=-1.1 found by Cacciari (1979) and with the value which will be adopted in section 2.2.

FPC83's figure 12 contains the $(V\text{-}K)$-$M_{K,o}$ and $(J\text{-}K)$-$M_{K,o}$ CMDs for their data. They chose to use $(m\text{-}M)_o$=11.60 to calculate $M_{K,o}$. This value, as will be seen later, is very high

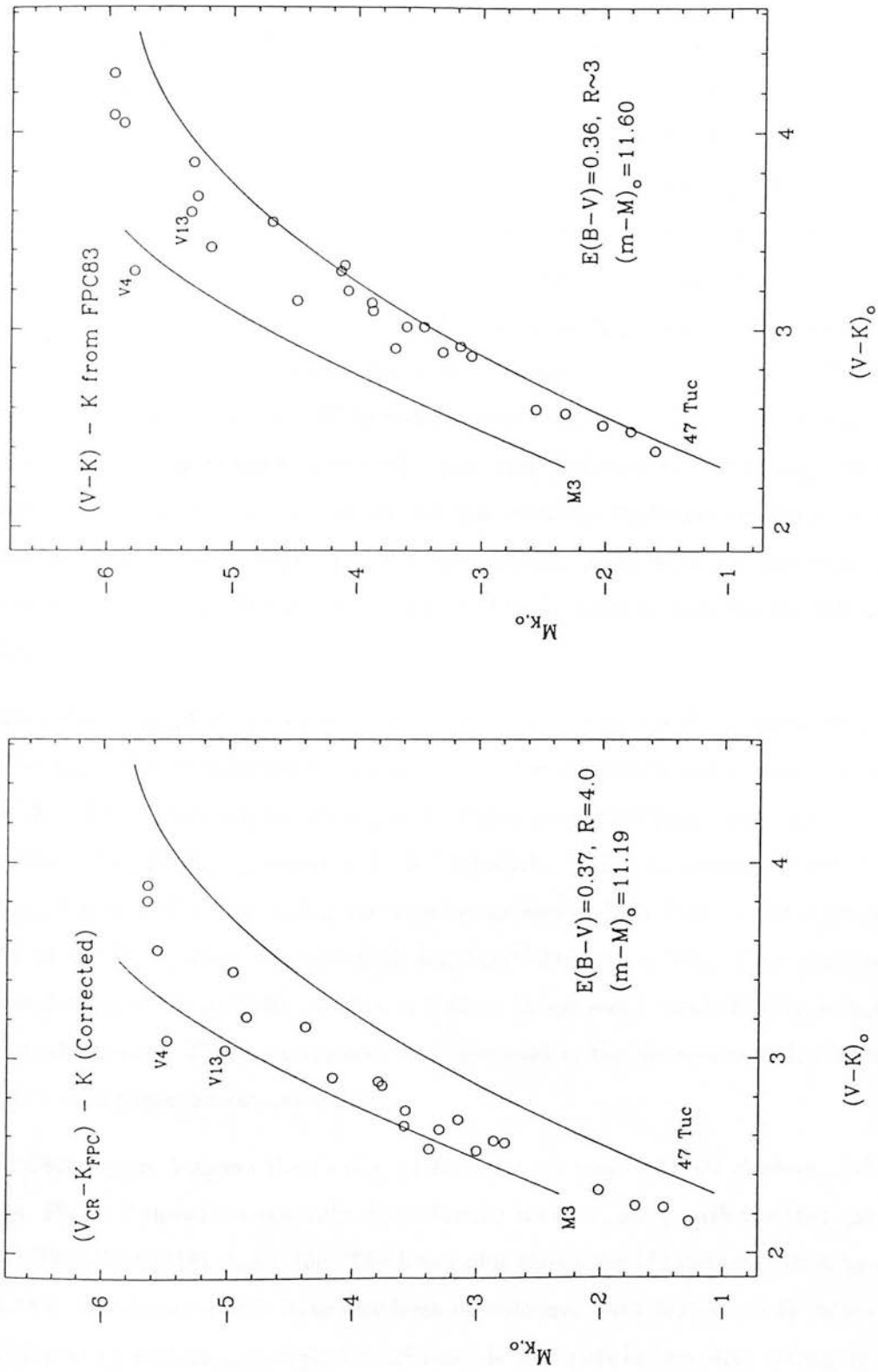

Figure 6: As in FPC83's figure 12, $(V\text{-}K)_o$-$M_{K,o}$ CMDs for M4 with the fiducials for M3 and 47 Tuc. The first plot is the revised one.

and FPC83 make no discussion of it. Figure 6 shows the FPC83 data as they plotted it with R~3, E(B-V)=0.36 and $(m-M)_o$=11.60 and the data (this time taking V from CR90 and applying their differential reddening correction, although this makes little difference) shifted to R=4.0, E(B-V)=0.37 and $(m-M)_o$=11.22 (which will be adopted as the best estimate of the distance modulus, in section 2.3). Also shown are the 47 Tuc and M3 fiducial lines ([Fe/H]~-0.6 and -1.7 respectively). FPC83's diagram showed the M4 stars to lie close to the 47 Tuc line and they again suggested that E(B-V) should be increased to 0.46 so that the CMD would be consistent with the intermediate-metallicity ranking of M4. The R=4 plot shows the M4 stars to lie roughly midway between the 47 Tuc and M3 curves, which is where FPC83 thought they ought to lie. The data are thus consistent with their estimated metallicity whilst still using E(B-V)=0.37. If $(m-M)_o$=11.60 is used the M4 stars lie slightly faint of the M3 line with the brightest stars lying furthest from the M3 data. In the (J-K)-$M_{K,o}$ plot (not shown), using R=4 and the smaller distance modulus again shifts the M4 stars so that they lie midway between the M3 and 47 Tuc lines.

The (V-K)-$M_{K,o}$ CMD is important because it is the source of the metallicity indicator, $(V-K)_{o,GB}$, the de-reddened (V-K) colour of the giant branch at an absolute K magnitude of -5.5. From their original diagram, FCP83 quoted $(V-K)_{o,GB}$=3.83 for M4. From the revised plot, $(V-K)_{o,GB}$=3.55 $\pm$ 0.15. Similarly, $(J-K)_{o,GB}$ becomes 0.92 $\pm$ 0.05 and $M_{K,o}$(GB)=-4.26 $\pm$ 0.2. Using the approximations in LDSJF90 to plot a line of M_{bol}=-3.0 in the (V-K)-$M_{K,o}$ diagram finds log T_{eff}(GB)=3.61 $\pm$ 0.01. This temperature was found using the T_{eff}-(V-K) relation in Cohen, Frogel and Persson (1978), to keep it on a consistent scale. These parameters are important in the discussion which follows of the other 1983 paper by the same group.

FPC83's figure 5 shows the $(V-K)_o$-$(J-K)_o$ plot for most of their clusters, although not M4. Figure 7 shows the two-colour plot for the M4 data, along with the M71 data and the M3/M13/M92/M71 mean line. The lower plot shows the M4 data modified by assuming R=4.0. The data for M71 have also been de-reddened with E(B-V)=0.27 rather than the 0.25 used by FPC83, although the difference is negligible in this plot. Changing the value of R has moved the M4 stars down the mean line but also to the blue in (J-K), so that they lie below the line. Interestingly, the M4 data now agree very well with those for NGC5927 and NGC5286 (not shown), for which Zinn (1980) quotes [Fe/H] as -0.16 and

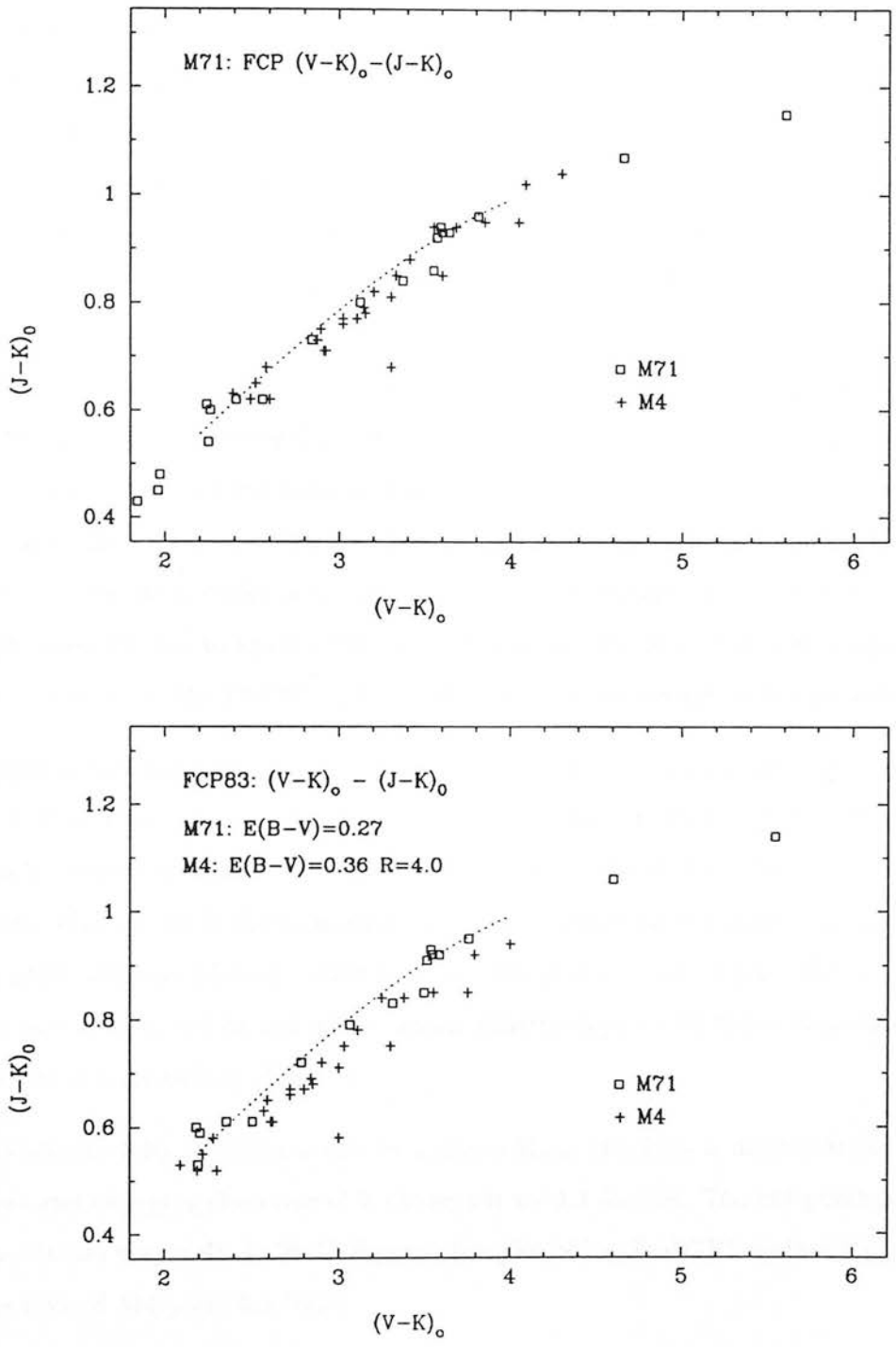

Figure 7: Two-colour plot for M4 with cluster mean line and M71 data from FPC83. The lower plot is for R=4.

-1.72, respectively, and which both have even higher quoted reddenings than M4. FPC83 decided that the (V-K)-(J-K) diagram was very insensitive to metallicity and that all the cluster giants should lie on a single intrinsic sequence. They asserted that clusters which did not follow the mean line were likely to have erroneous reddening determinations. The fact that three high-reddening clusters, covering the whole range of metallicity, all do not fit, by a similar amount and in the same sense, is suspicious. From the preceeding and subsequent discussion here it will be seen that the reddening and reddening law to M4 are now well determined. It is possible that the extinction in the J filter is not modelled adequately by the simple curves derived from MW90, so that the most obscured clusters will appear displaced from the lower reddening ones. Since (J-K) is sensitive to gravity, if the common high reddening is a red herring, it is possible that there is a systematic difference between the gravities of the stars in these three clusters and the other clusters in the sample, possibly due to age (or the second parameter ?). Of course there may simply be an error in some of the FPC83 J photometry. Further investigation is warranted.

FCP83 plotted five diagrams in which M4 was marked as a discrepant cluster. Their figures 2, 3, 4(a), 4(b) and 5 are reproduced together in figure 8. Their figures 2, 3 and 4(a) show Zinn's metallicity against log T_{eff} (GB), $(J\text{-}K)_o$(GB) and $M_{K,o}$(GB), respectively. The revised point for M4 is shown in each. In all three diagrams M4 becomes comparable with the other clusters plotted. Although the M4 point is now within the scatter of the other points it would fit better the mean relationships in all three diagrams if its metallicity were increased to -1.1.

In FCP83's figure 4(b), $[Fe/H]_{IR}$ is plotted against $M_{K,o}$. $[Fe/H]_{IR}$ is derived from the IR GB colours and changing the value of R changes it to -1.1 for M4. The M4 point now fits the mean relation very well. FCP83's figure 5 is a plot of log T_{eff}(GB) against $M_{K,o}$(GB). Again the revised M4 point fits well.

In their appendix on discrepant clusters, FCP83 again discuss increasing E(B-V) to 0.46 for M4, also suggesting that their mean giant branch could be shifted bluewards. This would remove M4's discrepancy in all their plots. Table 2 lists the original FCP83 GB parameters, the values with E(B-V)=0.46 and R$\sim$3 of their appendix and the revised values with R=4.0 and E(B-V)=0.37.

From this table it is clear that the increased value of R is just as good as an increased

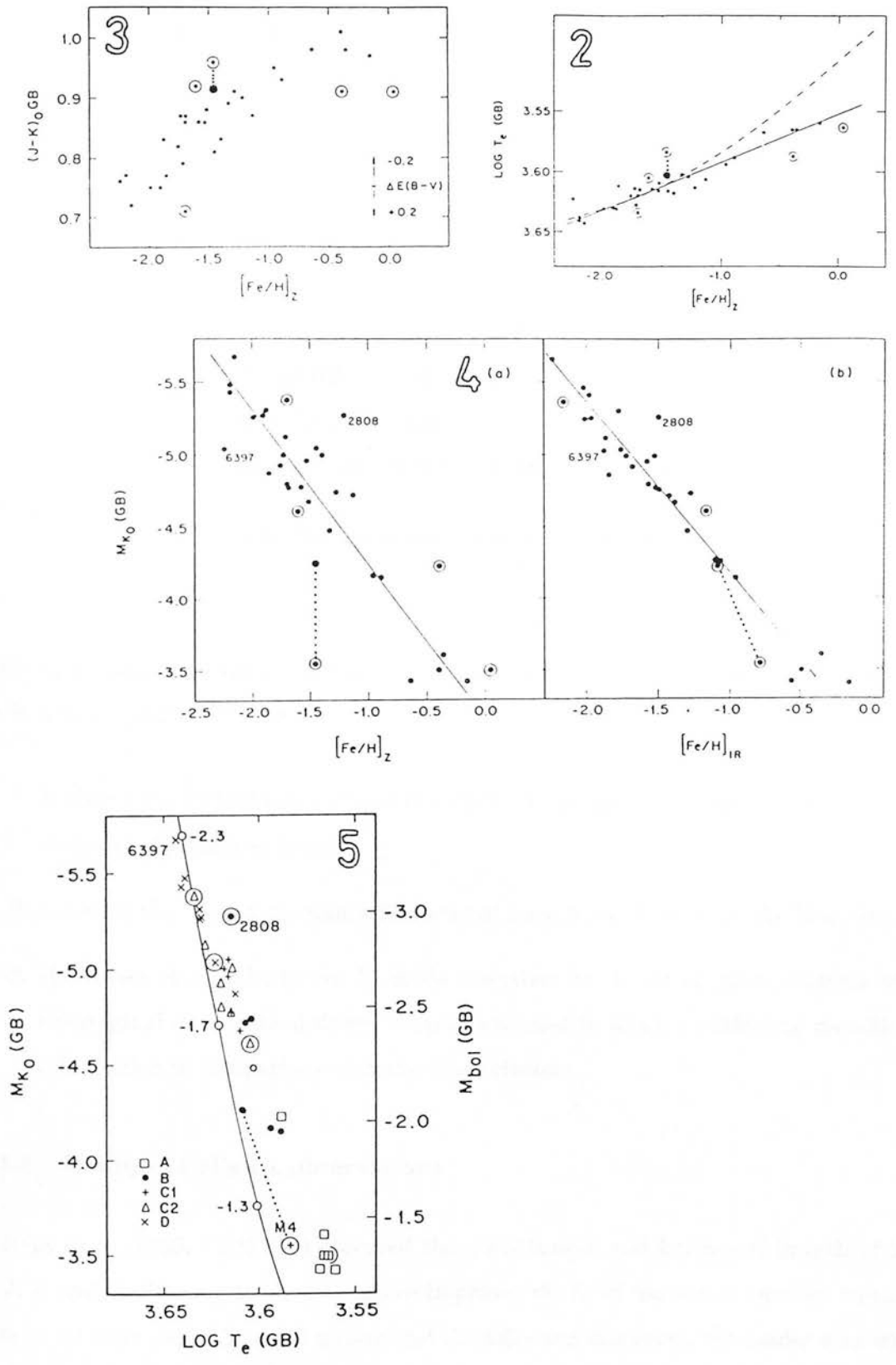

Figure 8: Figures 2, 3, 4(a), 4(b) and 5 from FCP83. The revised M4 points are shown as filled circles joined to the original points by dotted lines.

Table 2: Parameters derived from the FPC83 photometry

	FCP83	$FCP83_{App}$	R=4.0
$(V\text{-}K)_o$(GB)	3.83	3.6	3.55
$(J\text{-}K)_o$(GB)	0.96	0.90	0.92
$M_{K,o}$(GB)	-3.55	-4.3	-4.26
log T_{eff}(GB)	3.584	3.598	3.61

E(B-V) at explaining the deviation of M4 from the other clusters surveyed. An increase in R is to be preferred because:

1. it allows the FPC83's first choice of E(B-V) to be used, which agrees with the vast majority of estimates in table 1;
2. it means that the giant-branch fit does not have to be 'fiddled' to the blue, and
3. the values of metallicity can be made consistent at -1.1 in all plots, whereas with the original results the different diagrams seemed to present conflicting metallicity information in comparison with the other clusters.

2.1.3 Phillips et al's IR observations

Phillips et al (1986, PRMV86) observed the giant branch and horizontal branch of M4 at J, H and K. Shifting to R=4 equals or improves the fit of models or fiducials to their data in all their plots. To fully understand the following discussion the reader may wish to have a copy of the PRMV86 paper to hand.

PRMV86's figure 1 is a $(V\text{-}K)_o$-$M_{K,o}$ CMD, using $(m\text{-}M)_o$=11.28, in which the M4 stars lie redward of 47 Tuc's fiducial line. PRMV86 again invoke the 0.1 increase in E(B-V)

proposed by FPC83 to shift their photometry to where they expect it to lie. Once again using R=4.0 (even without changing the assumed distance modulus) shifts the M4 data so that they lie between the fiducials of M92 and 47 Tuc, as desired.

Their figure 2a shows the M4 stars lying below (redward in $(V\text{-}K)_o$) the field-star line in the $(V\text{-}K)_o$-$(B\text{-}V)_o$ plot. Since the reddening vector lies along the fiducial relationship PRMV86 were unable to invoke the 0.1 reddening increase and instead explained the difference between the M4 stars and the field stars as being the same as that in FPC83's $(V\text{-}K)_o$-$(U\text{-}V)_o$ diagram, that is, caused by "decreased atomic and molecular opacity terms in the blue to UV continuum," i.e. due to the difference in metallicity between the cluster and field. Applying R=4.0 shifts the M4 data into co-incidence with the field stars.

PRMV86's figure 2b attempted to fit model atmosphere calculations (from Kurucz 1979) to the BHB and RHB observations. The red stars were found to match the log g=3, [M/H]=-1 models, but the blue stars were too blue in (B-V) (or too red in (V-K)) to match even the log g=2, [M/H]=-2 models. Using R=4.0, the BHB stars shift exactly onto PRMV86's most probable BHB model with log g=3 and [M/H]=-1. Although the RHB stars now lie too red in (B-V) to match even the log g=4.5, [M/H]=0 line, they do not reach the field-star line. As PRMV86 note, the field-star line is not fitted by the appropriate models and it seems likely that the models are too blue in (B-V) at high (V-K) (see the discussion in section 7.1 of the last chapter). They do not discuss exactly how they produced their model lines but the Kurucz models do not include molecular transitions and provide few points in the infra-red, with the K flux having to be estimated from points at 1.8 and 2.7 μm, for instance.

In their figure 3, PRMV86 compared their GB and HB observations with models and field stars in the (V-K)-(U-B) diagram. Again the field stars are not well matched by the models and it seems likely that there is some missing opacity source in the model calculations. Putting in R=4.0 makes the giants shift close to the field-star line and the HB stars match the log g=2, [M/H]=-1 model. This is certainly a more likely solution that that found by PRMV86.

In PRMV86's figure 4, the M4 stars appear to match the intrinsic giant and main sequences well in the $(V\text{-}K)_o$-$(J\text{-}H)_o$ and $(V\text{-}K)_o$-$(J\text{-}K)_o$ diagrams. Changing to R=4 shifts the stars down the relations, so that the fit is just as good.

Finally, PRMV86 found the best-fit Kurucz (1979) model for each of the HB stars to calculate T_{eff} and log $L/L_{\odot}$. They decided to use E(B-V)=0.46, lest some of the stars end up in the instability strip. Using R=4 with E(B-V)=0.37 leads to the same T_{eff} shift, so also avoiding the instability strip.

Brief tests show that their calculated log $L/L_{\odot}$ (for E(B-V)=0.46) also do not change by much, being ~0.04 lower in the present analysis due to the use of the lower distance modulus that will be found in section 2.3. This does not substantially alter PRMV86's conclusions about the best-fit model.

Summarizing, PRMV86 were able to reconcile their CMD and atmospheric parameter calculations with expectations by invoking the FPC83 $0^{m}.1$ increase in E(B-V), but could not match models to their HB or GB stars in the two-colour diagrams. Changing R to 4.0 allows a successful fit to the models, as well as having the same effect as ΔE(B-V)=0.1 on the CMDs and 2CDs, and parameter calculations.

2.1.4 Liu & Janes Baade-Wesselink analysis of M4 RR Lyraes

LJ90 discussed reddening in detail and derived individual E(B-V)s for each of their four RR Lyrae variables from their UBV photometry. These reddenings compare well with those found by Cacciari (1979) and Sturch (1977) for the same stars. They noted that these were also consistent with the sense and magnitude of CR90's differential reddening gradient. They decided to use R=3.8, based mainly on the star σ Sco which is ~1° from M4 and for which Clayton and Cardelli (1988) found R=3.8 and E(B-V)=0.39. However, Liu & Janes have used the value of A_K/A_V=0.114 appropriate to R=3.1 from CCM89, whilst they should have used 0.122 for their assumed R=3.8. This implies that they used E(V-K)/E(B-V)=3.37 rather than 3.34. This makes very little difference to the derived parameters, but if the MW90 values are used and R is set to 4.0 so that E(V-K)/E(B-V)=3.61 and A_K/A_V=0.097, the derived parameters are altered somewhat more. Without repeating the fitting between the radial-velocity and photometric curves, it is possible to approximate the changes using the means of the curves. Working the changes through leads to slightly brighter values of $<M_K>$, the mean K magnitude, for each variable. Plotting this in the log P - K diagram (figure 9) shows that the revised points are a reasonable fit to the line derived for M4 in LDSJF90 from 26 variables (plus

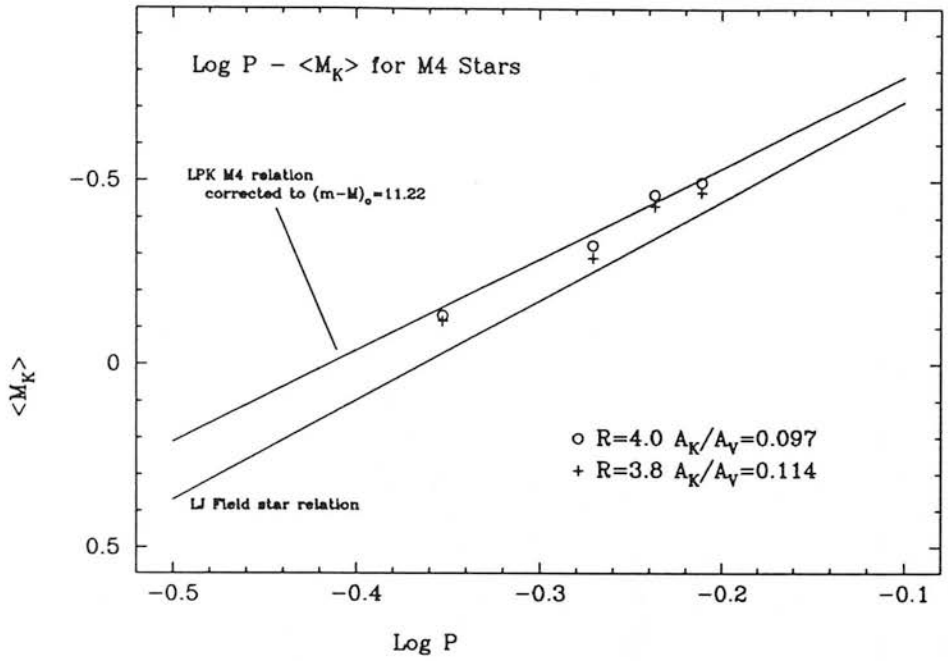

Figure 9: The log P - M_K diagram for the Baade-Wesselink points from LJ90. Also shown are the LJ90 field star relation and the relation found by LDSJF90 (slightly revised).

additional further observations by our group), when a de-reddened distance modulus of 11.22 is used (from section 2.3). The field star relation from LJ90 is also shown and does not fit the stars as well. Of course, simply by changing the distance modulus by $0^m.04$ the LDSJF90 relation could be made to agree with LJ90's original points.

2.1.5 Smith's 1984 ΔS work

Smith (1984) calculated Preston's ΔS metallicity parameter for stars in nine clusters. Combining these with previous determinations, he compared $[Fe/H]_{\Delta S}$ with various other estimates of metallicity, including the $(V\text{-}K)_{o,GB}$ values measured by FCP83 (and references therein). In this correlation he found two clusters to be so discrepant that they had to be excluded from the determination of the linear relation through the data. One of the clusters, NGC2298, was known to have an uncertain $(V\text{-}K)_{o,GB}$ value and the other, of course, was M4 with $(V\text{-}K)_{o,GB}$=3.83. From above, using R=4.0 and E(B-V)=0.37 finds a revised $(V\text{-}K)_{o,GB}$=3.55 for M4. This value moves the cluster into agreement with the others in the sample, as can be seen in figure 10. It is interesting to note that if [Fe/H]

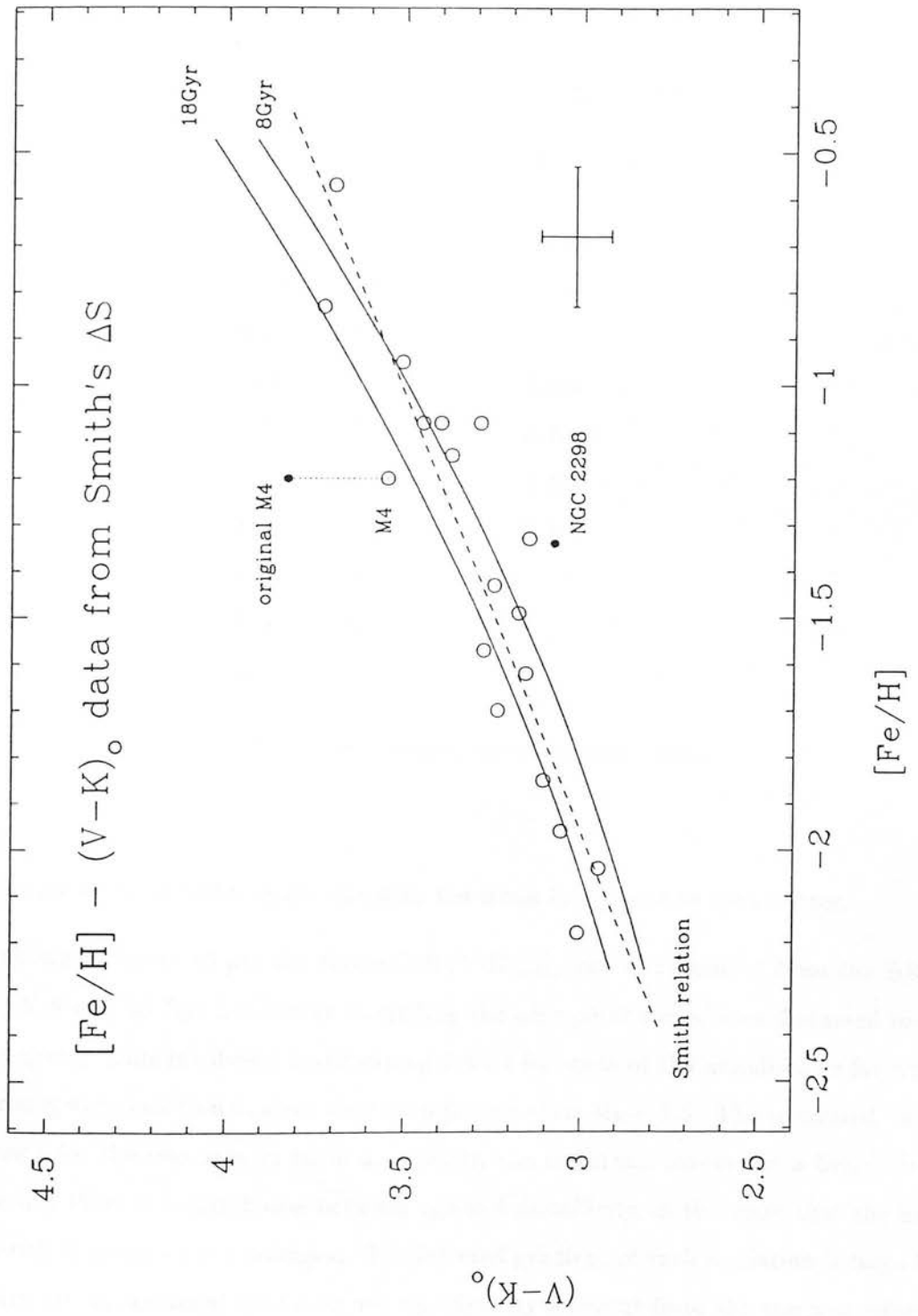

Figure 10: Smith's 1984 metallicity estimates and the effect of changing R to 4.0 for M4. The dashed line is that found by Smith and the curves are derived from the (V-K)-K isochrones.

Table 3: [Fe/H] - $(V\text{-}K)_{o,GB}$ measured for 8 and 18 Gyr

[Fe/H]	$(V\text{-}K)_{o,GB}^{8Gyr}$	$(V\text{-}K)_{o,GB}^{18Gyr}$
-0.47	3.92	4.04
-0.65	3.76	3.90
-0.78	3.67	3.77
-1.03	3.49	3.62
-1.26	3.32	3.45
-1.48	3.15	3.27
-1.66	3.10	3.21
-1.78	3.00	3.12
-2.03	2.93	3.03
-2.26	2.81	2.91

were increased to -1.1 the agreement with the mean line would be even better.

Also shown in figure 10 are the theoretical $(V\text{-}K)_{o,GB}$ curves measured from the BBVB (V-K)-K 8 and 18 Gyr isochrones (including the zero-point corrections discussed in the last chapter). This involves a small extrapolation for some of the metallicities for which isochrones were calculated, since they stop fainter than M_K=-5.5. The measured values are listed for the two ages in table 3. Clearly, the isochrone curves are a better fit to the data if there is a correlation between age and metallicity, in the sense that the most metal-rich clusters are the youngest. The inferred gradient of such a relation is large but the data are so scattered that it is not significantly different from the steepest relation found by Sandage and Cacciari (1990) from observations of 18 clusters.

2.1.6 Gratton, Quarta and Ortolani's metallicity work

Yet another confirmation of the higher value of R comes from the work of Gratton, Quarta and Ortolani (1986) who derived metallicities for M5, NGC6752, M71, 47 Tuc and M4 from both equivalent-width analyses and spectral synthesis, using the temperatures that FPC83 derived from their (V-K) values. In the course of comparing their values with previous metallicity estimates for these clusters, they plotted [Fe/H] against the $(V\text{-}K)_{o,GB}$ parameter. In this plot the M4 point lies well off the mean relation for the other four clusters, further in fact than its quoted errors allow. The revised $(V\text{-}K)_{o,GB}$ gives a point that agrees well with the other clusters, although this can only be a first-order correction because it ignores the fact that the (V-K) temperatures and log g from FPC83 contain systematic errors, if the revised reddening and distance modulus are correct. Simplistically applying the reddening correction to the $(V\text{-}K)_{o,GB}$ value gives a mean relation:

$$(V - K)_{o,GB} = 0.997[Fe/H] + 4.828$$

with a correlation coefficient of 0.95. The original relation had a gradient of 0.907 (and a correlation coefficient of 0.77).

2.1.7 TiO band strength metallicity work

An IR study carried out by Mould, Stutman and McElroy (1979) observed infra-red-optical colours to derive TiO band strengths for seven clusters. They used E(B-V)=0.42, an average from previous studies, for the reddening to M4. Fortunately, this reddening error was cancelled out by their use of R=3.08 rather than R=4. They found [Fe/H]=-1.06 $\pm$ 0.35 for M4 although the TiO bands are so faint that the cluster is at the metal-poor limit of their technique. They present a plot of their TiO band strength parameter against the integrated $(V\text{-}K)_o$ colour. Shifting the colour as given by R=4 brings M4 into closer agreement with the mean line.

2.1.8 Alcaino & Liller (1984) photographic CMD

AL84 determined the reddening to M4 to be E(B-V)=0.44 by fitting a zero-age main sequence to their photo-electric standards in the (B-V)-(U-B) diagram. For their reddening

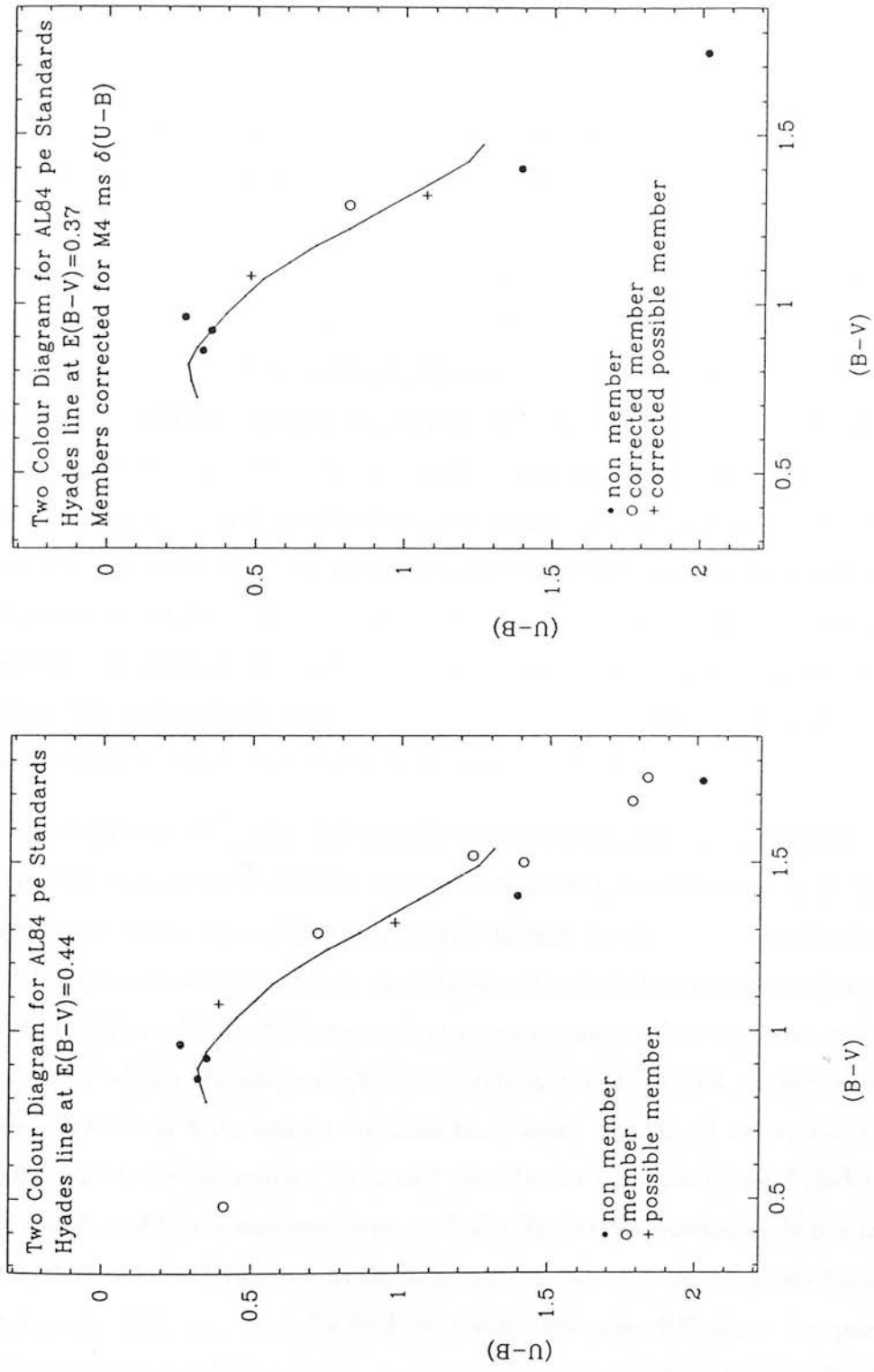

Figure 11: The (B-V)-(U-B) two-colour diagram for the AL84 data. The left-hand plot is the fit as AL84 found it to be, the other is after the cluster members have been corrected for UV excess.

vector they used E(U-B)/E(B-V)=0.73, which is correct for regions where R~4, although the value of 0.80 applicable to R~3 makes little difference compared to the re-analysis presented below.

RF84 used a similar technique, utilising the Hyades sequence of Sandage (1969), to find their value of E(B-V)=0.37. Simply fitting this Hyades sequence to the AL84 standards confirms their value of E(B-V)=0.44, showing that, at least for these data, there is no practical difference between the ZAMS and the Hyades sequence. Fitting the reddening in the (B-V)-(U-B) diagram is a difficult procedure since the position of any star is determined not only by its reddening but by the UV excess caused by the difference in metallicity between the observations and the fiducial sequence. Both RF84 and AL84 assumed that the stars they used were mainly foreground objects, near but not part of the cluster, so that they could be fitted to a near-solar metallicity sequence. CR90 contains 11 of the 13 stars selected by AL84 and shows that five are not members and six are 99% probable members. For example, AL84 concluded that star I was a foreground star about three-quarters of the distance to the cluster, but CR90 find that p=99%. With the excellent separation between cluster members and non-members found by CR90 it is highly likely that star I does indeed lie within the cluster.

RF84 plotted their M4 main-sequence observations on a two-colour diagram from which it is possible to measure δ(U-B) for a given $(B-V)_o$, being the difference in (U-B) from the Hyades sequence to a fiducial drawn by eye through the data. The AL84 photoelectric standards that are cluster members can now be corrected, at an assumed value of E(B-V), for their lower metallicity. Unfortunately only one member and the two stars not measured by CR90 lie within the range of (B-V) covered by the RF84 plot, so the correction (of δ(U-B)=-0.09) has been applied to these three stars. Figure 11 shows the two colour diagram for a) the uncorrected data with the Hyades line plotted for E(B-V)=0.44, as AL84 found, and b) the corrected data with the Hyades line plotted at E(B-V)=0.37. Of course, there is no information to say whether the two possible members belong to the cluster or the field, and even the field stars will show some UV excess compared to the Hyades sequence, which is probably more metal-rich than the Sun (e.g. [Fe/H]=0.12 from Cayrel, Cayrel de Strobel and Campbell, 1985). However, the figure shows that the data are not inconsistent with a cluster reddening of E(B-V)=0.37. The formal fitting error is the same $\pm$ 0.04 as found by AL84, although the systematic errors could be much larger

than this since the extinction towards the field stars has been taken to be the same as that to the cluster, the metallicities of the field stars are unknown and two of the stars assumed to be members may not be. RF84 appear to have been more successful in their selection of field stars, although they have not published the photometric data, so no re-assessment can be made.

2.1.9 The log P′-log T_{eff} Diagram

Following on from LDSJF90, Buckley, Longmore and Dixon (1992) use R=4 in their comparison of the log P′-log T_{eff} diagrams for the RR Lyraes of M3, M4 and ω Cen, where log T_{eff} comes from $(V\text{-}K)_o$ and log P′=log P+0.336M_{bol}. With R=4 the relations are all the same within the errors. With R=3 the M4 relation is significantly different, and more scattered, and implies a helium fraction, Y, of less than 0.20.

2.1.10 Summary

A detailed review of the previous estimates of the reddening to M4 has been conducted. In most cases, where it is possible, re-examining the data with R=4 makes them more consistent as a whole or does not change the estimates. Particularly important and convincing evidence comes from the work of FCP83, who had problems fitting in their M4 data with their other clusters and proposed an increase in E(B-V). Adopting R=4 solves all these problems.

The discrepant value of E(B-V) found by AL84 has also been shown to be in error and their data to be consistent with E(B-V)=0.37.

In conclusion, E(B-V)=0.37 $\pm$ 0.01 and R=4.0 $\pm$ 0.2 for M4.

2.2 Metallicity

LJ90 contains a detailed discussion of the large range of metallicity estimates for M4 available in the literature. As they say, it is too hard to work through these to include the effects of increasing R. Their adopted value is [Fe/H]=-1.3 $\pm$ 0.2, although the mean of the values in their table is -1.1 $\pm$ 0.3.

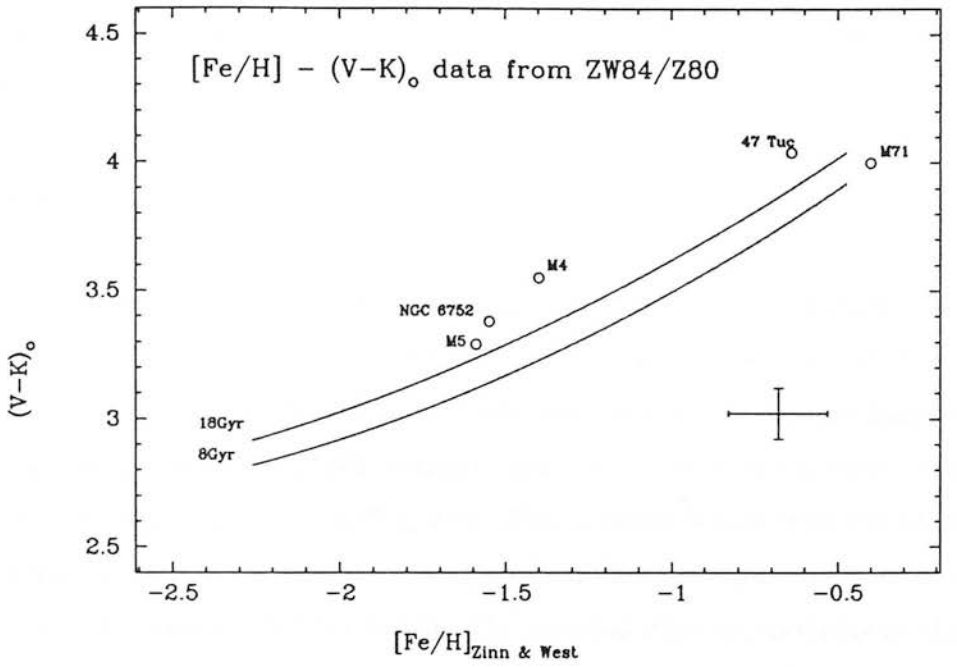

Figure 12: $(V\text{-}K)_{o,GB}$ against the Zinn/Zinn & West metallicity scale as listed by Bell (1987). The isochrone curves are shown as in figure 10, and it is not suggested that they should fit the data.

It is interesting to consider those determinations of metallicity that were discussed incidentally during the reddening discussion above, where the change in reddening *was* adequately taken into account. The value of -1.1 comes out of the work of Caputo, as discussed in section 2.1.1. This value also emerges from the work of FCP83, as both $[Fe/H]_{IR}$ from the GB IR colours and the value required to make M4 fit the mean relations in several plots. Again -1.1 would put M4 on the mean relation in Smith's 1984 ΔS work and in the Zinn/Zinn & West metallicities as tabulated by Bell (1987) and shown in figure 12. The TiO band strength work of Mould, Stutman and McElroy (1979) found -1.06 $\pm$ 0.35 from near-IR observations. Another IR study is that of Aaronson et al (1978) who correlated the integrated $(V\text{-}K)_o$ colour with metallicity for a sample of clusters. Correcting the integrated colour of M4 for the new value of R gives a value of [Fe/H]=-1.1.

It would seem that the IR colours point to [Fe/H]=-1.1, once the higher value of R has been taken into account.

All this suggests that [Fe/H] should be taken as -1.1 ± 0.25, bearing in mind the differing effects of the revised E(B-V) and R on the various methods used to determine the metallicity.

2.3 Distance modulus

Table 4 lists previous estimates of the distance modulus to M4 together with revised estimates using R=4 and E(B-V)=0.37 and, where quoted, the observed V magnitude of the HB. Clearly the revised values are more homogeneous. A simple mean (excluding the second Kron and Mayall (1960) estimate and the VBB85 value, since it is essentially the same data as RF84) gives 11.22 ± 0.11. This is rather better than the 11.37 ± 0.18 found from the raw values from the same studies, another confirmation of the success of the adopted values of E(B-V) and R. The adopted distance modulus to the cluster corresponds to 1750 ± 90 pc.

2.4 Age

Isochrone fitting has provided most of the estimates of the age of M4. RF84 found 13 ± 1 or 15 ± 1 Gyr depending on their choice of metallicity between -0.82 and -1.0. AL84 found 13 ± 2 Gyr from their CMD by assuming [Fe/H]=-1.3. VBB85 note that fits with the VB83 isochrones used by RF84 and AL84 come out ~10% too young because of a zero-point error in the magnitude scale. This makes the last two results approximately 14 or 16.5, and 14 Gyr, respectively. Clearly the zero-point change in the VB83 isochrones confers lower weight to these two results. VBB85 found 16 Gyr by re-fitting both the RF84 and AL84 data. ALA85 found 17 ± 1.5 Gyr, whilst the re-fitting in section 2.1 of this data with the SC91 isochrones and the adopted E(B-V) and $(m\text{-}M)_o$ finds 18 ± 1.5 Gyr. Buonanno, Corsi and Fusi Pecci (1989) find t_9=19.2 from their relation between cluster age and the V magnitude difference between the turn-off and the HB. Putting $(m\text{-}M)_o$=11.22, [Fe/H]=-1.1, R=4 and E(B-V)=0.37 into Buonanno's 1986 equation relating age to M_V(TO) and metallicity gives $16.6 \pm ^{2.5}_{2.2}$ Gyr. Faced with a range of apparently good age estimates, from 14 to 19 Gyr, the (unweighted) mean is 16 ± 2 Gyr is rather unsatisfactory.

Table 4: Distance modulus estimates to M4

Author	Quoted			Revised		
	(m-M)	$(m\text{-}M)_o$	σ	$(m\text{-}M)_o$	σ	V_{HB}
(1)	(2)	(3)	(4)	(5)	(6)	(7)
Greenstein 1939	13.97	11.4	(0.3)	—	—	
Kron & Mayall 1960	12.7	(11.57)		11.22		
(	12.4	(11.27)		10.92		)
Alcaino 1975	12.86	11.21		11.38		
Lee 1977		11.15	0.25	11.12[5]	0.25	13.35
Lloyd-Evans 1977[1]		11.7		11.36		13.5
Alcaino & Liller 1984[2]	12.52	(11.20)		11.14		
Richer & Fahlman 1984[2]	12.5	(11.37)		11.12		
(VandenBerg & Bell 1985	12.6	(11.47)	0.15	11.12	0.15	)
Caputo 1987	(12.76)	—	—	11.28	0.1	
Alcaino et al 1988[3]	12.7	11.39	0.14	11.12	0.14	
Buonanno et al 1989[4]	12.53	11.40	0.25	11.05	0.25	13.35
Cudworth & Rees 1990		11.47	0.2	11.27	0.2	13.45
LDSJF90		11.26		11.25		

1). Corrected for the zero-point error mentioned in note 13 of table 1.

2). Both RF84 and AL84 used the VandenBerg (1983, VB83) isochrones to fit their CMDs. VBB85 stated that the older isochrones were $0^m.1$ too faint, so this correction has been applied in the revised estimates of (m-M). The revised distance moduli agree well with the VBB85 result.

3). The revised estimate uses the apparent distance modulus found by refitting the ALA88 fiducial sequence with the SC91 isochrones in section 2.1.

4). Buonanno, Corsi and Fusi Pecci (1989) used an M_V(HB)-[Fe/H] relation based on matching the main sequences of a set of clusters with M30. Using the final derived value of $(m\text{-}M)_V$ for M30 (from their table 9) it is possible to get an alternative $(m\text{-}M)_V$ for M4 of 12.61 by using the main-sequence matching presented in their table 5. However, the two main sequences have somewhat different gradients and thus do not match well.

5). Lee found the distance by assuming $M_{V,o}$(HB)=1, the revised estimate assumes 0.8.

2.5 Summary

A consistent picture has emerged from the previous reddening estimates, once R is taken to be 4. The past uncertainty in the reddening has been a major block to studies of the cluster and has confused the values of distance modulus and metallicity that have been derived. Although the age estimates are hard to bring together, the other parameters seem to be reasonably well determined - comparable to those for M71, for instance.

The adopted parameters for M4 are:

$$E(B\text{-}V) = 0.37 \pm 0.01 \quad (m\text{-}M)_o = 11.22 \pm 0.11$$
$$t = 16 \pm 2 \text{ Gyr} \quad [Fe/H] = -1.1 \pm 0.25$$
$$R = 4.0 \pm 0.2$$

are used in the rest of this chapter.

3 The colour-magnitude and two-colour diagrams

The present data.

Unfortunately, contrary to expectations, the UBV photometry of RF84 was not available to match with the present K magnitudes. Similarly, the Penny, Lubenow and Dickens (1987) photometry, that includes one of the deep mosaic areas, proved to have problems and is awaiting re-reduction. Thus the K magnitudes could only be matched up with the AL84 photographic BV observations. Only 34 stars out of the total of ~880 measured on the large M4 mosaics are used in the CMDs and 2CDs.

The giant and HB observations of FPC83 and PRMV86 (with V from CR90 or Lee (1977) and Eggen (1972)) and the K observations of the RR Lyrae variables (from LDSJF90 and further work by our group, and with B and V from Sandage (1990)) are also plotted in the diagrams.

As mentioned at the end of chapter 2, there may be a zero-point discrepancy between the M4 main-sequence studies of AL84, RF84 and ALA88. AL84's photographic CMD agrees well with that of Lee (1977), which extends almost as faint as the base of the giant branch. AL84 also agrees with the observations of three giants by Clementini (1987) and

with CR90's photographic magnitudes. However, none of these studies reaches the cluster's turn-off. In chapter 2 it was shown that the main-sequence fiducial points of AL84 do not match well with those of RF84 and ALA88, but making the AL84 V magnitudes fainter by ~18%, whilst keeping (B-V) the same, would allow the three sequences to agree quite well. The agreement is good in the region of interest: from one magnitude above the turn-off to two magnitudes below. Secondary evidence comes from the V magnitude difference between the horizontal branch and the main-sequence turn-off, ΔV_{HB-TO}: AL84 measured this directly to be 3.2 ± 0.2, whilst ALA88 found 3.52 ± 0.1, by assuming a similar HB luminosity. This is a difference of 0.32 ± 0.22, in the sense that the AL84 TO is closer to the HB than ALA88's. ALA88 make no comment on this difference. Peterson (1986) found $\overline{\Delta V_{HB-TO}}$=3.46 ± 0.03 from 36 clusters, which makes the AL84 result seem suspect.

AL84's observations were taken using a Pickering-Racine wedge, so that the magnitudes were calibrated directly from photo-electric standards in the range $10 \leq V \leq 16$ and from the secondary images of these stars in the range $16 \leq V \leq 20$. AL84's value for the Δm of ~3.6 for one of the telescopes that they used agrees well with previous work and the measurements show only small internal scatter. However, the use of the Pickering-Racine wedge is fraught with dangers (see, for example, the discussion by Christian and Racine (1983) and Blanco (1982)) and it seems quite possible that, while the brighter stars are well calibrated, there is an error in those stars which were calibrated with the secondary images. Such an error could be magnitude- or colour-dependent. The stars used to produce the revised reddening from the AL84 two-colour data in section 2.1.8 were all measured photo-electrically and are brighter then V~16. The fiducial turn-offs are the same to 2% in (B-V) in the three optical studies, giving some small hope that B and V are affected similarly and that the (B-V) colours used later in the 2CD are reasonable.

The AL84 data have been used as published in what follows and the effects of a zero-point change are discussed where relevant: in the sections on isochrone fitting, model fitting in the 2CDs and in the comparison of the cluster to M71.

Membership probabilities are available for the brighter stars from CR90 and, in any case, the larger galactic latitude and better field-star separation for M4 mean that, although there are more stars measured than for M71, they are less likely to be foreground objects.

The next sections present the combined data in the CMDs and 2CDs.

3.1 The colour-magnitude diagrams

Figure 13 shows the (B-V)-V, (V-K)-V and (V-K)-K CMDs for M4. The same stars are shown in each plot. Stars shown by CR90 not to be members are excluded. One star measured in the present study is bright enough in V, because it is very blue, that it overlaps with the PRMV86 data. It is located at the red edge of the blue HB and its position in all three diagrams leads to some confidence in the relative zero-points of the different studies at bright magnitudes - since this star will have been directly calibrated from AL84's photo-electric standards it is not expected to show the zero-point problem that may exist for the fainter stars. Similarly, the independent observations of the RR Lyraes fit well into the PRMV86 HB gap. PRMV86 noted star 3314 as a field giant and it is apparent in all three diagrams well to the red of the giant branch.

The (B-V)-V CMD shows the classic features of M4: the well-populated horizontal branch and the large width of the upper giant branch. Because it falls between the PRMV86/FPC83 data and the present measurements, the well-populated sub-giant branch is almost not represented in these diagrams.

The (V-K)-V CMD shows unexpectedly large scatter in the upper giant branch, however this is entirely due to the PRMV86 data, with the FPC83 data being very similar in appearance to the same stars in the optical. The V magnitude for star 3209 is misprinted in PRMV86's table 1 although they have used the correct value in the body of the paper. The correct value has been used here. The four stars common to FPC83 and PRMV86 match well but three other giants appear $\sim 0^{\rm m}.6$ in (V-K) from the mean giant branch. The tightness of the RHB star sequence in the (V-K)-K CMD shows the quality of the PRMV86 K photometry, so it seems unlikely that the GB scatter is caused by either contamination or poor photometry.

The main-sequence points appear tighter in the (V-K)-V and (V-K)-K diagrams than in (B-V)-V because of the expanded colour scale and consequent reduction in significance of the photometric errors.

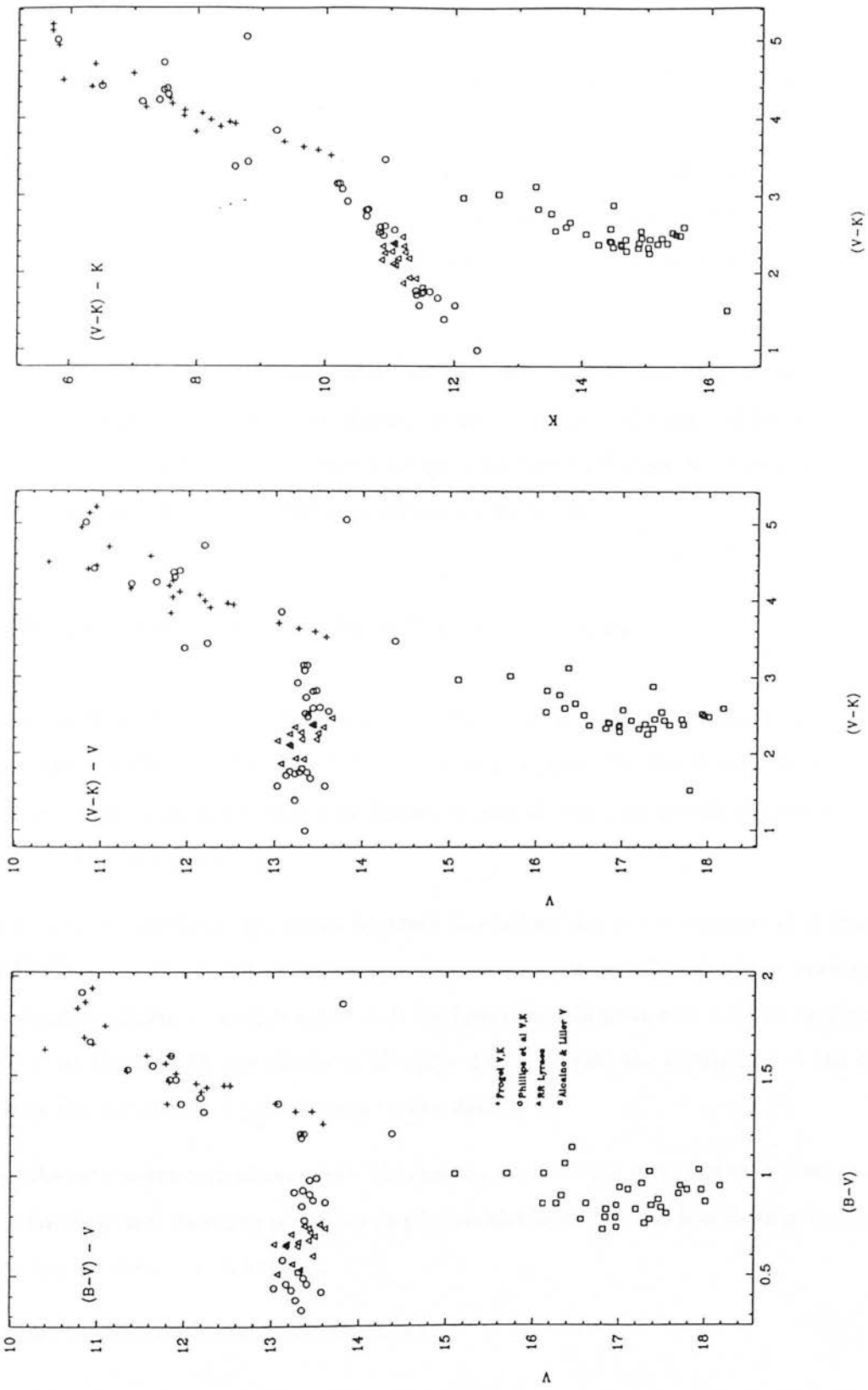

Figure 13: CMDs of M4. Each diagram contains the same stars.

3.2 The two-colour diagram

Figure 14 shows the (V-K)-(B-V) two-colour diagram of M4 and M71 together, after both clusters have been de-reddened by the appropriate amount, using R=4 for M4 and R=3.05 for M71 (the reddening vectors are shown in the plot). Also shown are three very blue stars from the M71 data which have *not* been de-reddened. Clearly these fit the sequence well and are most likely field stars. These stars were discussed in section 3.2 of the last chapter.

The two-colour sequences of the two clusters clearly match very well. As expected, the metallicity difference between the clusters is most apparent for the reddest stars, which are the brightest giants. It is difficult to quantify this difference because the M71 data are so scattered, but this is discussed further in section 6.

4 Matching the CMDs with isochrones

As in chapter 3, the (V-K)-V and (V-K)-K CMDs were matched with the full set of BBVB isochrones. The best fits for each CMD are shown in figure 15. The fitting parameters are listed in tables 5 and 6 and shown in figures 16 and 17, with the goodness of fit estimated on the scale A-E, as before.

Again there is excellent agreement between the colour shifts and ages derived from the two CMDs - as there should be, since they contain essentially identical information. The absolute distance moduli agree well for lower metallicities and are not significantly different at the best-fit metallicity of [Fe/H]=-1.03. Despite the sparseness of the CMDs the best fits are clearly a good match to the data.

Using the zero-point corrections to (V-K) and M_K discussed in section 4 of the last chapter, the reddening and distance modulus can be recalculated for the best-fitting isochrones. These values are listed in table 7.

Thus the isochrone-derived parameters are:

t=11 ± 1.5 Gyr	[Fe/H]=-1.0 ± 0.4
E(B-V)=0.34 ± 0.04	$(m\text{-}M)_o$=11.71 ± 0.15

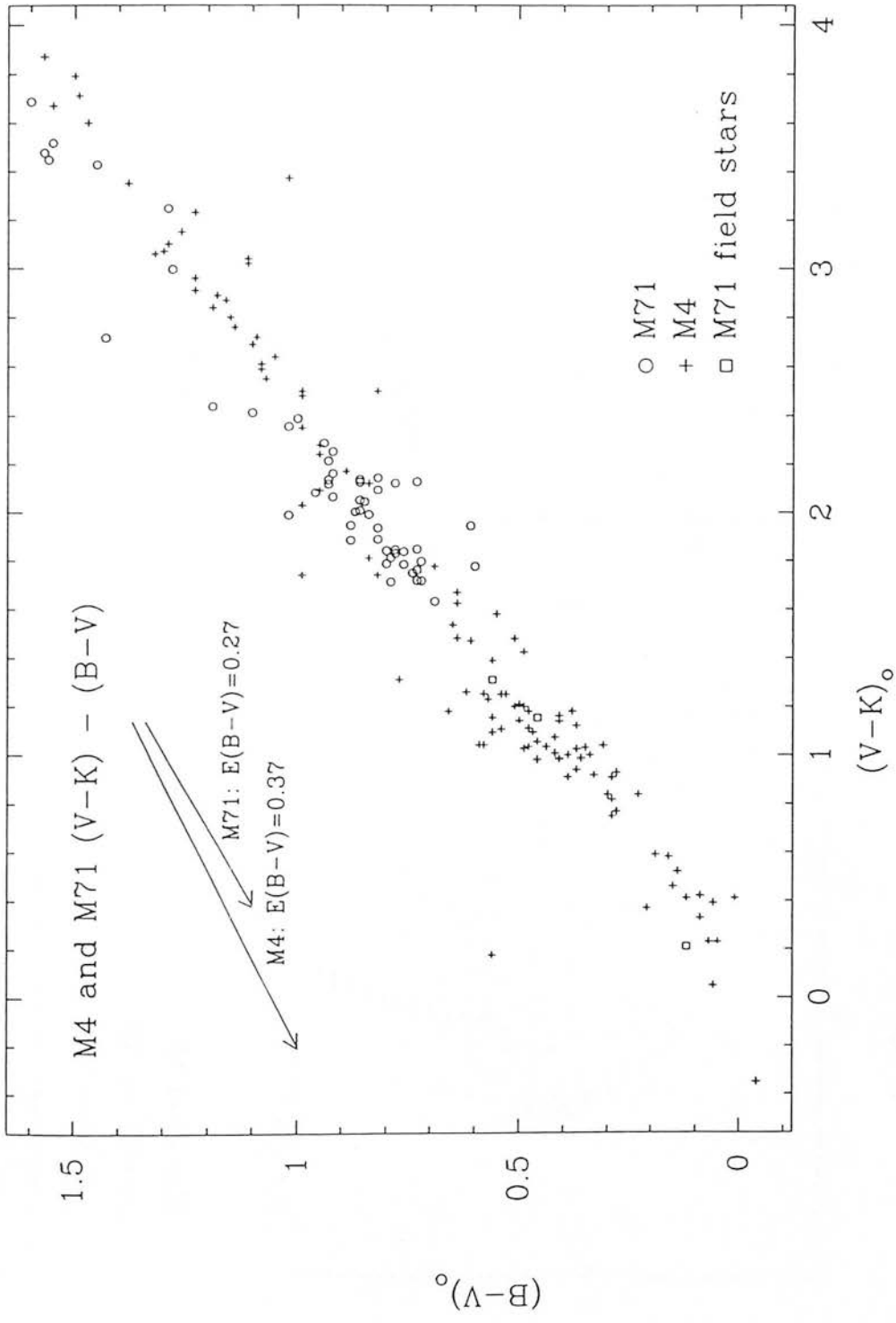

Figure 14: The (V-K)-(B-V) two-colour diagram for M4 and M71. The respective reddening vectors are shown. Three suspected field stars have been plotted without de-reddening. The AL84 B and V magnitudes have been used as published.

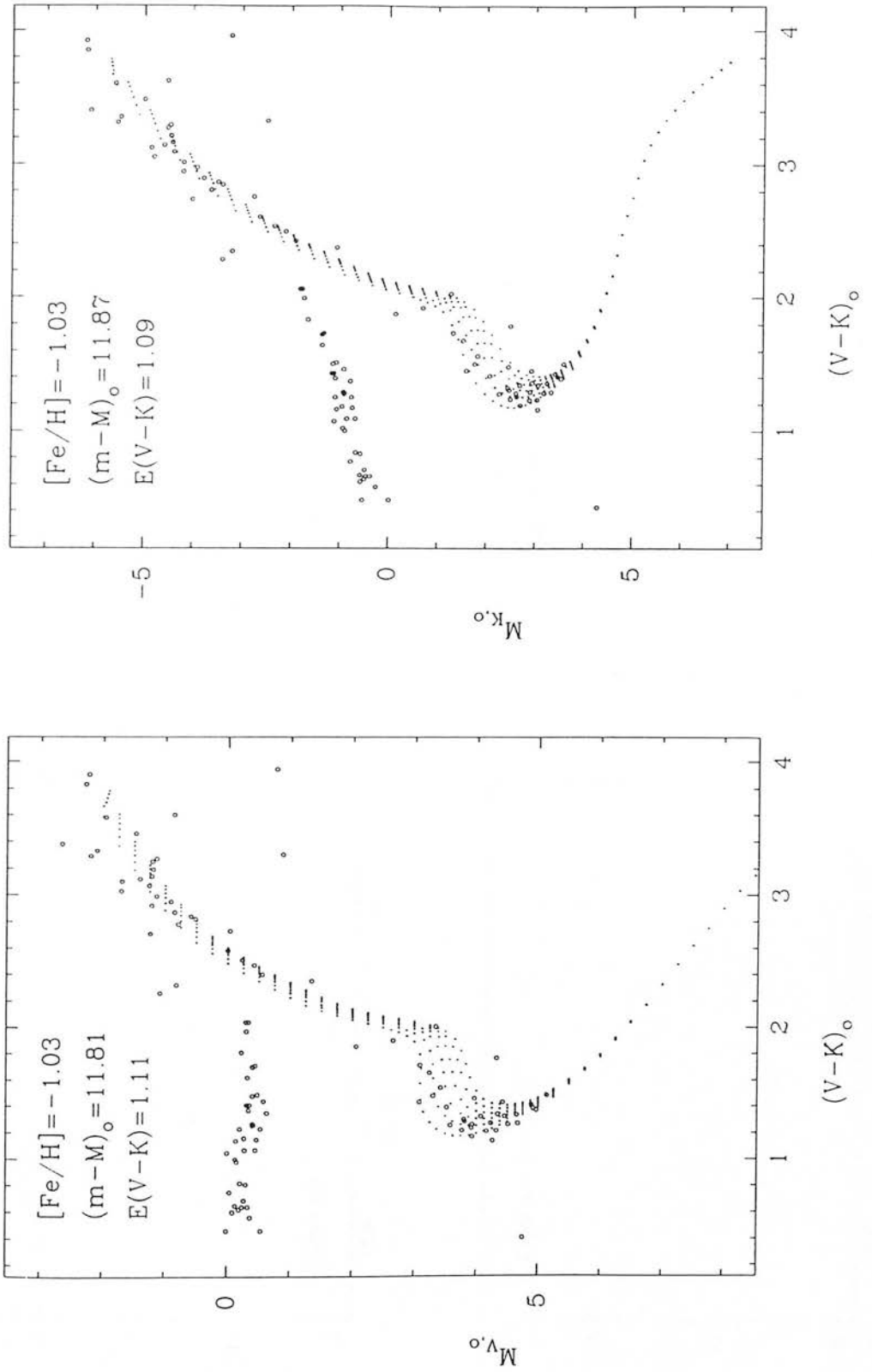

Figure 15: The best fits to the M4 CMDs from the BBVB isochrones.

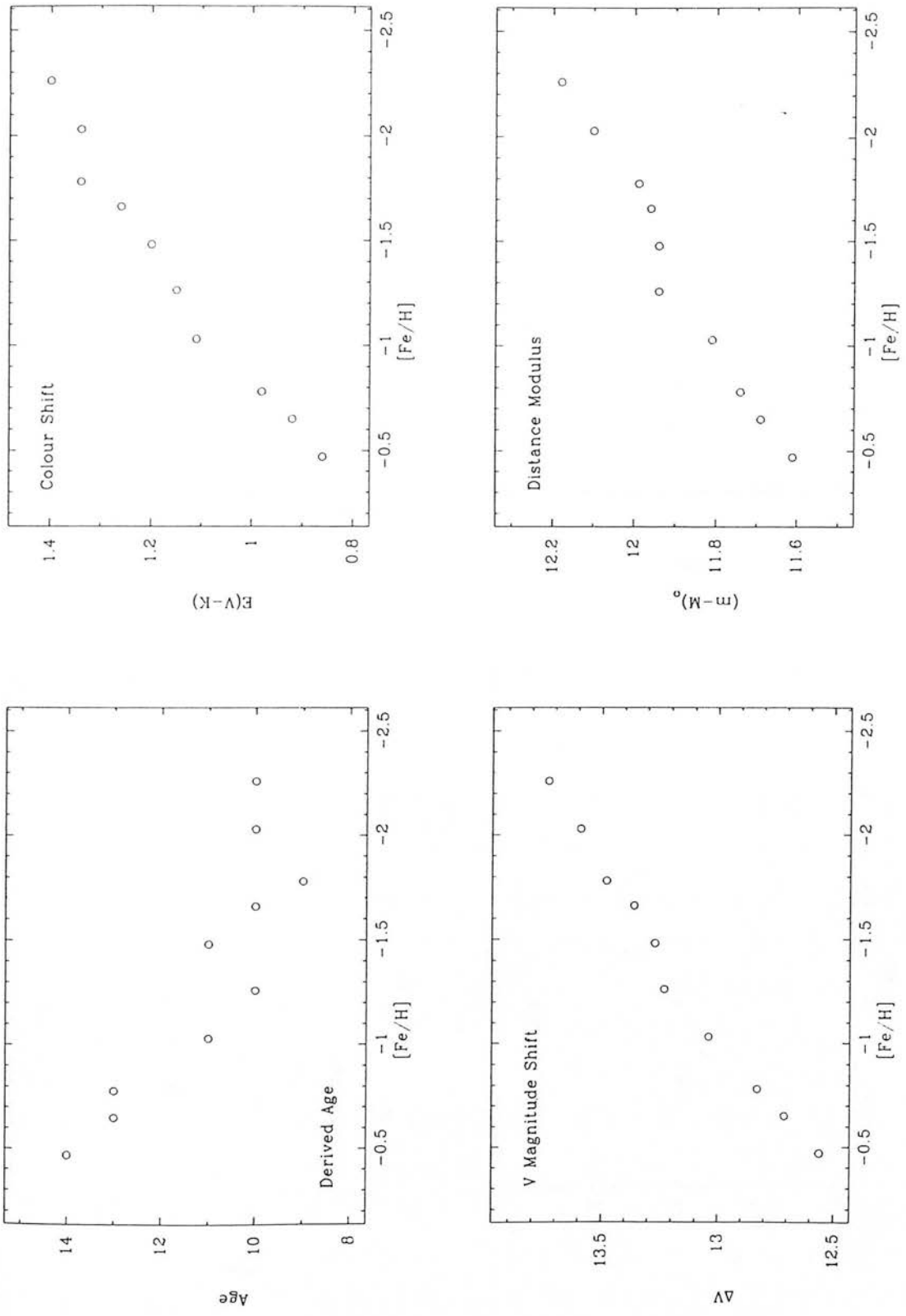

Figure 16: Fitting parameters for (V-K)-V CMD.

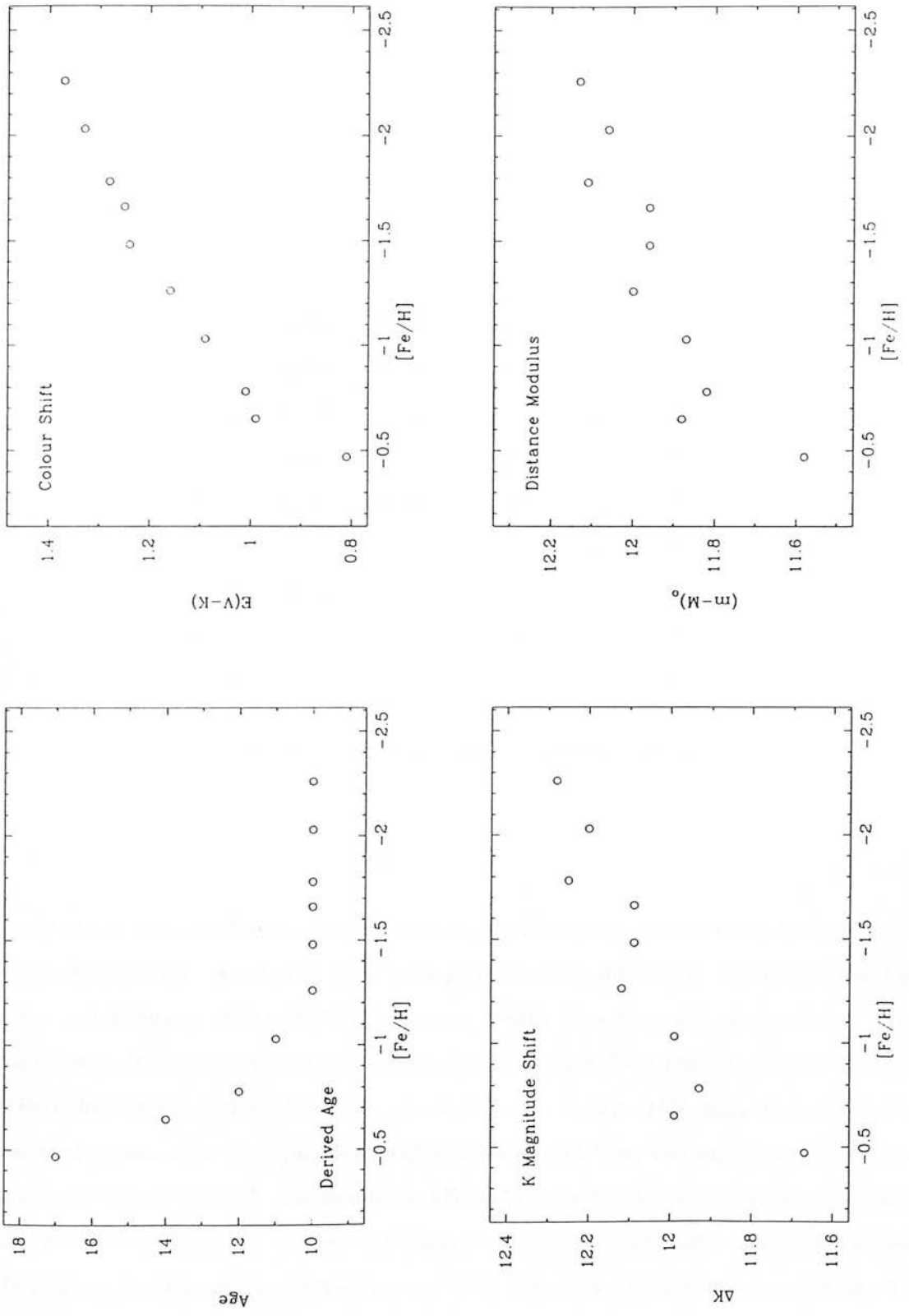

Figure 17: Fitting parameters for (V-K)-K CMD.

Table 5: Best fit parameters for (V-K)-V CMD

[Fe/H]	[O/Fe]	Δ(V-K)	ΔV	Age	Quality
-0.47	0.23	0.86	12.56	14	C
-0.65	0.30	0.92	12.71	13	B
-0.78	0.39	0.98	12.83	13	B
-1.03	0.50	1.11	13.04	11	B
-1.26	0.55	1.15	13.23	10	B
-1.48	0.60	1.20	13.27	11	C
-1.66	0.63	1.26	13.36	10	D
-1.78	0.66	1.34	13.48	9	D
-2.03	0.70	1.34	13.59	10	D
-2.26	0.75	1.40	13.73	10	E

Clearly the derived reddening and the best-fit metallicity are satisfactorily in agreement with previous work. An age of 11 Gyr is younger than previously suggested, but the oxygen enhancement of the BBVB isochrones means that they will predict lower ages than comparable isochrones with no enhancement. VandenBerg (1985a) showed that an [O/Fe] enhancement of 0.5 reduced the age of an isochrone by ~15%, regardless of [Fe/H]. This would mean that the equivalent [O/Fe]=0 age is 13 Gyr, although it is not known whether the present BBVB isochrones are affected in *exactly* the same way as the earlier VandenBerg isochrones. If the age difference is similar in magnitude to that found for M71 (with a slightly smaller [O/Fe]) an age of 11 Gyr may correspond to an age of ~15 Gyr from an unenhanced isochrone. Both values are consistent with the mean found from the literature in section 2.4 and close to the 14 Gyr AL84 derived from their optical data, which provides the main-sequence V magnitudes in the current CMDs. In any case,

Table 6: Best fit parameters for (V-K)-K CMD

[Fe/H]	[O/Fe]	Δ(V-K)	ΔK	Age	Quality
-0.47	0.23	0.81	11.67	17	C
-0.65	0.30	0.99	11.99	14	C
-0.78	0.39	1.01	11.93	12	B
-1.03	0.50	1.09	11.99	11	B
-1.26	0.55	1.16	12.12	10	B
-1.48	0.60	1.24	12.09	10	B
-1.66	0.63	1.25	12.09	10	C
-1.78	0.66	1.28	12.25	10	D
-2.03	0.70	1.33	12.20	10	D
-2.26	0.75	1.37	12.28	10	D

because of the steepness of the age-[Fe/H] fitting correlation, an error estimate of 1.5 Gyr must be assigned to the derived age.

If the AL84 zero-point were not already under suspicion, the derived $(m\text{-}M)_o$ would be puzzling, particularly because the same isochrones produce such good results for M71. The mean from the two CMDs of 11.71 makes the cluster half a magnitude, or 450pc, more distant than expected.

What if the value of R or E(B-V) were wrong ? Reverting to R=3.05 increases the equivalent (B-V) reddening to 0.45, but only changes the distance moduli to 11.67 and 11.71. If the reddening is increased from the 0.34 found to the 0.37 expected, the two values become 11.56 and 11.73. If the reddening is set at 0.37 *and* R=3.05 they are 11.91 and 11.76, respectively. The important point is that $(m\text{-}M)_K$ cannot be affected

Table 7: Revised parameters for fits to the [Fe/H]=-1.03, t=11 Gyr isochrone

Diagram	E(V-K)	$E(B-V)_{eq}$	Δm	$(m-M)_o$
(V-K)-V	1.23	0.34	13.04	11.68
(V-K)-K	1.21	0.34	11.87	11.74

much by changing the reddening or the reddening law, so that $(m-M)_o \sim 11.7$ from the K magnitude whatever the circumstances. Thus the present solution is 'self-consistent' in that the vertical shift in the (V-K)-V CMD produces a similar answer for $(m-M)_o$ to that in the (V-K)-K diagram.

Thus the present isochrone fitting procedure, which leaves reddening, distance modulus, metallicity and age as free parameters, has produced an anomalous result for the distance modulus, despite its success when applied to M71. The next few paragraphs address the question of whether a zero-point error in one or all of the studies or the isochrones could reconcile this anomaly.

If the cluster data are placed at the nominal offsets, from the adopted values of reddening and distance modulus, in relation to the [Fe/H]=-1.03, t=12 Gyr isochrone in the (V-K)-V CMD, the main-sequence points lie $0^m.2$ too blue in (V-K), while the giants are quite well fitted. If the K zero-point is adjusted so that the main sequence agreed with the isochrone, the bright giants would lie below all the [Fe/H]=-1.03 isochrones in V. To make the giants and main-sequence stars simultaneously fit an isochrone *and* derive the expected distance modulus from V (assuming E(B-V)=0.37) requires going to [Fe/H]=-0.65 where $E(B-V)_{equiv}$ would be 0.28. However, this correction would make the de-reddened distance modulus derived from the K magnitudes equal to 11.77 (or even worse if $E(B-V)_{equiv}$ is used).

An error of $0^m.2$ in the present K magnitudes, in the sense that the magnitudes are too faint, could produce an acceptable result from the (V-K)-V diagram but could not produce a consistent answer from the (V-K)-K diagram.

If there were a simple zero-point error in V of $0^m.2$ it would not be possible to obtain a satisfactory fit with the expected distance modulus. Since the giants and main-sequence stars are fitted together, the likely source of error is a zero-point difference *between* the sets of magnitudes, so that, for instance, the main-sequence points might lie too bright in V in comparison to the giants. This would mean that the CMD was compressed in V and would be fitted well by an isochrone with too high a metallicity or with too low an age.

As has already been seen, there is possibly an error in the fainter V magnitudes of AL84, which have been used to construct the main-sequence CMD points. Making AL84's V magnitudes $0^m.18$ fainter produces a good fit with the [Fe/H]=-1.03, t=16 Gyr (V-K)-V isochrone. Figure 18 shows the data thus adjusted and the [Fe/H]=-1.03 isochrones. The main-sequence points are still somewhat bluer than the isochrone, but the fit to the giants is very good. Shifting the MS points another 0.05 in (V-K) would make the fit very good (an A on the scale used earlier). Using the [Fe/H]=-1.26 isochrones would fit the main sequence better but would not reproduce the observed shape of the giant branch.

Thus, using the more usual isochrone fitting procedure of fixing E(B-V) and $(m-M)_o$, with an 18% shift applied to the AL84 data, the present CMD can be fitted by an isochrone of [Fe/H]=-1.03 and t=16 Gyr. Clearly the zero-point shift has not brought the data into perfect agreement with the theory. Sadly it seems likely that the AL84 data do require a V-magnitude zero-point change of some sort. This shift may be magnitude- or colour-dependent and seriously compromises the usefulness of the present data.

To summarize: the isochrone-fitting, rather than yielding accurate estimates of [Fe/H], E(B-V), age and $(m-M)_o$, has partly turned into a test of the AL84 V magnitudes, with the following results:

1. the giant branch of M4 is well fitted by the [Fe/H]=-1.03, t=16 Gyr isochrone at the adopted value of E(B-V) and $(m-M)_o$;

2. applying an 18% (or preferably slightly larger) shift to AL84's V magnitudes allows

the main-sequence points to agree with the same isochrone;

3. the CMD *with* the shift is better fitted by the isochrones than was possible without it;

4. The age estimate for the cluster is somewhat uncertain, with the metallicity being well determined from the shape of the giant branch. A revised age estimate of 16 ± 3 Gyr results if a shift of ~18% is assumed.

5 Matching the CMD with M71

Shifting the main-sequence zero-points again seems appropriate.

The nominal shifts between the two clusters (Δ(V-K)=0.59, ΔV=1.02 and ΔK=1.6 from the adopted parameters in section 2) produce excellent agreement of the HBs and of the GB stars near the HB. The turn-offs agree well, but by $1^{m}.5$ below in V, the M71 stars are $0^{m}.3$ redder. For the brightest giants the M71 stars are redder by $0^{m}.7$ at ΔV=2 above the HB, although the M71 scatter is large and the number of stars small.

If the offsets are set to agree with those found from the isochrone fitting of the two clusters (using the original AL84 magnitudes), the 'flat' section (between the TO and the base of the GB) in M4 lies ~$0^{m}.25$ above that of M71. This is in reasonable agreement with the $0^{m}.3$ predicted by the relation found for the brightness of this feature from the SC91 isochrones in section 5.5 of the last chapter. The HBs are $0^{m}.45$ apart, which is far more than the ~$0^{m}.06$ predicted by the log P - K relation (LDSJF90).

The 18% shift mentioned above is required to make the the lower main sequence points coincide at the nominal offsets. Figure 19 shows the two clusters matched in this way and also the respective best-fitting isochrones. Clearly, the shift again produces a result in better agreement with the models - with close matching of the lower main sequences - and again making the M4 main sequence bluer by $0^{m}.05$ would make the agreement even better.

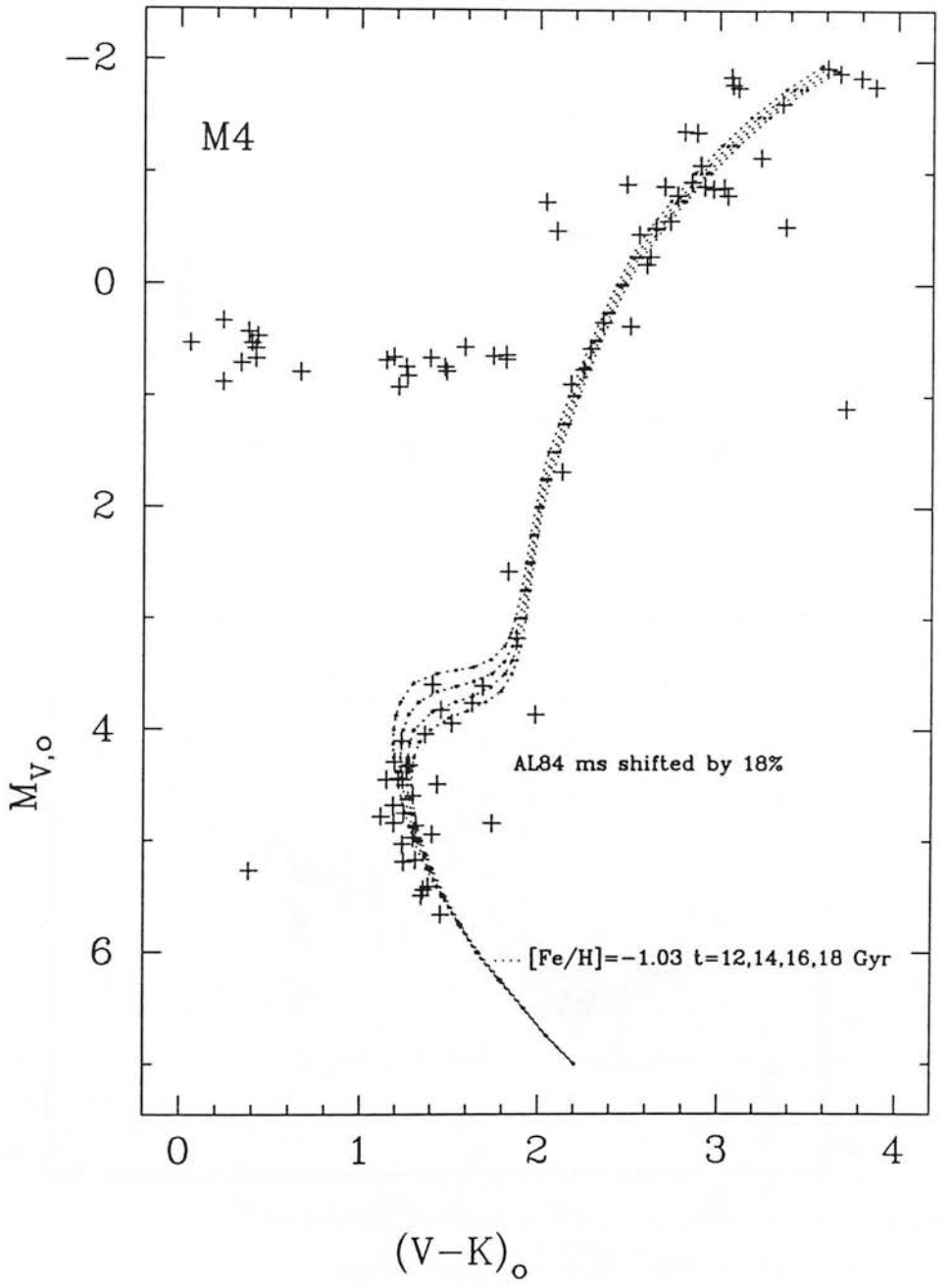

Figure 18: The BBVB [Fe/H]=-1.03 isochrones and the M4 data, with the AL84 V-magnitudes made fainter by $0^m.18$.

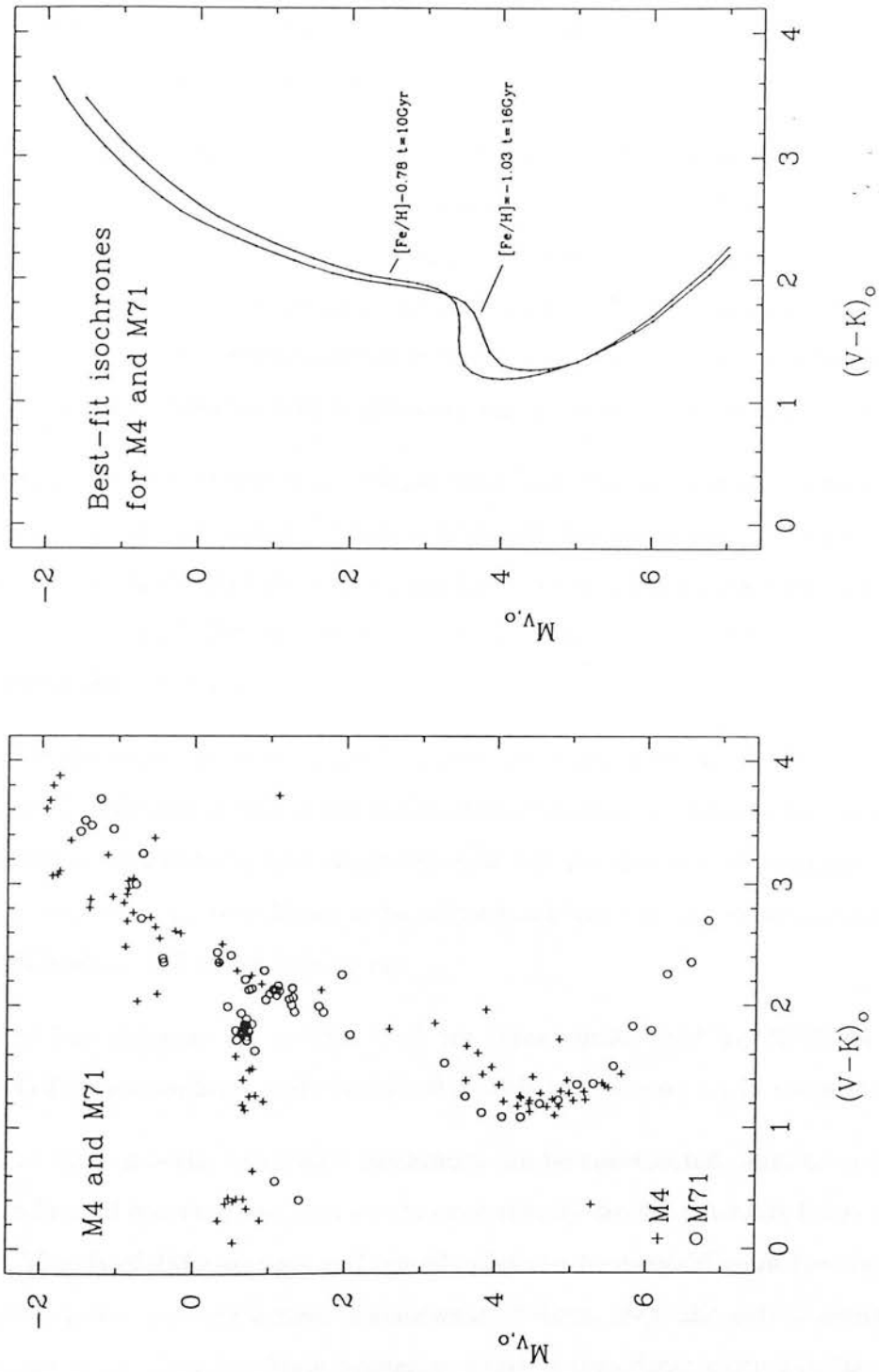

Figure 19: The M4 and M71 (V-K)-V data at their respective adopted reddenings and distance moduli. The AL84 V magnitudes have been made fainter by 18%. Also shown are the two best-fit isochrones for the clusters. Since there is no 11 Gyr isochrone for [Fe/H]=-0.78, the 10 Gyr curve is displayed, which is flatter between the turn-off and the giant branch.

6 Matching the two-colour diagram with models

The M4 observations are compared to the similar data in M71, model atmosphere calculations, and to two-colour isochrones.

As with M71, the (V-K)-(B-V) two-colour diagram allows observations to be compared with the results of model atmosphere calculations in a way that is independent of the distance to the cluster. As well as the giant and sub-giant observations that were plotted for M71, the M4 data-set also includes the large horizontal branch, including the RR Lyrae stars, and the stars in the region of the turn-off. The gravities of these stars are likely to range from log g=0.5 for the largest giants to almost log g=5 for the main-sequence stars.

How well the models fit has to be judged from how well the predicted gravities for the stars match up to expectations. There is little previous information on gravity: FPC83 derived log g for their giant stars, assuming $\mathcal{M}=0.8\,\mathcal{M}_{\odot}$; LJ90 derived log g for their four RR Lyrae stars and PRMV86 found best-fit model gravities for their HB observations, by assuming $\mathcal{M} \sim 0.65\,\mathcal{M}_{\odot}$.

As is often the case in a pioneering study, there are many parameters to be tested at the same time: in this case, how well the models match the observations depends both on how intrinsically accurate the models are *and* on how well the chosen reddening and reddening law have worked. If there is found to be a mismatch between theory and observations it will be difficult to tell which is in error.

As in the last chapter, the models used are those constructed by PRMV86 from the Kurucz (1979) atmospheres and the BGVB models (see section 7.1 in the last chapter).

As well as these models, two-colour isochrones can be constructed. Just as in the CMD, these are lines of constant age from stellar evolutionary models calculated over a range of masses. Models of different ages and metallicities can be overlaid upon the cluster data. Two-colour isochrones are a new, if somewhat obvious, idea, the only precedent is the special case of the Zero Age Main Sequence, which is sometimes plotted in the 2CD.

Unfortunately, the Bergbusch and VandenBerg (1991) (B-V)-V isochrones are not yet available, so that the SC91 (B-V)-V and BBVB (V-K)-V isochrones have been matched up, through the V magnitudes, for selected metallicities and ages. Since the two models use somewhat different physics, the results must be considered tentative. In particu-

lar, the BBVB isochrones contain [O/Fe] enhancement and the SC91 isochrones do not. No information is available on the masses or temperatures of the points in the BBVB isochrones, so these cannot be compared with the parameters in SC91.

6.1 Comparison with M71

It has already been seen in figure 14 that the observations of M4 and M71 match well. How good the match is may be tested by examining the difference between the two clusters where they overlap sufficiently. From the BBVB models, two stars of log g=2, one with [Fe/H]=-0.5 and the other with [Fe/H]=-1.0, will be separated by 0.05 in (B-V) at $(V-K)_o$=2, in the sense that the more metal-poor star will be the bluer. The separation of the mean lines through the stars in the two clusters, measured at $(V-K)_o$=2, is 0.03 $\pm$ 0.01. The difference between the adopted metallicities for the two clusters is 0.3. Thus the clusters are positioned, relative to one another, such that they are consistent with their nominal metallicities. Considering that both clusters have been de-reddened by over a magnitude in (V-K), along different reddening lines, this agreement is excellent and leads to confidence in the chosen reddening vectors for both clusters, and also in the *relative* accuracy of the models. For instance, increasing the reddening of M4 by $0^m.02$ in E(B-V) would close the separation between the two cluster sequences by $0^m.01$.

6.2 Comparison with models

Figure 20 shows the BGVB and PRMV86 models for [Fe/H]=-1.0 and various values of log g overlaid upon the de-reddened M4 data. The AL84 data has been shifted by 18% in V but not in (B-V) (i.e. the zero-point error in V is cancelled by a similar error in B). In the main, the agreement between the models and the observational expectations is excellent. For the bluest colours, the BHB stars cluster about the log g=3 model. Bearing in mind that the PRMV86 models are too blue in (B-V) at higher (V-K), the BHB, RR Lyrae and RHB stars form a sequence running along a line of log g$\sim$3. PRMV86 found log g$\sim$ 2.8 for the BHB and RHB stars from interpolation in their models. Similarly, LJ90 found log g$\sim$2.7-2.8 for their four RR Lyrae variables from modified Kurucz atmospheres.

Specific horizontal-branch evolutionary models do not agree: Rood and Crocker (1988), for instance, predict log g to go from 3 to 4.5 from the RHB to the BHB. They find rea-

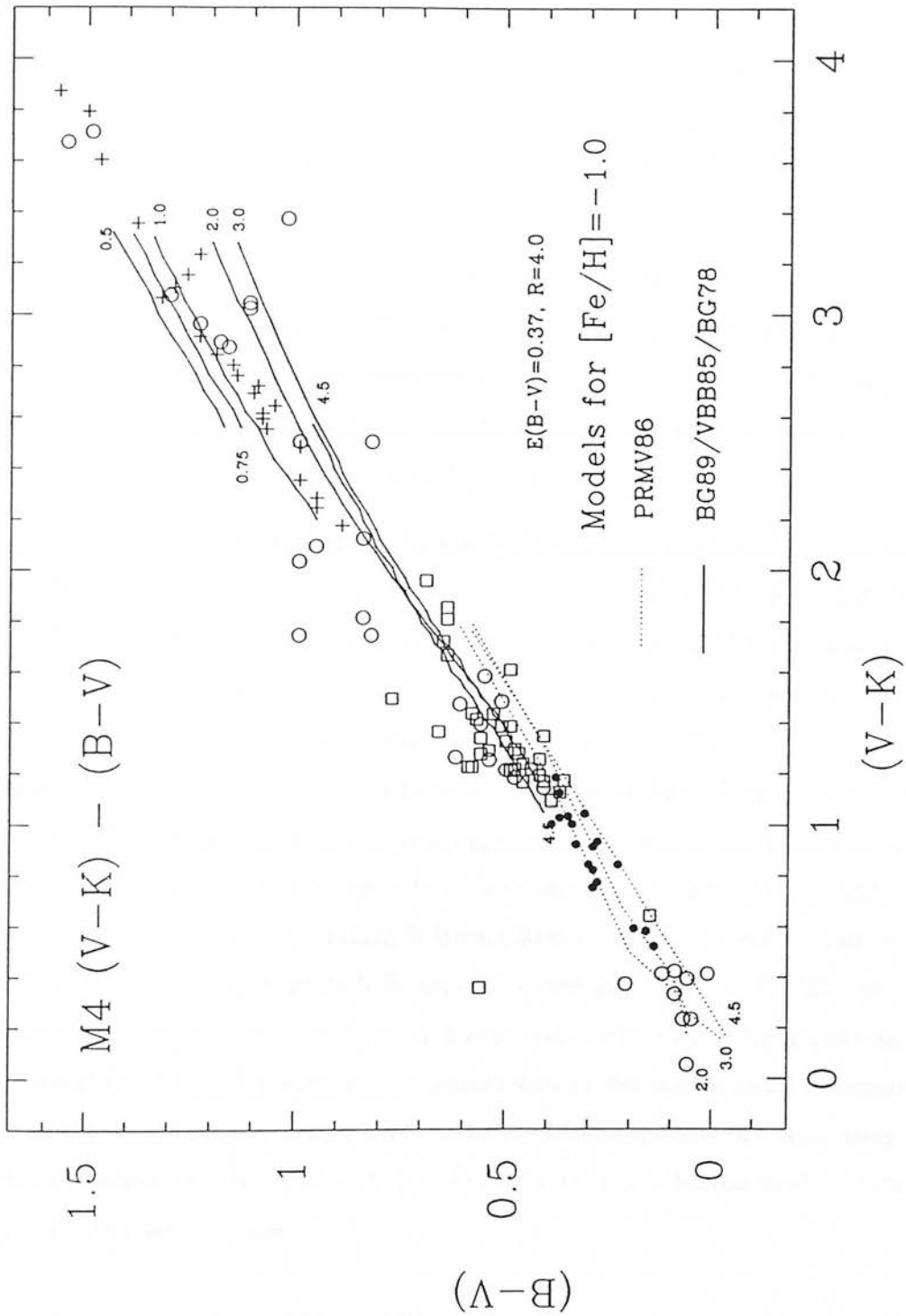

Figure 20: The M4 data compared to the BGVB and PRMV86 models for [Fe/H]=-1 in the (V-K)-(B-V) diagram. The main-sequence data have been shifted $0^{m}.18$ to the red in (V-K).

sonable agreement with these predictions from HB spectroscopic observations in NGC288, M5 and M92. However, if standard stellar atmosphere models accurately predicted parameters for HB stars, there would be no need for specific HB models, so it is neither surprising nor worrying that the present model gravities of log g=3 do not agree with the Rood and Crocker, and similar HB model, predictions. No HB models are available which include (V-K) colours.

The main sequence points coincide with log g=3 at the turn-off, with log g increasing for the fainter, redder stars. Unfortunately, the models do not extend above log g=4.5, so the variation of log g down the main sequence cannot be examined. It can be seen from figure 14 that if the 18% shift is not appropriate for the AL84 data, the main-sequence stars will have model gravities ranging from log g=4.5 upwards.

Allowing for the large scatter introduced by the PRMV86 observations, the giants form a sequence which runs from log g=1.5 at $(V\text{-}K)_o$=2.2 to log g=0.75 at $(V\text{-}K)_o$=3.8. These figures are in reasonable agreement with the gravities derived by FPC83, who found log g ranging from 0.4 to 2.2 for the same stars. The differences between the data-sets are more to do with the differences between the model atmospheres and assumptions used. Their calculations used $(m\text{-}M)_o$=11.60, E(B-V)=0.36, R=3.05 and $\mathcal{M}=0.8\,\mathcal{M}_\odot$. The mass is consistent with those found by SC91 for their upper main-sequence and giant stars at the appropriate [Fe/H] and age. If these gravities are recalculated with $(m\text{-}M)_o$=11.22, E(B-V)=0.36, R=4.0 and $\mathcal{M}=0.8\,\mathcal{M}_\odot$, taking V from CR90 and using the same relationships to determine T_{eff} and the K-magnitude bolometric correction, BC_K, as FPC83, the stars cover log g=0.5 to 2.35. At first sight, it seems odd that using what appear rather different values for the fundamental cluster parameters makes such a small difference to the derived values of log g. Starting from $L=4\pi R^2\sigma T^4$ and $g=G\mathcal{M}/R^2$, and using the approximate gradients of the log T_{eff}-$(V\text{-}K)_o$ and BC_K-$(V\text{-}K)_o$ relations used by FPC83, this approximate relation follows:

$$\Delta log\ g = -0.11\Delta R - 0.4\Delta(m - M)_o$$

for the dependence of the difference in gravities between FPC83 and the values recalculated using the presently adopted parameters. Thus, if the present parameters are correct, two-thirds of the error caused by FPC83's use of the wrong distance modulus was cancelled out by their also using the wrong value of R !

There are no spectroscopic gravities for M4 stars, but the gravities derived from these models agree well, at the same (V-K), with those stars in M71 that have values derived from high-dispersion spectroscopy. That is, if the giants in both clusters have the same T_{eff} (from (V-K)) and log g (from the models), the difference in metallicity translates into a shift in (B-V) colour, in the sense that the more metal-poor stars are the redder.

Thus the observations are found to agree satisfactorily with the models and the previous determinations of gravities. This means that, barring an unlikely conspiracy of errors, the reddening correction, the 12% zero-point correction in the models and the colours produced by the models are all consistent.

6.3 Comparison with two-colour isochrones

The BBVB (V-K)-V and SC91 (B-V)-V isochrones can be matched up through their V magnitudes for appropriate metallicities and ages. Because the BBVB isochrones contain [O/Fe] enhancement they will evolve faster, so that a BBVB isochrone of a given age needs to be matched to a somewhat older SC91 isochrone.

Figure 21 shows some two-colour isochrones overlaid upon the FPC83 giants and the present main-sequence data (including the 18% correction). The data have been dereddened with the adopted E(B-V) and the two-colour isochrones have been shifted by 12% in (V-K). The first isochrone, for instance, is constructed from the [Fe/H]=-1.03, t=8 Gyr BBVB (V-K)-V and [Fe/H]=-1.04, t=10 Gyr SC91 (B-V)-V isochrones. This age correction is based on ages being ~15% younger for [O/Fe]=0.5, as recommended by VandenBerg (1985a).

This is not an ideal situation. Had the Bergbusch and VandenBerg (1991) (B-V)-V isochrones been available, a set of two-colour isochrones could have been constructed which would have included the same physics and not needed any age correction.

Clearly, then, the present two-colour isochrones are not expected to be particularly accurate in shape or position in the two-colour diagram. They are none the less interesting, since the effects of metallicity and age changes on the sequences in the two-colour diagram can be judged from them.

The two-colour isochrones are approximately linear for all of the main sequence stars

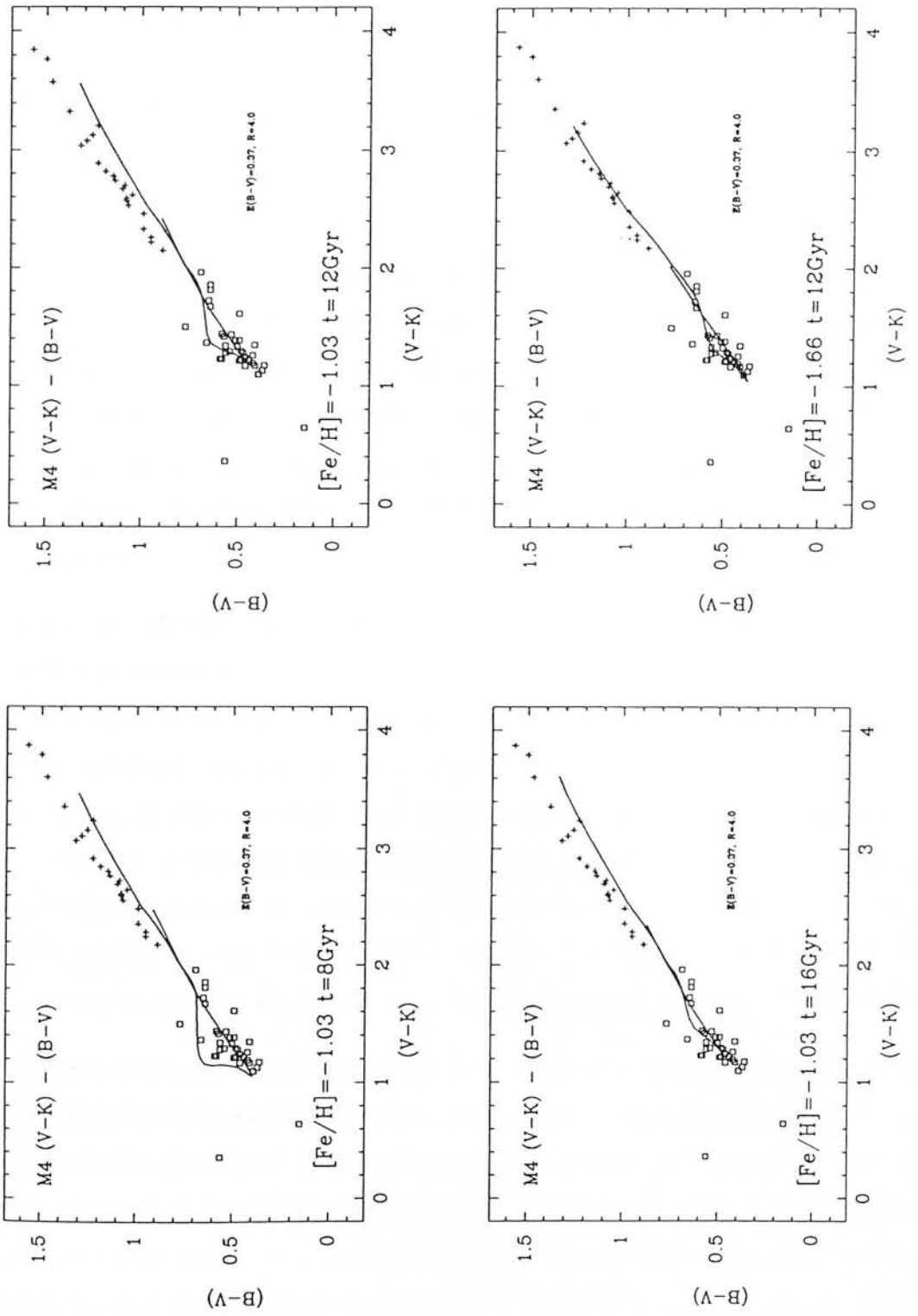

Figure 21: Two-colour isochrones for three different ages and two different metallicities, plotted with the FPC83 giant observations and the current main-sequence data.

below the turn-off. Stars that are turning off and on the way to the base of the giant branch form the loop seen in the isochrones, where the stars are redder in (B-V) by up to $0^{m}.2$ than the lower main-sequence stars of the same (V-K). After this loop the giants follow a similar line to the main sequence stars. Using isochrones of the same age, that is, not correcting for the [O/Fe] enhancement, makes no difference to the general form of the two-colour isochrones.

What are the effects of metallicity and age on the two-colour isochrones ? The more metal-poor isochrones have upper giant branches which are redder in (B-V) for a given (V-K) than those with a higher metallicity. The younger an isochrone the bluer the turn-off (obviously) and the larger the loop. The giant locus is relatively unaffected by age differences (for instance, for the [Fe/H]=-1.03 isochrones, the giant locus changes by only 0.02 in (B-V), at a constant (V-K)=3, between t=10 and 18 Gyr, while varying the metallicity between [Fe/H]=-0.5 and -2.25 leads to a difference of $\sim 0^{m}.2$ at a constant age of 12 Gyr).

From figure 21 the [Fe/H]=-1.03, t=16 Gyr isochrone fits the main sequence reasonably well. The isochrone for 12 Gyr appears to fit better, but if a larger shift than applied is appropriate for the AL84 V magnitudes, the 16 Gyr curve could fit satisfactorily. The giants are fitted better by the more metal-poor isochrone, but the reddest giants may not fit anyway (SC91 state that for the brightest and reddest stars their isochrones should be regarded as 'very tentative'). With the uncertainties in which ages to pair up in the two-colour isochrones, the AL84 B and V zero-points and the reddest SC91 (B-V) colours, little significance can be drawn from a best-fit two-colour isochrone, although they will certainly be useful in the future, when further developed and properly calibrated.

The loop is an odd feature and might be thought to be a simple mismatch between the two sets of models - this would not be surprising since the turn-off region is quite sensitive to the model parameters. However, figure 22 shows the loop in more detail, with the stars coded according to whether they are above or below the main-sequence turn-off. Had the loop been an accurate prediction of the behaviour of cluster stars, the upper main-sequence and sub-giant stars (open squares) would lie along the upper, curved section and the lower main-sequence stars (filled squares) would lie along the straight section, completing the loop. If the loop were completely spurious all the stars might be expected to lie along the straight section. The figure is inconclusive, because the number of stars

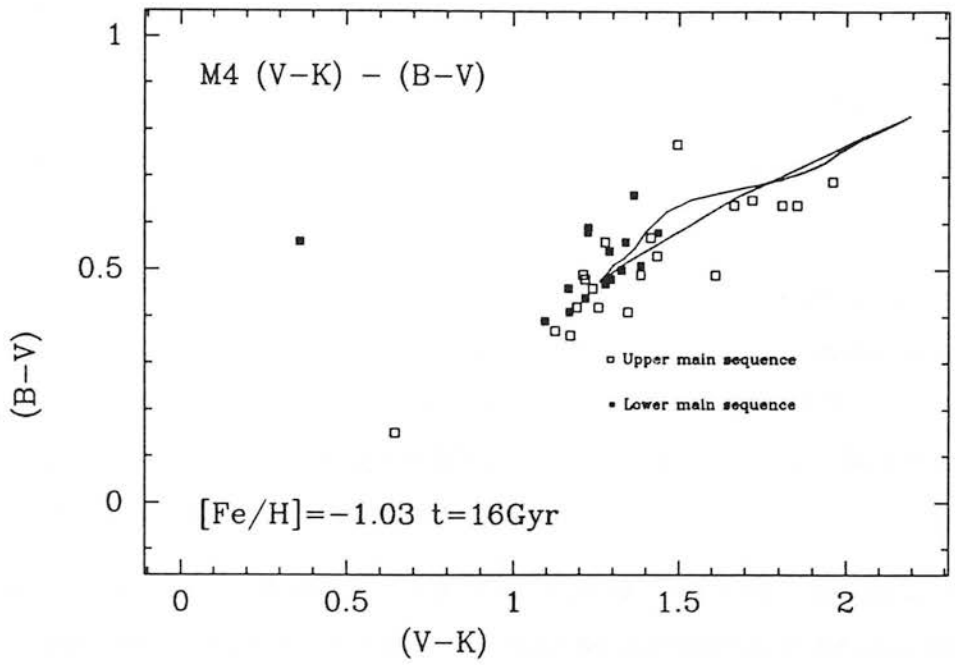

Figure 22: Detail of the loop in the [Fe/H]=-1.03, t=16 Gyr two-colour isochrone. The stars above and below the main sequence turn-off are differentiated.

involved is small and the scatter large, and because the models and observations clearly do not coincide, either because of the AL84 zero-point error or because of inadequacies in the models. If any result is seen it is that the stars actually lie in reverse of expectation, with the lower main sequence stars following the loop. One possible physical origin for the loop is seen in CMD evolutionary tracks calculated for more massive stars. In VandenBerg's (1985b) models there is a phase just after a star has turned off the main sequence when the star contracts, the hydrogen in the core having been exhausted, moving to the blue and brightening slightly. When conditions become right the hydrogen shell source starts up and, as the atmosphere expands again, the star resumes its redward movement toward the base of the giant branch (see also Iben, 1967). Such a back-track is not explicitly seen in either set of isochrones but a vestigial presence, affecting the stellar structure, and hence the gravity, in a minor way, or inducing the mixing of processed material could lead to the loops found. The effects of sudden temperature- or gravity-dependent opacity changes can be so strong that it would require detailed modelling to understand the physical mechanism that produces the loops.

6.4 Summary

Excellent agreement is found between the two-colour diagrams of M4 and M71, with the difference between them agreeing very well with the model predictions based on the nominal difference between their metallicities.

The BGVB and PRMV86 models for [Fe/H]=-1.0 fit the observations satisfactorily, predicting effective gravities consistent with those found from high dispersion spectroscopy of similar stars in M71, and with the Baade-Wesselink values for LJ90's four RR Lyrae stars. Again the chosen reddening for M4 has proven successful and the 12% blueward shift applied to the models yields consistent results.

Two-colour isochrones are found not to fit well. The two-colour isochrone loop *may* prove to be an age and metallicity diagnostic, although no information is yet available on the [O/Fe] dependence of its morphology. The slope of the giant stars is a good [Fe/H] indicator, little affected by age, but is not reproduced well by the isochrones because of the known problems with the (B-V) model colours.

To sum up, the present models fit well in the (V-K)-(B-V) two-colour diagram, suggesting a metallicity and a range of gravity in accord with expectations. The two-colour isochrones, will provide useful metallicity and age indicators, once the models are better tested against a range of well-observed clusters.

7 The luminosity function

The radial dependence of the K luminosity function is examined. An 'artificial' V luminosity function is constructed from the K data and compared to previous observations.

For a proper study of a cluster's luminosity function, observations are needed in an adjacent 'empty' field, so that the galactic background LF may be corrected for. Such observations were not taken in the present study, and would in any case be difficult in the area around M4, where the extinction is patchy. The M71 luminosity function was not considered because the field star contamination is expected to be severe, as is the crowding. The present data may be used in a differential way: one comparison that can be made is between two halves of the combined photometry for the large mosaic. Since the

observed area lies to the East of the cluster centre, with the long axis of the mosaic lying approximately radially, the data may be divided into an inner half, centred at about 4′ from the cluster centre, and an outer half, centred at $\sim 6.5'$. It is expected that the inner field will contain more stars of all types and thus suffer more from crowding problems. If significant mass or chemical composition gradients are present in the cluster, these might be expected to be manifested as differences in the LFs for the two regions, although the effect is likely to be very small at such large distances from the cluster centre.

Figure 23 shows both the linear and logarithmic luminosity functions for all the stars in the large mosaic (solid line), the LF for the inner set of stars (dashed line) and the LF for the outer set (dot-dashed line). The magnitude scale is in instrumental magnitudes, k, where the true magnitude is given by K=k-4.99 (from chapter 2). The figure shows an excess of stars in the inner field at all magnitudes brighter than k$\sim$23, with an extra 'bump' at k$\sim$21. Fainter than k=23 there are more stars found at each luminosity in the outer field. Because of the small areas involved it is not possible to derive separate completeness correction for the two halves of the image. Since the inner field suffers from greater incompleteness at faint magnitudes, because of its greater crowding, the excess of faint stars seen in the outer field is expected and unlikely to be real. Mass segregation would lead to a steeper LF for fields further out. When the counting errors and the incompleteness are considered, the two regions here cannot be said to be significantly different, except that there are nearly twice as many stars in a given magnitude interval in the inner field.

If the same image is divided horizontally into a Northern and Southern region, no significant difference can be seen between the two.

The only previous LF study which includes M4 is that of McClure et al (1986), who fitted theoretical LFs to their sample of nine cluster luminosity functions. The M4 observations came from the unpublished RF84 data and little information is included as to how the LF was calculated. In their figure 1 the M4 and 47 Tuc LFs match quite well, with the M4 function turning over at the faintest bin. McClure et al fitted theoretical LFs for [Fe/H]=-0.5, -1.3 and -2.3 and various values of the mass spectrum power-law index, x, where the number of stars with masses in the range $\mathcal{M}$ to $\mathcal{M} + d\mathcal{M}$ is given by the power law: $\phi(\mathcal{M})d\mathcal{M} = \mathcal{M}^{-(1+x)}\mathrm{d}\mathcal{M}$ (see McClure et al for definition). McClure et al (1987) presented results for two more clusters and a plot of the mass spectrum power-law index

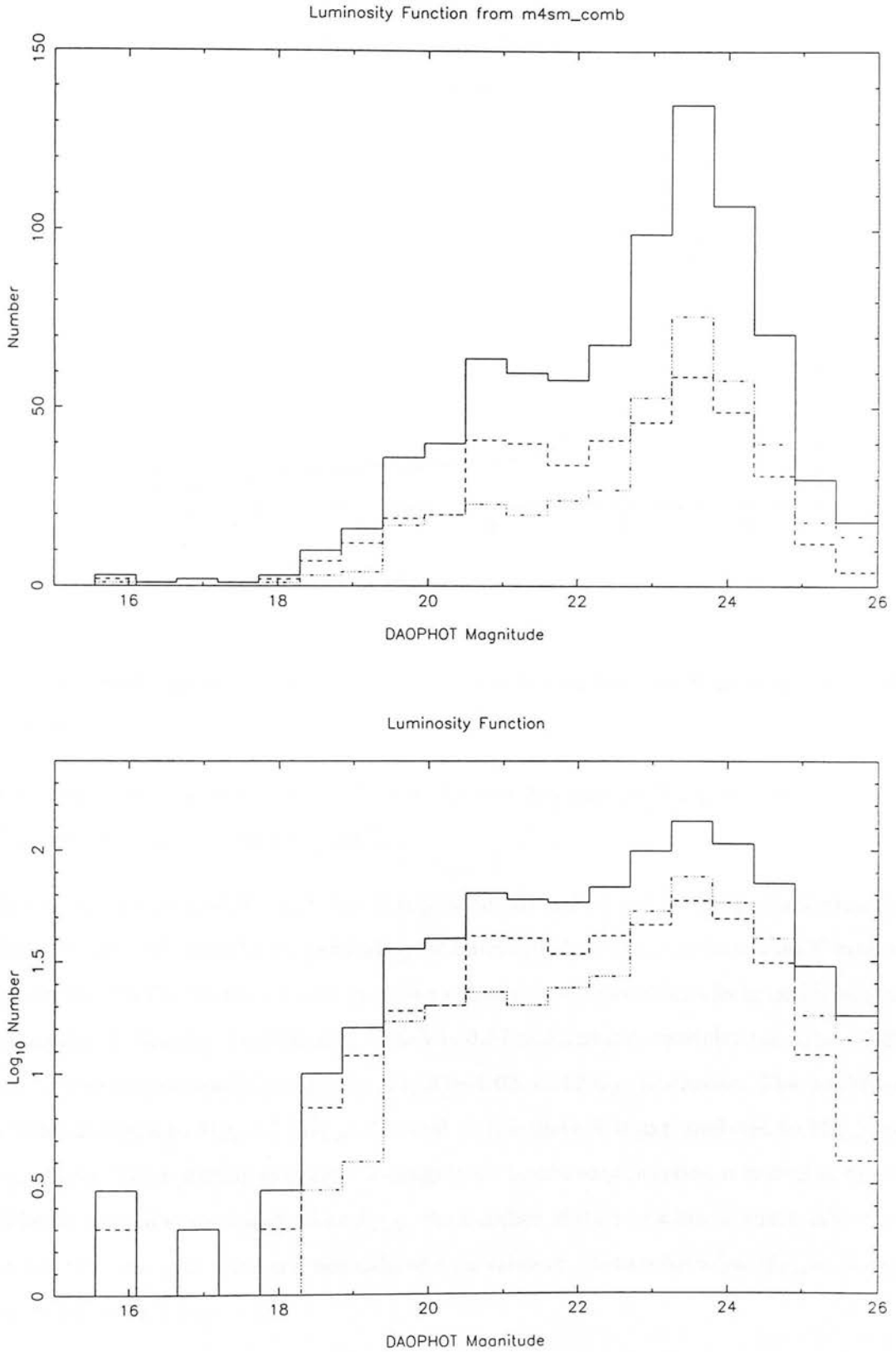

Figure 23: The K-band luminosity function measured for the combined data of the large images on logarithmic and linear number scales. The solid line is for all the stars, the dashed line for the outer field and the dot-dashed line for the inner one.

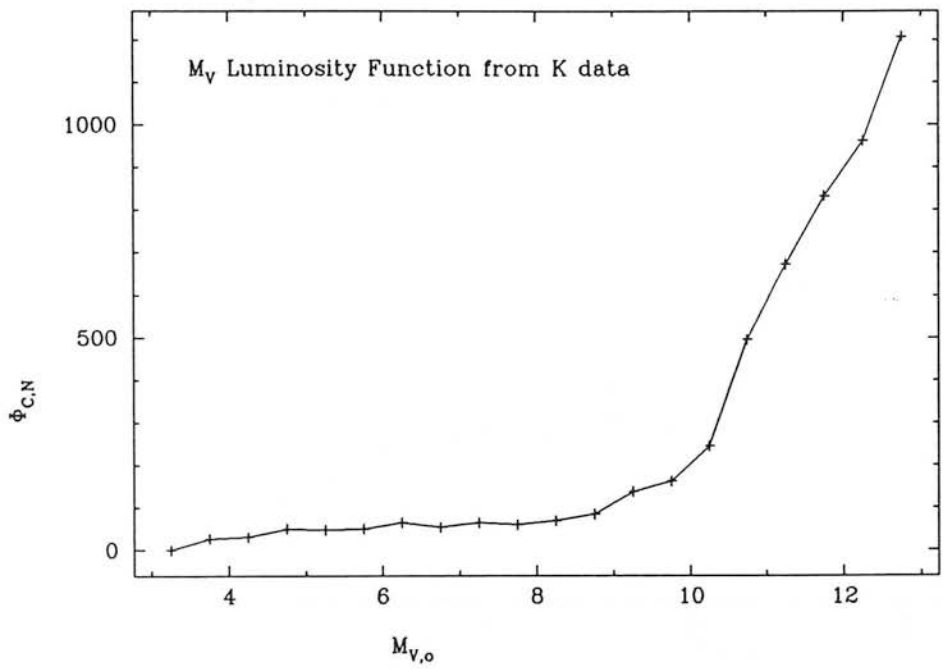

Figure 24: The V-magnitude luminosity function constructed from the K data via the BBVB isochrones.

against metallicity. The theoretical LF for [Fe/H]=-0.5 and x=-0.5 fitted the combined 47 Tuc and M4 observations adequately.

No K-magnitude LF models exist, but it is possible to make a rough comparison with the McClure et al (1986) data by transforming the current K-band observations into V magnitudes via the BBVB isochrones and applying completeness corrections from artificial star experiments. Assuming the reddening E(B-V)=0.37 and distance modulus $(m-M)_o$=11.22 the data were transformed through the [Fe/H]=-1.03, t=12 Gyr isochrone. The isochrone only extends down to $M_{K,o}$=7 ($M_{V,o}\sim$11) and so the curve was extrapolated to $M_{K,o}$=10 ($M_{V,o}\sim$14.5). The resulting synthetic V-magnitude luminosity function is shown in figure 24. The number of stars is plotted as $\Phi_{C,N}$, the number of stars in a bin of width ΔV=0.5, corrected for incompleteness and normalized to a value of 50 stars between $M_{V,o}$=5.0 and 5.5, as used by McClure et al.

The turn over in the Richer and Fahlman data is not seen in the present data, which extend to $M_{V,o}>10$ before the completeness correction factor exceeds 2. By $M_{V,o}$=12 this factor has reached 5. The dearth of stars around $M_{V,o}$=7.5 in the RF84 data is also not

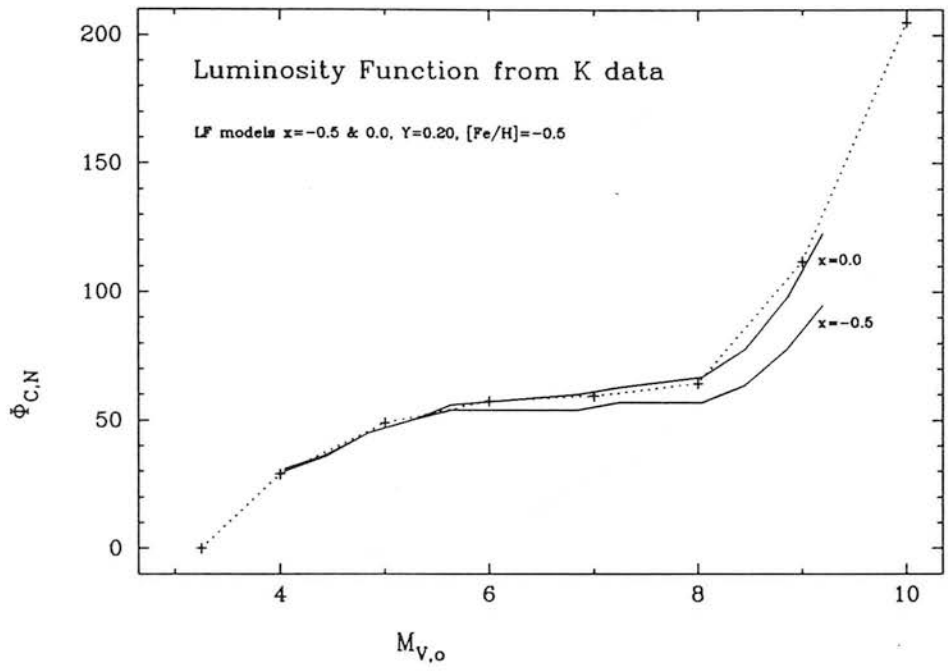

Figure 25: Luminosity function models from McClure et al (1986) matched to the present synthetic data.

found here, but the two data-sets are otherwise the same to within their errors.

Figure 25 shows the present data (resampled in half as many bins to make it smoother) plotted together with two of the models presented by McClure et al (1986). The faintest data point shown has been corrected with a factor of 1.9. The [Fe/H]=-0.5, x=0.0, Y=0.20 line is an excellent fit to the data - almost better than can be reasonably expected considering the process that the data have been through and the more probable values of [Fe/H]=-1 and Y=0.23 for M4. Also, no attempt has been made to correct for field-star contamination or the steepening of the LF by fainter stars scattering into the brighter, less-populous bins.

Given a knowledge of how the mass of a star is related to its K magnitude, it is possible to construct a model of the K luminosity function. Unfortunately, mass information is not available for the BBVB isochrones. Matching the BBVB and SC91 isochrones, through the V magnitude, allows the masses of the SC91 models to be related to the K magnitudes of the BBVB isochrones. The power-law index has been taken as 0, although the effect of varying x is small for the bright stars under consideration. Figure 26 shows the result of

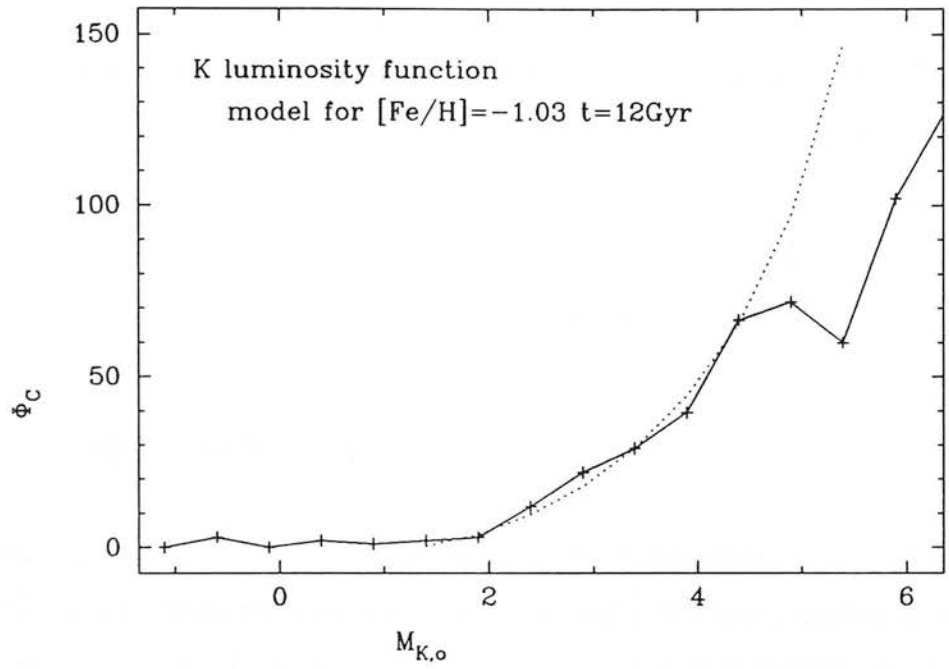

Figure 26: K luminosity function, corrected for incompleteness, with a model curve. The two are normalized to be the same at $M_{K,o}$=3.4.

this calculation together with the completeness-corrected K data. The model fits the data very well for all the bins which are complete. Beyond $M_{K,o}$=5 the K data are increasingly incomplete, although the completeness corrections would have to be considerably underestimated to explain the deficit of stars at the fainter magnitudes. Because the calibration of the mass-magnitude relation is so approximate, there is no need to further discuss this figure.

7.1 Summary

No significant difference was found between the stellar populations of the inner and outer halves of the large mosaic, given that the crowding is most significant in the inner region. A rough conversion of the K luminosity function into a V luminosity function allowed comparison with previous observations and models, with the conclusion that the power-law index of the mass function is close to -1 (i.e. x=0.0). This fits into McClure et al's (1987) x-metallicity correlation even better than their original result for the cluster, giving M4 a value of x between that of 47 Tuc and that of the combined intermediate-

metallicity clusters M5, M13 and NGC6752. On the other hand, Richer et al (1991) have used Cousins' I-band LFs to construct deep mass functions for 6 clusters and find no correlation between the mass spectrum power-law and metallicity. At present, this probably says more about the models used to convert between luminosity and mass than about the data or the intrinsic relationship.

Since the fainter main-sequence stars are very red observations at K are more efficient than at V at sampling a cluster's faint luminosity function.

8 Concluding remarks

At the start of this chapter, it was shown that the reddening results from most previous studies of M4 are consistent with a value of R of 4.0 $\pm$ 0.2 and a reddening of E(B-V)=0.37 $\pm$ 0.01. Although the value of R is important at optical wavelengths, it is only studies with large wavelength coverage that allow the value to be constrained. Important evidence for the larger value of R comes from several works:

1. Caputo (1987) conducted a 'self-consistent' examination of the properties of the RR Lyrae variables in the cluster. The different results for the distance modulus of the cluster, using either (B-V) or (V-K) to determine the temperatures of the variables, can be made to agree with each other and with the adopted values by choosing R=4.

2. FCP83 proposed an increase in reddening and a shift in their measured GB position to allow their M4 observations to fit their expectations in several observational diagrams. Simply, using R=4 and E(B-V)=0.37 does equally well, whilst still agreeing with the majority of other reddening determinations.

3. Similarly, PRMV86 invoked a reddening increase to explain why M4 did not fit their models. Setting R to 4 allows the more normal reddening to be used.

4. The revised $(V\text{-}K)_{o,GB}$, found by re-examining FCP83's observations in the light of the preferred form of the reddening law, allows M4 to agree better with correlations of this parameter with metallicity in the studies of Smith (1984) and Gratton, Quarta and Ortolani (1986), as well as in the present comparison with the Zinn

metallicities from Bell (1987).

In addition, some mistakes in previous work were revealed and the anomalous reddening estimate of AL84 was re-interpreted and the data found to be consistent with the presently adopted value.

Although it is hard to work through the effects of the revised reddening parameters on the various estimates of metallicity in the literature, those estimates which were examined, mainly based on combined optical and infra-red observations, were found to be consistent and to suggest that a value of [Fe/H]=-1.1 $\pm$ 0.25 might be appropriate. A similar mean, although with larger scatter, is found by taking all the metallicity estimates as given in the literature.

Applying the revised reddening parameters to previous determinations of the distance modulus of M4 clearly improves the overall agreement of the results, with a best estimate of 11.22 $\pm$ 0.11.

Although the age estimates from the literature cover a large range, a mean of 16 $\pm$ 2 Gyr was found. Fitting the ALA88 main-sequence fiducial with the new SC91 isochrones produced a best-fit age of 18 $\pm$ 1.5 Gyr at a reddening and distance modulus consistent with the adopted values.

Unfortunately, optical studies in the region of the present observations were not available or proved unsuitable, so that very few of the present data were used in the construction of CMDs and the 2CD. The RR Lyrae observations, based on LDSJF90 and further work by our group, fit well into the diagrams.

As in the last chapter, the present data were matched with the BBVB isochrones such that the reddening, distance modulus, age and metallicity were all left as free parameters. Although the results found for reddening, age and metallicity were consistent (within the errors) with the values found from the literature, the derived distance modulus was anomalous. If the possible zero-point error in the V magnitudes of AL84, mentioned in chapter 2, is included, the data are shown to fit the isochrones at the adopted reddening and distance modulus, with a derived age and metallicity consistent with the literature parameters. The AL84 zero-point uncertainty seriously compromises the usefulness of the data. Although the best-fit metallicity was well determined from the shape of the giant

branch observations, the derived age is very dependent on the main-sequence points. Thus the best that can be said is that the metallicity is found to be [Fe/H]=-1.0 ± 0.4, the age is t=16 ± 3 Gyr, and the giant-branch observations are consistent with the adopted reddening and distance modulus.

A comparison of the M4 CMD and (V-K)-(B-V) 2CD with those of M71 again suggested that a zero-point error in the AL84 magnitudes was spoiling an otherwise very satisfactory match. The match between the two-colour diagrams is in excellent agreement with the predictions of the BGVB models, based on the nominal metallicities of the two clusters.

Comparing the M4 data to these models in the two-colour diagram, the giant and horizontal branch stars agree well with the predictions of the models, although it again seems likely that the AL84 magnitudes contain a zero-point error.

Two-colour isochrones were constructed from the SC91 and BBVB colour-magnitude isochrones and were compared to the M4 data. These isochrones are rather uncertain because of the [O/Fe] enhancement difference between their progenitors and because of the possible scale errors in the reddest (B-V) colours, but are none-the-less of interest and certainly worthy of further work.

Throughout these comparisons it is evident that R=4 works very well for M4, certainly better than R=3. Where there are problems in comparing the M4 data with models this cannot be resolved by reverting to the standard value of R or changing the reddening.

The K-magnitude luminosity function for the large area mosaic image was converted into a V-magnitude LF, through an appropriate (V-K)-K isochrone, and found to compare very favourably with previous observations. Model LFs fit the data surprisingly well and suggest that the mass function power-law index is close to -1, consistent with McClure et al's (1987) assertion that the luminosity function is steeper for more metal-poor clusters.

The revision of the literature parameters has produced the most consistent set of parameters available for M4 and the present data have confirmed these values. However, a zero-point problem has meant that the parameters derived from the present data are rather uncertain. None-the-less the deepest globular cluster K-magnitude luminosity function yet published has been considered and the concept of two-colour isochrones has been introduced. There is much here to build on, for globular cluster studies in general and for M4 in particular when a deep optical study can be matched star-to-star with the K data.

References

Aaronson, M, Cohen, JG, Mould, J & Malkan, M, 1978. Ap.J., **223**, 824.

Alcaino, G, 1975. A.&A.Suppl., **21**, 5.

Alcaino, G & Liller, W, 1984. Ap.J.Suppl., **56**, 19 (AL84).

Alcaino, G, Liller, W & Alvarado, F, 1988. Ap.J., **330**, 569 (ALA88).

Bell, RA, 1987. In *'The Harlow-Shapley Symposium on Globular Cluster Systems in the Galaxy'*, eds. Grindlay, JE & Philip, AGD, p.79. Reidel (Dordrecht).

Bell, RA, 1992. Submitted to M.N.R.A.S.

Bergbusch, PA & VandenBerg, DA, 1991. In press.

Blanco, V, 1982. P.A.S.P., **94**, 201.

de Bruijn, J & Lub, J, 1987. In *'Stellar Pulsation'*, eds Cox, AN, Sparks, WM & Starrfield, SG, (Lecture Notes in Physics No.274), p.233. Springer-Verlag (Berlin).

Buckley, DRV, Longmore, AJ & Dixon, RI, 1991. Paper presented at the *'New Results on Standard Candles'* workshop, Trani, Italy 1991. To appear in Mem. Soc. Astron. Ital.

Buonanno, R, 1986. *Mem. Soc. astr. Ital.*, **57**, 333.

Buonanno, R, Corsi, CE & Fusi Pecci, F, 1989. A.&A., **216**, 80.

Burstein, D & McDonald, LH, 1975. A.J., **80**, 17.

Cacciari, C., 1979. A.J., **84**, 1542.

Caputo, F, 1987. A.&A., **172**, 67.

Caputo, F., Castellani, V., Di Gregorio, R. & Tornambé, A., 1984. A.&A.Suppl., **55**, 463.

Caputo, F, Martinez Roger, C & Paez, E, 1987. A.&A., **183**, 228.

Cardelli, J.A., Clayton, G.C. & Mathis, J.S., 1989. Ap.J., **345**, 245 (CCM89).

Cayrel, R, Cayrel de Strobel, G & Campbell, B, 1985. A.&A., **146**, 249.

Christian, CA & Racine, R, 1983. P.A.S.P., **95**, 457.

Clayton, GC & Cardelli, JA, 1988. A.J., **96**, 695.

Clementini, G, 1987. P.A.S.P., **99**, 637.

Cohen, JG, Frogel, JA & Persson, SE, 1978. Ap.J., **222**, 165.

Cudworth, KM & Rees, R, 1990. A.J., **99**, 1491 (CR90).

Eggen, OJ, 1972. Ap.J., **172**, 639.

Fernley, JA, 1989. M.N.R.A.S., **239**, 905.

Frogel, JA, Cohen, JG & Persson, SE, 1983. Ap.J., **275**, 773 (FCP83).

Frogel, JA, Persson, SE & Cohen, JG, 1979. Ap.J., **227**, 499.

Frogel, JA, Persson, SE & Cohen, JG, 1983. Ap.J.Suppl., **53**, 713 (FPC83).

Gratton, RG, Quarta, ML & Ortolani, S, 1986. A.&A., **169**, 208.

Greenstein, JL, 1939. Ap.J., **90**, 387.

Harris, WE & Van den Bergh, S, 1974. A.J., **79**, 31.

Herbst, W, Miller, DP, Warner, JW & Herzog, A, 1982. A.J., **87**, 98.

Iben Jr., I, 1967. Ap.J., **147**, 624.

Johnson, HL, 1966. Ann. Rev. Astron Astrophys, **4**, 143.

Kadla, ZI, Grashchenko, AN & Firmanyuk, BN, 1989. Sov. Astron. Lett., **15**, 57.

Kron, GE & Guetter, HH, 1976, A.J., **81**, 817.

Kron, GE & Mayall, NU, 1960. A.J., **65**, 581.

Kukarkin, BV, 1974. *'The Globular Cluster Stars'*, Acad. Sci. USSR (Moscow).

Kurucz, RL, 1979. Ap.J.Suppl., **40**, 1.

Lee, S-W, 1977. A.&A.Suppl., **27**, 367.

Liu, T & Janes, KA, 1990. Ap.J., **360**, 561 (LJ90).

Lloyd-Evans, T, 1977. M.N.R.A.S., **178**, 353.

Longmore, AJ, Dixon, RI, Skillen, I, Jameson, RF & Fernley, JA, 1990. M.N.R.A.S., **247**, 684 (LDSJF90).

Lub, J, 1986. In *'Stellar Pulsation: a Memorial to John P. Cox.'*, eds Cox, AN, Sparks, WM & Starrfield, SG, p.218. Springer (Berlin).

McClure, RD, Stetson, PB, Hesser, JE, Smith, GH, Harris, WE & VandenBerg, DA, 1987. In: *'The Harlow-Shapley Symposium on Globular Cluster Systems in the Galaxy'*, eds. Grindlay, JE & Philip, AGD, p.485. Reidel (Dordrecht).

McClure, RD, VandenBerg, DA, Smith, GH, Fahlman, GG, Richer, HB, Hesser, JE, Harris, WE, Stetson, PB & Bell, RA, 1986. Ap.J., **307**, L49.

Martin, PG & Whittet, DCB, 1990. Ap.J., **357**, 113 (MW90).

Mironov, AV & Samus, NN, 1974. Perem. Zvezdy, **19**, 337.

Moshkalev, VG, 1975a. Astronomicheskii Zhurnal An SSSR, **52**, 815.

Moshkalev, VG, 1975b. Sov Astron J, **19**, 495.

Mould, J, Stutman, D & McElroy, D, 1979. Ap.J., **228**, 423.

Newell, EB, 1970. Ap.J., **161**, 789.

Norton, AP, 1978. *'Norton's Star Atlas'*, ed. Satterthwaite, GE. Gall & Inglis (Edinburgh).

Penny, AJ, Lubenow, A & Dickens, RJ, 1987. In *'Stellar Evolution and Dynamics in the Outer Halo of the Galaxy.'*, eds. Azzopardi, M & Matteucci, F., ESO Conf. Workshop Proceedings, **27**, p.401. ESO (Garching bei München).

Peterson, CJ, 1986. P.A.S.P., **89**, 1258.

Philip, AGD, 1971. Bull Am. Ast. Soc., **3**, 8.

Phillips, JP, Martinez Roger, C, Sanchez Magro, C & Lazaro Vilchez, C, 1986. A.&A., **161**, 257 (PRMV86).

Racine, R, 1973. A.J., **78**, 180.

Richer, HB & Fahlman, GG, 1984. Ap.J., **277**, 227 (RF84).

Rood, RT & Crocker, DA, 1988. In *'The Harlow-Shapley Symposium on Globular Cluster Systems in the Galaxy'*, eds. Grindlay, JE & Philip, AGD, p.507. Reidel (Dordrecht).

Sandage, A, 1969. Ap.J., **158**, 1115.

Sandage, A, 1981. Ap.J., **248**, 161.

Sandage, A, 1990. Ap.J., **350**, 603.

Sandage, A & Cacciari, C, 1990. Ap.J., **350**, 645.

Sandage, A & Katem, B, 1982. A.J., **87**, 537.

Sarajedini, A & King, CR, 1989. A.J., **98**, 1624.

Smith, HA, 1984. Ap.J., **281**, 148.

Straniero, O & Chieffi, A, 1991. Ap.J.Suppl., **76**, 525 (SC91).

Sturch, C, 1966. Ap.J., **143**, 774.

Sturch, CR, 1977. P.A.S.P., **89**, 349.

van Albada, T.S. & Baker, N., 1971. Ap.J., **169**, 311.

VandenBerg, DA, 1983. Ap.J.Suppl., **51**, 29 (VB83).

VandenBerg, DA, 1985a. In *'ESO Workshop on the Production and Distribution of CNO Elements'*, eds. Danziger, IJ, Matteucci, F & Kjär, K, p.73. ESO (Garching bei München).

VandenBerg, DA, 1985b. Ap.J.Suppl., **58**, 711.

VandenBerg, D.A. & Bell, R.A., 1985. Ap.J.Suppl., **58**, 561 (VBB85).

Whittet, DCB & van Breda, IG, 1978. A.&A., **66**, 57.

Whittet, DCB & van Breda, IG, 1980. M.N.R.A.S., **192**, 467.

Zinn, R, 1980. Ap.J.Suppl., **42**, 19.

Concluding Remarks

What has been found ? Have the aims stated in the Introduction been achieved ? What next ?

This thesis did not set out to solve all the important problems that remain in globular cluster astronomy. Rather I have shown that near-IR array photometry has a valuable contribution to make to our understanding of the globular cluster system on a cluster-by-cluster basis. Observations at near-IR wavelengths have advantages over similar optical observations, particularly with regard to extinction and the stellar temperature scale, and it is clear that optical-IR CMDs are at least as good as traditional optical studies for assessing individual clusters and adding to the collection of reddenings, ages, and metallicities that are so vital to the study of the fundamental questions, such as the second parameter problem and the age range of the globular cluster system.

1 Summary of chapters

To begin with, here is a round-up of what happened in the last four chapters.

1.1 Chapter 1: photometry with IRCAM

The results of imaging observations of bright and faint standards in the J- and K-bands were presented. It was shown that IRCAM is certainly capable of photometry to better than the 1% level when appropriate flat-field frames are used. Linearity corrections were successful and any residual non-linearity is small over a large range of magnitude (<2% in the range $6^{m}.5$-$13^{m}.0$). Zero-point stability of the camera/telescope/atmosphere system was also found to be good.

1.2 Chapter 2: reduction and analysis

The present observations and observing philosophy were discussed. The reduction procedure for long exposure image frames, from raw frames to final mosaics, was discussed in detail. In particular, a mosaicing procedure involving fractional pixel shifts was investigated and found to improve, or at worst not change, the final measurements of stars. The use of DAOPHOT to analyse such frames was examined, and tests showed that the results were repeatable. Contamination corrections were established from artificial star experiments. Software to facilitate the reduction of this type of data was described (see also appendix B).

The zero-point calibration of the observations in both clusters was discussed. In M71 the K-magnitudes were calibrated from previous photometry by Frogel, Persson and Cohen (1979), specially-taken single-channel observations by ourselves and the IRCAM instrumental zero-points derived from the observations of standards discussed in chapter 1. For M4 specially taken single channel photometry of two stars and the chapter 1 results provided calibration. The K-photometry in both clusters is believed to be within 2% of the standard Johnson system.

The relative zero-points of different optical studies, were found to disagree, in the regions of interest, so they were put onto a common system.

1.3 Chapter 3: M71

Chapter 3 presented the observations of M71. A re-assessment of previous studies found the best set of self-consistent cluster parameters.

Newly calculated (V-K)-V and (V-K)-K isochrones were fitted to the data such that metallicity, age, distance modulus and reddening were all left as free parameters. The resulting best-fit estimates for these parameters were: -0.78 $\pm$ 0.3, 13 $\pm$ 1 Gyr (including oxygen enhancement), 12.85 $\pm$ 0.15 and 0.26 $\pm$ 0.03. These agree very well with the adopted values and are a more consistent and accurate set of parameters than has previously been derived from any single study of this cluster. Combining these with the parameters from the literature produces the finally adopted parameters: -0.7 $\pm$ 0.4, 14.5 $\pm$ 2 Gyr, 12.87 $\pm$ 0.07 and 0.266 $\pm$ 0.015.

A new scheme was proposed by which the CMDs of two clusters can be matched together in a 'self-consistent' manner, using models to relate the displacements of various morphological features to metallicity and age. In the present case, the solution is dominated by observational and theoretical uncertainties, but this is still, potentially, the way to maximize the use of the available information between two CMDs. (This scheme could equally well be applied to purely optical CMDs or to any combination of different CMDs).

A giant branch clump was discovered in the (V-K) CMDs. Fusi Pecci et al's (1990) $\Delta M_V^{HB-clump}$ parameter was used to derive a metallicity of -0.78. A second differential parameter, ΔV_{f-c}, being the V-magnitude difference between the GB clump and the mid-point of the sub-giant branch, was defined and calibrated against models as a function of metallicity and age, confirming that the models predict the clump to be brighter than it is actually observed to be.

Two-colour models in (B-V) and (V-K) were constructed from various models in the literature. Comparison between observations and theory in the (V-K)-(B-V) two-colour diagram showed an excellent agreement between expected and predicted stellar gravities. In particular, the available spectroscopic estimates of log g were found to agree well with the [Fe/H]=-0.5 models.

The model K fluxes, used in both the CMD isochrones and the 2CD, were made $0^m.12$ fainter, as recommended by Bell (1992). The present (independent) results confirm that this shift is appropriate, at least to first order.

1.4 Chapter 4: M4

A re-appraisal of all previous studies of M4 leads to the conclusion that R=4.0 $\pm$ 0.2. Using this value makes the metallicity, age, distance modulus and reddening more consistent between studies, and leads to the (revised) adopted parameters: [Fe/H]=-1.1 $\pm$ 0.25, age=16 $\pm$ 2 Gyr, $(m-M)_o$=11.22 $\pm$ 0.11 and E(B-V)=0.37 $\pm$ 0.01.

Unfortunately the Alcaino and Liller (1984, AL84) V-photometry that was used to produce (V-K) from the present observations, was suspected of containing a zero-point error. From comparison with other studies a correction was approximated by simply making V 18% fainter. It was not possible to further quantify the error but, since the V-magnitudes

come from Pickering-Racine wedge observations, it could be magnitude and/or colour dependent. Use of these data in the CMDs and 2CD confirmed that a zero-point error existed and suggested that the correction necessary might be closer to $0^m.23$, if a simple correction was appropriate. The main-sequence points are thus unreliable, although the conclusions drawn from the giant and HB stars are unaffected.

The suspect zero-point meant that a four free-parameter fit of the isochrones, like that for M71, could not be made, and the reddening and distance modulus were fixed at the adopted values, to derive a best-fit metallicity and age of -1.0 $\pm$ 0.4 and 16 $\pm$ 3 Gyr. These are in excellent agreement with the adopted values. The large uncertainty in the age determination reflects the zero-point difficulties.

The two-colour models predict exactly the offset that is seen between the dereddened M71 and M4 2CDs. The M4 data are well fitted by the [Fe/H]=-1 models, but unfortunately there are no spectroscopically determined gravities to compare with the model predictions.

Two-colour isochrones - a new concept - were constructed from normal CMD isochrones. Their use is limited, in this case, because the parent isochrones contain rather different physics, and, in particular, one set contains oxygen enhancement and the other does not. Also, the (B-V) colours for the reddest giants are uncertain. Thus the comparison with the data was inconclusive, but it is clear that 2C isochrones contain features that will be useful as age-independent metallicity and combined age and metallicity indicators, once a better set can be constructed (for instance, as soon as the Bergbusch & VandenBerg (1992) (B-V)-V isochrones become available, they can be matched with the BBVB (V-K)-K set, which they helped to generate).

The K-magnitude luminosity function was examined briefly. A comparison, through an appropriate isochrone, with models and previous observations of the V-magnitude LF shows close agreement, with a mass-spectrum power-law index of -1 (x=0.0) - consistent with the metallicity of M4 if McClure et al's (1987) power-law index - metallicity correlation is correct. This correlation is rather controversial and is discussed further in section 3.4 of this chapter.

Once again the Bell (1992) 12% shift in the model K magnitudes has been successful in the isochrones, the two-colour models, the two-colour isochrones and in the luminosity function colour transformation.

2 Have the aims stated in the Introduction been fulfilled ?

To show that IR arrays are capable of reliable and accurate photometry, and that images from such arrays can be analysed with profile fitting software, such as DAOPHOT.

Both of these have certainly been achieved.

To derive estimates for the physical parameters of reddening, distance modulus, metallicity and age for M4 and M71.

The isochrone fitting in both clusters has produced values of the cluster parameters in excellent agreement with the adopted values. The normally adopted method of fitting isochrones is to place the cluster data at the predicted absolute, dereddened colour and magnitude, and overlay the metallicity families of isochrones to find the best-matching age. For the M71 fit the data were sufficiently good to allow the isochrones to be fitted freely to the upper MS, TO and SGB. Thus the curve with the shape closest to that of the data was selected as best fit. The excellent agreement of the derived reddening and distance modulus with the adopted values, shows clearly the success of this approach and the accuracy of the models. The present agreement could not really be better, considering the discrepancies found between different optical CCD studies of a single cluster (see, for example, VandenBerg and Bell, 1985; Buonanno, Corsi and Fusi Pecci, 1989; Straniero and Chieffi, 1991).

To look for main-sequence binaries.

No significant number of binary candidates were found in the CMD of M71. M4 could not be searched because no colour information was available for the main-sequence stars. Potentially, examining the colour residuals from a main-sequence fiducial is a good way to find parallel sequences of binaries. Such binaries should be apparent in the IR because the main sequence has a gradient of about 4 in the (V-K)-V CMD, whereas in the optical the sequence is much more nearly vertical, so that any vertical shift translates into only a small colour shift away from the mean of the data.

To show that (V-K) CMDs are less affected by photometric scatter than (B-V).

This is obvious in the comparisons between the optical and optical-IR CMDs for the two clusters.

2.1 Additionally ...

Part of the motivation for exploring the new field of optical-IR CMDs and 2CDs was to look for unexpected effects. One such serendipitous discovery was the position of the three M71 blue straggler candidates in the two-colour diagram, showing them to be consistent with being field dwarfs.

3 Observational and astrophysical implications

3.1 Optical-IR studies

Clearly, if all other things were equal - that is, if IR astronomy were easy, arrays large and efficient and the (V-K) isochrones and models well developed - every-one should be observing clusters in V and K, because:

- photometric scatter in (V-K) translates into smaller scatter in T than for optical colours;
- (V-K) is likely to be more closely related to temperature than (B-V) and less metallicity sensitive;
- K-magnitude luminosity functions can sample the cluster mass function far more easily than observations at B, V or even I;
- reddening errors are 10x less important at K than at V (although they are 3x more important in (V-K) than (B-V) this is made up for by the 2-3x expansion in the colour axis in the move from (B-V) to (V-K));
- for clusters where R may be anomalous the long colour baseline confers good diagnostic powers.

Even though IR array photometry has yet to achieve the ease and convenience of similar work with CCDs, the rate of improvement of technology in the IR is swift and observing and reduction techniques can be automated to a large degree. There is certainly a large contribution to be made to the field of globular cluster research by optical-IR studies.

3.2 Photometry is difficult

One of the conclusions that can be drawn from the previous chapters is that photometry is difficult ! Even a very careful calibration cannot eliminate zero-point error, and this thesis contains numerous examples were errors are unreasonably large. Hesser et al (1987) state that the zero-points for their 47 Tuc BV observations are uncertain, in that the (B-V) colours may be 2% too blue. However, Straniero and Chieffi (1991) found a colour zero-point discrepancy of 4% between Hesser et al and another study. Cudworth (1985) found Arp and Hartwick's (1971) photometry to be out by 5% in both B and V. In M4, I find Lloyd-Evans' (1977) B and V magnitudes to be 7% different from those of Cudworth and Rees (1990), and of course, the worst of all, despite their careful discussion of the pitfalls of using the Pickering-Racine wedge, AL84's V magnitudes have turned out to be in error by perhaps 20% ! All of these discrepancies are larger than the various authors' estimates of how closely they were tied to the Johnson system.

Clearly, the lesson to be learnt is not to trust any-one else's photometry !

3.3 Luminosity functions

Although we did not start out intending to construct main-sequence luminosity functions for these two clusters, observations in the IR are very good for sampling LFs because (a) the stars are red and (b) the main sequence is quite flat in the (V-K)-V CMD so that, unlike in the V-band, a great many stars are packed into only a few magnitudes (that is, the stars are red and get redder). Also the V magnitude becomes a poor estimator of total luminosity for cool stars, since the peak of the energy distribution is to the red of the V filter and the bolometric correction is large (see figure 2 of the Introduction). On the other hand, the K filter provides a uniform measurement of energy output, sampling the tail to the red of the peak for objects hotter than ~1500K. The peak of the energy distribution of stars of T_{eff}~3500K is in the I band, so K is still better for looking for the

coolest stars.

Clearly it makes sense to observe in the near-IR to study the lowest mass stars, since they are also the reddest stars.

3.4 Mass functions

The observed present-day mass function, which is derived from the observed LF and an appropriate mass-luminosity relation, is not necessarily very closely related to the initial mass function of the cluster because of the effects of dynamical evolution (Lee, Fahlman and Richer, 1991) and of Galactic disc-passages (Chernoff and Shapiro, 1987). Also the derived mass function applies only to the stars at the radius of observation - if the relaxation time is short enough that significant mass segregation has taken place the global mass function must be estimated from the observed mass function and model calculations (as in Capaccioli, Ortolani and Piotto (1991, COP91).

The present result for the mass function power-law gradient for M4 (x=0.0) adds a little to the recent discussion of whether the present-day mass function of a cluster is dependant on its metallicity, as show by McClure et al (1987). Although Richer et al (1991) find there to be no such correlation in their data, Piotto (1991) and Ferraro and Piotto (1992) find very flat mass functions for the metal-rich clusters M4 and M107, respectively. COP91 suggest that the metal-rich clusters may have rather flat main-sequence mass functions, while those for intermediate and metal-poor clusters are not correlated with metallicity. It is interesting to note that if the M4 point in COP91's [Fe/H]-x correlation is moved from where it is plotted ([Fe/H]=-1.28, x=-0.7) to the values found here ([Fe/H]=-1.1, x=0.0), there are only two clusters (M12 and NGC6397) that do not agree with a correlation with a gradient of ~1, albeit with large scatter (particularly at the metal-poor end). McClure et al's (1987) gradient for the same relation was ~2.5. The revised M4 point still fits in with COP91's correlation between distance from the Galactic plane, Z, and x.

COP91 suggest that the Z-x correlation may be caused by the tidal stripping of low mass stars, and hence the flattening of the present mass function, during the passage of a cluster through the Galactic plane. However, they also point out that a correlation of any intrinsic parameter with the present distance of a cluster from the plane is suspicious, since that distance changes, at least for the halo clusters, quite rapidly. On this point,

the metallicity of the clusters in the COP91 sample is also reasonably well correlated with their distance from the plane (something they do not mention), so it is not possible to dis-entangle the effects of Galactic position *and* metallicity on the cluster mass functions.

Since there are a number of completing processes acting on the stellar population of a cluster, it is to be expected that the [Fe/H]-x diagram will show large scatter. Also some clusters simply will not fit because one of the normally-less-important processes has had a large effect on a particular cluster. For instance, it may be that M12 and NGC6397, which have flatter mass functions than predicted by the tentative [Fe/H]-x relation, may have ended up closer to the Galactic plane than most clusters of similarly low metallicity, with the result that tidal stripping has flattened their mass functions.

It is likely that the current differences between studies are partly due to their use of different mass-luminosity functions, which are very sensitive to the input physics for the lowest mass stars, to generate the mass functions and partly due to the small sample sizes, the intrinsic scatter of which obscure any relationship that exists.

It could be that the position at which a cluster formed in the Galaxy determines its metallicity directly and its present mass function slope indirectly, through the action of the Galactic potential and disc-passages. In this way a [Fe/H]-x relationship would be seen where there is in fact little or no causal connection between the two.

Another use of deep luminosity and mass functions is to look for the change in slope of the lower main sequence that should occur at $<\sim 0.5\,\mathcal{M}_{\odot}$ when the effects of H_2 molecules become important in the stellar atmospheres (see Renzini and Fusi Pecci, 1988).

3.5 The SPSE and the age of the globular cluster system

Since M71 is too metal-rich to contain any RR Lyraes it cannot be directly assessed for the Sandage Period Shift Effect. However the derived values of M_V(HB) and [Fe/H] can be compared with the various forms of the relation between the two quantities to be found in the literature.

The ages derived for the two clusters, 14.5 ± 2 Gyr for M71 and 16 ± 2 Gyr for M4, are not significantly different from Sandage and Cacciari's (1990) oxygen-enhanced result of 15.5 Gyr for all the clusters. However, since both clusters are metal-rich these ages

are also consistent with the Carney, Storm and Jones (1992, CSJ92) scenario of a simple oxygen-enhancement of 0.3 and a range of ages among the clusters of 15-20 Gyr.

Age determinations are one of the most significant astrophysical parameters to come from globular clusters. The ages of the clusters constrain the age of the Universe and hence the Hubble time, and the age range of the clusters constrains the speed at which the Galaxy formed.

At present there is a discrepancy between the ages of the globular clusters, as the oldest objects in the Galaxy, and the ages derived from nucleocosmochemistry - the use of the production and decay of radioactive nuclei to determine the duration of nucleosynthesis in the Galaxy before the formation of the Solar System, from the presently observed isotopic abundances. For instance, Fowler (1987) finds the age of the Universe to be 11.0 $\pm$ 1.6 Gyr from thorium and uranium isotopes, whilst Sandage and Cacciari (1990) find 15.5 Gyr for all of the Galactic globular clusters (including oxygen enhancement). Since the globular clusters probably did not form until at least 1 Gyr after the Big Bang (Fowler, 1987, for example) the discrepancy between the two ages is even worse. Also, Winget et al (1987) find the age of the Galaxy to be 9.3 $\pm$ 2 Gyr from the observed numbers of white dwarfs and models of their cooling rate. Many mechanisms have been proposed to produce younger ages for the globular clusters: rotation was mentioned in the Introduction, Willson, Bowen and Struck-Marcell (1987) proposed heavy main-sequence mass loss in the early stages of a star's life to reduce stellar ages to a maximum of $\sim$10 Gyr, and Noerdlinger and Arigo (1980) and Stringfellow et al (1983) constructed stellar models allowing ionic diffusion with the result that ages derived from present isochrones could be more than 20% too long. Although the tightness of the observed MSTOs of many clusters cast doubts on processes that rely on rotation or magnetic fields, where significant star-to-star variations might be expected (Renzini and Fusi Pecci, 1988), and ionic diffusion might be ruled out because it predicts an increase in the number of solar neutrinos where there is already a dearth, it is quite plausible that some form of one of these effects, or a combination of them, or even another as yet unidentified mechanism, does indeed reduce stellar ages from the high values presently favoured.

On the other hand, (if Ω=0) there are other results which support the longer timescale suggested by the globular cluster studies. For instance, Wheeler and Harkness (1986) find a Hubble time of 16.8 $\pm$ 1.4 Gyr (error estimate from Fowler, 1987) from studies of ^{56}Ni

in extragalactic supernovae. If Ω=1 this becomes 11 Gyr.

The problem seems intractable. At present the weight of evidence points to an error in the stellar evolutionary models that are used to construct isochrones. Very accurate CMD and LF studies are crucial to the detailed testing of models to confirm or deny the various mechanisms proposed to reduce the cluster ages.

3.6 The formation of the Galaxy

The Eggen, Lynden-Bell and Sandage (1962) model of the formation of the Galaxy and its revision by Searle and Zinn (1978) are still controversial (see Sandage, 1986). The most important factor in approving or disproving this model is the age range (or lack of it) amongst the globular clusters, which is still uncertain. Clearly the question of oxygen-enhancement must be addressed, since the currently proposed age range among the clusters depends crucially upon the correlation, or lack of it, of oxygen enhancement with metallicity. One complication is that the metal-rich clusters, being members of the thick disc subsystem, are generally more heavily obscured than the metal-poor clusters (47 Tuc is the only bright, metal-rich cluster to suffer very little extinction). Also the metal-rich end of the metallicity scale is the most controversial (see Bell, 1987). Both of these effects conspire to make the parameters for these clusters systematically less well determined than those for the more metal-poor ones. As has been shown, the use of IR magnitudes in CMD studies reduces the effect of reddening errors on the derived parameters and allows departures from the normal value of R to be detected.

3.7 Sub-dwarf fitting

The present data in M71 were not deep enough to match with the infamous sub-dwarf parallax stars, and there were no V magnitudes available to use with the faint M4 data. However, fitting sub-dwarf sequences in the optical-IR CMD is clearly a sensible thing to do, not just because of the reduced importance of reddening errors, but because of the reduced sensitivity of both (V-K)and K to metallicity in comparison with (B-V) and V. The sub-dwarfs are all of intermediate metallicity, averaging [Fe/H]=-1.4, so that model-derived corrections must be made if they are to be compared to cluster main-sequences of significantly different metal content. In the optical-IR CMD these corrections are

minimised (see Buckley and Longmore, 1992).

3.8 The optical-IR CMDs

The (V-K)-V CMD is morphologically very similar to the (B-V)-V CMD, albeit with an expanded colour scale.

Because (V-K) is more closely related to stellar temperature than is (B-V) (and less affected by metallicity), the (V-K)-V CMD is closer to the T-L plane of the theoretical HR diagram. All other factors being equal, this would mean that errors introduced by the colour-temperature and magnitude-bolometric correction relations, derived from model atmospheres, would be of less importance. Thus, with reduced sensitivity to systematic errors, the (V-K)-V CMD is a better diagram in which to fit isochrones than the (B-V)-V CMD. This is doubly the case when the smaller effects of reddening errors on the derived parameters are considered. In particular, the de-reddening of the distance modulus derived from fitting isochrones or sub-dwarfs in the (V-K)-K CMD depends on $\sim$0.1E(V-K), whereas in the (B-V)-V CMD it depends on $\sim$3E(B-V). Thus any error in the derived reddening has far less effect on the cluster distance found.

3.9 Two-colour diagrams

Two-colour diagrams are clearly useful because by assuming only the reddening (and the form of the reddening law) cluster data may be compared to other clusters or to the results of model calculations. The 2CD can be used to separate field and cluster populations because of both their differing reddenings and metallicities. Both M4 and M71 are close to the metallicity of the population I field stars, but for more metal-poor clusters this metallicity-induced separation will be more marked.

Another important use of the 2CD is to estimate physical parameters for the stars by overlaying a set of models of different gravity and appropriate metallicity. Thus the gravity of each star can be estimated and combined with a temperature derived from the (V-K) colour and the luminosity from the K-magnitude to calculate the stellar mass. This may prove important in testing whether the run of stellar masses near the turn-off agree with the predictions of standard isochrones, or with those that allow ionic diffusion. It

was seen in chapter 3 that the presently available models adequately predict gravities that are consistent with those derived from high-resolution spectral observations (although it must be remembered that these are also model dependent, so that a certain amount of circularity is involved).

Another approach is to use the (V-K) colour to estimate the effective temperature and the K magnitude to estimate the luminosity to calculate the stellar radius, which can be compared to model calculations. Again a certain amount of circularity is involved, since the necessary colour-temperature and BC-colour-magnitude relations are derived from models, with observational calibrations. The stellar models can thus be made to produce self-consistent physical parameters, constrained by observations.

3.10 Mixing-length theory

Since there is no adequate analytical treatment of convection, the mixing-length theory has to be employed when building stellar models (see, for example, Renzini and Fusi Pecci, 1988). While this approximation has been remarkably successful, there is still some controversy over its fundamental input parameter α, the ratio of the mixing length to the pressure scale height, and whether α is constant for all stars or a function of size, density, luminosity, temperature, metallicity, etc.

Because convection is important in the envelopes of MS and lower GB stars it is the values of radii and temperatures of these stars that must be used to test the results of the mixing-length theory. The current value of $\alpha \sim 1.6$ comes from solar models, MS models of young open clusters, sub-dwarfs with trigonometric parallaxes, binary star studies and detailed globular cluster CMD modelling (again, see Renzini and Fusi Pecci, 1988). In the present context the most important calibration of α comes from modelling the structure of the RGB and the T-[Fe/H] relation for RGB stars, with the temperature being determined from (V-K). Although there is generally good agreement, and α again comes out as ~ 1.6 there is so far a discrepancy between the models and observations for the temperature of stars at the tip of the giant branch (VandenBerg, 1984).

3.11 Interesting objects

The three blue straggler candidates in M71 have, unfortunately, been shown to be most likely to be field stars. White dwarfs and cataclysmic variables (CVs) are too blue and too faint to be found in the present study and, as intrinsically blue objects, it does not make sense to seek them in the infra-red. No cluster photometry yet goes deep enough to detect brown dwarfs.

3.12 The $(V\text{-}K)_{o,GB}$ metallicity indicator

It is well known that the giant branch becomes bluer for lower metallicity clusters. The Frogel, Cohen and Persson (1983) $(V\text{-}K)_{o,GB}$ metallicity parameter quantifies this change. For M4 the revised value of R and distance modulus changed this parameter by $\sim 0^{m}.3$, with a change of $\sim 0^{m}.2$ in M71. Figure 1 shows the relation between $(V\text{-}K)_{o,GB}$ and [Fe/H]

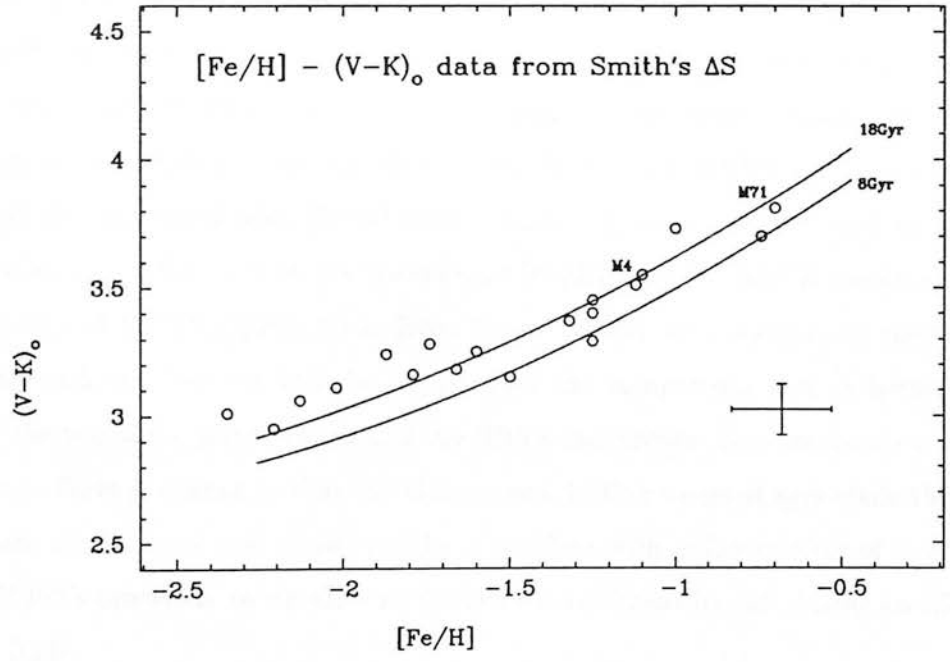

Figure 1: The relation between metallicity and $(V\text{-}K)_{o,GB}$. The points for M71 and M4 use the values adopted in this thesis. The curves are those derived from the BBVB isochrones (see section 2.1.5 of chapter 4 for further discussion).

(coming from Smith's (1984) compilation of ΔS metallicities), with M71 and M4 placed

according to the metallicities adopted here. (Smith's metallicities have been shifted onto a comparable metallicity scale by making them all 0.17dex more metal rich. This comes from a comparison of the Butler (1975) scale (as used by Smith) and the more recent ΔS calibration by Walker and Terndrup (1991)). Clearly the M4 and M71 points lie almost exactly on the mean line. This will perhaps convince researchers that the [Fe/H]-$(V-K)_{o,GB}$ relation has been rather under-valued, due to uncertainties in cluster parameters rather than any failing of the intrinsic relationship between the colour of the upper giant branch and a cluster's metallicity. Interestingly the third most metal-rich cluster in the plot is M107, for which a revised value of R may be appropriate, since it lies near M4 in the sky (see Longmore et al, 1990).

The lines of equal age, derived from the BBVB isochrones and plotted in figure 1, imply an age-metallicity relation covering ~14-25 Gyr over the range of cluster metallicities. Although these absolute values are rather higher, implying a low value of ~40 (Ω=0) or ~25 km/s/Mpc (Ω=1) for the Hubble constant for instance, this could easily be due to a small error in the [Fe/H]-ΔS relationship, meaning that the derived cluster metallicities are not quite on the same scale as those of the isochrones. The range of ~10 Gyr disagrees with the predictions of CSJ92, who found no significant age range amongst the clusters if the oxygen enhancement were correlated with [Fe/H]. The BBVB isochrones already contain [O/Fe] correlated with [Fe/H] with a similar gradient to that used by CSJ92, but a smaller zero-point so that, for instance, at [Fe/H]=-1.5 the BBVB isochrones have [O/Fe]=0.60 and CSJ92 [O/Fe]=0.85. Even though CSJ92 were comparing the turn-off luminosity with the Revised Yale Isochrones and the comparison here is between the colour at the top of the giant branch and the BBVB isochrones, there is clearly a serious discrepancy. Since it cannot be that the GBs cover a 10 Gyr range of ages while the turn-off stars are all the same age, there must be a problem with either one set of isochrones or with CSJ92's procedure to simulate an oxygen enhancement by calculating an effective Z for the RYIs.

3.13 Et cetera

There are areas of astrophysics that have not been mentioned where an accurate knowledge of the distance modulus, reddening, ages and metallicities of the globular clusters can be useful. Two of the most significant concern Galactic structure and the extragalactic

distance scale.

The metal-rich clusters delineate the thick disc, the metal-poor ones the halo. Both are useful to study the structure, kinematics and chemical composition of these Galactic subsystems.

Globular clusters in other galaxies can be used as distance indicators, for which a knowledge of the integrated light properties of those in our Galaxy is essential.

4 Future prospects

The future of IR imaging is rosy: ever larger and more efficient arrays are arriving at telescopes, and the currently-planned generation of very large telescopes are being designed with the needs of IR astronomy in mind. Buckley and Longmore's (1992, in preparation) 47 Tuc observations are an example of data taken with the next generation of instruments, in this case the Anglo-Australian Observatory's 128x128 pixel IRIS array camera. Already some 256x256 HgCdTe arrays are in operation in the 1-2.5 μm region and 256x256 InSb arrays, capable of working upto 5 μm, should be available on large telescopes in 1992.

Now that (V-K)-V isochrones are available there are many opportunities for optical-IR studies to make significant contributions to our understanding of individual clusters and the globular cluster system in general. In particular, Djorgovski's (1987) IRAS sample of $\sim$200 highly obscured globular cluster candidates are prime targets for optical-IR or purely IR studies. These objects are particularly important because many of them are likely to be metal-rich and members of the thick-disc population.

A precedent has been set in the determination of R=4 for M4. Several bright clusters need to be re-examined for a higher value of R, particularly M107 which also lies near the ρ Oph cloud. Recent CCD photometry of the cluster exists by Ferraro and Piotto (1992), who find that either a reddening almost $0^{m}.1$ larger than the accepted value or a α-element enhancement is desirable for their isochrone fitting. Amongst other clusters worthy of study are NGC6144, which is only 1° from M4 on the sky, and M69, a metal-rich cluster lying in Sagittarius which Frogel, Cohen and Persson (1983) found to be discrepant in several plots (see also Smith, 1989).

The GB clump certainly deserves further study, since its location is determined by pro-

cesses deep within the stars, and connected with predicted surface abundance changes (Rood and Crocker, 1985). Current models do not predict its location correctly (Fusi Pecci et al, 1990), so thorough observations could constrain the next generation of stellar models.

Observations in the turn-off/sub-giant region are particularly useful for isochrone fitting studies. A program of observations aimed at just this region could provide age and metallicity information on a uniform scale for a large sample of clusters, without using too large an amount of telescope time.

References

Alcaino, G & Liller, W, 1984. Ap.J.Suppl., **56**, 19.

Arp, HC & Hartwick, FDA, 1971. Ap.J., **167**, 499 (AH71).

Bell, R.A., 1987. In: *'The Harlow-Shapley Symposium on Globular Cluster Systems in the Galaxy'*, p.79. Eds. Grindlay, JE & Davis Philip, AG. Kluwer Academic Publishers (Dordrecht).

Bell, R.A., 1992. Submitted to M.N.R.A.S.

Bergbusch, PA & VandenBerg, DA, 1992. (In press).

Buckley, DRV & Longmore, AJ, 1992. Submitted to M.N.R.A.S.

Buonanno, R, Corsi, CE & Fusi Pecci, F, 1989. A.&A., **216**, 80.

Butler, D, 1975. Ap.J., **200**, 68.

Capaccioli, M, Ortolani, S & Piotto, G, 1991. A.&A., **244**, 298.

Carney, BW, Storm, J & Jones, RV, 1992. Preprint. (CSJ92).

Chernoff, DF & Shapiro, SL, 1987. Ap.J., **322**, 113.

Cudworth, KM, 1985. A.J., **90**, 65.

Cudworth, KM & Rees, R, 1990. A.J., **99**, 1491.

Djorgovski, S, 1987. In *'The Harlow-Shapley Symposium on Globular Cluster Systems in the Galaxy'*, p.527. Eds. Grindlay, JE & Davis Philip, AG. Kluwer Academic Publishers (Dordrecht).

Eggen, OJ, Lynden-Bell, D & Sandage, A, 1962. Ap.J., **136**, 748.

Ferraro, FR & Piotto, G, 1992. M.N.R.A.S. (submitted).

Fowler, WA, 1987. Q.J.R.A.S., **28**, 87.

Frogel, JA, Cohen, JG & Persson, SE, 1983. Ap.J., **275**, 773.

Frogel, JA, Persson, SE & Cohen, JG, 1979. Ap.J., **227**, 499.

Frogel, JA, Persson, SE & Cohen, JG, 1983. Ap.J.Suppl., **53**, 713.

Fusi-Pecci, F, Ferraro, FR, Crocker, DA, Rood, RT & Buonanno, R, 1990. A.&A., **238**, 95.

Hesser, JE, Harris, WE, VandenBerg, DA, Allwright, JWB, Shott, P & Stetson, PB, 1987. P.A.S.P., **99**, 739.

Iben Jr., I & Renzini, A, 1984. Phys.Rep. **105**, 329.

Lee, HM, Fahlman, GG & Richer, HB, 1991. Ap.J., **366**, 455.

Lloyd-Evans, T, 1977. M.N.R.A.S., **178**, 353.

Longmore, AJ, Dixon, RI, Skillen, I, Jameson, RF & Fernley, JA, 1990.

M.N.R.A.S., **247**, 684.

McClure, RD, Stetson, PB, Hesser, WE, Smith, GH, Harris, JE & VandenBerg, DA, 1987. In: *'The Harlow-Shapley Symposium on Globular Cluster Systems in the Galaxy'*, p.485. Eds. Grindlay, JE & Davis Philip, AG. Kluwer Academic Publishers (Dordrecht).

Noerdlinger, PD & Arigo, RJ, 1980. Ap.J., **237**, L15.

Piotto, G, 1991. In: *'Formation and Evolution of Star Clusters'*. Ed. Janes, K. A.S.P. Conference Series.

Renzini, A & Fusi Pecci, F, 1988. Ann.Rev., **26**, 199.

Richer, HB, Fahlman, GG, Buonanno, R, Fusi Pecci, F, Searle, L & Thompson, IB, 1991. Ap.J., **381**, 147.

Rood, RT & Crocker, DA, 1985. In: *'ESO Workshop on the Production and Distribution of CNO Elements'*, p.61. Eds. Danziger, IJ, Matteucci, F & Kjär, K. ESO (Garching bei München).

Sandage, A, 1986. Ann.Rev., **24**, 421.

Sandage, A & Cacciari, C, 1990. Ap.J., **350**, 645.

Searle, L & Zinn, R, 1978. Ap.J., **225**, 357.

Smith, GH, 1989. P.A.S.P., **101**, 1083.

Smith, HA, 1984. Ap.J., **281**, 148.

Straniero, O & Chieffi, A, 1991. Ap.J.Suppl., **76**, 525.

Stringfellow, GS, Bodenheimer, P, Noerdlinger, PD & Arigo, RJ, 1983. Ap.J., **264**, 228.

VandenBerg, D.A., 1984. In: *'Observational Tests of Stellar Evolution Theory'*, p.143. Eds. Maeder, A & Renzini, A. Reidel (Dordrecht).

VandenBerg, D.A. & Bell, R.A., 1985. Ap.J.Suppl., **58**, 561.

Walker, D & Terndrup, DM, 1991. Ap.J., **378**, 119.

Wheeler, JC & Harkness, RP, 1986. In: *'Galaxy Distances and Deviations from Universal Expansion'*, p.45. Eds. Madore, BF & Tully, RB. Reidel (Dordrecht).

Willson, LA, Bowen, GH & Struck-Marcell, C, 1987. Comments on Astrophysics, **12**, 17.

Winget, DE, Hansen, CJ, Leibert, J, Van Horn, HM, Fontaine, G, Nather, RE, Kepler, SO & Lamb, DQ, 1987. Ap.J., **315**, L77.

Appendix A: The Data

This appendix lists the results of DAOPHOT runs on the m71 and M4 mosaics. The data are listed in two columns of stars per page. For each star the following information is listed: number, x, y, instrumental magnitude, DAOPHOT error estimate.

M71DK

621	40.15	132.80	15.130	0.082	506	118.28	107.50	17.707	0.028
957	209.10	107.55	15.192	0.060	664	174.16	139.43	17.738	0.048
540	27.94	114.06	15.234	0.034	515	76.41	110.42	17.756	0.035
3	285.32	2.84	15.965	0.078	195	252.41	45.03	17.813	0.013
414	184.36	89.45	16.068	0.026	609	154.91	128.57	17.999	0.025
593	67.79	126.46	16.451	0.021	642	148.03	136.35	18.082	0.016
45	157.76	11.87	16.457	0.021	160	266.25	37.06	18.176	0.022
675	115.61	142.43	16.685	0.034	212	23.16	49.09	18.251	0.046
405	113.06	87.70	16.754	0.026	418	260.42	89.18	18.289	0.026
570	109.75	121.11	16.775	0.033	1114	212.35	133.62	18.315	0.026
395	218.30	85.95	16.802	0.024	569	87.64	121.14	18.355	0.031
109	75.74	25.64	16.815	0.045	433	153.47	92.44	18.372	0.024
421	131.21	90.41	16.831	0.023	34	227.21	10.31	18.403	0.017
652	73.27	138.12	16.832	0.029	360	282.53	79.03	18.417	0.027
702	43.12	146.84	16.839	0.032	401	82.94	88.09	18.431	0.023
647	116.00	136.96	16.842	0.019	548	244.76	115.18	18.482	0.037
614	87.89	130.22	16.844	0.021	42	41.92	12.29	18.484	0.037
640	86.83	136.29	16.858	0.033	541	182.75	114.55	18.494	0.042
594	88.19	125.68	16.866	0.039	501	126.85	107.24	18.505	0.017
243	200.68	55.10	16.895	0.018	625	135.84	133.71	18.510	0.032
37	68.07	10.90	16.897	0.030	636	122.12	135.20	18.550	0.018
121	185.51	28.08	16.899	0.024	453	249.11	96.13	18.556	0.046
354	61.60	77.72	16.905	0.031	298	150.37	66.85	18.605	0.041
729	140.03	151.80	16.910	0.032	495	297.23	105.51	18.627	0.085
219	189.72	49.77	16.919	0.014	561	142.03	119.04	18.630	0.032
551	272.25	115.69	16.933	0.031	338	179.75	75.06	18.635	0.015
448	234.52	94.99	16.939	0.017	592	59.68	125.55	18.727	0.032
518	132.72	110.32	16.951	0.016	173	175.46	40.30	18.779	0.036
496	46.50	105.58	16.955	0.038	555	176.57	118.45	18.785	0.033
591	255.94	124.59	16.978	0.031	344	164.98	75.84	18.798	0.038
231	263.56	52.09	16.998	0.012	556	278.78	117.74	18.840	0.036
105	170.74	25.36	17.035	0.042	451	201.52	96.08	18.841	0.061
643	209.09	135.55	17.045	0.013	533	116.15	112.58	18.850	0.041
84	77.51	20.87	17.147	0.043	927	111.73	120.51	18.884	0.222
369	177.23	81.32	17.153	0.019	585	241.79	124.07	18.905	0.048
505	24.30	107.74	17.168	0.045	412	62.89	89.42	18.937	0.045
409	278.93	88.35	17.199	0.036	610	190.06	128.74	18.970	0.040
510	264.13	108.48	17.208	0.028	116	98.78	27.43	18.982	0.041
20	293.05	6.98	17.210	0.035	367	215.71	80.20	18.986	0.028
388	140.17	84.01	17.236	0.015	227	71.60	51.66	19.018	0.033
480	93.54	102.01	17.278	0.018	124	16.64	29.14	19.043	0.059
617	47.42	130.92	17.343	0.035	328	255.81	73.01	19.047	0.032
509	258.56	107.51	17.374	0.029	193	84.64	45.37	19.066	0.034
626	142.48	133.88	17.472	0.021	300	254.39	66.71	19.069	0.026
577	71.28	122.67	17.490	0.044	598	172.86	127.16	19.077	0.084
565	60.65	119.81	17.530	0.034	684	219.88	143.34	19.101	0.033
645	35.16	137.17	17.628	0.016	488	142.75	103.64	19.148	0.031
524	250.63	110.53	17.649	0.026	553	167.15	116.50	19.199	0.074
8	7.98	5.05	17.688	0.076	291	53.47	65.72	19.203	0.058
470	109.39	100.48	17.696	0.026	597	19.39	126.73	19.206	0.051

1110	140.02	133.66	19.215	0.094
323	63.29	73.11	19.226	0.035
669	184.00	140.85	19.227	0.101
960	203.57	96.60	19.230	0.089
284	207.29	63.81	19.250	0.030
444	189.93	94.02	19.264	0.025
707	137.39	146.52	19.267	0.034
727	119.52	151.21	19.278	0.126
499	78.54	107.61	19.287	0.078
711	76.25	147.84	19.303	0.040
44	153.09	11.63	19.303	0.029
599	226.93	126.90	19.308	0.051
504	239.66	106.78	19.314	0.101
327	237.73	72.67	19.326	0.019
637	152.58	135.17	19.334	0.025
391	248.55	85.20	19.358	0.026
324	88.92	73.50	19.364	0.033
81	142.86	19.78	19.386	0.035
234	130.69	53.36	19.408	0.036
1113	215.85	133.26	19.431	0.069
215	8.74	50.02	19.432	0.066
611	232.81	128.82	19.440	0.041
486	200.12	103.43	19.456	0.048
170	66.19	39.59	19.465	0.038
283	190.62	63.90	19.470	0.033
313	188.60	70.53	19.473	0.040
350	253.53	77.26	19.483	0.036
310	262.03	69.29	19.484	0.033
337	160.97	74.73	19.508	0.035
390	64.00	85.04	19.511	0.049
269	277.64	61.51	19.548	0.040
339	230.80	74.91	19.552	0.049
91	179.71	22.30	19.573	0.031
184	124.45	42.93	19.598	0.027
52	36.22	15.30	19.615	0.035
189	229.95	44.45	19.617	0.047
473	175.53	100.70	19.641	0.050
422	139.87	90.00	19.649	0.053
682	125.71	143.13	19.664	0.032
528	193.85	111.98	19.674	0.041
271	183.91	62.01	19.682	0.059
210	131.02	47.89	19.689	0.066
349	97.70	77.45	19.699	0.081
406	175.44	87.85	19.707	0.031
590	199.97	125.30	19.711	0.074
493	133.92	104.52	19.733	0.065
618	76.69	131.50	19.735	0.049
416	235.34	88.85	19.742	0.051
481	121.21	101.74	19.760	0.066
649	203.71	136.98	19.775	0.049
83	42.05	20.78	19.784	0.054
596	176.24	127.02	19.793	0.205
11	63.88	6.45	19.802	0.155
334	22.42	75.29	19.830	0.065
872	280.86	88.12	19.854	0.425
159	249.01	37.49	19.860	0.041
115	88.94	27.29	19.860	0.060
698	288.88	145.39	19.875	0.050
169	186.45	39.37	19.876	0.044
194	157.96	45.26	19.878	0.068
47	12.40	12.65	19.888	0.075
521	217.09	109.88	19.892	0.069
454	261.74	96.25	19.894	0.057
955	190.70	131.77	19.900	0.093
397	211.70	86.61	19.902	0.048
717	103.02	149.43	19.913	0.093
503	198.85	107.29	19.915	0.043
1032	250.21	97.20	19.923	0.177
662	110.59	139.69	19.937	0.071
522	272.20	110.28	19.947	0.118
722	158.84	150.48	19.948	0.067
288	177.62	64.73	19.952	0.043
693	160.41	145.10	19.955	0.085
731	180.63	150.99	19.957	0.091
408	202.37	87.61	19.961	0.060
648	188.78	136.57	19.986	0.063
85	138.88	21.23	19.991	0.055
622	64.35	132.65	20.006	0.051
605	219.85	128.35	20.014	0.061
687	103.90	144.04	20.025	0.084
527	167.41	112.57	20.044	0.069
48	113.59	13.40	20.053	0.061
730	176.02	151.25	20.086	0.159
299	247.72	67.37	20.095	0.052
841	156.49	47.53	20.107	0.084
49	140.42	13.05	20.108	0.046
274	236.59	62.30	20.124	0.072
108	63.66	26.38	20.132	0.066
547	199.18	115.31	20.133	0.112
688	187.28	143.97	20.146	0.094
580	188.49	123.23	20.156	0.085
534	122.13	113.29	20.160	0.053
190	13.31	44.65	20.164	0.098
1112	196.76	115.00	20.169	0.113
924	72.80	142.38	20.180	0.078
256	172.25	57.90	20.197	0.072
443	182.26	93.92	20.200	0.081
424	200.08	89.66	20.205	0.127
1007	67.70	70.96	20.206	0.098
296	66.89	67.65	20.208	0.099
356	109.15	78.49	20.233	0.057
456	97.38	96.96	20.234	0.091
720	28.75	150.21	20.236	0.080
962	175.30	98.52	20.246	0.087
487	20.75	104.30	20.248	0.122
446	101.74	94.56	20.255	0.079
425	214.19	89.91	20.266	0.080
432	90.76	92.08	20.268	0.062
564	48.57	120.37	20.282	0.080
149	92.97	35.08	20.288	0.074
319	37.69	72.20	20.292	0.072
535	164.01	113.28	20.294	0.085
560	53.55	118.87	20.315	0.066
644	262.82	136.30	20.319	0.060
440	31.97	93.71	20.322	0.062
653	216.42	138.11	20.326	0.104
366	183.46	80.20	20.331	0.085
950	168.20	118.91	20.340	0.090
514	34.55	112.00	20.341	0.187
632	239.44	133.80	20.342	0.063
583	280.41	122.85	20.344	0.088
631	226.26	134.17	20.348	0.064
6	135.76	3.99	20.351	0.056
1031	246.97	95.09	20.356	0.102
199	79.19	45.68	20.360	0.095
122	211.58	27.84	20.363	0.077
200	209.36	45.96	20.364	0.087
111	225.41	25.74	20.385	0.077
706	108.69	147.35	20.387	0.121
312	79.24	69.82	20.388	0.087
961	179.66	87.64	20.397	0.095
714	170.69	147.68	20.400	0.087
363	71.28	79.52	20.400	0.111
54	135.00	14.58	20.401	0.061
549	124.92	116.36	20.403	0.057
567	130.99	120.19	20.403	0.085
73	299.05	18.34	20.406	0.067

920	77.09	122.96	20.428	0.135
246	128.10	55.96	20.428	0.109
315	109.35	70.75	20.432	0.097
297	132.54	66.71	20.438	0.109
386	5.63	83.88	20.451	0.072
1111	179.11	117.96	20.456	0.155
325	143.15	73.16	20.461	0.094
25	86.48	9.03	20.462	0.058
699	120.48	145.97	20.466	0.083
630	222.32	133.71	20.466	0.069
126	259.03	29.46	20.467	0.068
656	100.48	139.29	20.470	0.074
27	127.56	8.98	20.479	0.063
1115	211.50	131.21	20.480	0.177
676	146.59	141.01	20.480	0.087
877	238.31	64.46	20.480	0.101
512	66.31	109.03	20.481	0.100
259	119.28	58.85	20.485	0.064
944	151.06	138.39	20.491	0.076
958	215.62	104.76	20.495	0.205
204	107.42	47.10	20.499	0.071
482	217.95	101.72	20.501	0.150
183	105.46	43.00	20.505	0.085
389	165.61	84.37	20.507	0.082
943	144.38	142.76	20.509	0.118
385	278.81	83.03	20.510	0.158
308	167.26	68.93	20.514	0.093
341	37.90	75.51	20.518	0.090
148	79.66	35.06	20.519	0.075
330	102.30	74.49	20.523	0.063
713	129.33	147.78	20.530	0.073
396	101.63	86.48	20.532	0.061
826	81.37	24.41	20.535	0.127
842	132.19	49.26	20.536	0.146
165	86.03	38.95	20.539	0.072
221	30.40	51.13	20.539	0.083
39	182.75	11.07	20.542	0.102
130	197.32	30.25	20.545	0.073
956	192.50	136.25	20.547	0.127
461	255.71	96.86	20.548	0.102
139	57.58	33.20	20.552	0.092
242	163.50	55.42	20.559	0.075
670	213.92	140.81	20.572	0.130
1203	41.30	137.88	20.576	0.164
365	171.67	80.35	20.586	0.098
164	297.03	38.06	20.587	0.102
536	175.04	112.81	20.594	0.140
571	171.79	120.50	20.602	0.110
562	203.36	119.00	20.605	0.084
705	95.66	146.97	20.606	0.092
378	250.86	82.46	20.606	0.067
125	130.04	29.10	20.608	0.066
94	236.88	22.37	20.618	0.121
627	159.11	134.09	20.624	0.130
383	199.21	83.09	20.627	0.098
725	81.07	151.36	20.634	0.109
358	128.21	79.29	20.635	0.075
133	2.14	32.37	20.637	8.581
860	267.08	39.24	20.656	0.204
76	173.61	19.23	20.657	0.093
264	37.18	60.24	20.658	0.084
697	282.02	145.57	20.665	0.089
732	187.17	150.79	20.668	0.167
1033	255.03	121.01	20.672	0.186
207	288.03	47.44	20.672	0.078
261	299.61	58.76	20.673	0.105
635	107.38	135.27	20.675	0.091
72	244.18	18.02	20.675	0.079
726	107.47	150.63	20.678	0.183
392	263.94	84.52	20.680	0.138
566	125.25	119.88	20.688	0.073
364	153.10	79.92	20.693	0.111
18	152.38	6.37	20.694	0.137
146	240.35	34.30	20.699	0.082
254	108.74	58.53	20.709	0.096
348	83.46	76.55	20.715	0.073
22	2.26	7.76	20.716	4.928
502	149.35	106.65	20.717	0.118
959	212.54	112.86	20.721	0.105
639	79.75	135.93	20.724	0.101
492	106.16	104.99	20.726	0.099
931	122.86	105.46	20.727	0.133
696	255.13	144.88	20.728	0.085
437	95.28	93.40	20.728	0.070
60	197.11	16.38	20.730	0.071
659	166.94	138.57	20.735	0.092
118	51.50	28.38	20.737	0.105
253	176.61	56.65	20.738	0.094
690	20.79	145.10	20.744	0.092
712	113.23	148.58	20.747	0.113
516	94.81	109.48	20.750	0.118
257	186.96	57.99	20.752	0.101
138	275.35	31.81	20.757	0.081
218	161.55	50.34	20.763	0.076
701	247.54	146.08	20.763	0.102
335	50.80	74.74	20.763	0.074
151	147.05	35.52	20.770	0.086
602	54.43	127.71	20.771	0.093
377	189.60	82.69	20.771	0.093
357	79.44	79.21	20.772	0.089
252	115.75	57.41	20.776	0.083
402	88.19	88.03	20.779	0.122
824	39.51	20.75	20.780	0.129
119	56.51	27.97	20.786	0.095
683	148.98	142.91	20.790	0.119
182	75.21	43.01	20.790	0.116
141	176.85	33.01	20.796	0.117
874	260.16	93.17	20.804	0.145
666	44.24	140.44	20.805	0.153
543	17.14	115.43	20.812	0.128
572	248.49	121.60	20.813	0.104
933	145.92	117.96	20.815	0.121
233	106.41	52.84	20.816	0.076
208	90.87	48.26	20.822	0.125
679	2.31	143.28	20.827	0.143
175	11.94	41.80	20.831	0.153
14	162.17	6.35	20.836	0.160
954	185.87	124.91	20.848	0.145
1029	265.72	52.85	20.854	0.281
439	293.82	92.66	20.855	0.106
260	163.28	58.80	20.861	0.098
600	275.24	127.49	20.866	0.112
101	127.19	23.65	20.871	0.084
663	132.38	140.00	20.871	0.088
16	25.82	7.10	20.873	0.158
846	136.35	11.77	20.874	0.138
721	69.83	149.42	20.876	0.133
41	4.92	12.45	20.879	0.201
172	160.02	39.91	20.881	0.066
668	162.80	141.60	20.885	0.144
619	245.52	131.31	20.888	0.096
971	255.59	99.49	20.888	0.139
373	297.33	81.11	20.889	0.110
21	300.44	6.51	20.889	0.089
849	201.38	32.25	20.892	0.119
1103	54.61	67.53	20.892	0.276
558	21.14	118.80	20.899	0.166

430	42.24	92.03	20.902	0.151
217	53.15	49.97	20.903	0.118
925	73.93	145.93	20.914	0.122
86	258.92	21.06	20.915	0.094
431	51.67	92.17	20.922	0.177
209	98.45	47.94	20.923	0.108
123	245.94	28.34	20.929	0.089
80	35.71	19.97	20.932	0.103
10	233.77	5.49	20.934	0.108
303	171.76	68.11	20.939	0.118
110	161.57	26.11	20.942	0.091
129	135.95	29.52	20.943	0.133
563	212.52	118.83	20.945	0.091
399	301.76	86.94	20.947	0.103
604	132.86	128.15	20.947	0.090
657	104.03	138.88	20.953	0.145
464	215.47	97.92	20.953	0.103
374	45.53	81.54	20.953	0.134
941	124.36	133.47	20.955	0.139
434	159.89	92.04	20.956	0.103
368	39.32	80.93	20.958	0.105
104	141.68	25.34	20.964	0.091
99	52.82	24.15	20.969	0.114
301	89.51	68.41	20.969	0.087
1034	259.44	124.54	20.969	0.164
724	57.56	151.27	20.971	0.126
370	204.58	81.03	20.976	0.110
723	47.59	151.63	20.977	0.104
477	298.54	100.95	20.978	0.113
403	96.16	87.65	20.979	0.111
266	263.67	59.82	20.980	0.112
90	152.53	21.92	20.985	0.083
658	126.62	139.35	20.991	0.107
574	32.07	121.97	20.998	0.224
613	5.72	130.47	21.000	0.121
467	84.08	99.07	21.006	0.101
573	275.20	120.96	21.009	0.151
1116	208.24	129.90	21.009	0.311
232	19.66	53.27	21.020	0.125
460	241.57	96.74	21.021	0.176
153	180.95	35.61	21.021	0.099
191	30.44	44.91	21.022	0.116
46	270.71	12.37	21.032	0.105
949	162.73	120.30	21.038	0.154
309	198.27	68.72	21.046	0.120
450	170.04	95.75	21.046	0.149
249	268.02	55.68	21.047	0.137
805	29.52	140.60	21.049	0.153
624	23.55	134.28	21.050	0.153
667	57.12	140.79	21.051	0.157
939	132.99	130.83	21.054	0.119
681	34.75	142.72	21.063	0.576
361	20.58	80.01	21.070	0.240
106	13.77	26.12	21.073	0.183
248	259.88	56.15	21.081	0.117
823	65.07	36.84	21.082	0.111
155	21.80	36.71	21.084	0.149
875	238.29	89.93	21.095	0.180
695	234.73	144.82	21.100	0.120
280	73.03	64.26	21.102	0.131
69	239.40	17.41	21.102	0.110
964	154.07	46.91	21.105	0.192
98	296.52	22.88	21.110	0.142
537	219.13	113.14	21.113	0.174
929	99.58	101.06	21.115	0.110
19	243.23	7.16	21.116	0.124
362	53.80	80.33	21.116	0.108
53	83.19	14.82	21.117	0.094
531	65.13	112.95	21.120	0.136
607	97.49	128.89	21.125	0.138
455	267.78	95.68	21.125	0.136
546	106.95	115.00	21.126	0.142
733	190.67	149.11	21.127	0.194
972	262.12	98.32	21.131	0.154
840	152.21	70.39	21.136	0.129
873	284.48	90.78	21.142	0.124
1264	211.07	101.18	21.146	0.265
423	149.65	89.81	21.147	0.107
394	171.01	86.02	21.150	0.169
825	85.89	24.70	21.157	0.220
832	92.88	73.96	21.167	0.143
131	32.33	31.56	21.172	0.152
387	89.10	84.16	21.175	0.153
410	296.12	87.64	21.176	0.135
500	97.92	106.66	21.178	0.147
31	33.45	10.30	21.178	0.119
1205	29.40	118.73	21.179	0.207
578	102.68	122.92	21.179	0.121
237	223.63	53.90	21.179	0.122
582	219.08	123.16	21.182	0.165
36	300.90	10.33	21.182	0.121
484	156.36	102.79	21.183	0.151
286	261.60	63.53	21.183	0.160
855	231.33	37.31	21.185	0.131
462	44.61	97.65	21.189	0.143
458	187.06	96.21	21.191	0.143
801	22.35	146.95	21.192	0.146
871	281.91	82.10	21.193	0.247
719	276.25	149.31	21.193	0.158
96	209.89	23.47	21.194	0.138
811	39.53	92.33	21.195	0.192
457	115.99	96.71	21.195	0.183
371	238.16	80.99	21.196	0.130
559	24.33	119.39	21.197	0.208
638	15.20	136.06	21.198	0.165
273	220.82	61.93	21.202	0.161
206	215.79	46.60	21.202	0.137
1117	240.82	94.50	21.203	0.172
868	294.81	58.67	21.204	0.191
211	219.93	47.41	21.206	0.141
735	232.61	150.49	21.206	0.143
143	233.11	32.78	21.207	0.153
523	228.13	110.72	21.210	0.178
728	132.12	150.98	21.219	0.183
468	128.28	99.52	21.220	0.148
326	216.83	72.58	21.228	0.122
196	277.38	44.85	21.229	0.205
552	158.88	117.23	21.231	0.135
633	274.53	133.67	21.232	0.108
244	302.82	55.36	21.238	0.161
238	240.24	54.10	21.241	0.161
1016	120.21	86.66	21.241	0.165
942	122.07	139.64	21.241	0.157
466	53.32	98.60	21.242	0.127
1277	256.25	151.15	21.243	0.166
686	56.35	143.81	21.245	0.143
1220	66.68	13.36	21.252	0.384
239	52.44	54.42	21.252	0.125
938	131.81	125.81	21.254	0.143
186	101.38	44.53	21.256	0.132
848	179.72	30.94	21.262	0.163
262	22.77	60.16	21.266	0.146
479	79.81	102.23	21.266	0.166
428	266.23	90.96	21.269	0.165
472	167.58	99.57	21.270	0.132
294	288.89	66.03	21.274	0.186
187	166.53	44.28	21.275	0.126

435	299.57	92.54	21.279	0.155
134	103.42	32.32	21.280	0.251
114	67.88	26.70	21.281	0.206
376	147.61	82.27	21.281	0.156
483	65.80	103.08	21.283	0.131
359	143.60	78.96	21.286	0.144
436	16.60	92.92	21.286	0.117
276	126.58	63.38	21.289	0.133
588	120.80	125.54	21.289	0.167
163	233.30	39.04	21.289	0.138
867	289.84	36.14	21.292	0.237
438	173.84	93.13	21.297	0.220
426	222.89	90.94	21.300	0.172
1228	108.40	3.62	21.302	0.281
1230	90.32	77.35	21.307	0.224
144	157.64	34.36	21.308	0.091
804	25.40	141.17	21.313	0.203
568	194.47	120.55	21.323	0.165
1258	109.00	142.85	21.329	0.193
58	146.17	16.46	21.330	0.136
878	204.25	85.20	21.332	0.186
520	157.10	110.28	21.333	0.167
258	73.14	58.86	21.340	0.181
623	5.88	134.37	21.345	0.149
136	220.08	32.43	21.349	0.151
581	212.15	123.00	21.350	0.157
407	193.57	88.50	21.351	0.245
902	55.46	100.31	21.352	0.143
427	252.78	91.03	21.354	0.180
40	296.69	10.55	21.359	0.165
932	143.15	113.38	21.359	0.215
441	83.32	93.70	21.362	0.137
837	130.21	59.01	21.363	0.188
230	208.28	52.24	21.364	0.190
292	225.04	66.19	21.366	0.139
311	285.46	68.75	21.367	0.167
225	247.92	51.17	21.369	0.145
220	292.85	50.08	21.371	0.169
289	195.97	65.20	21.376	0.148
694	208.43	145.37	21.379	0.219
459	193.13	96.59	21.379	0.172
511	283.15	108.35	21.380	0.153
181	89.43	41.94	21.386	0.131
63	89.79	17.58	21.387	0.146
844	143.14	28.59	21.389	0.152
445	282.25	94.05	21.389	0.181
834	114.13	81.36	21.392	0.241
128	38.57	30.46	21.395	0.218
715	261.16	147.49	21.400	0.181
802	23.28	142.55	21.403	0.216
413	123.36	89.35	21.405	0.162
1020	168.94	93.03	21.406	0.185
465	4.73	99.35	21.408	0.160
442	121.96	93.95	21.410	0.154
176	45.73	41.33	21.411	0.127
9	37.06	5.32	21.416	0.300
948	147.60	104.49	21.416	0.185
923	79.07	140.63	21.418	0.163
532	108.94	113.05	21.433	0.192
250	286.76	55.60	21.434	0.202
420	74.28	89.70	21.438	0.181
59	178.21	15.51	21.441	0.151
616	23.35	131.28	21.443	0.207
70	101.37	18.00	21.445	0.148
61	256.33	16.36	21.446	0.160
347	224.19	75.83	21.448	0.188
285	245.39	64.78	21.448	0.179
606	263.11	126.78	21.453	0.238
922	79.25	130.33	21.453	0.224
1030	277.10	81.07	21.454	0.308
222	97.02	51.24	21.457	0.179
318	243.19	70.72	21.462	0.125
1259	99.94	145.81	21.464	0.196
819	47.36	66.85	21.466	0.233
75	58.92	19.10	21.467	0.208
293	276.19	66.31	21.468	0.159
704	86.31	146.76	21.468	0.229
1018	165.19	81.70	21.469	0.149
709	242.12	147.59	21.481	0.197
1017	160.05	88.90	21.482	0.206
576	42.06	124.24	21.484	0.297
178	238.70	40.73	21.484	0.153
475	237.71	100.75	21.486	0.196
224	229.56	51.20	21.487	0.136
316	178.62	71.23	21.490	0.144
381	121.50	82.59	21.493	0.117
329	80.85	74.34	21.494	0.133
1266	221.61	77.43	21.496	0.193
95	112.56	23.43	21.499	0.163
586	294.89	124.49	21.501	0.167
158	115.86	37.15	21.505	0.228
65	137.91	16.89	21.505	0.190
554	225.59	116.85	21.506	0.157
32	145.82	10.03	21.507	0.204
166	121.58	39.31	21.507	0.202
608	102.07	129.17	21.519	0.216
1265	208.97	96.56	21.519	0.211
478	68.91	101.74	21.525	0.168
379	300.97	82.55	21.526	0.201
35	233.80	9.38	21.531	0.165
908	59.56	34.99	21.535	0.239
393	16.69	86.11	21.539	0.158
921	73.94	134.79	21.542	0.891
858	252.99	36.18	21.545	0.215
449	163.41	96.05	21.545	0.232
691	36.92	145.32	21.550	0.187
270	85.36	61.65	21.558	0.142
404	106.54	88.25	21.558	0.141
861	268.82	41.34	21.562	0.308
93	198.33	22.25	21.563	0.142
641	97.23	136.40	21.566	0.202
235	140.75	52.93	21.566	0.140
142	228.93	32.80	21.566	0.213
557	14.16	118.95	21.570	0.265
263	27.51	59.96	21.570	0.196
978	279.31	124.88	21.571	0.241
140	64.26	33.44	21.572	0.173
517	99.99	110.07	21.576	0.253
281	87.95	63.99	21.579	0.153
661	93.68	139.63	21.583	0.176
708	198.62	147.02	21.583	0.145
26	103.73	8.95	21.584	0.181
275	49.01	63.18	21.585	0.223
167	128.80	39.57	21.588	0.214
171	140.67	40.12	21.591	0.233
382	126.82	83.27	21.591	0.168
489	276.37	103.89	21.596	0.195
835	107.85	68.49	21.596	0.276
429	21.51	92.67	21.601	0.222
447	137.64	94.57	21.602	0.171
198	8.52	45.94	21.606	0.341
807	9.35	129.72	21.608	0.216
692	67.01	144.53	21.610	0.276
307	33.64	68.89	21.615	0.216
137	246.55	31.81	21.616	0.166
384	225.64	83.39	21.618	0.242
162	171.10	37.77	21.622	0.185

1262	201.24	113.35	21.626	0.215
117	119.29	27.44	21.629	0.186
30	28.99	10.25	21.633	0.223
818	41.87	70.10	21.636	0.249
491	59.98	104.86	21.636	0.205
419	31.82	89.85	21.637	0.217
928	119.65	115.49	21.639	0.194
620	28.08	132.18	21.640	0.277
833	87.22	66.82	21.640	0.164
56	17.93	16.09	21.640	0.275
513	279.45	108.60	21.648	0.190
411	15.95	89.07	21.648	0.171
827	87.58	21.67	21.649	0.292
353	48.97	77.77	21.649	0.230
672	255.35	141.79	21.653	0.197
494	231.51	104.83	21.655	0.177
914	85.27	95.97	21.663	0.192
1212	50.33	67.36	21.664	0.311
57	129.34	15.33	21.666	0.209
64	124.31	16.72	21.667	0.213
62	62.96	16.89	21.670	0.212
1268	212.15	46.21	21.673	0.303
718	151.89	148.35	21.673	0.252
544	82.78	114.88	21.673	0.217
1	132.51	2.53	21.674	0.186
595	101.09	126.22	21.674	0.192
342	115.59	76.12	21.674	0.225
1263	209.21	115.58	21.675	0.245
803	22.84	139.44	21.676	0.215
295	32.20	66.69	21.676	0.224
550	150.16	116.32	21.678	0.160
38	110.10	10.97	21.679	0.222
333	152.53	74.22	21.679	0.160
703	51.17	147.22	21.679	0.276
135	141.06	31.51	21.680	0.166
1222	73.98	9.75	21.686	0.316
302	119.53	68.40	21.688	0.201
127	27.38	30.51	21.691	0.214
66	168.15	17.66	21.697	0.216
180	25.26	42.69	21.699	0.284
538	287.76	112.72	21.699	0.244
314	96.04	71.43	21.706	0.204
974	226.09	119.41	21.706	0.191
940	131.05	133.55	21.707	0.216
23	45.39	7.73	21.710	0.287
331	119.75	73.71	21.710	0.265
400	4.63	87.70	21.712	0.228
1210	51.94	77.65	21.713	0.207
290	301.69	65.02	21.714	0.267
213	140.02	49.15	21.715	0.161
120	111.60	28.37	21.716	0.197
716	60.63	148.71	21.717	0.250
304	232.39	68.40	21.722	0.208
33	173.87	10.48	21.723	0.221
463	155.61	98.45	21.727	0.184
7	274.63	4.09	21.727	0.213
584	46.14	124.18	21.728	0.286
317	206.88	71.37	21.728	0.224
152	107.11	35.72	21.732	0.246
828	95.60	33.82	21.733	0.234
279	37.46	63.46	21.734	0.226
700	202.20	146.10	21.738	0.164
340	262.84	74.70	21.738	0.182
1270	262.85	45.43	21.739	0.210
336	136.40	74.90	21.742	0.253
255	159.22	57.56	21.744	0.213
236	219.37	53.95	21.753	0.236
1015	130.91	101.07	21.758	0.242
866	287.84	26.13	21.758	0.312
1003	117.67	117.75	21.759	0.215
485	192.58	102.80	21.760	0.193
251	56.46	56.70	21.761	0.173
174	219.74	39.62	21.766	0.184
808	7.34	120.04	21.767	0.315
677	232.02	142.34	21.777	0.223
869	276.23	63.52	21.783	0.273
912	75.98	68.09	21.784	0.222
24	278.19	7.83	21.789	0.246
157	44.95	37.46	21.791	0.184
380	16.27	82.85	21.793	0.203
876	240.81	73.97	21.794	0.221
343	129.83	76.41	21.795	0.220
205	114.93	46.48	21.799	0.226
809	9.88	120.87	21.799	0.335
476	278.21	101.54	21.802	0.239
216	38.75	49.78	21.802	0.253
29	260.86	8.44	21.802	0.185
680	12.72	143.36	21.807	0.266
973	229.89	123.63	21.813	0.279
77	199.66	19.40	21.815	0.187
247	225.88	55.62	21.826	0.226
272	215.77	62.37	21.833	0.219
287	296.41	63.80	21.835	0.237
909	33.46	16.96	21.836	0.230
332	123.05	73.52	21.839	0.307
147	69.65	34.93	21.840	0.249
689	195.95	144.60	21.840	0.183
177	182.12	40.79	21.842	0.230
201	281.79	45.80	21.844	0.225
629	197.54	133.79	21.846	0.260
497	226.11	105.33	21.853	0.230
71	116.81	17.58	21.854	0.218
185	200.40	42.82	21.860	0.256
1224	83.09	37.90	21.866	0.245
321	276.21	72.01	21.874	0.255
278	30.81	63.89	21.877	0.263
154	218.47	35.49	21.879	0.242
268	194.89	60.90	21.881	0.274
507	162.55	108.01	21.882	0.244
1102	31.83	87.50	21.888	0.227
103	135.19	24.90	21.890	0.279
145	169.48	34.12	21.892	0.235
89	116.95	21.90	21.900	0.230
28	198.51	9.18	21.900	0.225
1209	56.76	80.81	21.908	0.307
1208	63.52	93.78	21.910	0.189
372	265.97	81.02	21.913	0.272
87	273.02	21.19	21.916	0.217
92	191.43	22.40	21.917	0.285
734	228.74	151.54	21.926	0.269
1211	57.38	70.82	21.928	0.223
88	105.35	22.21	21.929	0.242
1242	139.48	79.92	21.930	0.300
352	5.14	78.09	21.935	0.368
74	53.40	18.87	21.951	0.319
671	228.08	140.79	21.956	0.282
228	122.31	51.91	21.958	0.226
812	21.28	84.02	21.964	0.374
226	254.76	51.34	21.965	0.211
15	186.93	5.90	21.967	0.353
322	3.47	73.35	21.974	0.299
816	17.11	37.52	21.977	0.299
979	301.21	117.83	21.981	0.446
545	90.50	115.12	21.983	0.350
188	224.55	43.89	21.985	0.261
79	32.17	19.72	21.988	0.270
1241	124.60	81.41	21.990	0.233

490	54.30	104.83	21.990	0.238
2	192.23	3.23	21.991	0.281
100	96.94	23.85	21.997	0.347
179	281.57	41.47	21.998	0.317
1250	151.10	131.67	21.998	0.294
575	154.80	121.62	21.998	0.309
55	235.41	15.48	22.002	0.281
1244	119.53	91.48	22.003	0.262
197	4.51	46.17	22.007	0.419
113	42.41	26.82	22.008	0.250
917	83.40	109.16	22.011	0.248
1119	230.80	5.67	22.012	0.284
13	144.89	6.12	22.013	0.326
673	279.18	141.25	22.021	0.356
911	82.28	64.33	22.025	0.257
710	2.78	147.84	22.045	0.371
1026	233.74	42.62	22.045	0.301
1221	66.66	8.10	22.046	1.637
913	72.20	94.73	22.055	0.344
305	240.39	67.93	22.055	0.240
51	302.13	14.10	22.055	0.245
1225	100.51	32.66	22.058	0.500
214	147.10	49.44	22.074	0.169
1261	124.26	146.08	22.085	0.405
346	205.65	76.03	22.086	0.335
112	8.10	27.08	22.086	0.395
320	212.30	71.64	22.087	0.339
1006	118.77	80.23	22.090	0.183
813	18.49	67.15	22.091	0.357
132	149.37	30.99	22.093	0.279
229	149.53	51.98	22.098	0.172
1269	261.91	39.21	22.103	0.380
863	280.15	20.20	22.106	0.338
612	269.95	129.44	22.110	0.287
1013	120.76	43.39	22.112	0.267
839	137.04	66.11	22.119	0.234
810	29.16	101.14	22.119	0.335
665	240.68	139.76	22.121	0.282
603	107.63	128.00	22.121	0.421
375	134.04	82.25	22.124	0.342
469	139.65	99.04	22.124	0.364
415	208.61	89.11	22.126	0.365
814	33.57	75.19	22.145	0.315
102	201.96	24.04	22.145	0.339
685	292.90	143.41	22.147	0.402
845	145.68	29.30	22.150	0.319
1271	267.51	47.11	22.150	0.793
968	268.94	58.00	22.151	0.379
12	72.34	5.78	22.155	0.402
678	248.66	142.01	22.156	0.277
1014	139.77	46.28	22.157	0.270
977	251.76	129.84	22.163	0.271
615	121.63	129.99	22.165	0.400
937	128.80	124.04	22.168	0.263
1009	88.56	36.92	22.169	0.344
82	255.37	20.35	22.177	0.291
654	233.74	137.43	22.182	0.302
1243	132.39	95.90	22.185	0.300
1008	81.10	44.19	22.186	0.518
847	177.63	43.67	22.187	0.386
1267	234.28	79.70	22.194	0.411
1010	83.67	11.88	22.194	0.271
859	263.02	31.74	22.194	0.331
277	251.96	63.62	22.197	0.337
1274	280.22	61.15	22.198	0.428
519	149.30	110.00	22.198	0.345
1219	60.38	28.65	22.201	0.354
223	172.75	50.57	22.201	0.283
351	272.13	77.06	22.211	0.327
1035	266.01	145.35	22.212	0.334
1272	274.29	40.06	22.220	0.360
1216	13.42	19.72	22.228	0.408
203	34.41	47.40	22.236	0.427
17	54.67	6.64	22.237	0.292
68	192.45	16.43	22.248	0.459
345	194.39	75.81	22.250	0.345
589	159.70	124.96	22.251	0.497
1215	24.59	35.27	22.251	0.521
1257	134.26	147.99	22.264	0.519
471	135.15	100.29	22.268	0.335
1240	121.45	66.47	22.272	0.375
1239	129.67	68.11	22.273	0.578
1028	255.73	47.07	22.273	0.732
1109	153.92	51.86	22.280	0.349
963	173.03	45.77	22.280	0.476
1027	259.05	42.73	22.282	0.416
107	30.37	26.14	22.283	0.436
1120	284.70	48.19	22.286	0.416
398	288.97	87.72	22.288	0.409
854	219.09	20.55	22.289	0.320
1207	56.60	91.34	22.289	0.315
862	276.44	19.71	22.291	0.273
660	199.62	137.98	22.292	0.360
306	25.10	69.22	22.300	0.432
1256	131.88	143.06	22.305	0.392
417	246.20	89.15	22.307	0.299
474	39.88	100.83	22.313	0.355
4	79.09	4.12	22.317	0.465
240	102.42	55.28	22.325	0.254
97	268.26	22.80	22.327	0.340
865	280.50	15.12	22.330	0.406
1260	94.54	149.58	22.333	0.450
192	62.07	44.94	22.335	0.423
1012	127.94	26.84	22.338	0.363
856	227.74	48.45	22.344	0.300
1227	112.26	16.50	22.352	0.506
168	149.16	38.89	22.362	0.369
1232	125.38	55.18	22.364	0.517
1229	86.71	70.80	22.365	0.367
1118	230.19	12.25	22.366	0.650
150	129.68	35.13	22.373	0.361
245	5.06	55.63	22.376	0.372
1226	101.02	30.18	22.381	0.412
906	47.77	50.04	22.384	0.334
965	153.85	42.27	22.390	0.531
1245	137.47	86.68	22.393	0.478
651	300.17	137.72	22.406	0.491
542	5.20	114.99	22.411	0.506
1273	260.13	79.30	22.420	0.382
156	35.00	36.86	22.421	0.535
241	147.69	54.81	22.429	0.252
1214	10.43	67.46	22.434	0.603
529	233.98	112.56	22.435	0.349
1223	80.72	30.69	22.437	0.358
1235	144.89	53.88	22.440	0.454
1218	49.14	23.55	22.441	0.495
50	102.81	13.73	22.459	0.352
1238	146.09	66.59	22.483	0.449
78	207.47	18.45	22.504	0.345
43	61.13	12.07	22.508	0.427
907	43.65	44.02	22.529	0.363
1023	191.22	7.53	22.540	0.448
817	19.73	43.53	22.541	0.600
202	296.80	46.26	22.552	0.523
452	225.53	96.07	22.557	0.353
1233	125.46	48.55	22.559	0.376
1234	136.63	59.09	22.566	0.443

1019	161.32	85.01	22.566	0.436	1011	118.89	34.08	22.850	0.629
1206	27.73	82.01	22.570	0.410	1252	160.60	137.32	22.865	0.591
539	302.14	113.67	22.574	1.061	903	62.61	98.70	22.906	0.558
1106	105.61	50.12	22.606	0.488	905	27.40	88.79	22.916	0.564
966	157.64	37.95	22.610	0.380	526	48.16	112.32	22.989	0.813
650	271.85	136.37	22.640	0.398	1254	149.36	125.46	23.001	0.794
1251	154.50	137.45	22.653	0.530	1101	16.75	98.84	23.017	0.755
161	9.54	37.85	22.659	0.644	850	203.53	36.92	23.020	0.640
936	138.31	112.02	22.663	0.528	508	175.59	108.04	23.036	0.736
1024	203.53	15.94	22.669	0.487	1022	163.91	29.14	23.111	0.675
601	287.84	126.60	22.690	0.627	967	210.28	6.84	23.149	0.803
1236	141.65	68.72	22.698	0.413	1105	97.07	56.23	23.192	0.738
857	238.15	49.75	22.711	0.438	1217	36.88	25.99	23.225	1.112
864	278.35	13.31	22.711	0.508	930	105.15	111.25	23.294	1.156
901	34.65	101.51	22.713	0.502	634	285.85	133.78	23.342	1.410
587	5.74	124.78	22.715	0.493	870	292.26	68.43	23.374	1.127
530	54.37	113.12	22.733	0.637	525	295.01	110.50	23.393	1.653
853	219.54	27.15	22.740	0.469	579	136.36	123.26	23.476	1.384
1107	116.56	66.15	22.746	0.451	970	291.67	60.42	23.490	1.315
1237	138.09	69.80	22.758	0.427	1249	140.88	128.11	23.560	1.712
821	70.68	48.18	22.783	0.527	674	63.77	142.37	23.571	1.652
935	134.45	116.03	22.794	0.598	646	60.13	137.50	23.920	2.108
655	286.52	138.28	22.801	0.533	1246	142.84	95.73	24.026	1.895
67	187.75	17.44	22.841	0.523	498	287.96	105.58	24.141	3.597
919	86.67	106.97	22.846	0.593	1247	148.19	95.44	24.971	4.278

M71DEEP1_1

80	70.48	58.63	18.599	0.019	70	28.83	49.84	20.927	0.051
26	19.20	18.87	19.082	0.020	69	35.87	49.01	20.975	0.061
51	4.91	36.62	19.220	0.024	56	11.42	39.91	21.050	0.074
1	73.83	3.76	19.303	0.175	204	12.55	65.24	21.086	0.116
15	63.35	11.75	19.437	0.027	92	3.23	67.57	21.106	0.092
86	8.77	64.71	19.518	0.019	24	62.24	17.43	21.186	0.068
49	44.87	34.83	19.660	0.023	30	56.28	21.41	21.189	0.058
57	51.42	39.75	19.769	0.045	19	72.73	14.25	21.250	0.128
65	51.08	44.81	19.784	0.055	100	73.20	71.53	21.257	0.445
95	17.48	68.83	19.871	0.069	227	5.74	15.58	21.258	0.176
3	34.01	5.09	20.053	0.031	99	63.54	71.06	21.286	0.149
25	9.13	18.66	20.130	0.049	77	46.65	55.03	21.289	0.126
4	60.78	5.12	20.199	0.042	50	21.94	36.22	21.324	0.053
250	50.39	46.12	20.293	0.081	231	30.29	2.66	21.356	0.106
96	29.06	69.79	20.305	0.030	269	73.46	37.46	21.370	0.250
17	59.55	13.33	20.319	0.038	5	3.46	6.04	21.379	0.131
68	48.25	47.99	20.405	0.050	13	58.56	8.75	21.383	0.079
270	77.10	40.04	20.441	0.275	10	66.79	8.66	21.397	0.157
84	29.35	62.12	20.469	0.066	34	23.42	23.91	21.424	0.155
71	39.31	50.39	20.499	0.045	11	22.11	9.31	21.429	0.097
76	17.00	52.69	20.499	0.036	220	15.31	25.46	21.448	0.180
254	52.58	58.52	20.511	0.125	81	9.07	59.59	21.454	0.102
6	55.44	6.44	20.528	0.039	60	17.35	42.52	21.490	0.090
88	63.23	64.96	20.583	0.036	93	49.87	68.31	21.576	0.198
55	27.84	38.76	20.597	0.044	72	21.68	51.57	21.581	0.092
36	13.29	26.60	20.620	0.084	261	63.55	20.47	21.597	0.086
29	50.53	20.91	20.637	0.036	73	25.38	51.36	21.608	0.098
98	48.18	70.88	20.640	0.089	87	40.23	64.83	21.615	0.185
248	52.38	41.11	20.668	0.101	66	61.07	45.05	21.652	0.086
47	25.81	34.55	20.673	0.031	85	72.30	62.14	21.655	0.342
39	67.55	27.62	20.716	0.041	42	42.12	31.14	21.659	0.258
89	22.21	65.85	20.718	0.043	75	5.38	52.74	21.683	0.098
41	6.31	30.15	20.755	0.064	40	36.39	29.01	21.724	0.106
232	2.80	15.25	20.828	0.173	258	59.73	71.80	21.730	3.684
62	26.55	44.37	20.838	0.038	31	61.56	23.41	21.732	0.095
22	47.59	15.37	20.845	0.043	9	44.23	8.62	21.742	0.199
54	18.94	39.39	20.912	0.036	43	49.16	31.48	21.750	0.174

8	10.56	8.68	21.767	0.180	212	22.74	47.27	22.277	0.140
18	25.70	13.82	21.781	0.124	252	50.14	49.90	22.277	0.274
230	32.42	7.98	21.793	0.155	94	10.20	68.63	22.289	0.250
91	56.20	66.73	21.798	0.109	272	72.26	66.07	22.344	0.279
235	28.21	59.43	21.814	0.220	278	43.60	64.88	22.372	0.238
82	39.21	60.29	21.822	0.144	273	75.63	70.10	22.401	0.411
45	61.30	31.98	21.834	0.097	38	50.38	27.11	22.402	0.299
28	31.86	19.90	21.842	0.118	207	20.15	69.31	22.411	0.328
83	16.04	62.53	21.842	0.138	23	56.34	16.74	22.419	0.196
21	32.88	14.99	21.849	0.086	253	49.70	60.40	22.432	0.234
268	77.53	26.35	21.850	0.260	203	6.98	62.16	22.439	0.206
78	20.70	55.54	21.854	0.093	32	69.51	22.96	22.443	0.221
27	39.56	19.02	21.867	0.081	256	56.79	64.15	22.450	0.194
64	74.24	44.00	21.876	0.161	53	60.22	38.22	22.457	0.181
16	37.11	13.64	21.907	0.093	280	62.09	60.94	22.499	0.200
14	8.09	12.69	21.929	0.232	275	40.83	58.21	22.533	0.254
263	71.33	9.35	21.940	0.140	244	53.11	17.89	22.566	0.210
48	74.21	34.34	21.995	0.174	35	39.28	25.89	22.634	0.247
74	50.36	52.25	21.997	0.213	279	41.92	70.54	22.634	0.365
37	27.53	27.45	22.004	0.192	264	67.69	11.85	22.673	0.559
90	35.13	67.19	22.004	0.169	277	45.74	61.82	22.680	0.274
2	23.04	5.32	22.005	0.165	257	58.46	62.00	22.766	0.258
202	7.25	57.84	22.006	0.151	286	8.11	28.77	22.780	0.361
58	60.28	41.32	22.020	0.121	221	21.19	25.46	22.814	0.474
20	17.89	15.09	22.042	0.244	33	73.84	23.33	22.822	0.313
12	37.45	9.30	22.049	0.103	237	34.25	71.26	22.838	0.742
219	4.12	29.50	22.063	0.219	44	70.20	31.08	22.859	0.293
260	65.17	45.76	22.071	0.132	284	25.56	68.64	22.892	0.321
59	67.46	41.66	22.077	0.130	229	18.31	4.95	22.972	0.401
201	7.37	54.97	22.078	0.138	282	66.83	51.90	23.022	0.333
7	49.74	7.43	22.175	0.177	240	40.05	14.47	23.080	0.297
52	35.20	38.11	22.188	0.159	241	41.53	16.21	23.160	0.320
67	67.70	47.04	22.192	0.147	267	74.05	30.32	23.240	0.537
61	42.43	43.60	22.212	0.151	283	30.74	56.06	23.345	0.637
213	26.10	41.54	22.225	0.198	274	41.47	35.03	23.346	0.465
223	26.14	25.12	22.229	0.300	216	15.04	34.82	23.373	0.442
97	38.74	71.86	22.231	4.261	236	29.22	66.22	23.581	0.853
243	47.77	18.43	22.231	0.176	224	21.41	21.99	23.649	1.058
217	9.82	38.09	22.235	0.206	239	34.70	23.45	23.736	0.689
46	9.97	33.27	22.237	0.202	208	15.43	57.90	24.320	1.348
63	69.96	43.95	22.238	0.150	281	67.09	55.63	24.460	1.855

M71DEEP1_2

80	69.74	57.69	18.820	0.070	248	51.62	40.22	20.462	0.165
51	4.12	35.90	18.910	0.025	271	76.40	38.01	20.469	0.272
225	18.32	17.93	18.955	0.009	55	27.02	37.79	20.490	0.040
1	72.85	2.29	19.172	0.087	29	49.73	19.91	20.517	0.034
86	8.05	64.04	19.279	0.022	36	12.35	25.82	20.575	0.057
249	50.09	44.37	19.432	0.099	47	25.02	33.62	20.580	0.028
15	62.51	10.53	19.435	0.033	270	74.70	38.80	20.584	0.117
49	44.06	33.85	19.597	0.022	88	62.54	63.88	20.682	0.039
95	16.93	67.98	19.612	0.071	100	72.44	70.84	20.704	0.089
57	50.62	38.82	19.718	0.092	62	25.73	43.44	20.724	0.035
25	8.36	17.90	19.795	0.051	92	2.69	66.91	20.730	0.098
3	33.02	4.02	19.924	0.032	39	66.71	26.57	20.759	0.044
4	59.79	4.01	19.985	0.032	89	21.58	64.98	20.762	0.102
96	28.45	68.98	20.085	0.033	70	28.06	48.92	20.781	0.037
17	58.57	12.19	20.242	0.048	54	18.01	38.45	20.819	0.034
68	47.49	46.93	20.272	0.103	79	51.05	57.30	20.831	0.067
6	54.50	5.30	20.307	0.034	22	46.66	14.35	20.847	0.047
232	0.89	14.57	20.372	0.227	69	35.04	48.08	20.873	0.047
84	28.66	61.25	20.391	0.076	5	2.38	5.19	20.893	0.077
76	16.20	51.84	20.400	0.036	258	59.07	71.64	20.907	0.109
71	38.45	49.52	20.422	0.044	204	11.95	64.59	20.926	0.114
41	5.57	29.40	20.429	0.059	255	53.04	58.17	20.933	0.061
98	47.67	70.04	20.453	0.095	56	10.64	39.10	20.992	0.124

265	72.06	13.03	20.994	0.072
227	4.15	14.28	21.020	0.127
231	29.58	1.44	21.088	0.129
85	71.48	61.17	21.092	0.301
30	55.46	20.39	21.108	0.053
269	72.80	36.62	21.138	0.190
24	61.33	16.16	21.142	0.078
99	62.78	69.98	21.181	0.140
10	65.77	7.25	21.210	0.095
14	7.19	11.97	21.243	0.137
50	21.01	35.18	21.244	0.051
224	20.70	20.50	21.268	0.109
81	8.29	58.90	21.282	0.114
11	20.94	8.29	21.291	0.102
77	45.77	54.10	21.297	0.134
34	22.60	22.94	21.309	0.071
75	4.52	51.98	21.397	0.109
60	16.47	41.67	21.407	0.058
13	57.60	7.65	21.418	0.136
220	14.37	24.81	21.423	0.126
93	49.34	67.32	21.456	0.209
73	24.48	50.43	21.456	0.097
261	62.66	19.30	21.462	0.095
72	20.91	50.58	21.470	0.066
78	19.87	54.53	21.486	0.067
9	43.27	7.76	21.533	0.210
237	33.28	71.46	21.573	0.147
43	48.30	30.08	21.576	0.166
40	35.54	27.98	21.582	0.105
2	21.98	4.65	21.600	0.148
42	41.13	30.21	21.620	0.128
12	36.50	8.14	21.623	0.069
262	60.68	10.10	21.629	0.247
66	60.29	44.04	21.635	0.090
21	31.83	14.01	21.665	0.066
31	60.69	22.43	21.668	0.103
27	38.77	18.08	21.671	0.063
28	31.10	18.92	21.678	0.064
202	6.42	57.06	21.699	0.152
91	55.63	65.97	21.721	0.090
18	24.58	12.66	21.745	0.114
7	48.81	6.29	21.751	0.142
90	34.68	66.53	21.770	0.146
45	60.28	31.03	21.778	0.088
63	69.21	42.94	21.782	0.106
8	9.04	7.80	21.796	0.154
252	49.48	49.01	21.800	0.387
74	49.62	51.13	21.816	0.249
83	15.44	61.73	21.821	0.189
217	8.70	38.05	21.828	0.264
37	26.98	26.58	21.838	0.107
64	73.19	42.85	21.844	0.170
16	36.29	12.62	21.849	0.084
48	73.49	33.29	21.854	0.161
219	2.89	28.51	21.856	0.171
97	37.73	71.15	21.859	0.159
201	6.62	54.23	21.859	0.169
82	38.51	59.33	21.861	0.105
246	45.63	35.77	21.865	0.185
263	69.63	8.02	21.903	0.194
260	64.17	44.71	21.919	0.119
87	39.30	64.23	21.923	0.120
234	27.26	58.41	21.948	0.271
230	31.50	6.99	21.962	0.204
52	34.28	37.16	21.964	0.138
94	9.42	67.91	21.977	0.278
272	71.50	64.99	21.986	0.180
58	59.56	40.33	22.006	0.125
59	66.49	40.58	22.022	0.128
61	41.79	42.72	22.026	0.121
243	46.97	17.58	22.028	0.173
46	9.24	32.42	22.035	0.199
268	76.36	25.23	22.035	0.288
44	69.21	29.51	22.046	0.138
67	66.89	46.09	22.072	0.136
223	25.02	25.40	22.095	0.156
284	25.05	67.77	22.108	0.211
20	16.79	14.14	22.137	0.154
278	42.56	64.14	22.191	0.143
205	11.41	67.42	22.207	0.333
212	21.68	46.07	22.222	0.182
276	40.03	62.08	22.234	0.193
222	25.37	23.35	22.236	0.174
213	25.07	40.43	22.239	0.194
53	59.16	37.34	22.301	0.162
273	74.43	68.75	22.307	0.383
32	68.54	22.17	22.323	0.192
38	49.50	26.05	22.339	0.293
257	57.08	61.01	22.373	0.185
256	56.18	63.11	22.401	0.197
35	38.57	24.81	22.422	0.225
253	48.94	59.34	22.437	0.189
244	51.95	16.88	22.463	0.199
264	66.91	10.27	22.480	0.376
221	20.41	24.35	22.488	0.247
203	5.70	61.35	22.511	0.328
280	61.72	60.13	22.514	0.204
286	7.85	27.78	22.520	0.415
23	55.09	15.69	22.532	0.228
279	41.21	69.61	22.558	0.304
33	73.24	21.99	22.667	0.254
285	40.05	34.14	22.693	0.323
275	40.14	57.25	22.715	0.219
277	44.93	60.82	22.723	0.225
241	41.11	15.24	22.837	0.357
240	38.83	13.68	22.923	0.392
282	66.15	50.86	23.064	0.342
216	14.52	34.48	23.107	0.408
229	14.19	4.38	23.373	0.583
239	33.19	22.14	23.410	0.313
236	29.09	64.67	23.667	1.371
283	29.60	54.53	24.018	1.382
208	14.65	57.67	24.165	1.305
267	74.07	29.24	24.300	1.378

M71DEEP2_1

102	40.69	70.25	17.205	0.031
206	18.28	71.83	17.220	0.020
59	55.95	42.75	17.236	0.008
60	71.92	42.81	18.503	0.028
17	17.66	13.98	18.570	0.021
78	57.33	54.45	19.244	0.026
23	66.37	16.81	19.341	0.023
41	47.95	30.90	19.401	0.035
5	60.97	4.69	19.532	0.046
53	57.67	38.33	19.654	0.042
19	2.68	15.12	19.662	0.037
70	58.34	50.15	19.866	0.043
55	16.41	40.17	20.142	0.058
18	33.64	13.96	20.210	0.047

12	7.88	9.77	20.331	0.062	47	36.01	35.25	21.936	0.154
57	32.22	40.30	20.542	0.061	7	40.37	6.27	21.946	0.151
50	62.19	36.05	20.585	0.106	28	51.15	21.75	21.975	0.147
81	73.39	54.55	20.615	0.116	8	19.64	7.12	21.990	0.186
89	26.34	58.48	20.654	0.078	3	39.29	2.44	22.005	0.155
43	61.45	32.79	20.659	0.089	99	74.75	66.97	22.072	0.288
51	32.01	36.98	20.672	0.054	36	31.40	28.32	22.145	0.187
100	14.74	68.60	20.845	0.107	35	42.64	28.05	22.151	0.251
15	74.08	10.81	20.849	0.090	307	45.31	32.21	22.184	0.359
54	73.83	38.58	20.949	0.146	69	15.33	48.72	22.192	0.329
33	31.52	25.19	20.963	0.064	97	29.37	66.23	22.312	0.199
201	35.68	57.04	20.988	0.110	14	56.33	10.21	22.351	0.199
229	6.33	7.01	21.000	0.107	20	41.59	16.17	22.374	0.269
21	47.67	15.03	21.021	0.068	103	49.26	69.66	22.400	0.351
9	70.19	8.08	21.042	0.104	86	61.91	57.49	22.484	0.332
22	25.02	16.01	21.047	0.087	42	12.72	31.71	22.516	0.217
203	14.75	45.12	21.116	0.125	80	68.53	55.11	22.530	0.533
58	45.07	39.83	21.120	0.089	16	29.13	12.53	22.582	0.367
101	60.19	68.25	21.163	0.106	68	21.86	46.84	22.610	0.231
48	74.24	34.65	21.163	0.187	85	50.89	56.79	22.641	0.299
13	25.19	9.97	21.231	0.091	49	51.68	35.45	22.651	0.235
96	49.56	65.11	21.271	0.113	44	18.89	34.29	22.659	0.286
67	64.81	45.41	21.298	0.163	10	38.26	9.18	22.706	0.292
84	45.96	57.32	21.361	0.097	302	3.82	32.23	22.774	0.300
92	38.95	62.22	21.394	0.076	46	5.33	35.67	22.799	0.314
65	33.54	45.79	21.406	0.085	205	9.59	48.57	22.857	0.508
71	74.50	50.06	21.418	0.186	218	27.94	40.01	22.922	0.318
26	46.99	19.34	21.461	0.094	207	34.19	65.40	23.060	0.446
231	16.09	1.48	21.474	1.258	52	10.73	37.18	23.068	0.386
64	48.21	44.86	21.476	0.228	40	38.40	31.28	23.155	0.498
66	39.64	46.28	21.485	0.134	312	71.10	33.32	23.211	1.256
98	63.35	66.65	21.486	0.144	211	59.93	60.21	23.221	0.644
224	64.04	31.12	21.489	0.183	1	3.94	3.07	23.258	0.734
76	10.23	53.60	21.532	0.119	305	35.55	25.07	23.314	0.552
77	26.56	53.70	21.556	0.202	2	10.43	2.74	23.418	0.862
311	60.59	39.81	21.602	0.178	209	42.65	58.43	23.481	0.727
24	13.56	18.59	21.639	0.167	4	28.50	4.00	23.613	0.706
11	2.32	10.99	21.641	0.225	30	4.76	25.12	23.617	0.785
87	10.83	57.59	21.696	0.136	34	46.92	25.07	23.627	0.676
32	21.77	25.09	21.756	0.099	6	36.73	6.09	23.811	0.828
37	67.89	29.29	21.762	0.201	93	11.27	63.53	23.914	0.958
29	67.52	24.04	21.770	0.124	73	39.48	51.26	23.928	1.214
82	15.46	57.37	21.786	0.142	61	4.79	44.52	23.941	0.739
104	54.13	69.75	21.793	0.166	91	64.27	59.91	24.161	1.853
31	16.66	24.79	21.860	0.140	38	7.70	29.69	24.230	1.106
220	41.87	31.93	21.868	0.211	304	17.36	20.45	24.343	1.497
75	60.13	53.60	21.903	0.268	88	6.58	58.83	24.896	2.319
94	23.09	65.41	21.919	0.200	27	5.33	19.94	25.016	2.055
232	54.35	1.66	21.922	0.237	25	29.33	18.78	27.622	9.999

M71DEEP2_2

102	40.82	67.30	17.393	0.036	70	58.40	47.20	20.110	0.043
206	18.64	69.03	17.494	0.044	5	60.88	1.50	20.150	0.063
59	56.03	39.88	17.514	0.006	55	16.63	37.16	20.493	0.051
17	17.69	10.94	18.841	0.028	100	15.28	65.65	20.564	0.340
81	77.60	50.58	18.971	0.067	12	8.03	6.66	20.715	0.109
78	57.27	51.57	19.548	0.032	50	62.28	33.09	20.870	0.069
23	66.36	13.87	19.634	0.022	43	61.45	29.87	20.873	0.065
41	47.98	27.94	19.652	0.032	51	32.03	34.10	20.931	0.045
19	3.03	11.99	19.897	0.047	89	26.44	55.79	20.935	0.072
53	57.80	35.21	19.925	0.035	57	32.23	37.43	21.021	0.050

15	74.16	7.49	21.145	0.105	36	31.74	25.62	22.474	0.215
22	24.78	13.10	21.173	0.071	18	33.21	11.02	22.549	0.245
54	78.01	39.00	21.174	0.563	103	49.33	66.95	22.552	0.278
48	73.91	31.90	21.192	0.085	69	15.56	45.74	22.602	0.330
229	6.26	3.89	21.194	0.167	307	44.63	29.38	22.618	0.488
33	31.51	22.25	21.265	0.071	310	48.58	39.45	22.618	0.294
201	36.25	54.07	21.380	0.117	4	26.18	0.81	22.721	0.677
58	45.14	36.75	21.413	0.095	42	12.78	28.85	22.727	0.220
63	14.90	42.05	21.431	0.123	97	29.22	63.35	22.736	0.248
21	47.67	12.11	21.439	0.083	95	34.15	62.56	22.782	0.395
92	38.90	59.40	21.528	0.104	302	4.36	29.26	22.782	0.242
101	60.27	65.23	21.528	0.106	46	5.96	32.63	22.800	0.248
67	65.41	42.12	21.566	0.238	205	9.75	44.89	22.848	0.357
84	45.92	54.47	21.623	0.116	3	39.53	-0.42	22.879	9.999
98	63.58	63.92	21.639	0.117	56	27.93	37.09	22.895	0.283
65	33.65	42.93	21.642	0.116	94	24.62	60.95	22.919	0.309
66	39.73	43.39	21.645	0.115	44	18.62	31.30	22.935	0.352
26	46.97	16.50	21.649	0.094	210	58.02	56.01	23.037	0.408
9	70.24	5.13	21.725	0.177	49	52.18	32.68	23.050	0.336
96	49.96	62.12	21.744	0.113	207	35.13	66.43	23.053	0.521
99	74.16	64.27	21.783	0.136	30	5.14	21.92	23.060	0.350
13	24.98	6.70	21.801	0.119	10	38.69	5.90	23.104	0.369
208	47.61	60.83	21.816	0.158	68	21.72	43.57	23.128	0.398
215	59.82	50.83	21.832	0.265	75	63.28	48.97	23.155	0.425
24	14.04	15.31	21.840	0.175	306	41.90	15.03	23.178	0.399
37	67.72	26.38	21.853	0.143	2	11.54	0.24	23.209	4.323
29	67.59	21.18	21.878	0.107	93	11.23	60.79	23.225	0.412
87	10.81	54.89	21.893	0.150	40	38.28	28.30	23.261	0.373
76	10.21	50.83	21.927	0.187	61	5.37	40.79	23.347	0.534
60	73.94	41.47	21.966	0.238	52	11.67	34.79	23.358	0.434
1	4.49	-0.11	22.004	9.999	14	56.48	6.96	23.358	0.422
11	2.83	7.53	22.021	0.323	91	64.76	57.95	23.369	0.529
31	16.93	21.91	22.022	0.164	6	36.51	3.03	23.430	0.701
72	10.90	48.02	22.033	0.131	20	42.10	12.07	23.438	0.508
104	54.44	66.88	22.036	0.167	88	6.17	56.63	23.444	0.551
311	59.93	36.80	22.057	0.260	305	35.20	22.19	23.445	0.525
82	15.43	54.36	22.073	0.170	211	60.62	57.77	23.513	0.492
32	21.62	21.96	22.077	0.173	38	6.64	27.22	23.667	0.562
64	48.23	42.25	22.079	0.194	85	51.14	53.01	23.681	0.580
35	43.32	25.11	22.190	0.238	79	18.05	52.28	23.687	0.753
47	36.15	32.21	22.195	0.139	27	6.10	16.95	23.742	0.710
28	50.97	18.85	22.200	0.147	86	62.04	54.20	23.769	0.717
80	68.72	52.13	22.207	0.196	224	65.35	28.83	23.797	0.920
7	40.46	2.89	22.224	0.199	304	16.98	16.47	24.275	1.645
220	41.92	28.92	22.237	0.258	34	46.36	22.46	24.291	0.937
202	26.21	50.23	22.240	0.272	73	39.90	47.98	24.472	1.529
312	70.81	30.24	22.291	0.222	74	47.02	48.17	25.855	4.847
222	45.15	39.96	22.303	0.210	25	29.22	16.64	26.949	9.999
8	20.00	4.20	22.329	0.197	90	65.08	57.45	31.974	9.999
16	29.05	9.52	22.431	0.215	225	61.18	17.10	33.241	9.999

M4SM6

344	12.78	77.95	14.245	0.055	56	139.31	13.12	18.500	0.009
704	190.39	21.76	15.758	0.056	129	146.59	29.04	18.564	0.009
308	11.14	70.07	15.983	0.020	398	17.70	79.61	18.703	0.217
289	59.60	63.85	16.496	0.013	657	18.53	149.26	18.712	0.070
365	124.50	82.30	17.121	0.004	311	204.71	69.96	18.735	0.015
10	114.52	3.33	17.676	0.017	327	19.69	74.76	18.791	0.097
644	2.39	146.96	17.932	0.031	473	97.89	105.38	18.794	0.037
421	213.90	92.29	18.250	0.005	613	24.08	140.09	18.798	0.024
313	108.09	71.22	18.281	0.008	353	23.61	79.51	18.869	0.102
63	160.28	14.12	18.293	0.011	440	79.96	95.43	18.886	0.018

702	173.50	63.47	18.953	0.033
485	185.36	109.33	18.992	0.019
575	43.02	130.66	19.020	0.046
326	145.36	73.15	19.043	0.009
196	106.56	42.57	19.139	0.013
562	44.57	127.36	19.175	0.045
113	11.93	26.20	19.186	0.013
57	205.06	13.14	19.239	0.026
141	6.09	32.65	19.255	0.015
703	174.83	61.52	19.257	0.043
329	88.85	74.21	19.280	0.008
239	159.85	51.34	19.286	0.015
333	33.27	75.69	19.330	0.029
356	105.54	79.48	19.345	0.010
297	16.25	72.30	19.354	0.096
449	83.31	99.12	19.408	0.032
134	261.61	29.46	19.413	0.031
29	291.38	6.60	19.425	0.038
153	130.57	33.67	19.439	0.019
247	111.44	54.13	19.440	0.011
126	295.16	27.98	19.442	0.043
656	224.05	148.05	19.467	0.020
551	101.38	125.38	19.469	0.029
59	72.01	13.40	19.469	0.019
370	133.78	82.80	19.481	0.014
106	79.80	23.32	19.490	0.013
62	125.69	13.86	19.582	0.013
151	112.90	34.22	19.590	0.014
610	262.92	139.01	19.597	0.018
360	168.76	80.62	19.626	0.021
638	188.59	144.40	19.630	0.015
472	48.30	105.32	19.637	0.033
552	161.96	125.00	19.662	0.020
496	170.21	111.13	19.673	0.018
482	7.87	108.58	19.699	0.043
48	186.59	11.38	19.702	0.027
50	29.85	11.61	19.719	0.044
574	20.39	130.46	19.750	0.036
8	73.24	4.17	19.768	0.069
369	6.41	82.96	19.805	0.081
49	191.91	10.85	19.817	0.029
545	205.08	123.28	19.824	0.013
84	60.74	18.33	19.863	0.029
348	277.69	77.85	19.873	0.023
454	90.74	99.51	19.884	0.033
661	264.29	148.52	19.887	0.026
609	189.09	139.36	19.894	0.019
649	201.90	147.00	19.904	0.017
37	43.67	8.67	19.906	0.050
150	81.49	34.06	19.915	0.018
179	190.05	38.86	19.917	0.026
441	125.53	96.19	19.944	0.021
185	204.92	39.81	19.961	0.024
281	287.76	60.34	19.989	0.021
319	244.87	71.21	20.013	0.022
39	92.65	8.71	20.018	0.027
532	199.85	119.82	20.020	0.016
513	146.06	116.07	20.034	0.023
607	107.89	138.33	20.041	0.041
266	18.01	67.74	20.093	0.128
583	9.14	132.67	20.105	0.029
620	74.42	141.18	20.126	0.029
503	217.83	112.55	20.162	0.018
246	95.55	53.55	20.193	0.019
217	22.12	46.36	20.200	0.025
603	155.54	138.08	20.203	0.031
362	224.02	80.64	20.220	0.049
280	225.35	60.91	20.221	0.021
578	181.39	130.51	20.223	0.019
309	22.48	72.28	20.224	0.157
463	176.88	103.84	20.229	0.026
558	208.84	126.10	20.231	0.018
103	143.31	23.14	20.249	0.028
254	298.28	55.82	20.250	0.036
376	166.36	83.42	20.284	0.036
594	267.16	133.45	20.298	0.028
324	92.80	71.56	20.308	0.021
201	216.45	43.63	20.308	0.026
542	138.45	122.44	20.314	0.029
706	84.09	95.30	20.353	0.072
166	287.70	35.50	20.381	0.058
476	79.00	106.67	20.395	0.039
437	62.69	95.04	20.408	0.043
33	107.08	8.16	20.410	0.023
387	130.19	85.31	20.431	0.048
420	162.18	91.84	20.437	0.036
520	23.21	117.75	20.445	0.036
640	216.17	145.62	20.450	0.028
237	64.26	51.47	20.467	0.057
291	4.21	64.85	20.475	0.045
238	152.59	51.82	20.490	0.019
616	241.37	140.00	20.512	0.037
250	275.57	53.53	20.513	0.019
410	11.39	90.72	20.515	0.056
510	0.39	115.98	20.531	0.217
46	153.77	10.94	20.535	0.030
11	197.35	4.09	20.538	0.034
284	206.29	61.94	20.559	0.034
654	106.77	148.09	20.572	0.044
140	207.96	31.51	20.578	0.037
336	184.42	75.72	20.589	0.026
7	278.43	1.66	20.600	0.067
664	235.23	150.89	20.603	0.051
127	93.15	28.41	20.608	0.036
128	117.09	28.93	20.612	0.034
645	80.36	146.73	20.616	0.041
167	6.52	36.68	20.618	0.052
321	267.17	70.21	20.633	0.023
71	67.90	15.78	20.645	0.051
517	108.87	116.46	20.672	0.032
606	68.84	138.84	20.674	0.040
338	4.98	76.22	20.687	0.239
705	11.36	31.26	20.691	0.056
602	147.96	138.08	20.723	0.039
169	122.77	36.28	20.733	0.037
203	50.12	44.67	20.740	0.039
660	186.86	149.20	20.743	0.039
588	36.58	133.55	20.749	0.045
214	252.89	46.05	20.773	0.044
466	55.96	105.17	20.784	0.074
418	95.44	92.03	20.817	0.030
122	82.78	27.68	20.824	0.045
505	14.14	113.74	20.835	0.049
263	205.63	58.28	20.840	0.043
625	229.02	141.81	20.844	0.026
701	228.11	149.22	20.850	0.068
614	158.78	139.67	20.855	0.056
417	77.31	91.98	20.869	0.099
526	17.30	119.17	20.873	0.053
79	179.49	17.81	20.880	0.048
392	30.27	86.34	20.883	0.054
15	102.64	4.62	20.888	0.037
567	4.54	128.91	20.896	0.057
653	95.11	147.54	20.900	0.076
547	10.39	124.16	20.900	0.048
40	135.43	8.76	20.901	0.055
213	242.45	46.12	20.905	0.057

114	24.39	25.46	20.913	0.058
411	15.57	91.04	20.915	0.078
528	170.40	119.32	20.917	0.036
639	254.01	144.77	20.921	0.042
521	44.96	118.23	20.924	0.043
388	145.86	85.61	20.941	0.035
286	43.59	63.02	20.958	0.049
277	96.54	61.18	20.958	0.036
97	123.87	21.52	20.962	0.043
174	117.04	37.49	20.963	0.048
2	46.80	2.48	20.966	0.059
206	268.74	44.50	20.971	0.035
556	72.06	125.44	20.979	0.061
259	221.76	56.83	20.985	0.044
530	250.60	119.25	20.986	0.028
216	10.12	46.50	20.994	0.053
157	292.52	33.80	20.996	0.111
233	286.28	50.40	21.017	0.094
467	63.82	104.75	21.036	0.045
563	68.38	127.33	21.043	0.061
253	250.14	55.71	21.050	0.049
98	128.73	21.47	21.069	0.047
91	234.36	20.58	21.070	0.033
479	115.91	107.90	21.076	0.036
592	135.63	134.32	21.089	0.032
45	130.27	10.68	21.096	0.051
229	94.20	49.94	21.118	0.049
152	119.81	34.26	21.135	0.058
232	251.19	50.47	21.166	0.059
707	61.35	92.18	21.192	0.086
101	33.49	23.20	21.205	0.073
448	189.23	97.60	21.205	0.079
334	44.55	75.24	21.211	0.097
176	209.43	38.74	21.225	0.078
663	126.30	150.19	21.244	0.058
629	31.76	142.62	21.250	0.067
226	60.86	49.16	21.253	0.111
538	221.51	121.42	21.254	0.049
82	4.84	18.43	21.258	0.131
591	120.38	133.78	21.259	0.040
119	158.52	27.17	21.272	0.058
243	60.07	52.93	21.274	0.116
77	128.79	17.69	21.275	0.060
623	136.20	140.54	21.282	0.038
615	220.79	139.37	21.295	0.043
536	258.66	120.94	21.312	0.062
322	44.68	71.68	21.313	0.109
19	128.09	5.77	21.320	0.054
402	123.14	89.28	21.321	0.070
367	250.98	81.96	21.330	0.038
131	199.11	27.94	21.337	0.130
136	245.89	31.47	21.340	0.045
624	86.03	142.15	21.343	0.075
590	105.37	133.88	21.344	0.107
115	45.00	25.34	21.355	0.084
601	125.71	137.34	21.356	0.046
181	52.40	39.64	21.362	0.073
164	180.23	35.48	21.363	0.058
102	58.20	22.99	21.382	0.071
135	44.10	30.41	21.384	0.091
597	165.88	135.30	21.403	0.051
105	52.90	23.61	21.409	0.054
621	99.89	141.21	21.434	0.078
335	126.12	75.67	21.436	0.117
323	74.78	72.00	21.474	0.045
90	166.77	20.54	21.490	0.074
593	147.54	134.44	21.496	0.079
438	208.18	95.22	21.502	0.080
519	270.66	116.67	21.503	0.054
211	164.64	45.48	21.511	0.059
199	113.97	43.47	21.518	0.065
89	241.32	19.39	21.522	0.054
120	184.43	26.37	21.529	0.105
340	97.54	76.43	21.538	0.051
132	53.67	30.25	21.559	0.068
527	39.34	119.38	21.602	0.076
301	114.49	66.89	21.619	0.069
450	116.00	99.12	21.624	0.056
444	25.75	96.76	21.624	0.088
94	279.55	20.62	21.662	0.098
124	237.25	27.68	21.676	0.057
564	296.13	126.78	21.709	0.082
453	3.54	100.12	21.711	0.074
5	163.56	1.54	21.714	0.132
9	85.85	3.78	21.715	0.097
565	34.82	127.91	21.727	0.102
397	204.28	88.17	21.746	0.081
632	103.69	142.77	21.769	0.121
445	10.66	98.34	21.779	0.088
379	50.66	84.09	21.799	0.129
650	248.90	147.32	21.805	0.085
355	95.34	80.16	21.817	0.064
428	32.02	93.90	21.819	0.100
258	182.73	56.74	21.821	0.080
207	286.93	44.58	21.824	0.151
598	197.22	135.55	21.838	0.061
478	74.45	107.46	21.844	0.147
3	99.29	-1.27	21.850	9.999
32	80.77	8.07	21.852	0.117
20	181.66	7.09	21.863	0.148
304	40.82	68.14	21.867	0.133
294	223.43	64.71	21.870	0.095
230	242.57	49.58	21.881	0.140
261	12.19	57.94	21.885	0.155
342	193.85	77.10	21.905	0.079
310	118.42	69.91	21.906	0.094
587	29.21	133.91	21.910	0.083
182	57.61	39.51	21.916	0.112
477	71.00	108.18	21.926	0.134
403	177.61	88.66	21.933	0.074
459	110.81	103.31	21.942	0.072
139	191.87	31.70	21.948	0.103
447	146.39	97.63	21.954	0.087
509	293.78	115.40	21.997	0.099
4	139.77	2.77	22.004	0.085
231	10.01	55.02	22.006	0.135
271	22.39	60.35	22.009	0.182
572	244.50	130.26	22.018	0.088
406	141.49	89.79	22.027	0.096
109	7.75	26.92	22.032	0.147
641	238.57	149.00	22.033	0.101
525	215.12	117.80	22.033	0.094
290	267.24	63.72	22.033	0.073
461	21.55	104.02	22.054	0.148
634	275.60	142.64	22.055	0.099
55	104.34	12.29	22.066	0.103
251	37.31	55.80	22.067	0.135
107	217.98	23.36	22.075	0.107
160	204.70	34.81	22.076	0.160
658	57.67	149.63	22.110	0.126
34	120.53	7.43	22.135	0.178
241	6.61	53.07	22.138	0.182
96	88.60	22.23	22.145	0.076
183	134.85	40.01	22.154	0.101
512	99.63	115.40	22.157	0.096
550	91.93	123.88	22.181	0.088
375	152.22	83.60	22.188	0.139

357	160.76	80.28	22.205	0.157
480	163.21	107.81	22.211	0.088
659	110.29	147.82	22.216	0.139
424	235.63	93.16	22.221	0.130
236	53.11	52.03	22.244	0.123
504	289.78	112.86	22.250	0.120
451	216.75	98.34	22.261	0.132
121	27.64	28.09	22.275	0.205
498	223.17	111.56	22.275	0.126
24	266.25	5.10	22.282	0.141
67	147.03	14.42	22.324	0.181
223	191.12	48.15	22.330	0.115
581	263.60	131.09	22.348	0.171
275	149.30	59.61	22.350	0.115
306	53.36	69.00	22.357	0.147
497	106.33	112.74	22.371	0.139
276	272.17	59.68	22.375	0.106
76	78.72	17.64	22.390	0.164
531	8.33	119.79	22.404	0.189
429	48.20	93.79	22.404	0.129
458	146.67	101.23	22.418	0.134
219	138.53	46.49	22.438	0.146
180	23.71	40.07	22.440	0.193
293	161.22	64.65	22.445	0.207
47	170.51	10.59	22.449	0.191
381	186.79	85.35	22.456	0.133
604	184.97	137.73	22.458	0.183
605	270.03	137.16	22.459	0.205
221	118.20	47.70	22.483	0.152
431	168.99	93.46	22.497	0.214
358	188.16	79.50	22.510	0.139
72	172.12	16.08	22.515	0.214
442	226.72	95.88	22.524	0.143
474	144.31	105.46	22.544	0.145
30	8.13	7.60	22.545	0.339
154	155.11	34.26	22.553	0.132
209	44.74	46.03	22.560	0.193
475	202.67	106.32	22.584	0.124
662	285.37	148.80	22.587	0.156
244	181.82	53.28	22.606	0.167
395	84.08	88.09	22.611	0.132
6	254.39	2.60	22.620	0.190
192	72.51	41.70	22.623	0.164
252	75.97	55.60	22.625	0.146
270	235.32	58.85	22.636	0.128
396	116.80	87.17	22.637	0.211
400	51.87	87.79	22.643	0.203
87	139.41	19.77	22.649	0.294
413	65.63	91.53	22.665	0.186
240	233.76	51.21	22.666	0.125
523	64.76	117.93	22.676	0.211
78	144.62	17.28	22.726	0.318
81	258.53	17.86	22.735	0.203
407	248.01	90.42	22.742	0.134
541	5.76	123.44	22.776	0.282
296	281.50	64.02	22.788	0.258
386	44.19	86.01	22.789	0.223
630	50.80	143.59	22.795	0.206
302	168.71	66.51	22.797	0.378
41	175.40	9.13	22.804	0.268
307	213.17	68.39	22.818	0.178
23	231.63	5.85	22.828	0.144
409	297.84	89.15	22.831	0.246
267	26.46	59.55	22.837	0.318
298	99.54	66.34	22.844	0.197
436	22.61	95.13	22.847	0.277
341	119.56	76.54	22.860	0.230
13	224.53	3.19	22.861	0.184
222	185.08	49.68	22.865	0.199
168	68.14	36.39	22.871	0.196
543	176.37	122.08	22.875	0.215
272	103.07	58.96	22.884	0.206
100	18.00	23.62	22.886	0.321
260	269.59	56.17	22.887	0.160
399	47.14	88.90	22.910	0.244
456	229.71	100.81	22.915	0.206
184	197.59	39.26	22.917	0.173
548	51.38	125.23	22.924	0.292
292	144.59	65.49	22.930	0.226
225	299.51	48.65	22.938	0.455
312	239.92	68.47	22.941	0.304
35	146.77	8.66	22.946	0.257
380	64.98	83.26	22.951	0.225
204	180.29	44.50	22.953	0.225
143	72.39	32.96	22.957	0.243
173	29.93	41.12	22.960	0.232
622	130.57	140.20	22.967	0.186
371	180.63	82.79	22.978	0.219
393	192.31	87.02	22.996	0.197
518	206.56	116.83	22.997	0.197
483	62.09	108.42	22.997	0.295
514	154.04	115.32	22.997	0.189
560	264.86	126.32	23.011	0.265
314	125.77	70.60	23.019	0.377
144	138.99	32.71	23.021	0.286
146	177.18	33.90	23.023	0.265
60	111.56	13.42	23.025	0.290
274	142.05	58.35	23.038	0.288
147	274.26	32.04	23.044	0.348
529	187.47	118.19	23.044	0.174
318	180.58	69.04	23.050	0.255
337	251.65	75.23	23.062	0.174
382	231.47	85.46	23.076	0.192
652	51.74	148.37	23.086	0.263
584	89.96	133.60	23.112	0.191
589	97.46	133.07	23.127	0.197
627	282.38	142.17	23.132	0.346
14	242.83	3.02	23.148	0.232
555	56.19	126.89	23.150	0.338
419	133.73	91.04	23.159	0.482
573	249.88	130.79	23.160	0.253
373	39.90	83.26	23.176	0.299
577	127.37	130.47	23.176	0.222
248	135.26	54.12	23.185	0.330
149	19.95	34.86	23.192	0.375
414	151.25	90.37	23.195	0.311
27	278.09	6.49	23.195	0.530
269	164.95	57.65	23.203	0.375
600	5.99	136.04	23.209	0.450
553	245.07	124.42	23.246	0.255
242	11.48	104.74	23.248	0.280
582	202.04	131.81	23.264	0.225
299	192.89	66.79	23.268	0.232
568	230.99	127.46	23.273	0.362
460	220.44	101.99	23.273	0.283
224	272.05	48.33	23.281	0.290
305	141.64	68.52	23.283	0.357
389	215.52	85.49	23.294	0.380
228	19.75	49.62	23.320	0.476
283	114.23	61.53	23.322	0.327
608	177.07	138.81	23.322	0.307
508	259.48	117.22	23.331	0.399
366	140.59	82.19	23.333	0.331
384	283.02	85.22	23.343	0.414
651	279.77	146.29	23.358	0.324
85	12.78	19.86	23.384	0.576
618	8.48	142.26	23.386	0.474

43	237.72	9.15	23.402	0.280
464	260.03	103.64	23.418	0.289
300	90.22	68.73	23.418	0.382
524	135.90	116.96	23.429	0.454
99	282.20	23.29	23.435	0.631
484	135.01	109.09	23.441	0.288
278	121.32	61.42	23.445	0.363
554	26.73	127.38	23.453	0.352
569	274.23	129.60	23.455	0.326
21	188.17	6.00	23.471	0.559
446	104.06	99.39	23.474	0.244
469	264.84	102.13	23.486	0.301
195	82.27	43.17	23.490	0.240
345	140.10	78.03	23.491	0.408
325	226.80	71.85	23.495	0.286
486	233.17	109.07	23.498	0.350
515	162.04	114.78	23.514	0.254
626	248.63	141.58	23.518	0.384
175	149.58	38.23	23.521	0.437
112	256.30	24.28	23.528	0.441
489	277.85	109.21	23.533	0.347
378	269.35	82.79	23.540	0.337
288	246.31	62.88	23.550	0.266
88	153.31	19.87	23.571	0.312
372	278.73	83.17	23.571	0.541
443	285.28	95.33	23.578	0.375
54	60.22	13.74	23.585	0.524
596	63.56	135.09	23.585	0.510
642	290.25	144.95	23.589	0.428
188	65.22	41.20	23.593	0.391
73	235.55	15.56	23.593	0.317
586	288.64	132.22	23.603	0.422
58	45.80	13.58	23.609	0.744
540	289.13	123.57	23.621	0.465
186	281.93	40.24	23.629	0.703
295	255.77	65.01	23.632	0.320
194	231.30	41.65	23.656	0.411
172	279.42	36.80	23.663	0.851
507	177.36	114.35	23.668	0.280
234	25.15	51.06	23.670	0.428
390	256.98	85.20	23.671	0.359
159	97.91	34.93	23.692	0.389
38	59.11	7.70	23.699	0.486
361	212.77	80.96	23.722	0.491
197	159.89	43.69	23.725	0.454
315	133.13	71.67	23.726	0.429
455	132.81	99.95	23.790	0.322
516	238.39	115.32	23.792	0.535
264	262.62	58.38	23.800	0.403
317	156.24	71.04	23.806	0.355
220	32.28	47.79	23.810	0.713
502	208.71	112.70	23.818	0.393
579	206.74	130.27	23.841	0.447
218	88.57	47.31	23.843	0.607
256	122.31	56.87	23.845	0.508
83	45.56	19.50	23.850	0.714
177	257.59	38.10	23.861	0.451
430	155.03	93.06	23.868	0.574
53	296.70	11.96	23.874	1.109
178	39.58	38.41	23.883	0.486
95	65.13	23.37	23.900	0.683
249	147.10	53.47	23.902	0.451
262	153.99	57.96	23.907	0.380
36	14.45	8.45	23.907	1.090
108	274.49	23.85	23.908	0.628
279	160.49	61.08	23.922	0.758
12	217.60	3.44	23.935	0.587
42	244.34	8.14	23.939	0.443
111	231.88	25.06	23.944	0.443
347	260.68	77.15	23.949	0.465
506	94.58	114.96	23.965	0.502
359	145.19	81.07	23.967	0.610
425	252.70	92.40	23.980	0.420
351	84.12	78.24	23.993	0.529
488	272.33	111.44	23.995	0.579
350	288.50	78.11	23.998	0.605
104	159.90	22.99	24.007	0.697
303	283.27	72.55	24.019	0.624
118	137.27	26.43	24.034	0.708
161	231.38	35.13	24.049	0.601
571	292.07	127.26	24.068	0.701
432	200.32	93.22	24.069	0.682
631	64.43	144.67	24.082	0.676
494	35.19	111.47	24.085	0.735
539	278.08	124.73	24.094	0.515
452	280.42	100.03	24.112	0.577
462	30.70	103.01	24.135	0.516
415	270.27	90.06	24.139	0.641
499	237.90	111.83	24.164	0.724
585	113.80	133.20	24.176	0.552
544	193.98	123.32	24.186	0.548
208	35.26	45.80	24.195	0.926
611	285.95	140.30	24.195	0.929
405	292.71	89.37	24.197	0.878
434	264.26	94.33	24.209	0.713
595	58.40	134.54	24.212	0.884
423	3.63	92.84	24.219	1.233
646	148.89	145.01	24.227	0.450
383	240.08	84.65	24.236	0.686
331	61.57	73.64	24.236	0.868
501	89.40	114.23	24.247	0.635
580	236.83	130.87	24.313	0.927
75	53.88	17.81	24.315	0.848
227	224.31	49.86	24.324	0.529
92	264.44	21.20	24.328	0.885
155	253.18	33.25	24.336	0.653
28	283.31	6.64	24.342	1.700
158	89.34	36.66	24.359	0.816
133	69.34	31.77	24.391	0.896
162	11.67	36.64	24.416	1.460
320	261.82	70.41	24.425	1.061
500	63.93	113.11	24.434	1.044
330	295.75	69.72	24.468	0.975
189	176.98	41.54	24.482	0.880
481	298.95	108.70	24.483	0.927
576	62.68	130.53	24.488	1.153
487	266.90	109.44	24.492	0.992
22	208.58	5.61	24.494	0.719
533	238.73	120.60	24.499	0.982
354	59.16	79.70	24.505	1.154
385	289.08	88.19	24.509	1.014
110	212.32	25.26	24.534	1.150
190	247.73	40.89	24.534	0.948
468	241.57	104.70	24.534	1.018
433	240.19	93.50	24.541	1.100
148	280.40	33.73	24.542	1.790
26	34.22	6.74	24.546	1.694
80	217.66	17.77	24.547	1.002
491	93.08	110.22	24.560	0.893
394	69.47	90.07	24.579	1.299
245	212.79	54.88	24.593	0.786
215	295.29	45.64	24.594	2.140
408	258.06	89.02	24.605	0.808
557	120.74	125.87	24.655	0.869
495	46.01	110.26	24.684	2.395
198	262.72	42.87	24.689	1.024
328	69.73	73.43	24.731	0.930

65	96.49	14.31	24.749	1.824
265	281.39	57.98	24.757	1.630
535	83.53	120.60	24.762	1.089
316	137.86	70.83	24.804	1.272
426	276.91	93.85	24.898	1.384
116	242.44	25.16	24.945	1.137
537	283.94	121.54	25.008	1.585
255	31.42	57.95	25.141	2.285
282	297.13	59.88	25.144	3.085
401	102.83	88.29	25.160	1.353
612	300.85	138.34	25.192	3.053
549	218.02	124.09	25.317	2.005
285	260.13	61.01	25.414	1.757
1	36.86	2.88	25.432	2.646
170	263.65	37.74	25.491	2.049
412	39.12	90.54	25.506	2.475
212	171.32	46.35	25.506	2.176
332	265.47	75.19	25.704	2.769
202	279.84	43.92	25.733	5.019
457	239.43	100.67	25.753	3.074
130	178.65	29.41	25.938	3.602
145	168.72	32.96	26.225	4.916
346	177.23	77.26	26.376	5.240
635	35.63	144.29	26.464	6.696
163	11.94	59.82	26.467	6.668
193	172.27	41.94	26.820	7.354
636	42.80	145.18	26.868	8.671
200	152.63	43.08	27.355	9.999
377	266.59	81.65	27.608	9.999
470	280.74	100.66	27.626	9.999
68	232.62	15.11	28.200	9.999
363	246.00	80.44	28.272	9.999
511	35.36	117.01	28.468	9.999
61	118.84	14.01	28.594	9.999
633	177.97	142.81	28.651	9.999
416	276.55	90.13	28.750	9.999
268	90.14	59.41	29.086	9.999
570	294.20	140.77	29.332	9.999
492	125.01	110.17	29.789	9.999
343	238.22	77.80	29.978	9.999
648	173.54	146.25	30.193	9.999
339	79.15	76.26	30.239	9.999
352	208.61	78.01	30.343	9.999
465	40.77	104.15	30.506	9.999
647	165.52	145.14	30.555	9.999
171	275.53	37.48	30.829	9.999
156	268.90	32.85	31.011	9.999
534	312.19	128.81	32.912	9.999
165	224.13	35.62	33.133	9.999

M4S_2M4

1	21.74	1.98	23.277	0.323
11	15.39	4.59	23.123	0.268
45	14.79	9.75	23.606	0.390
30	8.25	8.21	22.084	0.109
54	10.35	13.47	22.893	0.216
62	15.10	14.00	24.068	0.606
53	5.38	12.96	21.787	0.090
78	10.92	17.40	22.879	0.205
85	15.08	18.67	23.272	0.318
96	18.31	20.39	23.170	0.295
104	24.15	21.37	23.709	0.472
126	24.37	26.32	20.862	0.035
137	19.03	28.18	23.926	0.647
138	27.13	29.20	22.151	0.116
153	17.98	31.69	25.274	1.983
175	30.59	35.93	24.550	0.956
152	11.05	32.07	20.391	0.025
181	12.48	36.61	23.451	0.354
182	24.83	36.26	24.731	1.371
203	23.68	40.77	22.298	0.120
191	30.38	39.94	26.069	3.564
130	11.61	27.11	19.162	0.009
161	5.70	33.59	19.249	0.008
186	6.04	37.47	20.507	0.025
233	21.73	47.27	20.218	0.020
232	16.64	46.55	23.469	0.376
204	44.73	41.44	26.164	3.954
215	34.53	45.13	32.615	9.999
234	33.57	47.07	24.544	0.962
5	277.71	2.16	20.773	0.058
22	275.77	6.39	23.047	0.451
3	70.54	2.36	20.350	0.082
4	163.10	2.72	21.639	0.059
7	46.83	3.60	20.879	0.051
18	53.00	5.64	23.396	0.410
9	173.29	3.62	23.223	0.282
8	139.17	3.78	21.901	0.102
10	223.63	4.39	22.960	0.274
26	219.31	5.81	23.620	0.499
38	222.44	8.24	25.077	1.942
14	113.89	4.46	17.668	0.009
58	116.95	13.29	24.563	1.471
63	110.98	14.67	23.085	0.356
88	118.95	18.66	32.533	9.999
35	106.52	9.24	20.448	0.034
110	123.19	22.59	21.033	0.061
19	102.12	5.77	20.868	0.052
57	104.05	13.13	22.056	0.148
111	127.95	22.41	21.054	0.067
13	85.22	4.70	21.746	0.081
16	196.54	4.77	20.499	0.035
15	187.18	4.87	24.449	1.449
31	181.41	8.17	21.714	0.141
51	185.69	12.08	19.778	0.033
59	176.45	12.49	25.058	2.146
47	191.05	11.48	19.893	0.034
50	171.17	11.55	22.819	0.280
76	171.14	16.29	22.501	0.210
94	178.51	18.58	21.034	0.060
17	266.06	5.49	22.292	0.124
28	255.35	6.10	24.562	1.343
20	204.73	6.15	23.361	0.321
21	212.48	6.77	23.885	0.667
27	237.63	6.40	23.837	0.568
32	242.44	8.32	24.361	0.901
44	237.06	10.50	24.185	0.782
39	247.12	8.65	24.386	0.924
25	127.44	6.80	21.386	0.082
48	129.65	11.96	21.097	0.066
43	134.96	10.05	20.973	0.072
71	125.14	14.92	19.612	0.020
64	138.70	14.25	18.540	0.009
97	138.79	20.65	22.084	0.195
117	142.77	24.20	20.298	0.038

146	145.95	30.23	18.597	0.016
24	33.09	7.63	24.291	1.652
55	29.47	12.76	19.715	0.032
37	146.63	8.97	22.827	0.167
34	79.84	9.44	21.995	0.076
40	43.41	9.74	19.909	0.033
69	44.78	13.77	23.484	0.738
79	50.43	17.21	24.038	0.864
90	53.49	18.84	24.343	1.248
115	57.85	24.05	21.384	0.092
121	52.37	24.84	21.442	0.079
91	60.33	19.46	19.967	0.028
148	53.26	31.40	21.792	0.102
42	92.19	9.81	20.030	0.017
60	270.22	12.03	23.988	0.809
77	274.00	15.95	26.903	9.999
49	153.17	12.14	20.481	0.037
65	204.33	13.86	19.214	0.023
70	71.59	14.62	19.538	0.018
80	67.63	17.02	20.722	0.052
72	159.78	15.25	18.325	0.016
75	146.30	16.19	22.028	0.109
83	232.24	17.30	23.814	0.523
99	233.92	21.29	21.022	0.041
100	240.66	20.52	21.445	0.059
101	245.46	21.08	23.528	0.398
81	97.93	16.82	23.374	0.316
86	91.37	18.81	23.631	0.384
93	87.03	18.69	23.662	0.377
108	87.84	23.51	22.543	0.133
132	88.31	27.42	22.960	0.218
139	82.25	28.74	20.844	0.035
144	92.68	29.52	20.678	0.029
122	79.38	24.49	19.527	0.011
169	81.08	35.23	19.951	0.017
92	77.68	19.74	22.232	0.147
143	294.44	28.63	19.470	0.022
174	291.61	34.51	21.100	0.091
180	286.99	36.10	20.445	0.044
84	262.29	17.02	25.557	3.652
102	265.35	20.88	26.098	5.921
103	278.53	21.21	21.876	0.146
125	274.92	25.24	23.065	0.386
105	166.34	21.86	21.629	0.087
128	171.55	25.60	25.630	3.722
109	103.92	22.93	24.914	1.035
112	206.71	23.04	23.189	0.274
120	33.16	24.43	21.207	0.075
127	44.35	26.31	21.447	0.084
118	217.12	23.98	22.186	0.156
116	111.38	24.53	23.801	0.498
123	115.53	24.45	25.429	2.325
145	116.58	30.01	20.753	0.032
149	110.45	31.68	22.242	0.141
171	119.33	35.28	21.251	0.048
170	112.33	35.36	19.579	0.011
188	122.15	37.44	20.755	0.030
194	116.39	38.47	20.981	0.039
218	113.52	44.38	21.596	0.064
244	117.34	49.00	22.662	0.160
136	157.96	28.31	21.376	0.061
163	158.07	34.52	22.256	0.147
164	164.52	34.85	24.968	1.661
209	166.81	41.11	22.989	0.244
229	164.07	46.44	21.746	0.075
247	168.82	51.11	23.529	0.349
141	236.55	28.59	21.757	0.085
140	198.49	28.76	21.432	0.074
156	194.97	31.22	22.946	0.288
155	190.74	32.24	22.096	0.125
147	260.90	30.08	19.420	0.019
154	65.29	31.16	24.312	0.767
183	67.39	37.77	23.407	0.322
168	72.44	35.60	24.352	0.804
187	61.12	39.39	23.573	0.367
207	67.05	40.83	23.152	0.253
206	57.48	40.81	22.064	0.105
205	51.94	40.70	21.362	0.068
228	50.01	45.80	20.814	0.041
178	217.81	36.40	26.439	6.857
158	245.29	31.99	21.337	0.059
159	273.64	32.20	23.077	0.300
212	275.90	44.88	27.742	9.999
226	275.41	45.11	23.395	0.352
249	270.05	49.25	23.247	0.318
225	268.09	45.00	20.949	0.040
264	274.78	54.13	20.616	0.045
271	269.12	55.38	24.019	0.680
294	270.39	60.22	22.992	0.275
311	281.88	64.19	23.518	0.428
309	266.56	64.77	22.015	0.100
299	286.82	61.25	19.996	0.017
322	261.46	66.74	23.364	0.352
337	266.23	70.81	20.748	0.033
259	285.80	51.44	21.095	0.064
279	297.37	56.63	20.554	0.043
227	286.48	45.34	22.037	0.165
214	288.98	42.99	23.706	0.688
157	207.11	32.37	20.365	0.048
195	208.64	39.08	21.117	0.103
210	204.14	40.56	19.953	0.034
172	130.05	34.79	19.475	0.019
173	233.51	35.15	25.117	1.686
184	239.34	38.91	23.718	0.422
196	233.14	38.52	23.597	0.418
201	227.76	39.84	24.634	1.006
221	232.25	44.04	24.681	1.128
224	223.33	45.57	25.297	1.698
245	223.84	49.31	23.871	0.456
179	253.75	35.65	23.907	0.637
189	257.18	38.48	23.475	0.428
199	183.32	40.16	24.224	0.842
223	178.94	44.73	23.386	0.335
200	189.09	39.52	19.935	0.018
252	175.89	50.80	23.707	0.420
198	151.16	39.65	25.087	1.423
208	134.21	40.96	22.343	0.096
202	299.18	42.34	27.974	9.999
211	92.35	42.23	22.963	0.275
216	98.99	43.63	23.009	0.300
217	106.04	43.67	19.179	0.016
222	75.86	43.99	24.145	0.749
239	73.97	48.31	30.474	9.999
220	215.52	44.27	20.207	0.027
230	199.23	49.03	27.311	9.999
238	252.05	46.81	20.756	0.037
254	250.43	51.05	21.214	0.057
274	249.34	56.19	21.236	0.055
237	241.79	46.98	20.791	0.060
240	138.31	47.59	22.391	0.128
242	295.40	47.38	24.352	1.517
243	299.13	48.84	23.699	0.806
241	190.22	48.58	23.045	0.293
253	184.13	50.64	22.728	0.205
260	63.32	52.34	20.630	0.060
255	52.40	52.78	22.098	0.161
261	128.59	50.20	33.943	9.999

251	93.51	51.10	21.137	0.052
256	88.93	51.51	23.655	0.484
269	94.77	54.54	20.183	0.022
258	233.94	51.76	22.987	0.160
257	159.08	52.23	19.321	0.022
262	151.76	52.76	20.497	0.018
268	27.94	54.33	26.962	8.860
272	22.55	55.94	23.706	0.426
295	22.34	60.99	22.392	0.138
267	15.10	55.83	24.684	1.144
285	11.78	59.10	22.252	0.145
270	110.62	55.17	19.427	0.015
281	117.08	57.59	23.608	0.433
304	119.58	62.42	22.846	0.202
287	124.44	58.59	24.108	0.681
273	133.97	55.68	23.578	0.529
297	134.81	61.26	24.694	1.329
277	75.34	56.68	22.347	0.158
276	68.54	57.17	22.472	0.220
275	36.10	56.92	22.073	0.093
278	181.72	57.26	21.750	0.090
280	43.46	57.59	24.270	0.845
306	42.30	63.86	20.840	0.038
325	39.44	68.35	22.170	0.130
283	220.86	57.63	21.134	0.040
302	224.49	61.58	20.296	0.018
321	222.63	65.14	21.809	0.070
320	216.78	66.90	23.283	0.275
284	231.02	58.35	24.432	0.855
282	191.25	58.73	23.229	0.284
288	196.22	59.39	24.194	0.661
291	261.21	58.99	24.818	1.461
298	257.10	60.96	23.877	0.565
289	204.72	59.06	20.825	0.044
305	205.49	62.75	20.600	0.036
293	147.79	60.29	22.221	0.092
296	101.69	60.54	22.966	0.221
300	95.41	62.23	20.939	0.036
324	98.36	67.06	22.759	0.190
290	244.21	61.65	28.839	9.999
316	241.12	65.80	23.556	0.362
331	238.70	69.47	23.500	0.342
343	244.02	71.84	20.035	0.014
357	236.64	73.94	23.282	0.275
301	161.02	61.37	24.312	0.685
319	160.29	65.59	23.146	0.223
328	166.91	67.21	22.928	0.175
342	163.19	71.43	24.855	0.988
347	168.30	73.47	23.568	0.296
314	76.87	64.60	23.855	0.363
317	3.32	65.79	20.618	0.047
318	142.87	66.57	22.703	0.201
326	113.40	67.63	21.681	0.076
335	117.58	70.90	21.971	0.094
346	122.33	72.90	22.830	0.206
368	116.11	77.47	23.192	0.280
327	126.00	68.43	24.508	0.852
361	125.26	76.22	21.502	0.073
330	230.63	68.39	24.156	0.653
350	225.92	73.26	23.572	0.392
336	203.76	70.71	18.775	0.009
340	107.02	72.05	18.261	0.007
341	132.94	72.21	23.311	0.267
339	91.59	72.35	20.237	0.028
353	87.78	75.03	19.265	0.010
367	83.03	77.97	23.704	0.513
386	85.13	83.23	23.298	0.348
393	89.06	83.79	24.116	0.743
381	94.36	81.19	21.647	0.074
365	96.62	77.40	21.741	0.084
345	73.64	72.95	21.359	0.062
360	68.47	76.96	23.265	0.378
373	60.57	79.83	25.213	2.432
349	144.23	74.02	19.045	0.018
354	151.77	74.63	24.242	0.735
382	159.79	80.94	22.162	0.114
396	165.28	84.11	20.271	0.024
385	167.66	81.49	19.676	0.015
355	210.18	74.93	23.996	0.411
352	47.15	75.10	21.387	0.106
358	43.20	75.82	21.756	0.138
379	40.49	80.38	22.347	0.185
452	47.05	93.72	22.607	0.211
356	217.66	75.12	26.606	5.691
362	183.45	76.49	20.625	0.020
383	186.80	80.45	22.571	0.115
369	193.22	77.93	22.138	0.078
405	185.81	86.74	23.201	0.199
413	191.22	88.17	23.034	0.170
438	181.62	91.43	23.358	0.217
425	176.65	90.02	21.892	0.053
447	172.59	92.38	23.162	0.173
459	168.40	94.34	22.752	0.119
364	32.01	76.50	19.404	0.052
376	268.29	79.95	24.360	0.745
401	261.39	86.29	24.271	0.672
406	265.05	85.96	26.353	5.169
422	255.24	89.07	24.015	0.589
374	104.49	80.31	19.287	0.011
375	255.89	80.21	24.697	1.275
389	250.02	82.46	21.444	0.061
384	223.12	81.22	20.315	0.065
388	239.76	82.75	23.461	0.259
414	236.39	87.45	24.724	0.961
421	239.29	89.26	24.905	1.108
400	230.87	83.78	23.611	0.342
454	234.45	93.67	22.447	0.110
387	123.44	83.20	17.079	0.003
409	129.25	86.41	20.492	0.048
423	122.17	90.04	21.472	0.084
394	132.66	83.82	19.506	0.015
412	116.10	88.14	22.151	0.124
445	120.85	92.92	22.211	0.147
399	112.45	84.88	24.061	0.720
458	115.06	95.29	23.083	0.274
468	124.79	96.89	20.116	0.023
408	109.08	86.58	23.470	0.415
477	115.70	99.62	21.591	0.069
436	107.64	93.05	24.104	0.715
485	110.25	103.19	21.999	0.103
427	102.86	90.43	24.311	0.836
395	151.49	84.38	22.331	0.117
398	76.59	84.80	25.893	2.955
403	279.95	85.03	23.472	0.362
404	67.79	85.84	23.278	0.281
410	144.66	86.48	20.931	0.028
428	139.99	90.59	22.084	0.087
462	139.12	95.81	23.164	0.222
470	145.62	98.00	22.071	0.078
483	145.67	102.16	22.550	0.125
489	140.62	103.67	22.877	0.168
505	134.59	105.87	23.407	0.259
510	128.06	108.68	25.383	1.566
513	121.72	109.34	24.356	0.638
509	115.84	107.97	21.055	0.034
534	123.81	113.91	25.631	1.992
420	203.35	88.75	21.786	0.049

426	297.32	89.39	23.131	0.396
424	157.75	89.45	23.274	0.337
446	161.12	92.52	20.468	0.026
437	152.40	92.67	23.513	0.384
430	246.80	91.18	22.873	0.144
432	10.52	91.65	20.491	0.036
433	14.82	91.98	21.078	0.060
466	16.19	97.95	24.702	1.435
456	22.56	96.28	24.131	0.996
472	10.34	98.77	22.077	0.118
467	25.05	97.25	21.985	0.135
484	21.32	103.51	22.773	0.233
451	30.42	94.41	22.235	0.123
443	75.80	92.65	20.842	0.079
442	70.56	92.70	24.279	1.458
461	78.84	95.88	18.957	0.022
460	68.70	96.15	24.151	1.312
444	94.42	92.82	20.699	0.035
448	212.98	93.15	18.289	0.009
463	207.63	95.77	21.592	0.144
453	220.62	94.06	22.907	0.183
469	226.62	96.20	23.671	0.325
480	229.87	100.69	23.160	0.202
464	259.10	96.15	25.986	3.981
486	259.08	103.14	23.208	0.275
501	262.49	104.37	23.523	0.375
471	188.81	98.06	21.349	0.068
473	184.41	99.41	22.562	0.204
476	90.12	99.84	19.899	0.034
481	280.86	100.85	23.611	0.326
479	36.77	101.73	24.845	1.305
493	41.02	105.29	24.575	1.005
492	219.98	103.13	22.943	0.149
490	158.38	103.82	24.230	0.782
511	163.27	107.31	22.116	0.117
525	162.02	112.08	25.310	2.213
491	176.56	103.99	20.384	0.028
500	210.12	104.19	24.942	1.070
496	63.43	104.65	21.222	0.059
512	62.92	108.69	22.936	0.281
502	270.29	104.96	23.959	0.402
494	48.18	105.20	19.818	0.017
495	56.02	105.21	21.056	0.077
497	97.81	105.30	18.834	0.019
498	195.74	105.48	26.171	4.374
499	202.52	105.78	22.472	0.154
504	78.75	106.29	20.414	0.050
518	297.22	108.37	23.838	0.578
536	293.69	114.38	22.177	0.131
549	287.17	115.97	24.363	0.928
516	231.19	108.71	24.411	0.627
517	234.54	109.57	23.712	0.337
530	231.74	112.54	23.080	0.184
540	237.66	114.49	23.028	0.192
547	234.00	116.08	25.514	1.864
571	238.59	121.29	23.853	0.379
563	243.95	118.75	24.377	0.629
531	244.94	113.05	24.767	0.933
564	250.32	118.79	21.066	0.029
589	246.84	123.28	25.860	2.264
535	253.88	114.21	22.705	0.142
617	244.32	129.78	22.304	0.082
644	245.15	134.82	25.035	1.135
667	241.09	139.60	20.559	0.019
652	235.96	136.78	23.844	0.375
674	235.19	140.79	23.410	0.245
648	231.95	135.93	25.662	2.044
679	228.73	141.74	20.868	0.024
515	185.42	109.26	18.959	0.017
539	187.99	114.09	22.887	0.490
519	27.93	109.24	23.726	0.407
514	152.25	110.09	24.239	0.766
538	153.73	114.61	23.571	0.410
522	170.20	110.94	19.607	0.023
521	104.48	111.41	22.681	0.188
543	99.59	115.30	22.120	0.108
544	108.83	116.28	20.736	0.030
581	110.26	122.20	23.636	0.392
604	110.10	127.00	23.308	0.296
523	260.70	111.53	23.255	0.380
532	263.92	112.97	23.989	0.747
529	217.77	112.52	20.122	0.022
557	215.44	117.67	21.951	0.119
528	205.46	112.82	23.942	0.566
551	206.00	116.74	23.211	0.318
568	199.78	119.52	20.049	0.019
584	205.12	123.08	19.854	0.018
598	208.90	125.81	20.234	0.028
533	41.34	113.37	23.539	0.367
553	44.63	117.94	20.905	0.036
561	39.30	119.11	21.573	0.066
560	36.77	118.37	28.048	9.999
542	87.99	114.70	24.233	0.667
570	89.69	121.22	22.983	0.210
588	91.98	123.82	22.339	0.118
610	96.02	128.81	25.163	1.618
637	88.57	133.74	25.415	2.018
626	100.80	131.69	23.883	0.489
625	92.63	132.00	23.464	0.362
633	96.84	132.58	24.361	0.796
647	93.73	135.33	25.121	1.650
592	101.32	125.07	19.478	0.010
634	104.83	133.03	21.554	0.073
654	107.84	138.13	20.041	0.019
672	114.57	140.09	25.103	1.486
677	103.97	142.35	21.834	0.075
671	99.74	140.77	21.354	0.047
700	106.72	147.82	20.480	0.024
537	136.15	114.92	23.607	0.327
545	130.09	116.57	32.002	9.999
555	134.01	117.89	24.355	0.688
567	128.79	119.68	24.136	0.482
574	138.49	122.06	20.323	0.020
593	125.03	125.06	31.985	9.999
611	133.93	125.82	24.353	0.707
573	121.28	121.73	25.426	1.603
605	130.11	127.00	24.041	0.476
554	117.60	117.64	24.422	0.638
627	142.13	132.23	24.368	0.643
639	135.64	133.82	21.131	0.034
640	147.59	134.39	21.471	0.041
651	131.50	135.91	23.464	0.274
666	136.27	140.27	21.240	0.037
655	147.86	137.86	20.711	0.020
650	125.85	136.99	21.431	0.041
673	131.21	140.99	23.045	0.174
638	120.39	133.72	21.268	0.037
546	145.94	115.72	19.985	0.024
548	270.65	116.13	21.546	0.050
577	270.55	122.20	23.744	0.407
595	268.03	125.42	24.037	0.551
590	262.97	124.85	23.147	0.235
572	258.62	120.61	21.296	0.044
618	263.62	130.78	22.114	0.102
629	258.84	131.82	24.546	0.893
635	266.99	133.18	20.350	0.020
657	256.13	136.64	24.815	1.166

653	269.84	137.15	22.350	0.120
663	262.77	138.75	19.653	0.011
550	64.54	116.97	22.795	0.134
556	178.30	118.30	24.842	1.114
575	177.03	121.87	23.197	0.253
582	183.29	123.47	23.704	0.382
562	170.37	119.00	20.922	0.039
558	8.42	119.18	22.331	0.164
579	6.54	123.02	23.897	0.736
586	10.43	124.05	20.957	0.048
607	4.42	128.33	21.141	0.067
624	9.25	132.38	20.199	0.031
576	221.60	121.34	21.291	0.058
583	193.02	121.84	33.507	9.999
597	62.76	125.81	24.228	0.609
596	55.86	126.20	23.791	0.364
603	68.36	126.77	21.157	0.038
587	51.18	123.45	23.217	0.216
632	58.06	132.54	24.084	0.500
591	71.75	125.01	21.141	0.038
614	73.05	129.45	22.687	0.144
594	161.83	124.74	19.688	0.020
601	296.47	125.80	21.793	0.086
578	338.48	169.53	27.696	9.999
636	295.86	132.48	24.103	0.683
623	288.28	131.80	24.019	0.705
622	281.33	130.74	23.348	0.350
645	279.18	135.23	23.730	0.501
675	289.59	141.34	24.459	1.008
681	283.35	141.87	22.862	0.264
619	274.23	129.59	23.323	0.305
694	291.68	144.35	23.023	0.253
692	280.37	144.61	23.798	0.630
710	285.57	148.54	22.552	0.179
687	298.51	143.85	23.195	0.289
680	275.72	142.39	21.960	0.095
608	34.80	127.81	21.743	0.223
612	232.60	127.60	23.004	0.179
616	154.78	129.65	23.399	0.253
613	20.38	130.07	19.785	0.019
641	18.43	134.70	23.259	0.428
621	181.46	130.51	20.232	0.028
628	220.62	131.38	24.672	0.733
630	29.26	133.47	22.355	0.110
642	165.65	135.08	21.447	0.044
643	197.23	135.33	21.886	0.070
656	155.48	137.81	20.174	0.027
660	158.73	139.28	20.919	0.055
659	68.62	138.50	20.724	0.049
670	74.33	140.73	20.116	0.029
662	220.70	139.24	21.190	0.038
661	189.06	139.39	19.837	0.029
690	188.65	144.42	19.612	0.021
708	186.87	149.15	20.731	0.049
664	24.11	139.76	18.827	0.014
668	11.98	140.41	24.064	0.610
678	176.86	141.31	25.104	1.738
684	172.76	143.46	33.525	9.999
669	39.69	141.29	31.664	9.999
676	85.74	141.84	21.293	0.083
682	31.61	142.49	21.324	0.042
683	50.21	143.36	23.249	0.281
685	121.53	144.51	25.455	1.809
686	253.77	144.35	20.898	0.045
699	248.71	146.98	21.649	0.080
688	63.75	144.97	23.316	0.256
691	216.10	145.32	20.511	0.030
695	80.30	146.40	20.627	0.036
696	2.47	146.68	17.926	0.008
698	201.89	146.71	19.907	0.027
702	195.67	149.05	23.351	0.576
697	95.15	147.32	20.924	0.080
703	224.05	147.97	19.436	0.022
701	139.65	148.50	30.736	9.999
714	145.15	151.38	23.884	0.638
704	264.16	148.23	19.966	0.021
705	57.52	149.38	21.800	0.078
713	126.51	149.84	21.259	0.053
715	234.83	150.96	20.488	0.052
712	33.00	150.96	21.265	0.050
2	62.22	2.04	20.578	0.078
6	295.60	2.34	23.433	0.745
23	299.55	5.78	23.580	0.821
29	290.73	7.26	19.438	0.023
12	73.00	5.55	19.898	0.068
36	119.12	8.51	22.370	0.176
33	57.85	8.92	23.872	0.333
89	220.00	17.10	23.554	0.350
133	164.98	24.45	23.439	0.441
135	183.81	26.65	21.109	0.153
131	73.53	28.40	24.107	0.643
213	199.71	46.35	34.266	9.999
231	9.63	47.33	21.117	0.068
312	333.86	-6.13	34.276	9.999
246	255.81	49.41	24.125	0.699
250	59.71	50.45	21.329	0.100
263	59.24	53.73	21.491	0.118
266	5.87	54.18	22.668	0.247
308	172.96	63.60	18.627	0.073
313	58.36	64.64	16.519	0.014
348	278.76	72.74	23.556	0.444
329	52.93	69.26	22.227	0.176
366	156.61	77.42	34.248	9.999
378	22.77	80.41	19.126	0.069
380	57.42	80.52	23.060	0.239
397	46.01	84.75	21.817	0.121
419	50.44	88.49	22.287	0.193
402	268.46	84.53	30.323	9.999
351	214.31	33.13	34.287	9.999
407	29.08	87.28	21.073	0.038
449	281.01	93.27	23.069	0.358
475	82.66	99.28	19.461	0.057
478	2.93	100.50	21.837	0.067
503	13.89	106.91	22.633	0.254
507	7.84	108.23	19.728	0.029
527	14.04	113.34	20.781	0.041
559	17.36	118.87	20.833	0.042
552	23.14	117.48	20.487	0.031
508	72.35	107.60	21.705	0.119
524	285.06	111.63	23.180	0.392
526	289.98	112.08	22.069	0.135
541	280.89	113.45	23.293	0.418
565	280.29	119.18	23.528	0.538
620	42.90	130.32	19.107	0.048
631	36.59	133.18	20.681	0.135
609	87.44	127.62	25.098	1.464
615	137.59	130.14	24.652	1.099
162	26.07	33.91	24.189	0.832
177	179.06	35.96	21.629	0.069
332	276.34	68.13	27.966	9.999
370	276.79	78.57	19.903	0.020
602	44.43	127.11	19.238	0.056
119	16.55	23.85	22.645	0.172
193	38.97	38.83	23.791	0.446
197	277.41	36.87	24.779	2.134
219	121.33	40.00	24.224	0.641
303	275.90	52.64	29.512	9.999

334	10.16	70.97	15.891	0.022	418	42.97	88.82	23.914	0.853
363	299.11	75.33	21.639	0.148	441	59.76	92.39	21.375	0.067
474	18.77	99.42	23.949	0.769	711	18.52	149.05	18.809	0.084
416	303.64	107.01	27.707	9.999	68	31.98	12.67	21.802	0.212
693	282.89	144.88	25.743	4.908	95	2.97	19.59	20.528	1.080
106	189.73	22.52	15.459	0.051	606	297.57	131.24	28.068	9.999
124	255.02	29.89	22.273	0.138	46	27.17	12.30	22.409	0.405
167	33.91	35.49	24.253	0.579	371	283.02	78.64	23.624	0.436
235	42.58	44.77	23.517	0.313	435	47.46	90.38	22.832	0.185
457	61.18	95.31	20.507	0.060	434	17.92	104.78	23.380	0.348
709	284.99	151.75	29.746	9.999	190	270.76	38.29	23.820	0.642
114	36.32	22.18	22.309	0.105	600	281.66	127.97	24.410	1.161
185	277.69	23.71	24.383	1.009	344	13.13	76.27	17.319	0.373
372	282.31	86.80	31.282	9.999	392	10.96	80.28	16.703	0.611
431	284.72	91.74	24.516	1.082	286	15.56	73.08	19.256	0.168

M4DEEP

42	13.19	45.33	20.206	0.024	34	18.71	36.75	23.775	0.804
6	40.01	8.81	20.207	0.021	19	73.96	20.27	23.894	0.446
67	49.49	66.36	20.506	0.028	50	1.90	38.18	23.938	0.671
25	51.25	26.69	20.626	0.015	44	70.35	46.77	24.098	0.442
59	22.05	56.05	20.655	0.036	36	72.77	38.29	24.160	0.603
40	20.75	44.34	20.752	0.035	15	40.08	17.48	24.167	0.530
43	53.46	45.20	21.034	0.025	52	12.94	50.85	24.200	0.510
5	67.17	8.32	21.193	0.056	12	9.50	16.12	24.258	0.577
46	47.77	47.48	21.255	0.030	21	36.97	22.64	24.285	0.587
69	25.11	67.24	21.278	0.045	38	39.38	43.09	24.383	0.497
48	20.75	48.30	21.408	0.065	61	45.74	61.14	24.417	0.932
71	56.58	68.37	21.644	0.075	63	71.38	61.70	24.451	1.028
11	56.02	15.49	21.796	0.078	62	74.29	60.82	24.462	1.049
65	9.96	64.40	21.799	0.112	18	18.68	19.69	24.566	0.556
73	61.93	71.05	21.957	0.099	51	73.10	50.16	24.624	0.770
57	37.97	54.11	22.069	0.113	14	3.69	17.44	24.698	1.451
53	35.29	51.22	22.069	0.111	20	69.68	22.07	24.718	0.999
22	28.82	23.77	22.133	0.070	39	64.72	43.24	24.763	0.713
64	31.58	64.47	22.424	0.121	37	60.15	38.84	24.931	0.814
66	71.49	65.70	22.516	0.159	30	68.11	31.75	24.952	1.160
7	18.00	9.87	22.574	0.168	17	5.45	20.23	24.968	1.826
32	46.77	35.28	23.086	0.243	16	45.89	18.37	25.031	1.168
68	63.36	65.69	23.104	0.270	8	72.84	11.54	25.195	2.215
35	30.80	38.61	23.134	0.146	47	66.17	47.40	25.319	1.259
72	67.15	68.06	23.178	0.297	33	75.19	35.86	25.442	2.056
27	23.37	30.60	23.289	0.271	41	44.54	43.78	25.468	1.445
60	74.55	56.57	23.299	0.312	24	66.82	26.49	25.875	2.523
13	26.29	16.13	23.325	0.198	26	17.54	28.09	25.970	3.166
28	41.73	31.42	23.380	0.312	23	70.63	24.87	27.708	9.999
3	12.61	6.40	23.563	0.443	10	63.26	14.48	28.782	9.999
49	59.17	46.96	23.630	0.263	54	17.86	37.63	30.423	9.999
70	13.99	68.62	23.634	0.564	31	71.38	31.88	30.883	9.999
1	45.62	4.09	23.668	0.472	29	9.70	33.14	34.763	9.999
56	26.42	52.75	23.711	0.573					

M4DEEPM1

41	13.08	45.24	20.248	0.012	54	21.94	55.95	20.694	0.029
8	40.02	8.80	20.253	0.018	39	20.66	44.27	20.767	0.034
65	49.30	66.22	20.552	0.019	42	53.39	45.12	21.051	0.025
26	51.17	26.60	20.651	0.018	7	67.30	8.28	21.233	0.051

44	47.68	47.39	21.267	0.028	68	34.41	68.73	23.880	0.530
66	24.91	67.08	21.312	0.036	60	74.02	61.03	24.010	0.474
46	20.65	48.21	21.417	0.061	43	71.64	46.41	24.023	0.383
69	56.42	68.20	21.693	0.104	21	73.85	20.25	24.056	0.490
15	55.98	15.46	21.816	0.074	49	72.90	50.14	24.076	0.417
61	9.74	64.26	21.881	0.072	36	72.86	38.25	24.135	0.475
71	61.62	70.65	21.978	0.158	19	39.90	17.42	24.252	0.415
50	35.27	51.18	22.069	0.098	38	64.61	43.13	24.496	0.531
53	37.93	54.07	22.093	0.103	58	9.76	60.71	24.584	0.865
24	28.72	23.69	22.155	0.061	37	59.93	38.78	24.669	0.621
63	71.41	65.38	22.349	0.154	22	65.91	21.19	24.709	0.778
62	31.44	64.30	22.420	0.138	45	66.15	47.21	24.811	0.723
9	18.05	9.83	22.616	0.148	18	3.47	18.82	24.814	1.323
33	46.67	35.15	23.058	0.133	48	7.89	50.29	24.859	0.936
35	30.69	38.51	23.080	0.122	40	41.50	41.10	24.940	0.713
57	74.66	56.52	23.162	0.199	20	6.22	20.61	25.165	1.843
29	23.31	30.45	23.196	0.149	31	67.87	31.57	25.591	1.815
3	19.49	4.15	23.220	0.268	11	72.96	11.51	25.973	4.215
17	26.22	16.07	23.300	0.178	23	70.51	21.84	26.225	3.887
1	34.49	3.68	23.447	0.295	25	70.90	24.73	26.804	6.770
47	58.70	46.56	23.499	0.232	5	72.93	7.35	28.027	9.999
52	26.33	53.28	23.546	0.403	59	62.60	60.77	28.257	9.999
2	45.40	3.96	23.550	0.357	27	66.58	26.87	29.550	9.999
34	18.54	36.79	23.552	0.242	30	8.80	32.55	32.760	9.999
67	13.94	68.34	23.581	0.322	32	71.42	31.85	33.069	9.999
4	12.61	6.40	23.588	0.374	28	13.26	27.31	33.880	9.999
10	2.34	11.15	23.605	0.416	51	8.52	54.03	34.127	9.999
14	11.67	14.92	23.772	0.278	56	66.52	55.94	34.602	9.999
55	44.93	56.81	23.832	0.240	0	0.00	0.00	0.000	0.000

M4DEEPM2_2

6	43.54	6.17	20.347	0.059	23	4.71	19.85	23.890	0.694
52	16.77	42.82	20.390	0.036	12	64.39	12.85	23.896	0.738
29	54.86	24.15	20.825	0.039	81	15.15	66.68	23.953	1.087
77	53.04	63.64	20.874	0.049	33	67.83	26.45	23.957	0.650
68	25.59	53.56	20.889	0.048	55	63.80	45.53	24.005	0.737
51	24.36	41.77	20.982	0.060	42	50.96	33.20	24.069	0.622
70	2.75	57.78	21.206	0.063	62	72.14	49.88	24.121	0.621
4	70.83	5.86	21.207	0.068	59	16.02	48.18	24.144	0.890
53	56.94	42.65	21.281	0.055	76	72.84	62.04	24.145	0.718
54	51.33	45.03	21.513	0.076	28	7.00	23.34	24.185	0.886
79	28.68	64.69	21.568	0.079	56	2.53	45.94	24.238	1.227
57	24.43	45.81	21.617	0.108	19	43.93	16.94	24.239	0.832
11	59.57	12.95	21.711	0.099	69	68.50	55.80	24.258	0.729
72	13.48	61.76	21.975	0.145	61	59.62	48.56	24.288	1.024
60	38.96	48.68	22.266	0.163	64	61.98	51.94	24.363	1.095
80	60.11	65.47	22.352	0.186	66	68.58	52.96	24.421	0.848
25	32.36	21.15	22.452	0.106	34	21.78	28.05	24.471	1.026
63	41.61	51.46	22.517	0.205	43	68.04	33.35	24.498	0.996
73	35.07	61.84	22.872	0.227	67	75.81	53.44	24.536	1.615
5	21.75	7.48	23.124	0.436	74	8.01	63.56	24.562	1.567
78	3.29	65.74	23.137	0.478	71	72.95	57.70	24.599	0.987
44	4.77	33.54	23.258	0.534	65	10.13	53.16	24.680	1.342
37	27.31	28.59	23.273	0.316	50	37.12	40.62	24.695	1.392
2	14.79	4.97	23.381	0.622	15	17.53	16.37	24.769	1.831
47	34.44	35.69	23.449	0.503	31	32.19	25.92	24.799	0.931
14	28.83	14.14	23.458	0.281	16	22.10	15.90	24.814	1.930
17	8.27	16.92	23.592	0.558	24	19.56	21.87	24.815	1.498
7	2.60	8.43	23.643	0.844	30	19.40	24.75	24.818	1.481
35	45.31	28.52	23.767	0.548	41	62.73	31.86	24.826	1.720
46	21.83	34.74	23.779	0.562	45	29.88	33.82	24.888	1.853

48	46.18	37.69	24.934	1.628	49	72.54	38.49	25.542	3.139
27	67.07	23.09	24.948	1.640	18	34.64	17.34	25.627	2.027
1	52.84	3.23	24.959	2.200	22	11.49	17.49	27.542	9.999
39	35.36	30.09	24.984	1.101	13	10.78	14.82	29.094	9.999
21	38.47	17.92	25.132	1.308	32	36.32	25.74	31.814	9.999
8	35.05	9.25	25.170	2.786	3	61.85	6.04	32.122	9.999
26	63.41	20.27	25.241	2.182	40	57.93	31.87	32.157	9.999
10	36.27	12.04	25.308	3.170	75	23.21	63.37	32.951	9.999
36	14.71	29.50	25.312	3.643	58	6.96	46.71	33.856	9.999
20	29.30	17.82	25.329	1.551	9	13.95	10.58	34.225	9.999
83	43.41	68.12	25.436	3.086	82	74.97	66.61	34.296	9.999

Appendix B: Reduction Software

There follows a summary of some of the software that has been written to handle IRCAM frames and DAOPHOT/ALLSTAR data files. It is hoped that some of these routine will be of use to other researcher.

LINCORR.FOR - performs polynomial linearity corrections on bias-subtracted frames.

DAO_COMBINE.FOR - matches 2 NST/ALS files to a given pixel tolerance and outputs to COMB file. Optional prompting for confirmation of match.

DAO_COMBINE_IRSETS.FOR - matches two ALS/NST files, passing through any stars found in only one set, averaging parameters for those in both sets. Out to ALS file.

DAO_MATCH_INFO.FOR - produces magnitude and separation residual plots for given cut-offs in separation and errors.

DAO_DOUBLES.FOR - reads COMB and 2 ALS/NST files to display maps for stars in 1st set matched with more than one star in second set, for user to decide between them or reject both.

DAO_COMB3.FOR - combines COMB files by matching chosen indices and outputing a COMB3 file.

DAO_C3_EXTRACT.FOR - reads COMB3 file and outputs n1 m2-m1 m1 using error cut-offs in both magnitudes.

DAO_FIND_MATCH.FOR - writes stars that have matched through to another ALS/NST file. Prompts for which set in COMB file is to be used to search input ALS file numbers.

DAO_INPUT.FOR - typed in data is output to ALS/NST format file.

DAO_MAP.FOR - plots maps from ALS/NST files on any display, overlaying if required, between input limits.

DAO_REFIT.FOR - program to search combine output and for those pairs matching to better than n pixels copy them through to a new ALS file for a 2nd run of DAO_XYFIT. - to refine co-ordinate transformation.

DAO_REMOVE_STARS.FOR - find stars by co-ordinates and offer to remove them from ALS/NST file.

DAO_RMS.FOR - program to generate RMS plots from DAOPHOT NST/ALS files, allowing interactive definition of a cut-off and filtering of the data. - allows fitting of upto 9th order polynomial to cut data. Outputs to ALS and RPLT files.

DAO_SUBSELECT.FOR - a program to select an x,y subset from an NST/ALS file, and subtract x and y offsets.

DAO_XYTRAN.FOR - to apply a linear transformation of an ALS/NST format file. (From EDRS XYTRAN and XYLTRN).

XYFIT and its subroutines

DAO_XYFIT.FOR - to obtain a least-squares linear position transformation between two sets of x,y postions in ALS/NST files. (From EDRS XYFIT).

DAO_FITLST.FOR - subroutine to control the fitting of a linear transformation between two sets of x,y positions and to display the results. Calls dao_xymtch to match numbers and dao_xyfitr to do the fit, then displays results. (From EDRS FITLST).

DAO_LINTRN.FOR - subroutine to obtain least-square fit of linear transformation to 2 sets of x,y positions. (From EDRS LINTRN).

DAO_XYFITR.FOR - to obtain a least-squares linear transformation between two sets of x,y positions, rejecting erroneous data. (From EDRS XYFITR)

DAO_XYMTCH.FOR - to sort two lists so that items with the same identifier occur in the place in each. (From EDRS XYMTCH).

Appendix C: Publications List

Refereed publications

Longmore, AJ, Dixon, RI, Skillen, I, Jameson, RF & Fernley, JA, 1990. M.N.R.A.S., **247**, 684.
'Globular cluster distances from the RR Lyrae log(period) - infrared magnitude relation.'

Simon, M, Chen, WP, Forrest, WJ, Garnett, JD, Longmore, AJ, Gauer, T & Dixon, RI, 1990. Ap.J., **360**, 95.
'Subarcsec resolution observations of the central parsec of the galaxy at 2.2 μm.'

Guarnieri, MD, Longmore, AJ, Fusi Pecci, F & Dixon, RI, 1990. Mem Soc Ast It. **61**, 143.
'Infrared Colour-Magnitude diagrams of the globular cluster M3.'

Guarnieri, MD, Dixon, RI & Longmore, AJ, 1991. P.A.S.P., **103**, 675.
'The accuracy of infrared photometry with arrays.'

Unrefereed publications

McLean, IS, Aspin, C, Longmore, AJ & Dixon, RI, 1987. In *'IR Astronomy with Arrays'*, eds Wynn-Williams, CG & Becklin, EE, University of Hawaii (Honolulu).
'The January 1987 Galactic Centre Occultation Observed with IRCAM.'

Longmore, AJ, Dixon, RI & Guarnieri, MD, 1990. *'Astrophysics with Infrared Arrays'*, ed. Elston, R, p.121. Publications of the Astronomical Society of the Pacific (San Fransisco).
'Colour-magnitude and colour-colour diagrams of globular clusters.'

Longmore, AJ, Dixon, RI, & Buckley, DRV, 1990. In *'Confrontation Between Stellar Pulsation and Evolution'*, eds. Cacciari, C. & Clementini, G., A.S.P. Conference Series 11, 36.
'How infrared observations of RR Lyrae stars enhance their usefulness in distance & pulsation studies.'

Buckley, DRV, Longmore, AJ & Dixon, RI, 1991. Paper presented at the *'New Results on Standard Candles'* workshop, Trani, Italy 1991. To appear in Mem. Soc. Astron. Ital.
'The RR Lyrae log (period) - mean K magnitude relation: intrinsic scatter, applications & remaining uncertainties.'